FINAL REPORT

Alternative Copper-Beryllium Alloys Development

SERDP Project WP-2138

MAY 2015

Ralph Jaffke
Parviz Yavari
Northrop Grumman Corporation

Distribution Statement A
This document has been cleared for public release

SERDP
DOD ▪ EPA ▪ DOE

This report was prepared under contract to the Department of Defense Strategic Environmental Research and Development Program (SERDP). The publication of this report does not indicate endorsement by the Department of Defense, nor should the contents be construed as reflecting the official policy or position of the Department of Defense. Reference herein to any specific commercial product, process, or service by trade name, trademark, manufacturer, or otherwise, does not necessarily constitute or imply its endorsement, recommendation, or favoring by the Department of Defense.

REPORT DOCUMENTATION PAGE

Form Approved
OMB No. 0704-0188

Public reporting burden for this collection of information is estimated to average 1 hour per response, including the time for reviewing instructions, searching existing data sources, gathering and maintaining the data needed, and completing and reviewing this collection of information. Send comments regarding this burden estimate or any other aspect of this collection of information, including suggestions for reducing this burden to Department of Defense, Washington Headquarters Services, Directorate for Information Operations and Reports (0704-0188), 1215 Jefferson Davis Highway, Suite 1204, Arlington, VA 22202-4302. Respondents should be aware that notwithstanding any other provision of law, no person shall be subject to any penalty for failing to comply with a collection of information if it does not display a currently valid OMB control number. **PLEASE DO NOT RETURN YOUR FORM TO THE ABOVE ADDRESS.**

1. REPORT DATE *(DD-MM-YYYY)*
16-02-2015

2. REPORT TYPE
FINAL REPORT

3. DATES COVERED *(From - To)*
JUNE 2011 - MARCH 2015

4. TITLE AND SUBTITLE
ALTERNATIVE COPPER BERYLLIUM ALLOYS DEVELOPMENT PROGRAM

5a. CONTRACT NUMBER
W923HQ11C0031

5b. GRANT NUMBER

5c. PROGRAM ELEMENT NUMBER

6. AUTHOR(S)
JAFFKE RALPH E. / YAVARI PARVIZ et al.

5d. PROJECT NUMBER
WP2138

5e. TASK NUMBER

5f. WORK UNIT NUMBER

7. PERFORMING ORGANIZATION NAME(S) AND ADDRESS(ES)
NORTHROP GRUMMAN CORPORATION

AEROSPACE SYSTEMS
1 HORNET WAY
EL SEGUNDO, CA. 90245

8. PERFORMING ORGANIZATION REPORT NUMBER

9. SPONSORING / MONITORING AGENCY NAME(S) AND ADDRESS(ES)
STRATIGIC ENVIRONMENTAL
RESEARCH DEVELOPMENT PROGRAM
UNITED STATES AMERICA
CORP ENGINEER

10. SPONSOR/MONITOR'S ACRONYM(S)
SERDP
USACE

11. SPONSOR/MONITOR'S REPORT NUMBER(S)

12. DISTRIBUTION / AVAILABILITY STATEMENT
DISTRIBUTION AUTHORIZED TO U.S. GOVERNMENT AGENCIES AND THEIR CONTRACTORS: CRITICAL TECHNOLOGY; MARCH 2015. OTHER REQUESTS FOR THIS DOCUMENT SHALL BE REFERRED TO SERDP.

13. SUPPLEMENTARY NOTES
EXPORT RESTRICTIONS APPLY

14. ABSTRACT
ALTERNATIVE COPPER BERYLLIUM ALLOYS DEVELOPMENT WAS PERFORMED IN THIS PROGRAM. A DOWN SELECTION FROM TWO BASE MATERIAL COMPOSITIONS (COPPER & COBALT). NOT ENOUGH EXPERIMENTAL MATERIAL WAS AVAIALBLE TO FURTHER INVESTIGATE THE COPPER BASE (CUPRIUM) ALTHOUGH PROPERTIES AND PERFORMANCE CHARACTERISTICS OF THE COBALT BASED MATERIAL WERE AS GOOD AS OR BETTER THAN THE STANDARD COPPER BERYLLIUM. MATERIALS CHARATERISTICS TESTS AND SIDE BY SIDE COMPARISONS WERE PERFOMED AND EVALUATED. RESULTS SHOWED THAT THE COBALT BASED MATERIAL HAS AS EQUAVILANT OR SUPEROR PERFORMANCE THAN THOSE OF THE STADNDARD COPPER BERYLLIUM MATERIAL AND ACHIEVED MOST OF THE DESIRED PEEFORMANCE LEVELS REQUIRED FOR THE PROGRAM EXCEPT FOR THAT OF THE TENSILE YIELD STRENGTH.

15. SUBJECT TERMS
DESIGN & DEVELOPMENT

16. SECURITY CLASSIFICATION OF: UNCLASIFIED			17. LIMITATION OF ABSTRACT	18. NUMBER OF PAGES	19a. NAME OF RESPONSIBLE PERSON
a. REPORT	b. ABSTRACT	c. THIS PAGE			RALPH JAFFKE
UNCLASSIFIED	UNCLASSIFIED	UNCLASSIFIED	SAR	122	19b. TELEPHONE NUMBER *(include area code)* (310) 332-1134

Standard Form 298 (Rev. 8-98)
Prescribed by ANSI Std. Z39.18

Use or disclosure of data contained on this sheet is subject to the restriction on the title page of this proposal.
Northrop Grumman Private/Proprietary Level I

TABLE OF CONTENTS

Page

EXECUTIVE SUMMARY 1

1.0 OBJECTIVE 3

2.0 TECHNICAL APPROACH 4

2.1 BACKGROUND 4

2.2 METHODS 6

2.3 MICROSTRUCTURAL CONCEPTS 9

2.4 PRELIMINARY ALLOY DESIGN AND PROCESS MODELING 10

2.4.1 Copper Based Alloy Designs (Ngcu-1a / Ngcu-1b / Cuprium) 10

2.4.1.1 Design of NGCu-1A Sn-Free 11

2.4.1.1.1 Final NGCu-1A Alloy and Process Selection 16

2.4.1.2 Design of NGCu-1B Containing Sn 17

2.4.1.2.1 Final NGCu-1B Alloy and Process Selection 19

2.4.1.3 Design of Cuprium Containing Sn 20

2.4.1.3.1 Final Cuprium Alloy and Process Selection 26

2.4.2 Cobalt Alloy Design 26

2.4.2.1 Design of NGCo-1A 28

2.4.2.1.1 Final NGCo-1A Alloy and Process Selection 31

2.4.2.2 Design of NGCo-2A 31

2.4.2.2.1 Final NGCo-2A Alloy and Process Selection 38

2.4.2.3 Design of NGCo-3A Alloy 38

2.4.2.3.1 Final NGCo-3A Alloy and Process Selection 47

2.4.2.4 Optimized Design of NGCo-3A 48

3.0 ALLOY CHARACTERIZATION AND DISCUSSION 56

3.1 CHARACTERIZATION TESTING PERFORMED AND RESULTS 57

3.1.1 Tension Test Results of Evaluation Materials 58

3.1.2 Compression Test Results of Evaluation Materials 62

3.1.3 Pin-on-Disk Wear Testing Results of Evaluation Materials 64

3.1.4 Reciprocating-Ball-on-Flat Test Results of Evaluation Materials 69

Use or disclosure of data contained on this sheet is subject to the restriction on the title page of this proposal.
Northrop Grumman Private/Proprietary Level I

TABLE OF CONTENTS (Continued)

Page

3.1.5 Alternative Alloys Testing Evaluation & Material Down-Selection 73

3.1.6 Galling Test Results of Evaluation Materials 76

3.1.7 Fatigue Life Cycle Test Results of Evaluation Materials 81

4.0 ENHANCED BUSHING DEVELOPMENT EVALUATION 83

4.1 FINITE ELEMENT SIMULATION TOOLS 83

4.2 GENERAL PROPERTIES 84

4.3 PARAMETRIC CASE STUDIES 87

4.3.1 CASE 1: Increasing Load 87

4.3.2 CASE 2: Shaft Rotational Velocity 88

4.3.3 CASE 3: Coefficient of Friction 89

4.3.4 CASE 4: Shaft Boundary Conditions, Loading Conditions, and Tilt 92

4.3.5 CASE 5: Bushing Yield Stress 94

4.3.6 CASE 6: Effect of Bushing/Shaft Tolerance 97

4.4 SUMMARY AND CONCLUSIONS OF MODELING EVALUATION 98

5.0 FULL SCALE ENVIRONMENTAL BUSHING TESTING 99

5.1 BUSHING THRESHOLD TEST AND EVALUATION 102

5.2 BUSHING ENDURANCE TEST AND EVALUATION 112

6.0 ALTERNATIVE COPPER BERYLLIUM HEALTH RISK ASSESSMENT 120

7.0 CONCLUSIONS 120

REFERENCES: 123

APPENDIX A 124

Use or disclosure of data contained on this sheet is subject to the restriction on the title page of this proposal.
Northrop Grumman Private/Proprietary Level I

LIST OF FIGURES

Page

Figure 1. Overall Program Schedule 4

Figure 2. Flow Diagram for Design of Ferrium 6

Figure 3. Example of a Wear Mechanism Map for Steel[5] 8

Figure 4. Systems Design Chart for a Precipitation Strengthened Copper or Cobalt Alloy System 9

Figure 5. Calculated Lattice Parameters for FCC Cu-X Binary Alloys (left) and $L1_2$ Precipitates (right) at 500°C 11

Figure 6. Observation of the Presence or Absence of Cellular Growth in Different QuesTek Alloys and their Correlation with the Predicted Lattice Misfit 12

Figure 7. A Constrained Cu-Ni_3Mn-Ni_3Al Pseudoternary 13

Figure 8. Calculated Thermodynamic Equilibria Step Diagram for the NGCu-1A Design 14

Figure 9. Calculated Solidification Curves for NGCu-1A Under Two Different Models 15

Figure 10. As-Cast and As-Homogenized Calculated Segregation Profiles, Illustrating that 975º C/48hrs Should be Sufficient to Eliminate Most of the Residual Micro-Segregation in the Alloy 15

Figure 11. NGCu-1A Round Stock Evaluation Material 17

Figure 12. Prior Published Work Demonstrating that a Cu-Ni-Mn-Sn-Al Alloy can be Successfully Hot-Worked at 850° C 18

Figure 13. Step Diagram of the NGCu-1B Design, and the Calculated Scheil Solidification Plot. The Final Solidification Temperature is Calculated to be 750° C 18

Figure 14. (a) NGCu-1B 20

Figure 15. Images of Spray-Metal Forming Facility at Penn State's Applied Research Lab 22

Figure 16. As-Cast Micrographs from the SMF Cuprium Billet. Left: Etched Optical Micrograph Revealing the Fine Grained Structure, Right: SEM Micrograph Indicating the Presence of Very Fine (~1 Micrometer or Less) Grain Boundary Precipitates 23

Figure 17. Schematic Detailing the Production Path for the SMF Cuprium Alloy 23

Figure 18. Image of the As-Cast SMF Cuprium Billet 24

Figure 19: Optical Micrographs of Extruded SMF Cuprium at Different Magnifications 25

Figure 20. Optical Micrograph of the Fully Tempered USMC B86 Alloy, Revealing the Absence of any Cellular Growth and the Presence of Annealing Twins 27

Figure 21. The Re-Design Strategy to Obtain the Required Strength 28

Figure 22. Step Diagram for the Previous QuesTek B86 Alloy, and the Desired Stability Lines for the Current Design 29

Use or disclosure of data contained on this sheet is subject to the restriction on the title page of this proposal.
Northrop Grumman Private/Proprietary Level I

Figure 23a, b. Calculated Iso-Contour Plots of the Gamma Prime Volume Fraction and Lattice Misfit as a Function of the Ti and Fe Content 30

Figure 24. Step Diagram of the NGCo-1A Design, and the Calculated Values of the Key Design Metrics 30

Figure 25. NGCu-1A Round Stock Evaluation Material 31

Figure 26. Grain Structure Parallel to the Rolling Direction in NGCo-1A 32

Figure 27. Grain Structure Perpendicular to the Rolling Direction in NGCo-1A 32

Figure 28. Calculated Thermodynamic Step-Diagram for NGCo-1A Alloy, Showing the Phases Present and their Equilibrium Amounts at Different Temperatures 33

Figure 29. Atom-probe Reconstruction of the NGCo-1A Alloy, Showing the Presence of $L1_2$ Particles in a FCC Matrix, as Predicted 34

Figure 30. Measured X-ray Diffraction Peaks of the Gage-Section of a Fractured Tensile NGCo-1A Specimen, using a Cu Kα Source 35

Figure 31. Composition by Weight % of NGCo-2A after Minor Modifications 36

Figure 32. Temper Evaluation Shows Increased Hardness at Lower Temperature for Longer Time 37

Figure 33. Production Process of NGCo-2A 2nd Generation Material 37

Figure 34. Forging Failure of NGCo-2A at 1175º C 38

Figure 35. Schematic Detailing the MetalWerks Production Path for the NGCo-3A Alloy 39

Figure 36. Example images of the GFM at MetalWerks 41

Figure 37. NGCo-3A, Immediately after Forging to the Intermediate 4 Inch Round Product Size. Total Length is 86 Inches 41

Figure 38. Example Image of NGCo-3A 4 Inch Round Product During Dye Penetrant Testing (Prior to Peeling to 3.875 Inch Diameter) 42

Figure 39. NGCo-3A, after Forging to the Final 2.1 Inch Round Product Size 44

Figure 40. NGCo-3A VAR End Crop - Hardness Response Study at an Aging Temperature of 780° C 45

Figure 41. Optical Micrographs of Rotary Forged NGCo-3A, 2.1 Inch Product, at Different Magnifications 46

Figure 42. Gantt chart showing tasks to be performed for NGCo-3A Material Optimization 48

Figure 43. Experimental LEAP Analyses of the NGCo-3A used to Calibrate QuesTek's Co Thermodynamic Databases in Preparation for PrecipiCalc Simulations 49

Figure 44. Example of Experimental Diffusivity Data (from literature) used to Calibrate QuesTek's Co Kinetics Databases in Preparation for PrecipiCalc Simulations 50

Figure 45. Calculated Isothermal Aging Curves for the NGCo-3A 51

Use or disclosure of data contained on this sheet is subject to the restriction on the title page of this proposal.
Northrop Grumman Private/Proprietary Level I

Figure 46. Tensile Yield Strength Results from Task 1 Heat Treatment Optimization Study (NGCo-3A 4" Round Material) 52

Figure 47. Predicted increase in tensile yield strength with refinement in grain size from its current level of 75 µm down to 30, 20 and 10 µm, respectively 53

Figure 48. Schematic of Production Path for 30 lb Scale Manufacture of NGCo-3A alloy..... 54

Figure 49. Chemistry Analysis of the Round 3 Production of NGCo-3A at MetalWerks 55

Figure 50. Images of the Round 3 NGCo-3A Prototype Ingot after Fracturing During Hot Rolling..... 56

Figure 51. Configuration of Tensile Specimen per ASTM E8 58

Figure 52. Typical ASTM E8 Tensile Test Fixture and Tensile Specimen..... 59

Figure 53. Typical Tension Test Results 60

Figure 54. Configuration of Compression Specimen per ASTM E9..... 62

Figure 55. Typical ASTM E9 Machined Compression Specimen 62

Figure 56. Typical Compression Test Results 63

Figure 57. Configuration of Pin-on-Disk Specimen 65

Figure 58. Typical ASTM G99 Machined Pin-on-Disk Wear Specimen..... 65

Figure 59 - Schematic Illustration of Pin-on-Disk Wear Test Setup 66

Figure 60. Visual Wear of Track # 1 of the Disk and Associated 440C Steel Ball for AMS 4533 Cu-Be, NGCu-1A, NGCo-1A, NGCo-3A (2") and NGCo-3A (4") Respectfully..... 68

Figure 61. Visual Wear of Track # 10 of the Disk and on the Associated 440C Steel Ball for AMS 4533 Cu-Be, NGCu-1A and NGCo-1A Respectfully 69

Figure 62. Configuration of Wear Testing Reciprocating-Ball-on-Flat Test Specimen..... 69

Figure 63. Typical ASTM G133 Machined Reciprocating-Ball-on-Flat Specimens 70

Figure 64. Schematic Illustration of Reciprocating-Ball-on-Flat Wear Test Setup..... 70

Figure 65. Visual Wear of Track #1 of Reciprocating-Ball-on-Flat Wear Test 72

Figure 66. Visual Wear of Track # 10 of Reciprocating-Ball-on-Flat Wear Test 73

Figure 67. Alloy Tensile Characteristics Comparison Chart 74

Figure 68. Compression Yield Strength Comparison of NGCo-3A & Copper Beryllium..... 75

Figure 69. Friction Factor Comparison of NGCo-3A and Baseline Copper Beryllium 76

Figure 70. Configuration of ASTM G98 Galling Test Specimen..... 77

Figure 71. Typical ASTM G98 Machined Galling Button Specimens..... 77

Figure 72. Typical ASTM G98 Test Setup Fixture 78

Figure 73. ASTM G98 CuBe Test Specimens with Highest Loaded Specimen 79

Use or disclosure of data contained on this sheet is subject to the restriction on the title page of this proposal.
Northrop Grumman Private/Proprietary Level I

Figure 74. ASTM G98 NGCo-3A (2”) Test Specimens along with Highest Loaded Specimen 80
Figure 75. ASTM G98 NGCo-3A (4”) Test Specimens along with Highest Loaded Specimen 80
Figure 76. ASTM E606 Fatigue-Life Cycle Specimen Details 81
Figure 77. Typical ASTM E606 Machined Fatigue-Life Specimens (NGCo-3A and Copper Beryllium) 82
Figure 78. Fatigue Life Cycle Comparison Test Results of the NGCo-3A Alternative and the Standard CuBe Alloy 82
Figure 79. General Mesh of the 1" Width Bushing Showing the Bushing, Shaft, and Plate Geometry 85
Figure 80. General Mesh for 1/4" Width Bushing 86
Figure 81. General Mesh for 1" Width Bushing 86
Figure 82. Geometry of the 1/4" Width Bushing with Chamfer 87
Figure 83. Bushing Stresses Versus Applied Load 88
Figure 84. Bushing Stresses versus Rotation Velocity 89
Figure 85. Bushing and Shaft Von Mises Stresses versus Static Coefficient of Friction 90
Figure 86. Bushing and Shaft Contact Pressures versus Static Coefficient of Friction 91
Figure 87: Bushing Contact Pressures & Contact Shear Stress versus Static Coefficient of Friction 91
Figure 88. Shaft Stresses versus Boundary Conditions (with Asymmetric Rotation) 93
Figure 89. Bushing Stress Distribution versus Shaft Tilt 94
Figure 90. Shaft Stresses as Affected by Symmetric or Asymmetric Rotation 94
Figure 91. Load vs. Strain for Different Yield Stresses 95
Figure 93. Von Mises Stresses Under 10 kips of Load for 140 ksi Yield Strength Bushing 96
Figure 94. Von Mises Stresses Under 10 kips of Load for 200 ksi Yield Strength Bushing 96
Figure 95. Effect on Strain from Bushing/Shaft Tolerance 97
Figure 96. Effect on Bushing Stress from Bushing/Shaft Tolerance 98
Figure 97. Images of Bushing Test System Rigging 100
Figure 98. Configuration of Chamfer and Radius Type Bushing Specimens 100
Figure 99. Configuration of the Test Pin made from MP35N Material 101
Figure 100. NGCo-3A-1C Bushing Threshold Test Result Plotted 102
Figure 101. Photos of NGCo-3A-1C Bushing and Pin Inspection Post Threshold Test 102

Use or disclosure of data contained on this sheet is subject to the restriction on the title page of this proposal.
Northrop Grumman Private/Proprietary Level I

Figure 102. NGCo-3A- 2C Bushing Threshold Test Result Plotted 2,000 lb Load for 100 Cycles 103

Figure 103. Photos of Bushing and Pin Post NGCo-3A-2CThreshold Test 2,000 lb Load for 100 Cycles 103

Figure 104. CuBe-1C Bushing Threshold Tests (1, 2 & 3) Result Plotted 104

Figure 105a. Photos of CuBe-1C Bushing and Test Pin Post Initial Test of 2,000 lb Load & 100 Cycles 105

Figure 106. CuBe-2C Bushing Threshold Test (1 & 2) Results Plotted 106

Figure 107. Photos of CuBe-2C Bushing & Pin Post Threshold Tests (1 &2) 106

Figure 108. NGCo-3A-3C Bushing Threshold Test (1, 2, 3, 4 & 5) Result Plotted 107

Figure 109. Photo Sets of NGCo-3A-3C Visual Inspection Results of Bushing & Pin for 0-100 Cycles, 200-300 Cycles and 400-500 Cycles Respectively All at 500 lb Static Load 108

Figure 110. NGCo-3A-1R and CuBe-3C Bushing Threshold Test (1, 2, & 3) Result Plotted 109

Figure 111. Results of Initiation of Galling Repeatability of NGCo-3A-1R 100 Cycles and 300 Cycles Followed by CuBe 100 Cycles and 300 Cycles Visual Inspections 110

Figure 112. Results of CuBe-4C Bushing Being Incrementally Loaded with 500 lb Increase Every 100 Cycles out to 10,000 lbs. 111

Figure 113. Results of Visual Inspection of CuBe-4C Tested Out to 1,700 Cycles and 10,000 lbs 111

Figure 114. Results of Initial NGCo-3A-4C Endurance Test at 500 lb Load for 100 Cycles 113

Figure 115. Visual Inspection results of NGCo-3A-4C at 500 lb load 100 Cycles 113

Figure 116. Results of NGCo-3A-5C Endurance Test at 250 lb Load for 100 Cycles 114

Figure 117. Results of NGCo-3A-5C Visual Inspection of 250 lb Load for 100 Cycles 114

Figure 118. Results of CuBe-5C Endurance Test at 250 lb Load for 100 Cycles 115

Figure 119. Results of CuBe-5C Visual Inspection of 250 lb Load for 100 Cycles 115

Figure 120. Results of CuBe-6C Endurance Test at 100 lb Load for 100 Cycles 116

Figure 121. Results of CuBe-6C Visual Inspection of 100 lb Load for 100 Cycles 116

Figure 122. Results of NGCo-3A-6C Endurance Test at 100 lb Load 0-100 Cycle 117

Figure 123. Results of NGCo-3A-6C Visual Inspection of 100 lb Load for 100 Cycles 117

Figure 124. Results of NGCo-3A-7C Endurance Test at 100 lb Load 0-100 & 100-200 Cycles 118

Figure 125. Results of NGCo-3A-7C Visual Inspection of 100 lb Load for both 0-100 Cycles and 100-200 Cycles Tests 119

Use or disclosure of data contained on this sheet is subject to the restriction on the title page of this proposal.
Northrop Grumman Private/Proprietary Level I

LIST OF TABLES

Page

Table 1. Risk Factors and the Mitigation Strategies for the Two Copper-Based Designs 10

Table 2. NGCu-1A Summary of Microstructural Features that Enable the Design Properties 16

Table 3. Comparison of the Properties and Processability of NGCu-1A and NGCu-1B 19

Table 4. Target Composition of Prototype Alloy Cuprium 20

Table 5. Grain size measurements on NGCo-1A alloy..... 33

Table 6 Comparison Between Measured and Predicted FCC and $L1_2$ Phase Compositions..... 34

Table 7. Chemistry Results (in weight %) Measured from the VIM Electrode and the VAR Ingot of NGCo-3A, Compared against the Production Target Ranges 40

Table 8. Summary of Tensile Test Data Collected from the 2nd Generation Prototype Alloys..... 47

Table 9. Summary of ASTM G98 Galling Test Results..... 79

Table 10. General Geometric Properties of Bushing, Shaft and Plate..... 87

Table 11. Model Properties for Case Study 1 (Increasing Load) 88

Table 12. Model Properties for Case Study 2 (Shaft Rotational Velocity) 89

Table 13. Model properties for case study 3 (coefficient of friction)..... 90

Table 14. Model Properties for Case Study 4 (shaft Boundary Conditions, Loading Conditions, & Tilt)..... 92

Table 15. Effects of Tilt and Boundary Conditions with Non-Tilting Load and Asymmetric Rotation 92

Table 16. Effects of Shaft Tilt with Tilting Load Asymmetric Rotation..... 92

Table 17. Effect of Shaft Tilt with Tilting Load and Symmetric Rotation..... 93

Table 18. Model Properties for Case Study 12 (Bushing Yield Stress)..... 94

Table 19. Model Properties for Case Study 6 (Effect of Bushing/Shaft Tolerance) 97

Table 20. Full Scale Bushing Test Matrix for Alloy Performance Comparison 101

Table 21. Summary of Threshold Test Conditions and Visual Inspection Notes..... 112

Table 22. Summary of Endurance Bushing Testing Conditions and Visual Results 119

Use or disclosure of data contained on this sheet is subject to the restriction on the title page of this proposal.
Northrop Grumman Private/Proprietary Level I

LIST OF ACRONYMS

1. ABAQUS – A Software Suite for Finite Element Analysis and Computer Aided Engineering
2. ACGIH – American Conference of Governmental Industrial Hygienists
3. AQMD – Air Quality Management District
4. AR –Argon
5. ARL – Applied Research Laboratory
6. ASTM – American Society for Testing and Materials
7. BC –Boundary Conditions
8. BCC – Body Centered Cubic Structure
9. BEI – Biological Exposure Indices
10. CBD – Chronic Beryllium Disease
11. Co-Cr-Mo – Cobalt Chrome Molly
12. CoF – Coeficient of Friction
13. COTS – Commercially Off-The-Shelf
14. CRES – Corrosion Resistant Steels
15. Cu-Be – Copper Beryllium
16. DICTRA – Diffusion Controlled Transformation Software
17. DICTRA – Diffusion Transformation
18. EDM – Electrical Discharge Machining
19. FCC – Face Centered Cubic Structure
20. GFM – Rotary Forging (Geselschaft für Fertigungstechink und Maschinebau)
21. HBN – Hexagon Boron Nitride
22. HCP – Hexagonal Close Packed Structure
23. HRC –Hardness Rockwell
24. $L1_2$ Phased – Phase for FCC Alignment
25. LEAP – Local Electrode Atom Probe
26. M_2C Particles – Even Distribution of Particles in the Matrix
27. M_s – Martinsite Start Temperature
28. NAVAIR – Naval Air Command Center
29. PM – Powder Metallurgy
30. PPT – Percipiatate
31. RR – Reduction Ratio
32. SAE Getters – Used to Maintain Ultra High Vacuum (Insure Purity)
33. SBIR – Small Business Innovation Research
34. SCC – Stress Corrosion Cracking
35. SDAS – Secondary Dendrite Arm Spacing

Use or disclosure of data contained on this sheet is subject to the restriction on the title page of this proposal.
Northrop Grumman Private/Proprietary Level I

36. SEM – Scanning Electron Microscope
37. SHT – Solution Heat Treat
38. SMF – Spray Metal Formed
39. TLV – Threshold Limit Values
40. USMC – United States Marine Corps
41. VAR – Vacuum Arc Re-Melting
42. V_f – Volume Fraction
43. VHN – Vickor Hardness
44. VIM – Vacuum Induction Melting

Use or disclosure of data contained on this sheet is subject to the restriction on the title page of this proposal.
Northrop Grumman Private/Proprietary Level I

EXECUTIVE SUMMARY

Copper Beryllium (CuBe) is considered the standard material extensively used for highly loaded low wear bushing applications on military aircraft and many other military platforms. This material has an exceptional suite of performance characteristics; strength, stiffness, density, wear resistance, galling resistance, and corrosion resistance that meet the demanding requirements for high stress in articulating mechanical joints. CuBe is an acknowledged hazardous material and there is a genuine concern about its continued utilization because of the severe health effects associated with its use. During the 1990's multiple studies were conducted and results identified sensitized immune system post exposure. Symptoms of exposure are sometimes not immediate and can occur well after contact. Exposure to beryllium has been reported to produce a range of diseases including lung cancer and Chronic Beryllium Disease (CBD). In May of 2002 OSHA had prepared one of its latest bulletins recommending the lowering of the exposure limit to $0.2\mu g/m_3$ down from the $2\mu g/m_3$ for a time-weighted average of 8 hours. This lower level was adopted after research had identified exposure incidents with the previously recommended levels. The lower levels along with the additional protection recommendations to prevent skin contact from the dust were acknowledged to further prevent the ill effects from the materials exposure. Hazardous health effects identified by the use of CuBe have raised industry's concerns and this is the key driver behind this programs efforts.

This programs main objective was to design and develop an environmentally safe alternative alloy that exhibits equivalent or better performance than incumbent AMS 4533 Copper-Beryllium Alloy; 98Cu – 1.9Be; Solution Heat Treated, and Precipitation Heat Treated material. One of the preferred goals in this program effort is to design and produce a material alternative that does not vary with component size and in doing so this program has relied upon solid solution alloying and/or precipitation-hardening so that the alloy strength maintains uniform performance properties in the larger-diameter materials.

Northrop Grumman as prime contractor partnered with QuesTek Innovations who are well known for their; computer aided modeling of alloy phase transformations and kinetics, and the practical application of models to materials system design. QuesTek utilized several of their own design tools in the development of the alternative alloy materials. A step-wise building block approach was executed which began with a thorough investigation into the materials that supported the performance requirements being pursued. Program criteria were set to meet the following requirements; (1) Tensile strength greater than 165,000 psi, (2) Yield strength at 0.2% offset greater than 140,000 psi, (3) Hardness of 36 to 45 Rockwell C (HRC) and (4) meet or exceed the performance of Cu-Be alloys in terms of friction coefficient in dry sliding conditions against low-alloy steels, wear resistance, resistance to galling and spalling, axial fatigue, and rolling contact fatigue.

Utilization of QuesTek's Systems by Design Chart which focuses on Processing, Structure, Properties and Performance led to the identification of the preferred alternative alloy types in the initial base materials down-selection. The two material types; (1) high-strength precipitation strengthened copper alloy, (2) high strength precipitation-strengthened cobalt alloy, were identified as the two most promising alloy design concepts for further development. The next step in the systems engineering process sketched out the microstructures within each concept material to identify the components that had the potentials in achieving the desired properties while maintaining thermal processing capabilities that supported kinetic and thermal phase

Use or disclosure of data contained on this sheet is subject to the restriction on the title page of this proposal.
Northrop Grumman Private/Proprietary Level I

transformation. A thorough material component analysis was performed to ascertain which components provided the desired benefits and supported a microstructure with nano-scale precipitation strengthening to achieve higher strength levels to meet the programs performance goals. Developed materials were produced utilizing typical melt processing methods and characterization testing performed to evaluate alternative material performance comparison to the AMS 4533 standard material. Tests include: ASTM E8 Tensile strength, ASTM E9 Compression strength, ASTM E606 Strain Life, ASTM G98 Galling, ASTM G99 Pin-on-Disk, and ASTM G133 Reciprocating Ball-on-Flat. Six alternative alloys were designed, developed, produced and tested during this programs period of performance.

Conclusions provided from the various program results show that both the Cuprium (a copper tin alloy that was spray metal formed at Penn State University) and the NGCo-3A alloys have favorable properties with the NGCo-3A having the superior performance properties from the alloys evaluated and being the material of choice for down-selection. While the tensile strength of the NGCo-3A is highest among all the alloys, yield strength is lower than the baseline material. The fatigue life, friction and galling behavior of the NGCo-3A are superior to the baseline material.

As an addition to the design and development of an alternative alloy material this program with the help of Dr. Christiane Beyer at the California State University at Long Beach assisted by her team of students funded by the program has prepared some finite element modeling simulations to explore and evaluate the stress and wear effects of loaded bushing with and without performance enhancements. A finite element model was developed utilizing the standard and alternative bushing alloy materials property information. Full scale bushing and test setup geometry measurements were entered into the ABAQUS modeling software to support the simulation. The theory was based on mimicking the full scale bushing tests so a comparison could be performed to support simulation proof of concept. Several case studies were run to help build a simulation data base that would emulate the wear behavior of a material so predictive wear analysis could be performed for developmental purposes.

Full scale environmental bushing testing was the final program task requirement in supporting the ultimate in material performance comparison results of the standard copper beryllium to the down selected NGCo-3A alternative alloy. The supplier performing these tests had a special testing rig to apply the high load conditions to the bushing samples. Two test methods were performed in evaluating the comparison of the baseline and alternative alloy materials. One was a threshold test which evaluated the comparison of a high load low frequency oscillation where the pin was rotated back and forth 25-degrees in each direction through 0-degrees. The other was an endurance test which evaluated the comparison effects of a high static load while rotating around and around at a low speed. Comparison of the visual effects and charted data results identified that the NGCo-3A alternative alloy had equivalent to and slightly better performance than that of the standard copper beryllium.

One enhanced bushing design identified in the modeling effort, which incorporated a radius as an alternative to the standard chamfer on the bushing ID, was tested along with the standard bushings although no substantial improvement in bushing performance was identified.

Future work if funding is awarded would include: improved yield strength of NGCo-3A by refining the grain size, optimization of heat treat and the development of the production and commercialization plans.

Use or disclosure of data contained on this sheet is subject to the restriction on the title page of this proposal.
Northrop Grumman Private/Proprietary Level I

1.0 OBJECTIVE

The objective of the program is to develop an environmentally safe alternative to the current baseline AMS 4533 Copper Beryllium (Cu-Be) alloy currently employed for highly loaded nonlubricated bushing and bearing wear applications. The program will work to develop an alternative material and thermomechanical processing route which results in a suite of mechanical properties that satisfies design requirements for such applications and exhibits compatibility with legacy structural alloys and mechanisms, as well as the sealant, primer, topcoat, and corrosion prevention protocols in place. In meeting this objective the following key challenges will be addressed:

- **Alloy/Process Development.** Alloy composition and thermomechanical processing parameters development is central to the objective and goal of the program. Variables which will be evaluated for mechanical properties/performance development will include composition, degree of cold work, and thermal treatment.
- **Material Performance Demonstration.** Detailed design requirements will be developed in the initial portion of the program. These requirements will be the basis for which the candidate alternatives to Cu-Be will be evaluated. Thorough static mechanical properties as well as wear and galling testing will be executed. Additionally, corrosion resistance/environmental exposure testing will be conducted to assess performance in relevant operational environments.
- **Bushing Design Development.** Current studies suggests that the bushing/pin contact geometry (i.e., the shape of the interface between the inner diameter of the bushing and the pin within it) may dominate frictional performance. Bushing designs will be developed to explore the opportunity to extend overall dynamic wear performance of nonlubricated bushings via investigation of these alternative design concepts.
- **Production Demonstration.** Potential implementation into the production environment requires that the alternative candidate material possess a reasonable Manufacturing Readiness Level (MRL) of 7 and thus can be readily manufactured. Material will be alloyed and processed in accordance to the parameters developed in the alloy and process parameter development task and fabricated into rod stock in diameters up to 4.0 inches.
- **Bushing Performance and Design Demonstration.** Dynamic, rotating, highly loaded full-scale component-level testing will be conducted to assess the performance of the alternative Cu-Be material in standard parts design configurations, as well as in the design configurations in the bushing design development task to establish an operational level means of comparison of bushing material and design performance.
- **Production and Environmental, Health, and Safety Impact Assessment**. Challenges that may impede implementation of the candidate Cu-Be alternative will be identified and addressed. Compatibility with legacy structural alloys and mechanisms, as well as sealant, primer, topcoat and corrosion prevention protocols will be evaluated. Environmental, health, and safety precautions and impacts will also be identified.

Use or disclosure of data contained on this sheet is subject to the restriction on the title page of this proposal.
Northrop Grumman Private/Proprietary Level I

2.0 TECHNICAL APPROACH

The team is working to develop a "drop in" alternative to the currently employed AMS 4533 Cu-Be material for highly loaded bushings and bearings in wear applications. This effort was initiated with the identification of a series of alternative Cu-Be alloys for further investigation and development. Multiple iterations of materials and process computational modeling were performed, considering compositional alterations and thermal, mechanical, or thermomechanical processes for performance optimization. After every computational modeling iteration, coupon-level specimens were fabricated and subsequent initial properties evaluation/characterization were performed. After the final computation modeling iteration, detailed mechanical properties data were generated and tribological characterization performed. Bushing design and surface morphology optimization were also conducted and integrated into a full-scale component-level test/demonstration.

The program schedule shown in Figure 1 below displays the tasks that have been accomplished.

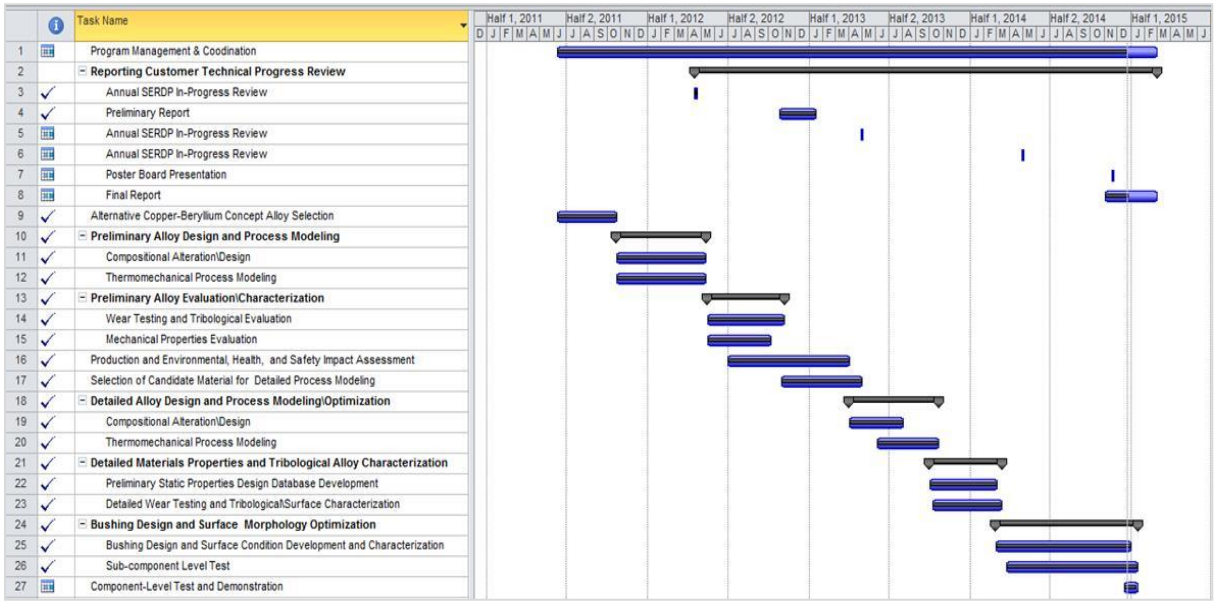

Figure 1. Overall Program Schedule

2.1 BACKGROUND

Cu-Be alloys exhibit a unique balance of static and dynamic properties that make their alloy systems especially attractive for use in highly loaded wear applications. In the recent past as the challenges associated with beryllium exposure have become more apparent, material suppliers have labored to bring alternative beryllium free alloys to market. It is well understood that there are a multitude of commercially available alternatives to Cu-Be bushings. These include a variety of options from Corrosion Resistance Steels (CRES), Powder Metallurgy (PM) 304 stainless steel sintered with Hexagonal Boron Nitride (HBN) solid lubricant, spinodal copper-nickel-tin alloys, cobalt-chromium-molybdenum alloys, as well as low friction surface treatments and liner systems. Each of these offers an option for substitution in varying conditions or applications. However, none has been identified that meets all of the design requirements which Cu-Be alloys currently satisfy.[1]

Use or disclosure of data contained on this sheet is subject to the restriction on the title page of this proposal.
Northrop Grumman Private/Proprietary Level I

In previous internal platform support development programs as well as internal research and development projects conducted at Northrop Grumman Aerospace Systems (NGAS) or in which NGAS participated, several alternative Cu-Be commercial off-the-shelf (COTS) and emerging materials were identified for potential implementation in place of Cu-Be in highly loaded wear applications, evaluated, and characterized. These programs investigated raw materials as well as a wear resistant liner system. The raw materials evaluated included: Brush Wellman's fine-grained spinodal ToughMet AT and ToughMet TS materials, the iron-based, high nitrogen annealed and mechanically strengthened Nitronic60[2,3], and k Technology Corporation's (kTC's) powder metallurgy 304 stainless steel sintered with hexagonal boron nitride solid lubricant. The wear-resistant coating evaluated was Kamatics' V-type KAron bearing liner system, which was placed on a PH13-8Mo steel substrate in the H1000 condition. Materials evaluations ranged from static mechanical testing for initial performance rank and screening to wear testing. The wear testing included ASTM G 98 for threshold galling stress determination, and ASTM G 99 Pin-on-Disk for development of coefficient of friction and wear rate data against 0.393 inch diameter SAE 100 Cr-6 steel. All of the alternative materials displayed limitations preventing the ability for consideration as a suitable "drop in" replacement in place of Cu-Be alloys.[1] In most cases, the challenge resided in meeting both the static strength target within the entire range of diameters in which Cu-Be in the AMS 4533 condition is employed and attaining comparable resistance to wear and galling.[1] For example, Nitronic 60 is effective in meeting the strength as well as wear and galling resistance, but as in the case of ToughMet TS, Nitronic 60 is mechanically strengthened and can only be work hardened to strengths comparable to AMS 4533 up to a maximum of 2.0 inches in diameter and thus not applicable to the full size range of targeted bushings. Similarly, the bearing liner systems are effective in galling and wear resistance but only at limited strengths significantly below that of AMS 4533.

One of the initial tasks in the program that the team has addressed is further screening of the current state of potentially viable commercial off-the-shelf (COTS) Cu-Be alternative materials. From the body of data developed in previous investigations on alternative Cu-Be materials as described above as well as the further screening projected in the current program, a series of candidate alternative Cu-Be materials was identified. These were included, high strength Cu-alloys and high-strength Co-Cr-Mo alloys. Each of these material systems has exhibited a shortfall in material performance in comparison to the incumbent AMS 4533 Cu-Be alloy. To address this, a series of computational modeling iterations were conducted on the material systems identified for potential Cu-Be substitution. These computational modeling iterations will investigate the effects of composition, and thermomechanical processing on materials properties and tribological performance.

Baseline bushing designs employed in legacy as well as currently developing platforms have remained unchanged for decades. As described earlier, current studies suggest that a significant increase in bushing performance may be achievable via modification of the contact geometry at the interface of the bushing inner diameter and outer diameter of the pin within it. Moreover, the initial results of the work being conducted at the University of Florida propose that this design feature may dominate frictional performance. Thus, a task within the program evaluated bushing designs with variable contact geometries to explore this opportunity to extend the overall dynamic wear performance of nonlubricated bushings.

Use or disclosure of data contained on this sheet is subject to the restriction on the title page of this proposal.
Northrop Grumman Private/Proprietary Level I

2.2 METHODS

The objective of the program was to develop a "drop in" alternative to the currently employed AMS 4533 Cu-Be material for highly loaded bushings and bearings in wear applications. This effort was initiated with the identification of a series of alternative alloys for further investigation and development. Multiple iterations of materials and process computational modeling were performed, considering both compositional alterations and thermal, mechanical, and/or thermomechanical processes for performance optimization. After each computational model iteration, coupon-level specimens were fabricated and subsequent initial properties evaluation/characterization was performed. After the final computation modeling iteration, detailed mechanical properties data will be generated and tribological characterization performed. Bushing design and surface morphology optimization was also conducted and integrated into a full-scale component-level test/demonstration.

Computational modeling was conducted by QuesTek Innovations; QuesTek utilized their Materials by Design® development methodology, which has been proven in previous materials development programs. An example of QuesTek's Materials by Design® process can be illustrated by the Ferrium S53 alloy development program. Under Strategic Environmental Research Development / Environmental Security Technology Certification Programs (SERDP/ESTCP) seed funding QuesTek used its Materials by Design technology to design S53 as an ultra-high-strength corrosion-resistant drop-in replacement for 300M to eliminate the need for toxic cadmium (Cd) coatings on landing gear components.

Guided by systems engineering principles, QuesTek developed a system-flow block diagram to illustrate the microstructure needed in order to achieve the alloy property objectives, and the processing route required in order to obtain the desired microstructure (Figure 2).

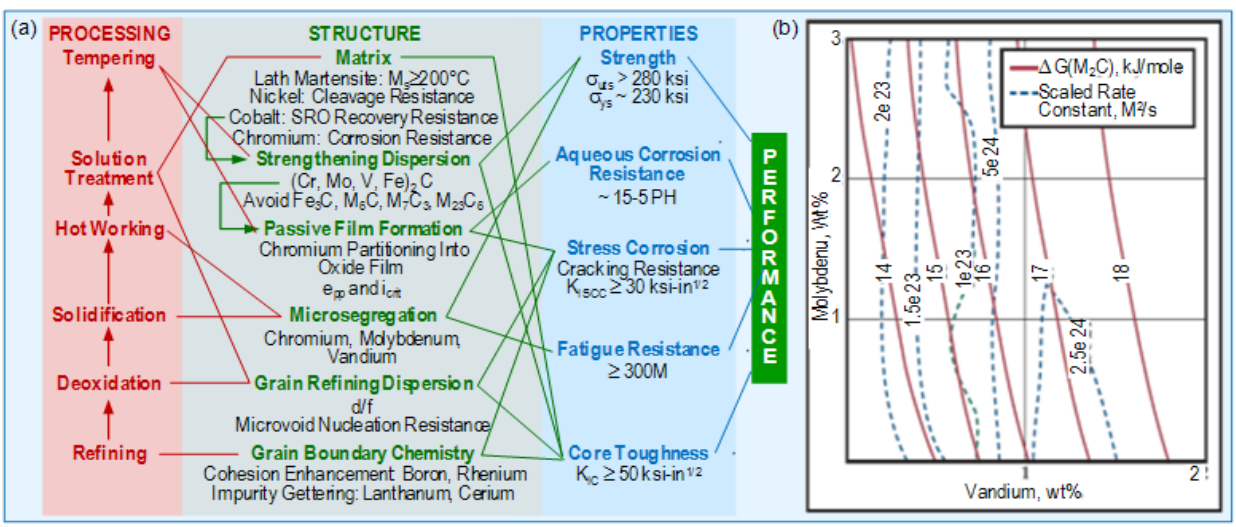

S53 (b) Calculated Overall Precipitation Driving Force and Coarsening Rate Constant for M2C Particles in S53 Alloy as a Function of the Alloy Mo and V Content.

Figure 2. Flow Diagram for Design of Ferrium

This is often the first step in the Materials by Design process. As the diagram shows, S53 was designed to be a secondary hardening steel strengthened by efficient M2C carbide precipitates. It also contained sufficient chromium to provide passivation against general

Use or disclosure of data contained on this sheet is subject to the restriction on the title page of this proposal.
Northrop Grumman Private/Proprietary Level I

corrosion. Stress Corrosion Cracking (SCC) resistance was obtained by designing the grain boundary chemistry for maximum cohesion.

In order to achieve the strength goals, S53 was designed to be strengthened with nanoscale dispersions of M2C carbides, which are an efficient strengthener in steels due to their high modulus misfit with Body Centered Cubic (BCC) iron (the martensite matrix), and the ability to precipitate coherently at the nanoscale. It is important to note that the coherency leads to significant complications in predicting the precipitation kinetics, because the coherency strain energy must be accommodated in the precipitation model. This has been well studied and reported in the literature, and such models were used in Figure 2, where the overall precipitation driving force and the normalized coarsening rate constant are reported as a function of molybdenum and vanadium content in the S53 alloy. This design calculation maximizes the resulting strength through the precipitation driving force, while ensuring that this strength can be achieved with reasonable tempering parameters.

Another key design tradeoff was to achieve high strength while maintaining adequate martensite kinetics to ensure a martensitic alloy. Quantitative martensite kinetic models can predict the martensite start temperature along with the M2C precipitation driving force as a function of cobalt and nickel. These designs maximize strengthening while requiring a sufficiently high Ms-temperature to maintain a predominantly martensitic alloy.

Design for corrosion resistance used the results of prior efforts studying the stability of passivating films in secondary hardening alloys. Multicomponent thermodynamic effects are analyzed to maximize chromium partitioning in the spinel oxide, primarily driven by cobalt content. In addition, the nanoscale M2C carbides are designed to be sufficiently smaller than the oxide scale to enable their oxidation during passivation. This frees the chromium to be incorporated into the passive film.

Additional constraints on ductile fracture, grain-boundary chemistry, and grain-pinning dispersions complete the design optimization and uniquely identify the alloy composition that represents the best compromise of the diverse design goals and constraints.

QuesTek used a similar Material by Design approach for designing a nontoxic Cu-Be drop-in replacement alloy for aerospace bushing applications. The primary property objectives for a nontoxic Cu-Be drop-in replacement alloy are high-strength and tribological performance, or wear behavior. Similar to S53, high strength can be achieved in the system by nanoscale dispersions of coherent strengthening particles that can impede the motion of dislocations. In order for the strengthening efficiency to be maximized, the nanoscale particles need to be coherent with the matrix, i.e., in a Face Centered Cubic (FCC)-matrix the particles need to be FCC-type. Thus, in a Copper (Cu) or Cobalt (Co)-based concept where the matrix is Cu-based or Co-based FCC, the particles can be FCC-type L12-phased Ni_3Al (commonly referred to as γ'). The composition of the alloy has to be designed such that the L12 phase can be precipitated as nanoscale particles in the system, and upon precipitation the lattice mismatch between the matrix and the particles is minimal. Additionally thermodynamic and kinetic tools were used to optimize the volume fraction and size of these particles after aging treatment, in order to obtain the desired strengthening response.

Wear behavior, including both wear resistance as well as galling resistance, is the other key property objective for a nontoxic Cu-Be drop-in replacement alloy. For abrasive wear, mechanisms of wear may involve processes such as plowing, microfatigue, wedge formation,

Use or disclosure of data contained on this sheet is subject to the restriction on the title page of this proposal.
Northrop Grumman Private/Proprietary Level I

cutting and microcracking. QuesTek employed its Materials by Design tools to reduce the work of adhesion (Wad) between the wearing pair, as reduction of the adhesion improves the wear resistance. This can be achieved by reducing the surface energy of the bushing alloy by controlling its melting point. Additionally, the size, shape, and thermo-mechanical properties of wear debris play an important role in tribological performance, and thus hard wear debris such as oxide films should be avoided. Abrasive wear may become very relevant to wear of Cu-based or Co-based alloys when sufficient aluminum is present in the alloy to form abrasive alumina wear particles at the surface, thus establishing upper bounds for the critical amount of oxide forming elements that can be used in these systems. For a wide range of FCC single-phase alloys, wear rate decreases with decreasing stacking fault energy γ_{sf}, which can also be estimated from first-principles calculations, and considered within the computational alloy development phases.

Depending on the pressure and the sliding velocity, the wearing behavior of a given material may be best described by a wear mechanism map. Figure 3 shows an example of a wear mechanism map for steel.

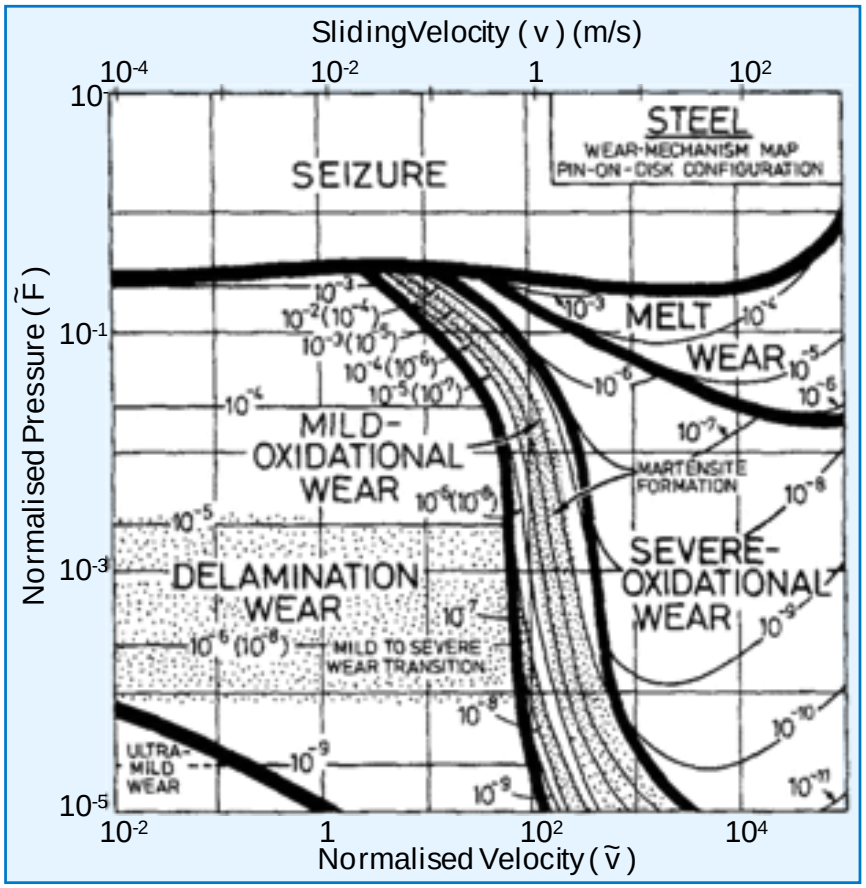

10NP06-011

Figure 3. Example of a Wear Mechanism Map for Steel[5]

The wear rate ψ, is given by the Archard empirical equation as:

$$\psi = k\frac{Lv}{H}$$

Use or disclosure of data contained on this sheet is subject to the restriction on the title page of this proposal.
Northrop Grumman Private/Proprietary Level I

Where L is the applied load, v, sliding velocity, H, the hardness of the softest material and the constant k varies with the thermomechanical properties and the adhesion between the wearing pair, the wear debris, the environment and the initial wear.

A wear mechanism map can assist our understanding of pin-on-disk results of prototype alloys with varying composition and microstructure, and can be used to feedback into the design iteration of the bushing alloy.

Static performance of materials developed for wear application is generally readily available. However, the tribological characterization of candidate Cu-Be alternative materials which is the key to obtaining a full assessment of the ability of the proposed material to perform in highly loaded wear applications is rarely available for the design or engineering communities. Tribological subcomponent-level evaluations were conducted to develop a greater understanding of the performance of an alternative Cu-Be material and contact geometries in a dynamic representative test environment prior to full-scale, component-level demonstrations.

2.3 MICROSTRUCTURAL CONCEPTS

The systems design chart for a precipitation strengthened copper or cobalt alloy system, illustrating the performance-properties-structure-processing links is shown in Figure 4.

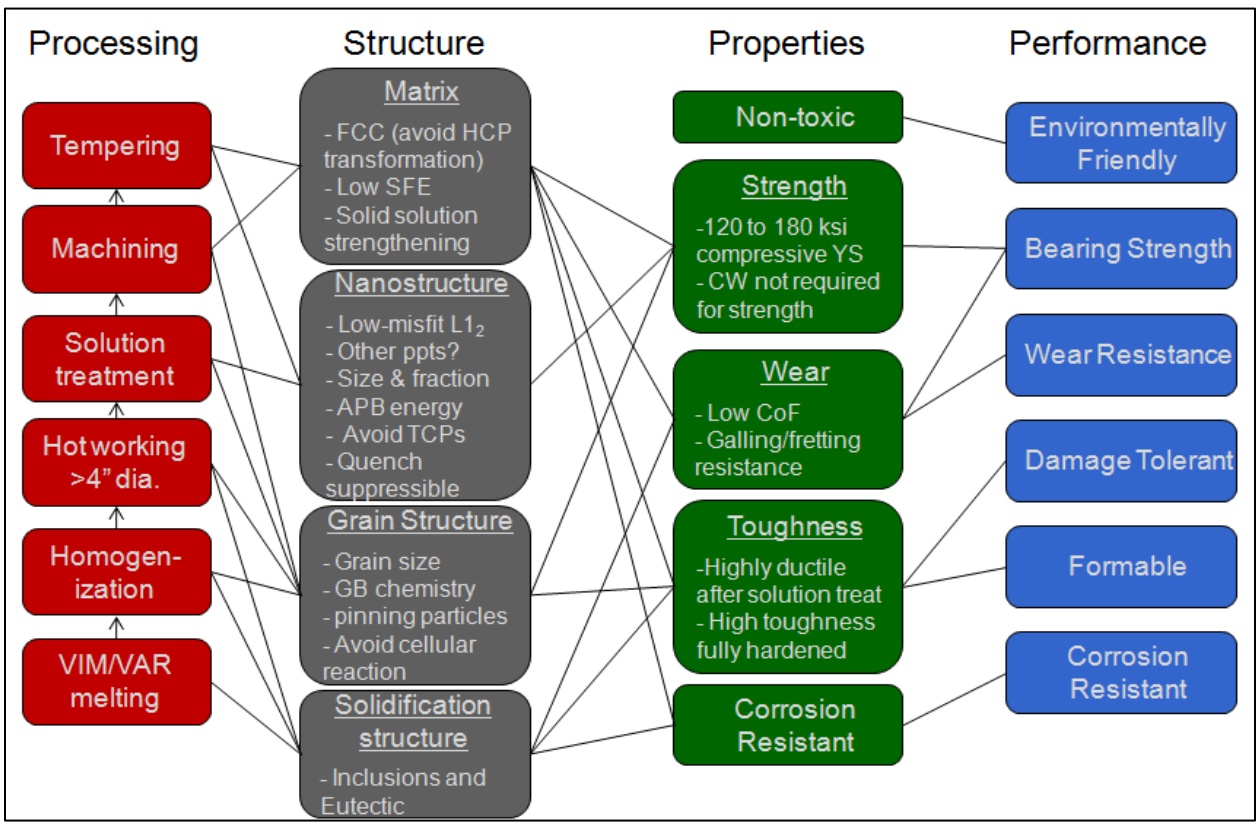

Figure 4. Systems Design Chart for a Precipitation Strengthened Copper or Cobalt Alloy System

Use or disclosure of data contained on this sheet is subject to the restriction on the title page of this proposal.
Northrop Grumman Private/Proprietary Level I

The performance objectives of the high-strength Cu-Be alternative alloy system are that the alloy needs to be environmentally benign, needs to achieve the strength of Cu-Be without the need for additional cold work, needs to be wear resistant and damage tolerant for the bushing performance, needs to have the ability to be formed into the bushing shapes, and also, because the target platform is a Naval aircraft, needs to have adequate corrosion resistance. These performance objectives then translate to a series of quantitative/qualititative property requirements as shown in the green boxes in the above figure. The next step in the systems engineering process is to sketch out the microstructures within each concept that can achieve the desired properties. This is discussed in more detail in the following sections.

2.4 PRELIMINARY ALLOY DESIGN AND PROCESS MODELING

Three alternative alloys were initially down selected from the most prospective candidate's in support of replicating those superior characteristics and performance properties of the standard copper beryllium alloy. The three candidates were two copper alloys; one with tin (Sn) and one without tin and the third one was a cobalt alloy.

2.4.1 Copper Based Alloy Designs (NGCu-1A / NGCu-1B / Cuprium)

Based on QuesTek's previous experience in designing $L1_2$-strengthened Copper alloys in the Naval Air Systems Command (NAVAIR) Small Business Innovation Research (SBIR) program[6], the design risk factors associated with the Cu-alloy concept, and their mitigation strategy was identified. These are listed in Table 1:

Table 1. Risk Factors and the Mitigation Strategies for the Two Copper-Based Designs

Incipient melting	• 1 Sn-free design + 1 with Sn • No other low-melting components/eutectics
Cellular growth	• Match lattice parameters of $L1_2$ and matrix (<-0.6%) • Grain-pinning dispersion to pin grain boundaries
Quench suppressibility	• Lower solvus of $L1_2$
Strength	• Volume fraction of strengthening particles > 20% (ideally 25%) at 450-500°C

Incipient melting and cellular growth are the two biggest risk factors for the copper alloy concept. The alloying element Tin (Sn) tends to lower the solidification temperature of the Cu-alloys, as the final solidification product is a low-melting eutectic ($D0_3$ Cu_3Sn – Complex ordered cubic crystal structure). Due to the lower solidification temperature, the maximum homogenization temperature and the hot-working temperature are restricted, in order to avoid incipient melting during high temperature processing. An obvious mitigation strategy is to avoid using Sn in the designs. However, Sn has a beneficial effect in matching the lattice parameters of the FCC and $L1_2$, and thereby preventing cellular growth in the system. Thus QuesTek designed one Sn-free alloy and one Sn-containing alloy, in order to maximize the probability of achieving the alloy property objectives. Quench suppressibility of the alloys can be controlled by controlling the $L1_2$ stability (from thermodynamic design). To achieve the required strength of the alloy, a minimum $L1_2$ volume fraction of 20% is needed (based on QuesTek's NAVAIR alloys[6]).

Use or disclosure of data contained on this sheet is subject to the restriction on the title page of this proposal.
Northrop Grumman Private/Proprietary Level I

2.4.1.1 Design of NGCu-1A Sn-Free

Since the NGCu-1A design does not contain Sn (to achieve easier processability), the design focus is to achieve the desired strength and quench suppression, without the formation of cellular growth in the system. Cellular growth is a function of several factors, such as lattice misfit between particle and matrix, the driving force for precipitation, and the mobility of the FCC grain boundaries (GB). Reducing the lattice mismatch, reducing the driving force for precipitation, and making the FCC GBs immobile helps prevent the occurrence of cellular growth.

FCC-$L1_2$ lattice parameter models were constructed to aid in the alloy design process, and identify phase equilibrium which results in the lowest lattice misfit. The elevated temperature (500° C) lattice parameters for various Cu-X binary alloys and various Ni_3X $L1_2$ particles are shown in Figure 5. The lattice mismatch between $L1_2$ Ni_3Al and FCC Cu is -1.76%. Therefore in order to reduce the precipitate-matrix lattice parameter mismatch in Cu alloys, strengthened with Ni_3Al-type precipitates, solutes that will either reduce the lattice parameter of FCC Cu matrix or increase the lattice parameter of Ni_3Al are needed. As seen from Figure 5, the lattice parameter model demonstrates that most solutes (Sn, Mn, Ti, Si, and Al) increase the lattice parameter of Cu. Ni and Co are the only solutes that decreases the lattice parameter of Cu, but they do not decrease the lattice parameter enough to match Ni_3Al. At 15 at% Ni in a Cu solid solution, the lattice parameter of the binary Cu-Ni alloy is 3.632 Å compared with 3.583 Å for Ni_3Al.

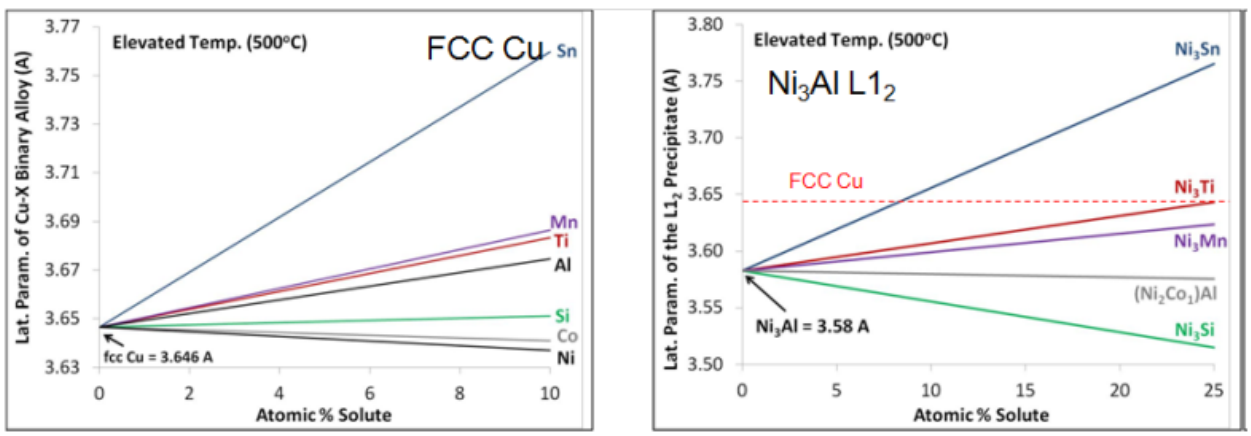

Figure 5. Calculated Lattice Parameters for FCC Cu-X Binary Alloys (left) and $L1_2$ Precipitates (right) at 500°C

These results suggest that decreasing the lattice parameter mismatch cannot be achieved by simply reducing the lattice parameter of the FCC matrix. The lattice parameter model also demonstrates that it is possible to increase the lattice parameter of the $L1_2$ with Sn, Ti, or Mn. Since the design is Sn-free, Mn was selected as the alloying component of interest to help reduce the $L1_2$-FCC lattice mismatch, and suppress the cellular growth in the system. Ti was not selected since it is known to form a stable Ni_3Ti phase which reduces quench suppressibility of the system.

Microstructural observations, coupled with the predictions from the lattice parameter model, were used to define a threshold value of the lattice mismatch, below which cellular growth is not expected to occur.

Use or disclosure of data contained on this sheet is subject to the restriction on the title page of this proposal.
Northrop Grumman Private/Proprietary Level I

Figure 6 shows the microstructure of various Cu alloys fabricated by QuesTek, along with the predicted lattice misfit based on the calculated phase equilibria. For the Cu-15Ni-2.5Al alloy, a lattice mismatch of -1.7% is predicted, and this agrees with the observation of strong cellular growth in the system. Even when the lattice misfit is reduced to -1.1%, marginal cellular growth is still observed. However, when the lattice misfit is below -0.6%, the cellular growth is completely suppressed. Thus -0.6% can be taken as the lattice parameter design objective in order to completely suppress cellular growth in these systems.

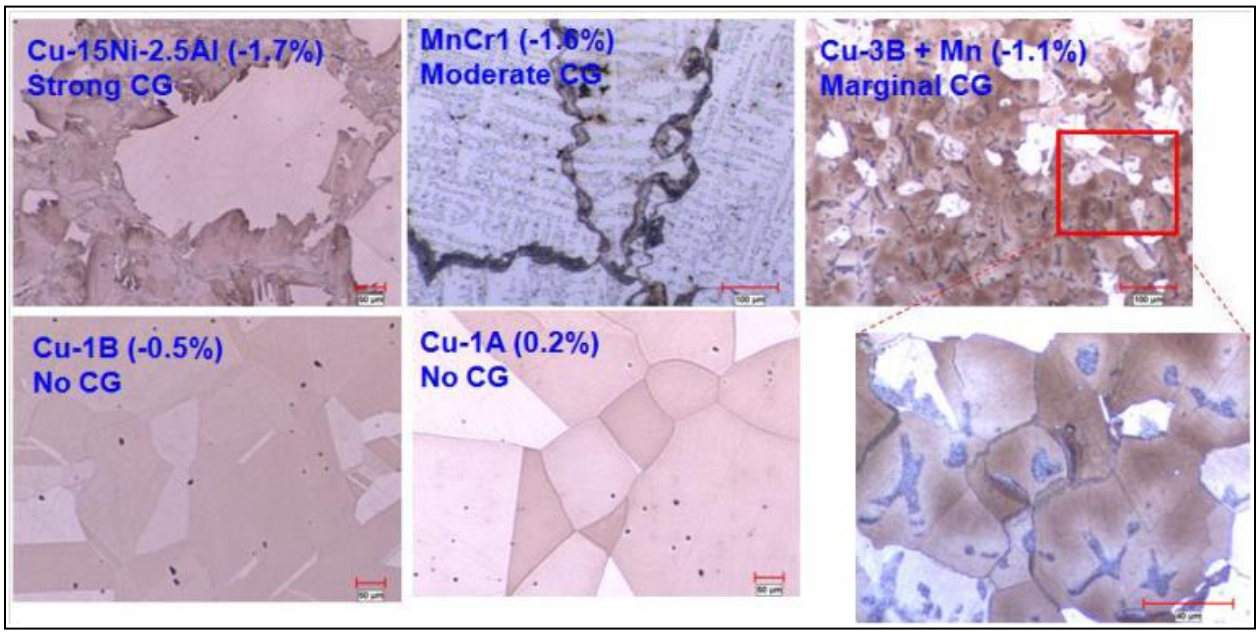

Below a Threshold Value of -0.6%, no Cellular Growth was Observed, and this Represents the Design Goal for this Program.

Figure 6. Observation of the Presence or Absence of Cellular Growth in Different QuesTek Alloys and their Correlation with the Predicted Lattice Misfit

Having identified the lattice misfit goal, the next step was to thermodynamically explore the Cu-Ni-Mn-Al system, and identify the FCC-$L1_2$ phase equilibria which satisfied the dual constraint of achieving > 20% $L1_2$, as well as minimize the lattice misfit as much as possible. The calculated Cu- Ni_3Al-Ni_3Mn constrained pseudoternary phase diagram is shown in Figure 7. The two-phase FCC-$L1_2$ region is shown, and the dashed lines represent the tie-lines between the FCC and the $L1_2$ phase. The numbers shown adjacent to the tie-lines represent the lattice misfit for an alloy composition lying on that particular tie-line. For the constrained equilibrium calculation shown in Figure 7 (where the Ni:(Mn+Al) is 3:1), the lowest lattice misfit that can be achieved is -1.2%. The red-star shown on that plot represents an alloy composition that achieves the -1.2% lattice misfit, as well as >20% $L1_2$ after an aging temperature of 500° C. This represents a starting point for further composition optimization to reduce the lattice misfit even further, to bring it as close as possible to the design objective of -0.6%.

Use or disclosure of data contained on this sheet is subject to the restriction on the title page of this proposal.
Northrop Grumman Private/Proprietary Level I

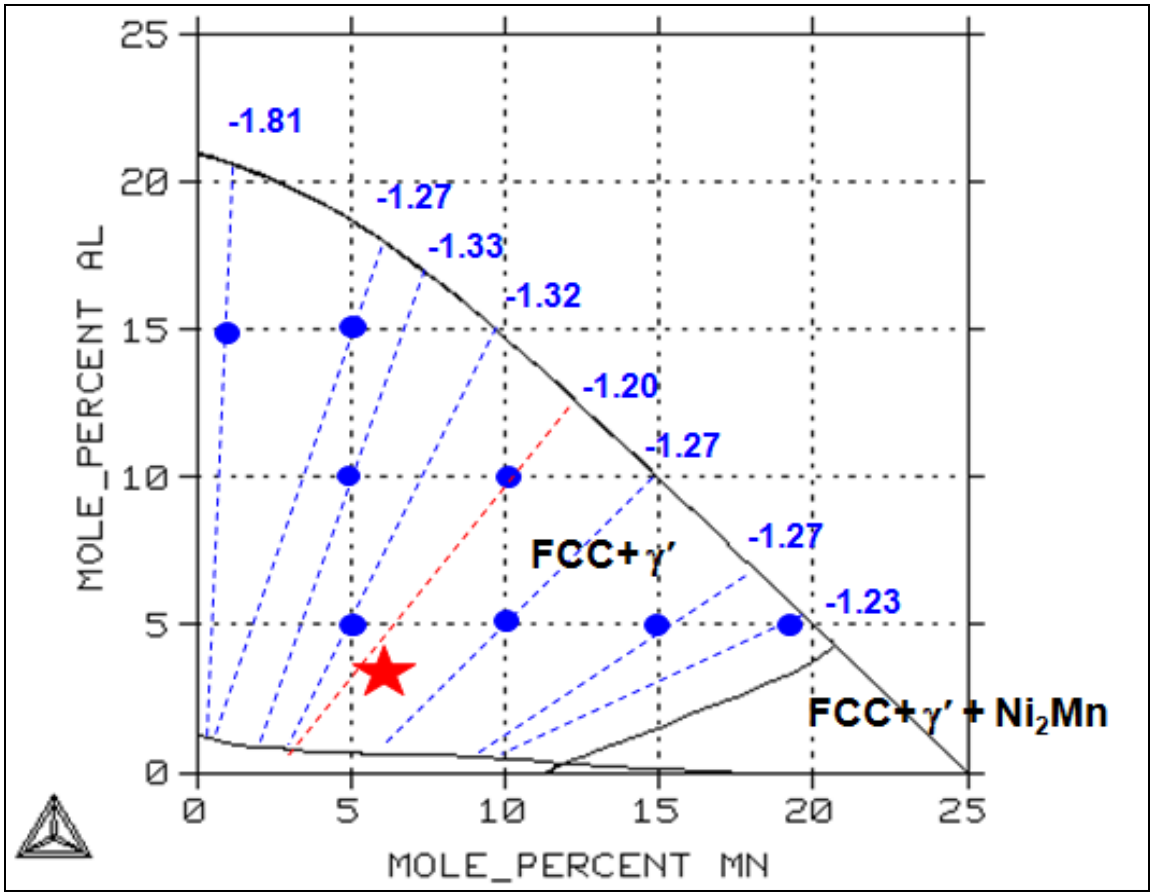

Thermodynamic Plot, where the Dashed Red Line Represents the Lowest Misfit Achievable in this Constrained System. Further Reductions in Misfit can then be Achieved by Relaxing the Ni:(Mn+Al)=3:1 Constraint.

Figure 7. A Constrained Cu-Ni_3Mn-Ni_3Al Pseudoternary

Starting with this baseline composition, the Ni content in the alloy was increased to reduce the lattice misfit further, and bring it closer to the design objective. The calculated thermodynamic step diagram of the final alloy composition is shown in Figure 8. It shows the equilibria phase fractions of the phases present in the system, as a function of temperature. By increasing the Ni in the system, and by selecting a lower aging temperature of 450° C, the final lattice misfit was reduced to -0.75%. While this is still higher than the design goal of -0.6%, the expectation is that most of the cellular growth will be eliminated in this system, and a small amount of cellular growth can be tolerated in the alloy. As seen from Figure 8, the final alloy also includes Vanadium to extend the $L1_2$ solvus so that a sub-solvus treatment (which helps pin the FCC grain boundaries) can be carried out. The range of solution heat-treat, sub-solvus, and aging temperatures for this alloy is also indicated on Figure 8.

Use or disclosure of data contained on this sheet is subject to the restriction on the title page of this proposal.
Northrop Grumman Private/Proprietary Level I

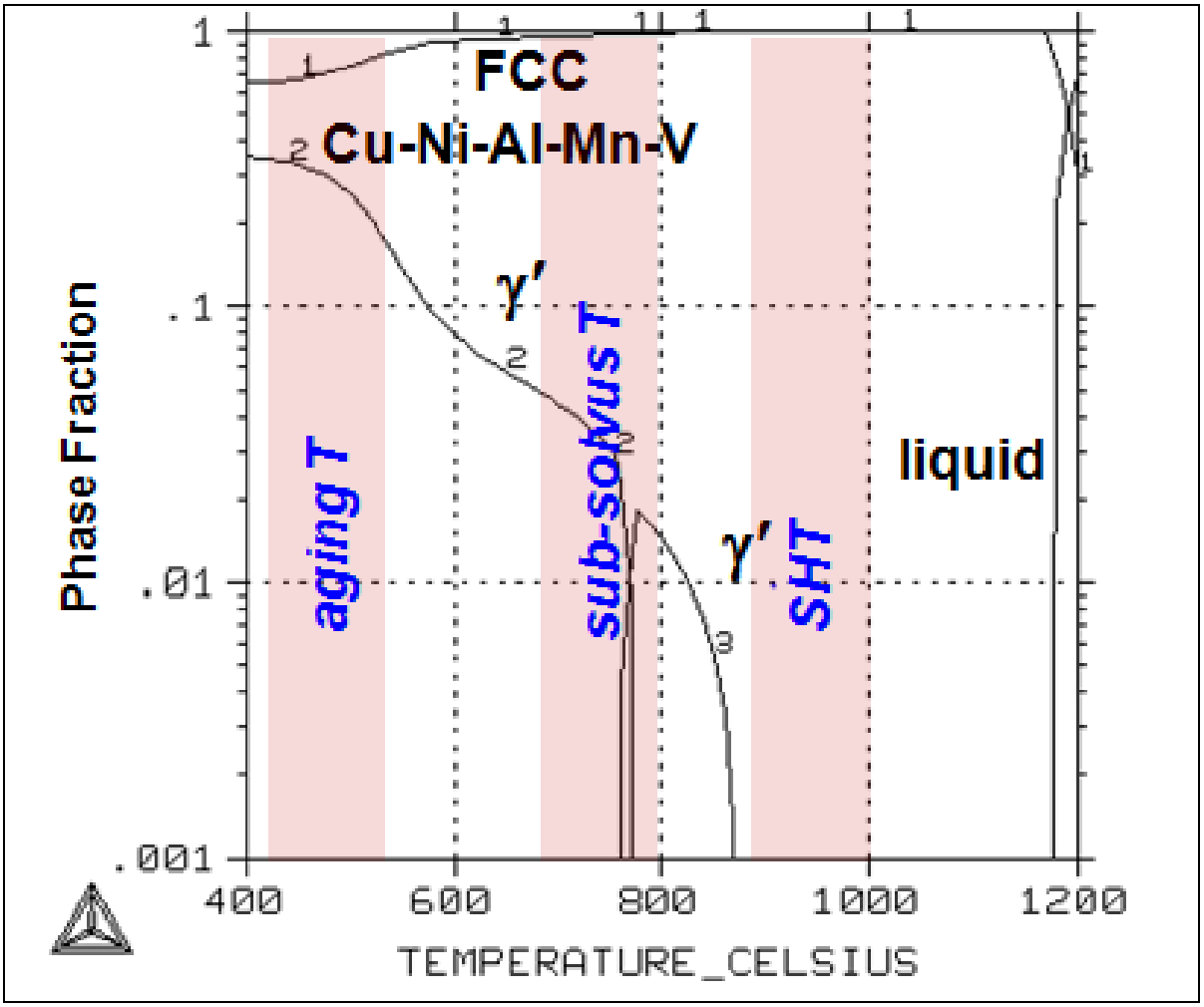

The Highlighted Regions Represent the Ideal Processing Temperatures.

Figure 8. Calculated Thermodynamic Equilibria Step Diagram for the NGCu-1A Design

The solidification curves of NGCu-1A, calculated under two different assumptions, are shown in Figure 9. Scheil solidification assumes no back-diffusion in the solid and infinite diffusion in the liquid, and usually represents the worst-case scenario in terms of residual segregation and final solidification temperature. A moving-boundary solidification model implemented in the Diffusion Controlled Transformations software (DICTRA), accounts for back-diffusion in the solid during the solidification process, and represents a more realistic case. The solidification temperature calculated from the Scheil model is 1018° C, while that calculated from the DICTRA model is 1075° C.

Use or disclosure of data contained on this sheet is subject to the restriction on the title page of this proposal.
Northrop Grumman Private/Proprietary Level I

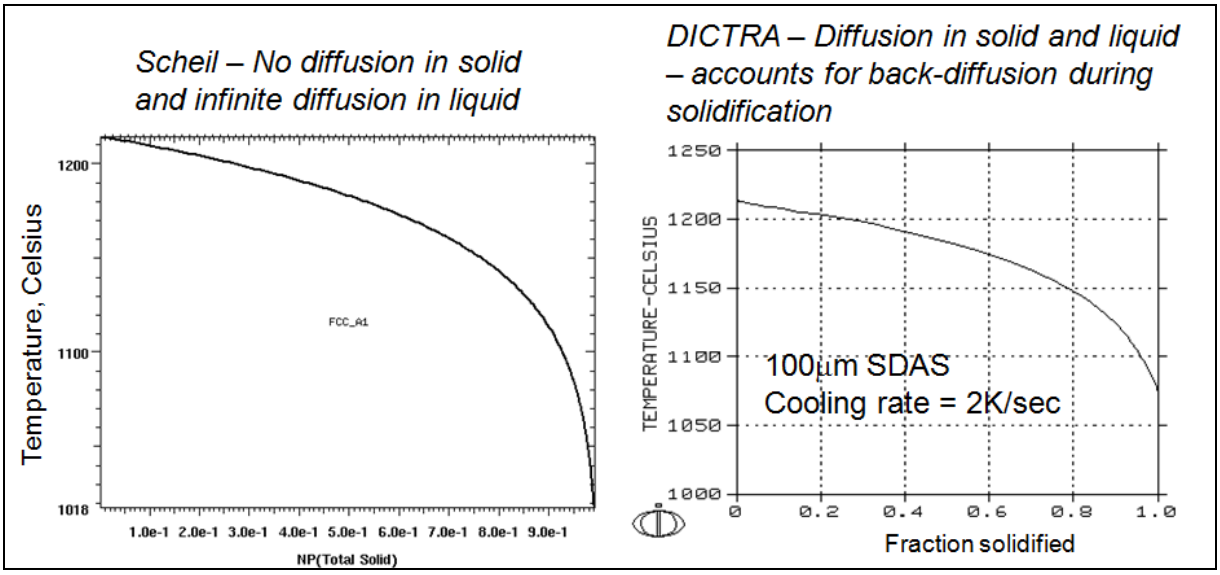

1) Scheil, which Represents the Worst Case Scenario, and 2) DICTRA – which Represents a More Realistic Scenario.

Figure 9. Calculated Solidification Curves for NGCu-1A Under Two Different Models

Figure 10 shows the calculated as-cast residual segregation in the solid FCC dendrite of NGCu-1A after solidification, using the DICTRA model. The Ni-segregation across the secondary dendrite arm-spacing (SDAS) is calculated to be quite significant. However, after homogenization at 975° C for 48hrs, the bulk of the segregation is predicted to have been eliminated. 975° C was selected as the homogenization temperature as it is 43° C below the worst-case solidification temperature of 1018° C, and hence should be safe to avoid any incipient melting during the homogenization process, while still being high enough to eliminate segregation effectively.

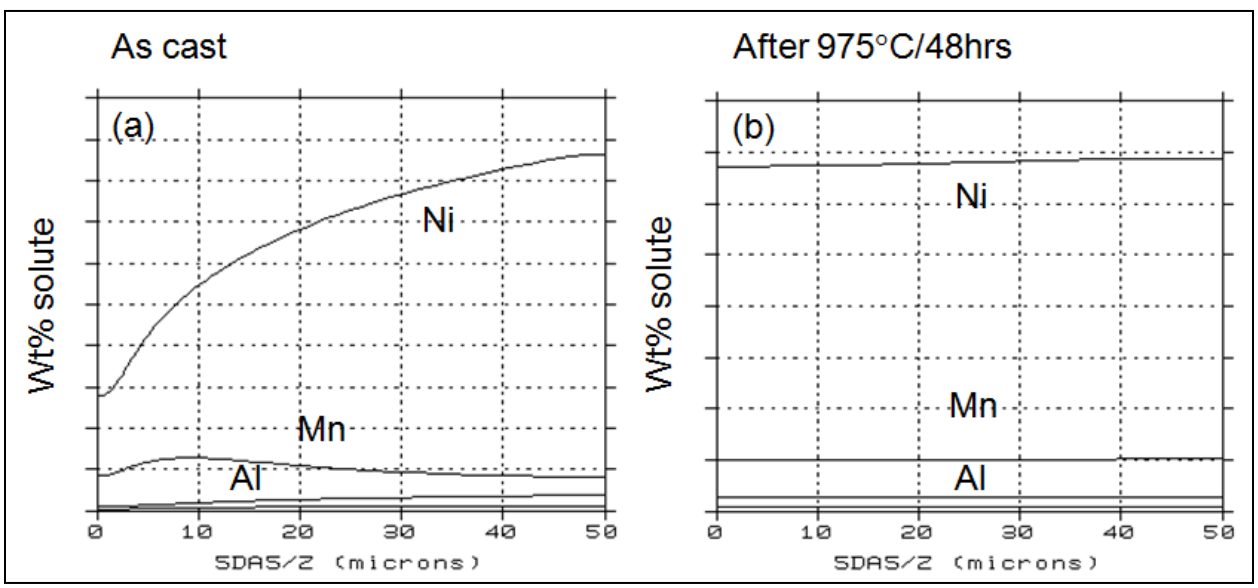

Figure 10. As-Cast and As-Homogenized Calculated Segregation Profiles, Illustrating that 975º C/48hrs Should be Sufficient to Eliminate Most of the Residual Micro-Segregation in the Alloy

Use or disclosure of data contained on this sheet is subject to the restriction on the title page of this proposal.
Northrop Grumman Private/Proprietary Level I

The primary design constraints of this alloy, the microstructural features which enable the design properties, and the associated risk factors for this design are summarized in Table 2.

Table 2. NGCu-1A Summary of Microstructural Features that Enable the Design Properties

Design constraint	Microstructural feature and properties	Risk factors
Easy to forge	• No Sn in alloy – No incipient melting • No other low-melting components/eutectics • Scheil solidification T of 1018° C	• High Ni in alloy – Can we eliminate segregation effectively?
Minimize cellular growth	• Lattice misfit of $L1_2$ and matrix reduced to ~ -0.75% • Grain-pinning dispersion to pi grain boundaries at lower end of gorging (-0.5% of NI-V Fcc#2 at 850° C • ~ 4% V_f of $L1_2$ at 700° C for sub-solvus treatment	• Biggest risk – Is the lattice misfit small enough to eliminate cellular growth • Can a certain amount of cellular growth be tolerated?
Wear behavior	• Low SFE matrix	• Will high Ni in matrix promote galling behavior?
Quench suppressibility	• Lower solvus of $L1_2$ (580° C in absence of V)	• None – No issues in prior Navy alloys
Strength	• Volume fraction of strengthening particles ~ 28% at 450° C (assuming 4% ppt at 700°C) • Expected YS> 135ksi	• Role of Mn or APB energy? • Can we get optimal size at 450° C?

2.4.1.1.1 Final NGCu-1A Alloy and Process Selection

Alloy:

- Cu-Ni-Mn-Al-V
- Achieves a FCC- γ' microstructure after heat-treatment

Process:

- Melt alloy at 30 lb sub-scale (SAES - Getters) – 4" Vacuum Arc Re-melting (VAR)
- Homogenize - 975º C/48hrs
- Grind outer layer to 3.5" Round bar
- Extrude bar at 950º C down to 1.0" Round (12¼:1 reduction ratio)

  *Extrusion was performed at Special Metals Corp. Huntington, West Virginia
- Optimize heat treatment to eliminate cellular growth and provide required strength

  *Sub-solvus temperature – As low as possible that does not lead to cellular growth at that temperature (as upper limit of cellular growth is usually 0.9 Solvus)
- Aging temperature – lower is better as it minimizes lattice misfit – However at low temperature the kinetics is slower

Pictures below in Figure 11 provide a visual appearance of the as received NGCu-1A round stock sections provided by QuesTek Innovations prior to the evaluation materials being shipped to the machining house.

Use or disclosure of data contained on this sheet is subject to the restriction on the title page of this proposal.
Northrop Grumman Private/Proprietary Level I

Figure 11. NGCu-1A Round Stock Evaluation Material

2.4.1.2 Design of NGCu-1B Containing Sn

The biggest risk factor associated with the NGCu-1A design was the possibility of occurrence of cellular growth, which if not completely eliminated, can limit the mechanical properties of the system. From QuesTek's previous experience in the NAVAIR program, Sn has been shown to effectively suppress cellular growth due to its role in minimizing the lattice parameter mismatch (see Figure 5 and Figure 6). However, as discussed in the previous section, Sn introduces a risk factor of incipient melting and limited alloy processability. In previous Navy program QuesTek was unable to hot-work alloys which contained >4wt% Sn due to the incomplete dissolution of the low-melting $D0_3$ Cu_3Sn compound. The alloys in that program had been hot-worked at 900° C, which led to incipient melting during the hot-working process. However, researchers have shown that Cu-Ni-Mn-Al-2wt%Sn alloys can be successfully hot-rolled between 800-850° C[6] (see Figure 12). Thus, the motivation of this design was to increase the probability of suppressing cellular growth by the introduction of Sn and minimizing the lattice misfit, while still keeping the amount of Sn low enough that it does not introduce any incipient melting during hot-working.

Use or disclosure of data contained on this sheet is subject to the restriction on the title page of this proposal.
Northrop Grumman Private/Proprietary Level I

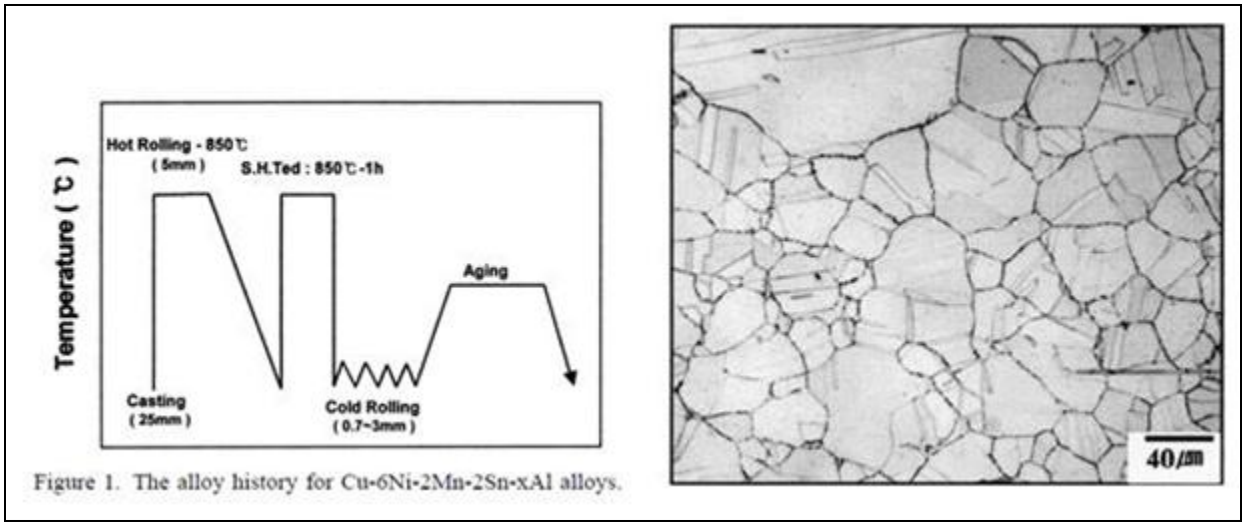

Figure 12. Prior Published Work Demonstrating that a Cu-Ni-Mn-Sn-Al Alloy can be Successfully Hot-Worked at 850° C

Using the NGCu-1A alloy as the baseline, the relative amounts of Mn and Sn were balanced, and the amount of Sn is limited to <2wt%. The final designed alloy composition had 1.9wt % Sn and the alloy misfit was successfully lowered to -0.57%, which satisfies the design goal of <0.6%. Figure 13 shows the step diagram of this design (designated as NGCu-1B), as well as the Scheil solidification curve.

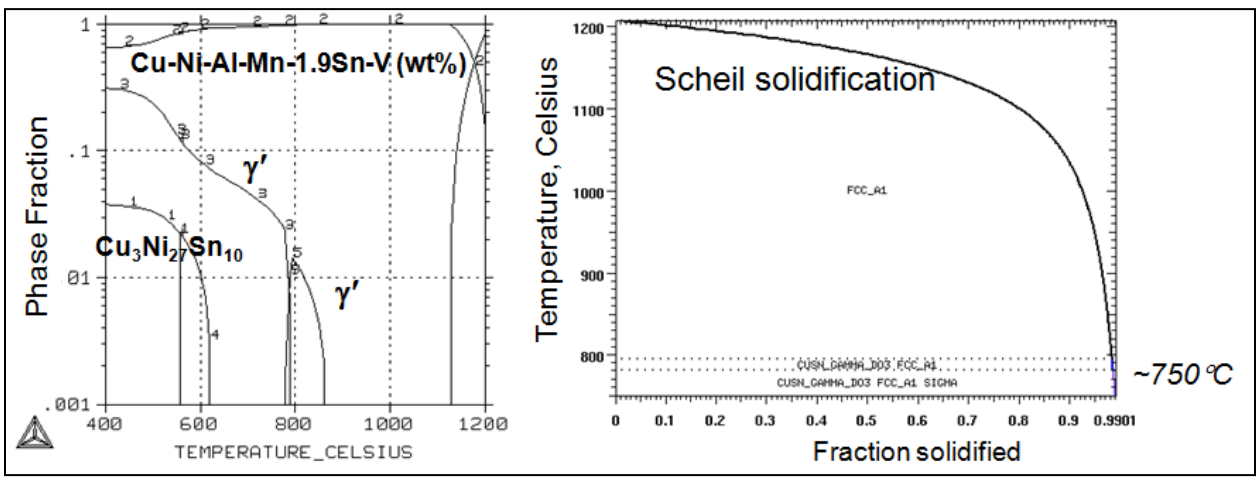

Figure 13. Step Diagram of the NGCu-1B Design, and the Calculated Scheil Solidification Plot. The Final Solidification Temperature is Calculated to be 750° C

The recommended homogenization temperature for the above design is a multi-step process: 700º C/8hrs + 750º C/16hrs + 800º C/8hrs + 825º C/16hrs.

A comparison of the expected properties and processability of the NGCu-1B design against the NGCu-1A design is shown in Table 3.

Use or disclosure of data contained on this sheet is subject to the restriction on the title page of this proposal.
Northrop Grumman Private/Proprietary Level I

Table 3. Comparison of the Properties and Processability of NGCu-1A and NGCu-1B

Alloy	NGCu-1A (Sn-free) Lower-risk Lower-reward	NGCu-1B (with Sn) Higher-risk Higher-reward
Composition (wt%)	Cu-Ni-Al-Mn-V – ppm B	Cu-Ni-Al-Mn-Sn-V
Biggest risk	• Cellular growth leading to low ductility of aged alloy	• Forgeability
Main advantage	• Alloy is processable with no risk of hot-tearing during hot-working	• Addition of Sn has been shown to mitigate cellular growth and provide strength
Prototype size in current round	• Melt as 30lb VIM/VAR billet • Extrude to required dimensions for NG testing	• Melt as 5 lb arc-melted button • Extrude to 0.75″ round rod
Wear behavior	• Expected to be equivalent	
Quench suppressibility	• Expected to be marginally better for NGCu-1A	
Strength	• Expected to be marginally better for NGCu-1B due to the role of the high diffusivity of Sn in helping the γ′ growth kinetics – They reach optimal size faster	

2.4.1.2.1 Final NGCu-1B Alloy and Process Selection

Alloy:

- Cu-Ni-Mn-Al-V-1.9Sn
- Contains < 2wt% Sn to mitigate incipient melting

Process:

- Melt alloy at 5 lb sub-scale (Pittsburgh Materials Technology, Jefferson Hills, PA)
- Homogenize - 700º C/8hrs + 750º C/16hrs + 800º C/8hrs + 825º C/16hrs
- Extrude to 0.75” round at 800º C
- Optimize heat treatment to eliminate cellular growth

  *Sub-solvus temperature – As low as possible that does not lead to cellular growth at that temperature (as upper limit of cellular growth is usually 0.9T solvus)

  *Aging temperature – lower is better as it minimizes lattice misfit – However at low temperature the kinetics is slower

The NGCu-1B Prototype material encountered a processing failure that prevented the manufacturer of the alloy. Metallographic specimens showed indications of both the early stages of cellular precipitation and incomplete homogenization Figure 14. The hardness measured from the small button sample produced separately at QuesTek did not attain the value desired by the program.

Use or disclosure of data contained on this sheet is subject to the restriction on the title page of this proposal.
Northrop Grumman Private/Proprietary Level I

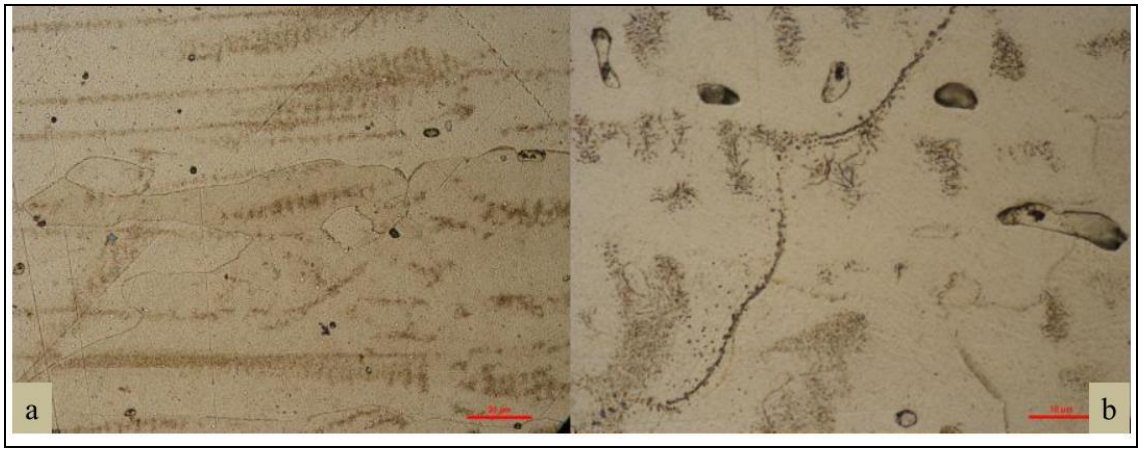

Tempered specimen shows porosity and undissolved particles (white); (b) NGCu-1B tempered specimen shows grain boundary particles that suggest mild cellular precipitation.

Figure 14. (a) NGCu-1B

2.4.1.3 Design of Cuprium Containing Sn

While the 1st round prototype (NGCu-1A) alloys achieved the necessary wear performance to compete with the baseline CuBe alloy, they both lacked the necessary strength for the program targets. A 2nd generation redesign was initiated to address this issue and adjust the alloy composition and processing for greater strength. For the Cu-based concept, QuesTek's NAVY SBIR alloy design – Cuprium – was selected.

QuesTek designed a precipitation-strengthened Cu-based material concept to achieve the desired property goals. This alloy is similar in characteristic to the NGCu-1B alloy composition - Ni_3Al, $L1_2$-type precipitation, Sn-containing for low lattice misfit. To mitigate issues with low-melting eutectic phases associated with the Sn content (which resulted in failed prototyping in (round 1), a novel processing route known as Spray-metal Forming (SMF) was utilized. The target chemistry of the Cuprium alloy is shown in Table 4 below.

Table 4. Target Composition of Prototype Alloy Cuprium
Values are in weight percent.

Element	min	target	max
Carbon	--	--	0.010 (100 ppm)
Manganese	--	--	0.05
Tin	3.8	4.0	4.2
Phosphorus	--	--	0.01 (100 ppm)
Sulfur	--	--	0.005 (50 ppm)
Aluminum	1.1	1.2	1.3
Nickel	23.5	24	24.5
Silicon	--	--	0.05
Iron	--	--	0.02
Zinc	--	--	0.05
Lead	--	--	0.05
Vanadium	0.7	0.8	0.9
Oxygen	--	--	0.005 (50 ppm)
Nitrogen	--	--	0.002 (20 ppm)
Boron	0.004 (40 ppm)	0.005 (50 ppm)	0.006 (60 ppm)

Use or disclosure of data contained on this sheet is subject to the restriction on the title page of this proposal.
Northrop Grumman Private/Proprietary Level I

A ~50 lb heat of *Cuprium* was produced for characterization under this program. This alloy is known to be difficult to process by conventional hot working practices as previously mentioned due to a high risk of incipient melting during thermal processing. To mitigate this risk, a spray metal forming process was utilized to cast a highly homogeneous billet. Spray metal forming, or SMF, is a casting process by which pre-alloyed material is re-melted in a crucible under an inert cover gas (typically Ar) and poured through an array of inert gas jets to break the stream of molten metal into droplets in a process called inert gas atomization. These droplets are then accelerated towards a substrate by the gas jet (typically Ar), and an alloyed billet is built up by semi-solid state deposition. The solidification rates experienced during the SMF process are very high, resulting in minimal alloy segregation during casting. The homogeneity of the billet after casting is sufficient enough that a post-casting homogenization step is unnecessary.

The SMF process was completed with laboratory-scale equipment at the Penn State University's Applied Research Laboratory (ARL). The image to the left of Figure 15 shows an overall view of the SMF equipment. The green arrow points to the crucible for re-melting the pre-alloyed billet. The image to the lower right shows this re-melt crucible in more detail. The SMF chamber circled in red is shown in greater detail in the image to the upper right. The red arrow points to the substrate arm that the SMF billet is deposited into. This substrate arm is capable of rotating, extending and retracting, in order to fully control the final shape of the SMF billet. By controlling the movement of this substrate arm, cylindrical, rectangular, and even tubular billets can be fabricated.

Use or disclosure of data contained on this sheet is subject to the restriction on the title page of this proposal.
Northrop Grumman Private/Proprietary Level I

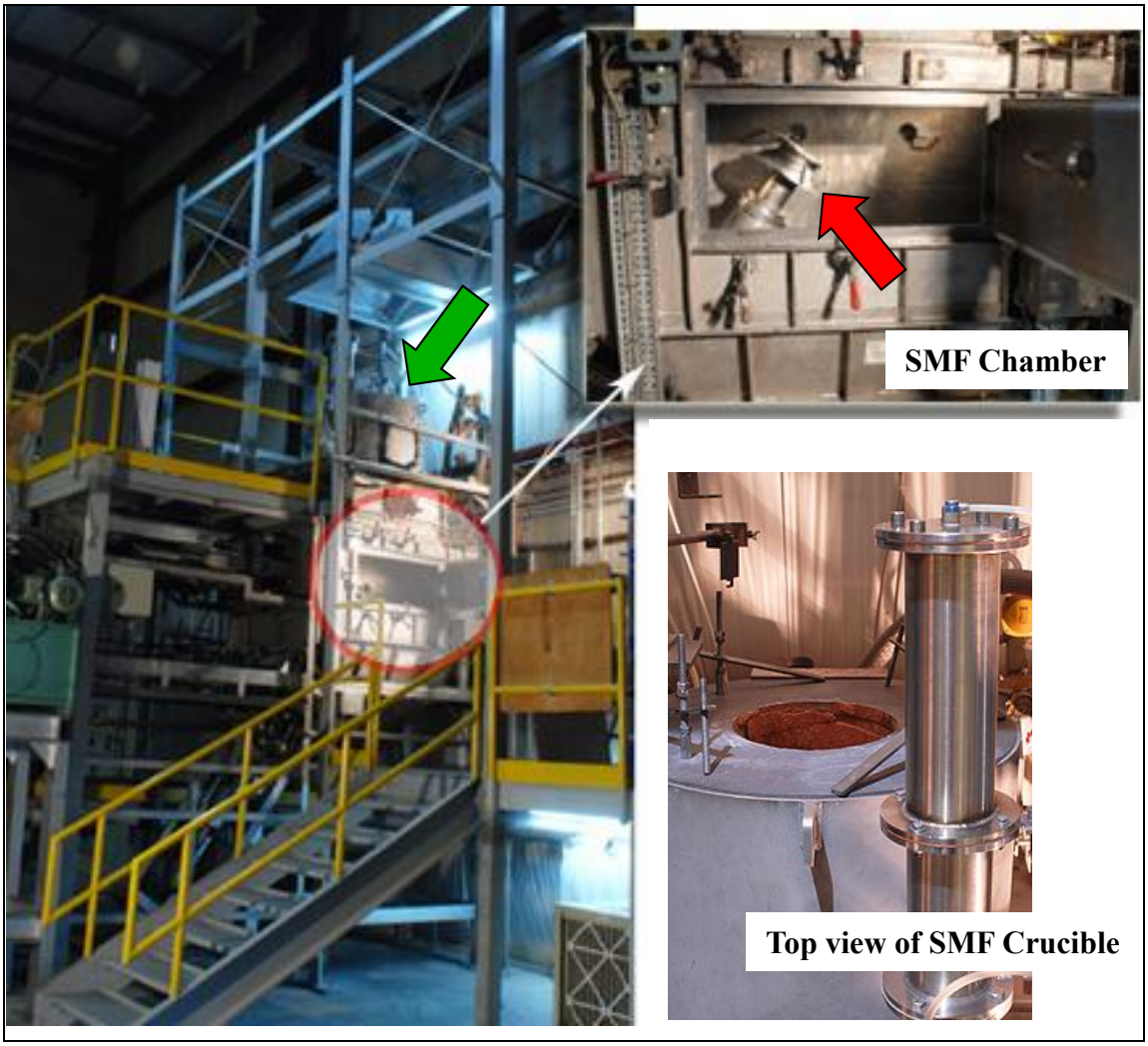

Figure 15. Images of Spray-Metal Forming Facility at Penn State's Applied Research Lab

Three SMF billets were produced in total, two small-scale trial runs to establish and verify process parameters and billet properties ahead of one final run to produce a larger billet for testing. Process parameters such as gas-to-metal ratio, gas jet velocity, pour rate, etc. were varied in order to minimize porosity and grain size and maximize yield. Microstructural characterization completed at ARL indicate the achieved level of porosity in the casting was on the order of 5-10% porosity near the center of the billet, and slightly higher at around 15% at extreme top and bottom. As shown by optical micrograph in Figure 16, as-cast grain sizes were on the order of 10-20 micrometers in diameter, a very fine scale for an as-cast structure. The micrographs shown in Figure 16 were polished by standard metallographic techniques, and etched in a solution of 5 g $FeCl_2$ + 10mL HCl + 80 mL H_2O in order to reveal the grain structure through selective etching of the grain boundaries. SEM analysis indicates only a minor amount of alloy segregation in the form of fine V- and Sn-rich grain boundary precipitates.

Use or disclosure of data contained on this sheet is subject to the restriction on the title page of this proposal.
Northrop Grumman Private/Proprietary Level I

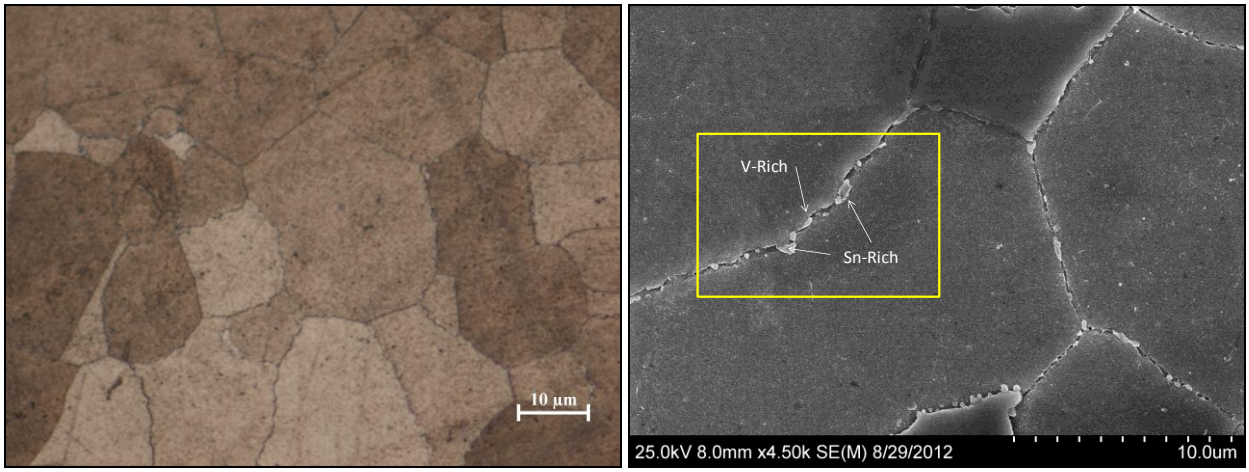

Figure 16. As-Cast Micrographs from the SMF Cuprium Billet. Left: Etched Optical Micrograph Revealing the Fine Grained Structure, Right: SEM Micrograph Indicating the Presence of Very Fine (~1 Micrometer or Less) Grain Boundary Precipitates

Figure 17 presents a schematic detailing the overall production path utilized to fabricate and process the SMF Cuprium material. Processing steps include casting, machining into an extrusion billet, hot extrusion and final heat treatment. SMF casting and EDM preparation of an extrusion billet was completed at Penn State ARL. Figure 18 details the approximate location the extrusion billet excised from the SMF billet. Hot extrusion into 1.25 inch round product was completed at the AFRL Materials Processing Laboratory located at Wright Patterson Air Force Base. Extrusion was completed at 850° C at a slow feed rate of 90 inches per minute. The billet was reduced from an initial diameter of 2.95 inch to a final diameter of 1.25 inch (reduction ratio of ~5.6), yielding about 24 inches of usable material.

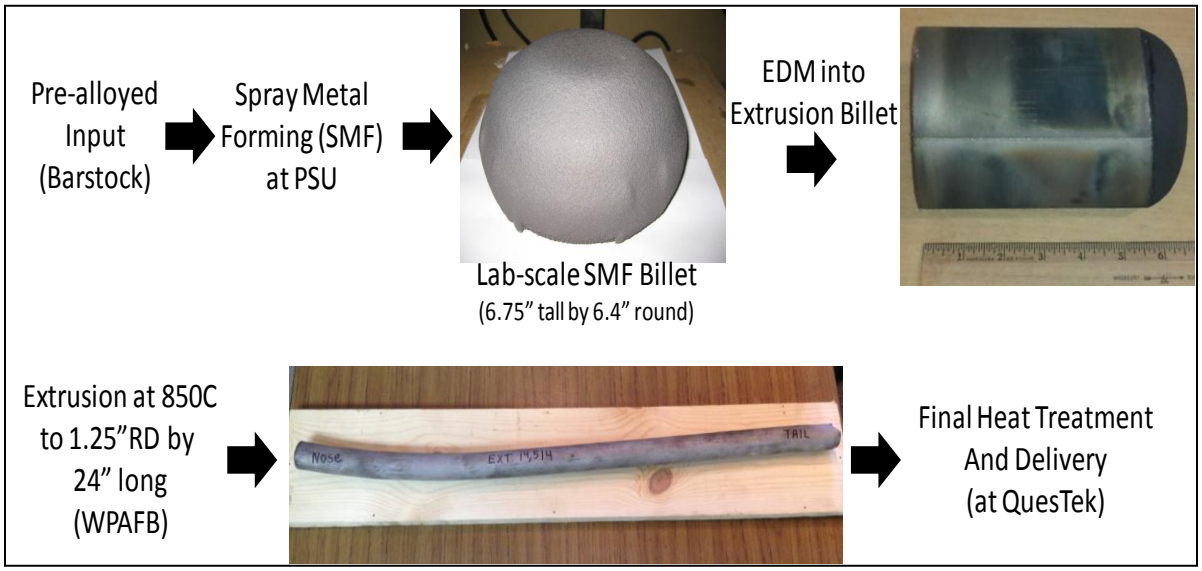

Figure 17. Schematic Detailing the Production Path for the SMF Cuprium Alloy

Use or disclosure of data contained on this sheet is subject to the restriction on the title page of this proposal.
Northrop Grumman Private/Proprietary Level I

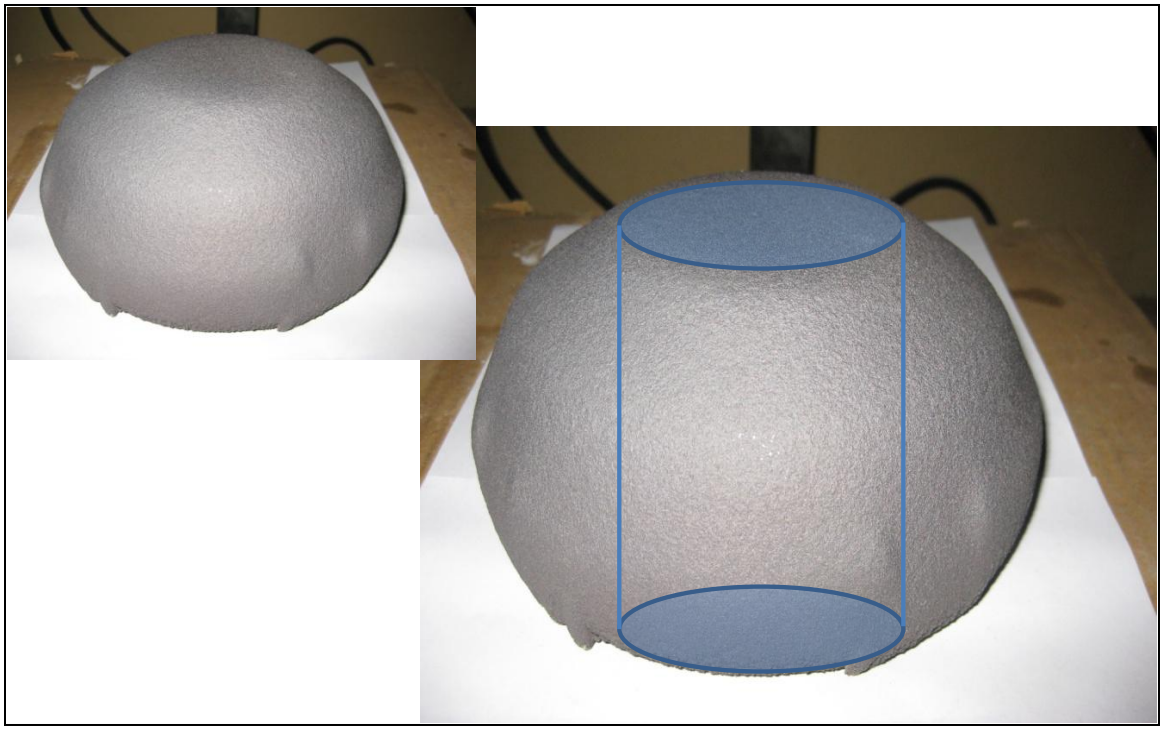

The schematic overlay in the image to the right indicates the location from which an extrusion billet was excised.

Figure 18. Image of the As-Cast SMF Cuprium Billet

Following extrusion, the bar was sectioned into two bars, one 11-inch long and one 12-inch long. Using results of prior heat treatment optimization studies, the bars were heat treated at QuesTek using laboratory-scale air furnaces. The heat treatment schedule applied to the bars prior to final delivery for property characterization was:

1. Solution Heat Treat at 825° C for 2 hours + Water Quench
2. Sub-Solvus Anneal at 700° C for 30 minutes + Water Quench
3. Age at 500° C for 8 hours + Water Quench

The Cuprium bar was heat treated at QuesTek in its full 1.25-inch-diameter product form. A small segment of material was removed from the nose-end of the bar (that is, the forward end of the billet during extrusion). One ASTM E8 standard tensile specimen (0.25” gage diameter) was excised from the center of the bar. Hardness and microstructure samples were excised from the mid-radius of the bar. Hardness was measured by both Rockwell C (HRC) and Vickers (HV) methods, taking a minimum of 12 measurements per sample. Average hardness was measured at 32.2 HRC, or 318 HV.

Figure 19 contains detailed optical micrographs of the extruded and heat treated SMF *Cuprium* microstructure. Comparison to the as-cast microstructure in Figure 16 it shows that the extrusion process has resulted in some grain refinement. The extruded and heat treated microstructure contains a fine, equiaxed distribution of grains on the order of 5-10 micrometers in diameter. Fine, equiaxed precipitates are visible at grain boundaries, a byproduct of the high temperature, sub-solvus annealing step. This step intentionally allows these fine grain boundary precipitates to form, in order to prevent cellular growth from occurring.

Use or disclosure of data contained on this sheet is subject to the restriction on the title page of this proposal.
Northrop Grumman Private/Proprietary Level I

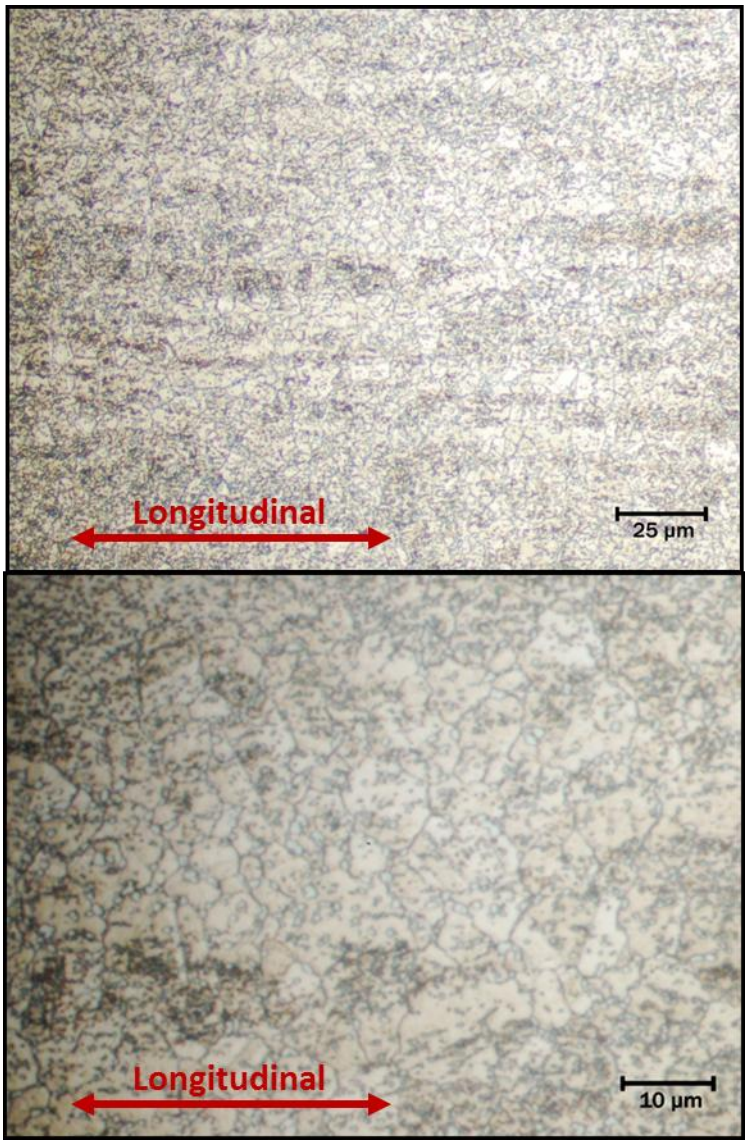

Sample etched in standard copper alloy etchant solution (5g FeCl2+10mL HCL+ 80mL H2O). The longitudinal direction of extrusion is oriented horizontally.

Figure 19: Optical Micrographs of Extruded SMF Cuprium at Different Magnifications

Strength results are comparable to previous results obtained from VIM/VAR and press forged Cuprium material, an indication that the SMF and extrusion processes were successful in producing acceptable material. These comparison results are presented in the Design of NGCo-3A Alloy section Table 8 that follows. The ductility of this prototype material is significantly better than obtained in prior material, with percent elongation increasing from ~6% to 16% and percent reduction in area increasing from ~8% to 34%. The prior prototype material had significant issues with incipient melting during press forging, resulting in a poor microstructure that SMF casting process has successfully reduced or eliminated the incipient melting risk during forming of this alloy.

Use or disclosure of data contained on this sheet is subject to the restriction on the title page of this proposal.
Northrop Grumman Private/Proprietary Level I

2.4.1.3.1 Final Cuprium Alloy and Process Selection

Alloy:

- Cu-Ni-Mn-Al-V-Sn
- Contains < 4wt% Sn to mitigate incipient melting

Process:

- Melt alloy at 50 lb sub-scale (Penn State University Applied Research Laboratory)
    a. A successful 2000 lb melt was recently produced at (Penn State ARL)
- Spray Metal Formed (SMF) Billet (improved homogeneity)
- Hot extrusion from 6.4" round to 1.25" round at 850° C (5.6 reduction ratio)
- Optimize heat treatment after forging to eliminate cellular growth
    - Solution Heat Treat at 825° C for 2 hours + Water Quench
    - Sub-solvus Anneal at 700° C for 30 minutes + Water Quench
    - Age at 500° C for 8 hours + Water Quench

2.4.2 Cobalt Alloy Design

QuesTek's cobalt alloy design for this program was based on a modification of a previously designed alloy for a US Marine Corps funded project[6]. The United States Marine Corps (USMC) designed alloy (designated B86) had excellent strength (hardness) behavior, but had low quench suppressibility, resulting in precipitation occurring during the quenching process. The motivation of the current design exercise was to improve the quench suppressibility of the alloy, while achieving the same strength response.

Co-Cr alloys are promising to satisfy the current program objectives due to the following reasons:

- They have the best sliding wear resistance of any class of engineering metal
    - Carpenter's ACUBE 100 is a CoCrMo alloy showing excellent sliding wear performance
- Excellent Coefficient of Friction (CoF)/wear resistance due to low 'stacking fault energy' of FCC-Co phase
    - Tendency to transform FCC to HCP structure
        - Used in metastable FCC state @ room temperature (RT)
        - Alloy to suppress martensitic transformation

    Significant work-hardening associated with the phase transformation

    - Existing Co-Cr alloy relies upon cold- or warm-work to achieve high strength (size dependent!)
    - Excellent chemical/erosion resistance

Use or disclosure of data contained on this sheet is subject to the restriction on the title page of this proposal.
Northrop Grumman Private/Proprietary Level I

The basic microstructural features of QuesTek's cobalt alloy design are summarized below (and illustrated schematically in Figure 20):

- High Cr content – for optimal wear and corrosion-resistance behavior
- Minimize the hardness and maximize ease of machining in annealed state
  - Minimize interstitial elements (C, N)
- Design for a precipitation-strengthening dispersion
  - Solution-treatable following (rough) machining in annealed state
  - Efficient precipitation during tempering > ~700º-900° C
  - Coherent phase is ideal: ($L1_2$ or γ) – Co_3Ti
  - Ensure good lattice parameter matching between the FCC matrix and ordered FCC ($L1_2$) particles
- Design for good solidification and hot-working

Due to the low misfit between the FCC Co-Cr phase and the Co3Ti $L1_2$ phase, the Co_3Ti phase was selected as the strengthening dispersion for the design. As mentioned previously, the design was based on a previously designed alloy B86 for a Marine Corps application. The B86 alloy was a Co-Cr-Ti-Ni-Fe-V alloy. It was designed such that the FCC-$L1_2$ lattice parameters were closely matched, in order to suppress the cellular growth reaction. This alloy had been fabricated at button scale, and subsequently characterized. An optical micrograph of the alloy in the fully tempered state, and the measured hardness values at different stages of tempering are shown in Figure 20. As seen from Figure 20, the microstructure did not reveal the presence of any cellular growth in the system, and revealed the existence of annealing twins, which implies that the FCC phase had low stacking fault energy (the intent of the design). Also, the alloy achieved high hardness after tempering, and the estimated tensile strength after full aging satisfies the current program objectives. However, the alloy had a very high hardness after quenching from homogenization/solutionization temperature. This implies that the alloy lacked sufficient quench suppressibility, and this might introduce processing difficulties if the alloy has a high as-quenched hardness. Hence the focus of the redesign is to make the alloy more quench suppressible.

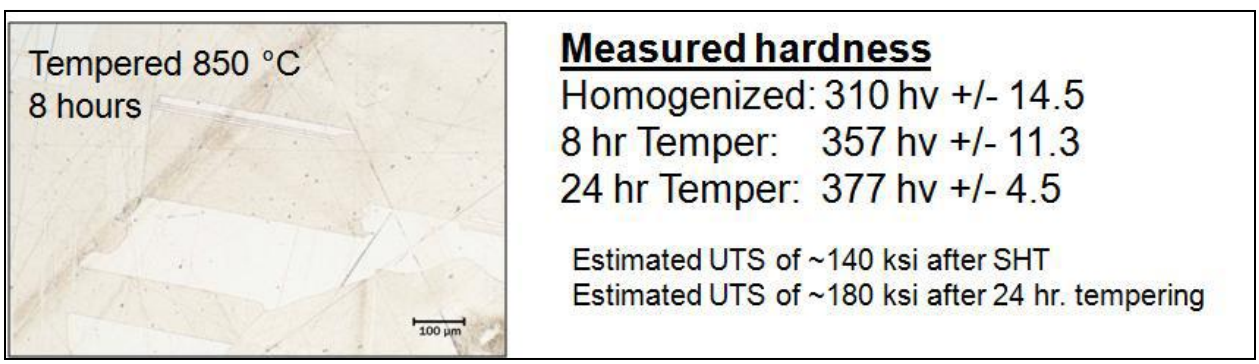

The Hardness Values of 350-380 VHN Achieved After Tempering Satisfy the Strength Goals of the Current Program. However, the As-Homogenized Hardness is Quite High, Indicating that the USMC Design is not Quench Suppressible, Which Might Introduce Processing Difficulties.

Figure 20. Optical Micrograph of the Fully Tempered USMC B86 Alloy, Revealing the Absence of any Cellular Growth and the Presence of Annealing Twins

Use or disclosure of data contained on this sheet is subject to the restriction on the title page of this proposal.
Northrop Grumman Private/Proprietary Level I

2.4.2.1 Design of NGCo-1A

The re-design strategy of the B86 noted as NGCo-1A is shown in Figure 21, and focuses on the primary design goal of achieving a yield strength level of > 140 ksi. The key is to achieve enough volume fraction of the strengthening $L1_2$ particles after full tempering, without increasing the driving force so much that these particles are precipitated during the quench from the solution treatment.

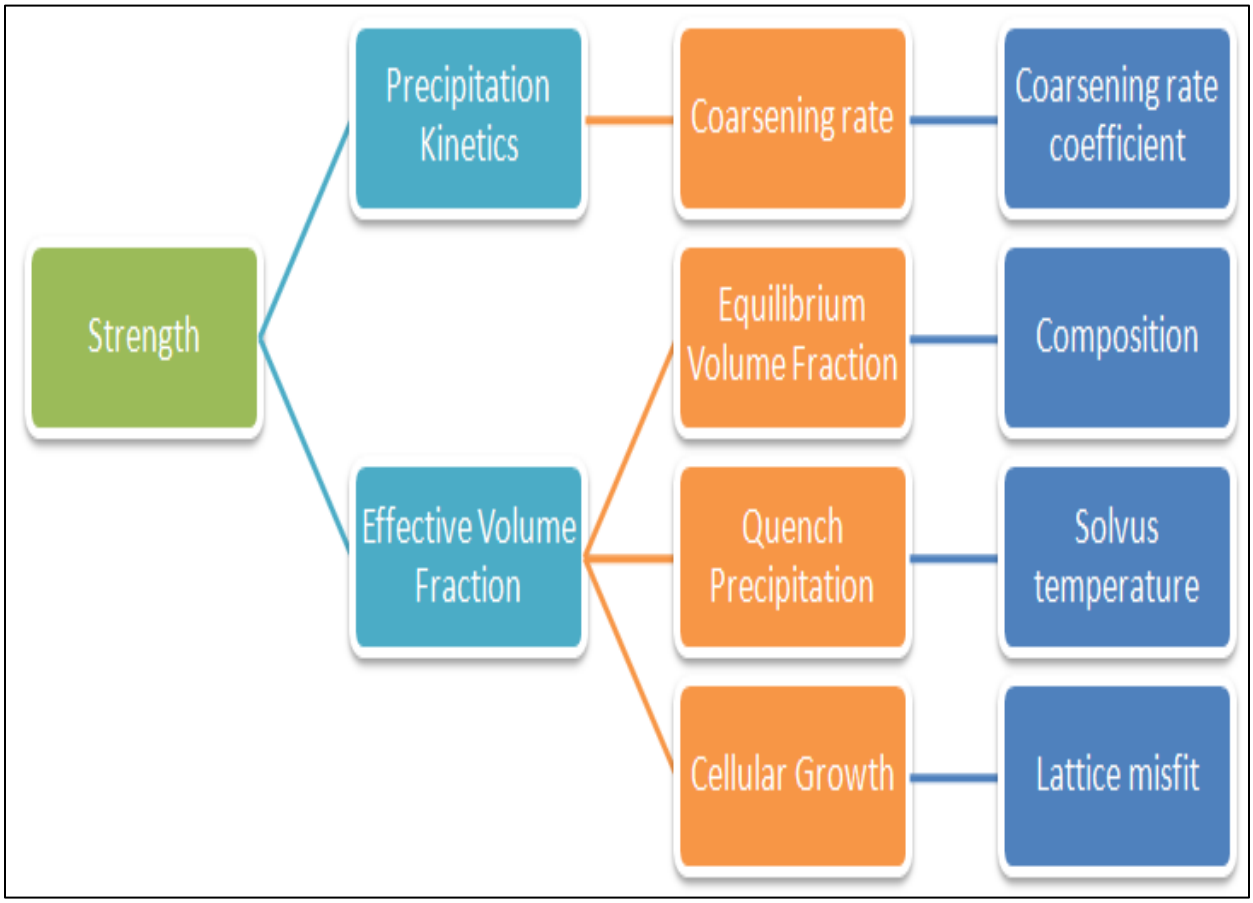

While Also Increasing the Quench Suppressibility of the Alloy.

Figure 21. The Re-Design Strategy to Obtain the Required Strength

The step diagram of the previous B86 design (represented by the solid lines) is shown in Figure 22. Also superimposed on Figure 22 are dashed lines representing the desired stability of the $L1_2$ phase and the Co_4Cr_2Ti phase for the current program. The gamma prime solvus should be reduced to increase the alloy quench suppressibility. However, the gamma prime solvus cannot be too low, as this leads to slow precipitation kinetics and low phase fraction. Also, the solvus of the undesirable Co_4Cr_2Ti phase should be reduced in order to avoid precipitation of this phase during the aging/tempering treatment. Lastly, depending on the final aging temperature for gamma prime precipitation, the solvus of the HCP phase should be just below the aging temperature.

Use or disclosure of data contained on this sheet is subject to the restriction on the title page of this proposal.
Northrop Grumman Private/Proprietary Level I

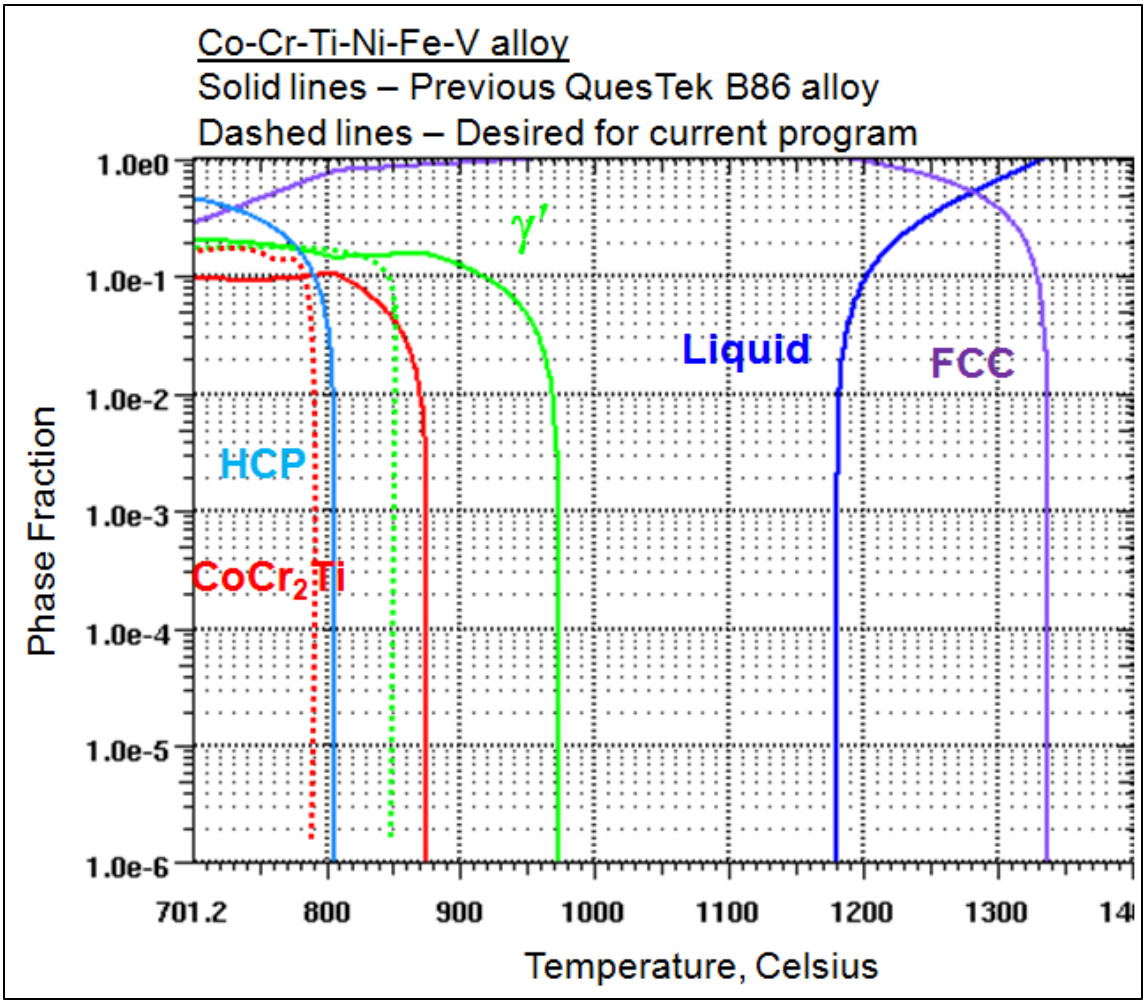

Figure 22. Step Diagram for the Previous QuesTek B86 Alloy, and the Desired Stability Lines for the Current Design

As seen from Figure 22 above, reducing the gamma prime solvus temperature is critical to achieving quench suppressibility in the design. Figure 23 shows two calculated iso-contour plots for two different tempering temperatures, as a function of the amount of Fe and Ti in the alloy. The purple lines represent the volume fraction of gamma prime at that temperature, and the green lines are the iso-contours for the corresponding lattice misfit with the FCC matrix. Figure 17(a) is the plot for a tempering temperature of 850° C, and the highlighted region in pink shows the USMC B86 design, which achieved a gamma prime volume fraction of 16%, a lattice misfit of 0.4%, and a gamma prime solvus temperature of 950° C. Increasing the amount of Fe has an effect of lowering the gamma prime solvus temperature. Figure 23(b) shows that by increasing the Fe to 7.5-wt%, and by reducing the Ti slightly, the gamma prime solvus can be reduced to 890° C (a 60º C reduction), and the same gamma prime volume fraction of 16%, and the lattice misfit of 0.4% as the B86 design can be realized at a lower tempering temperature of 780° C.

Use or disclosure of data contained on this sheet is subject to the restriction on the title page of this proposal.
Northrop Grumman Private/Proprietary Level I

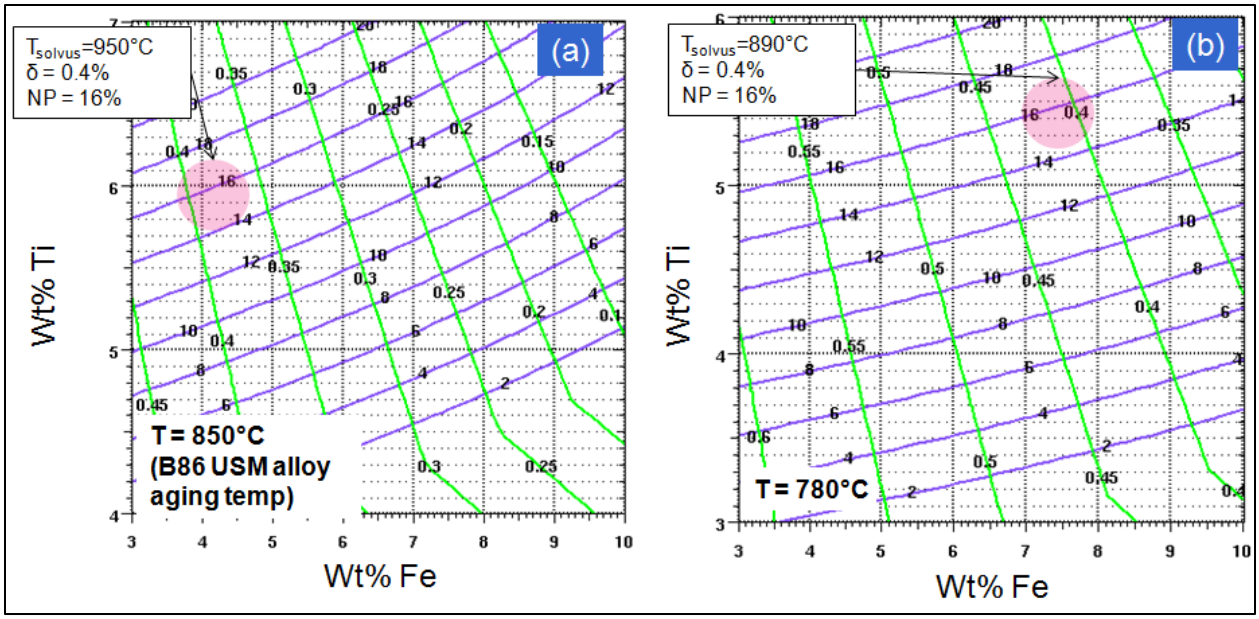

Illustrating that by Increasing Iron Content and Lowering the Aging Temperature, the same Lattice Misfit and Phase Fraction is Obtainable as the B86 Alloy, While Achieving Lower Solvus Temperature.

Figure 23a, b. Calculated Iso-Contour Plots of the Gamma Prime Volume Fraction and Lattice Misfit as a Function of the Ti and Fe Content

The final step diagram of the NGCo-1A design, and the key design metrics are shown in Figure 24.

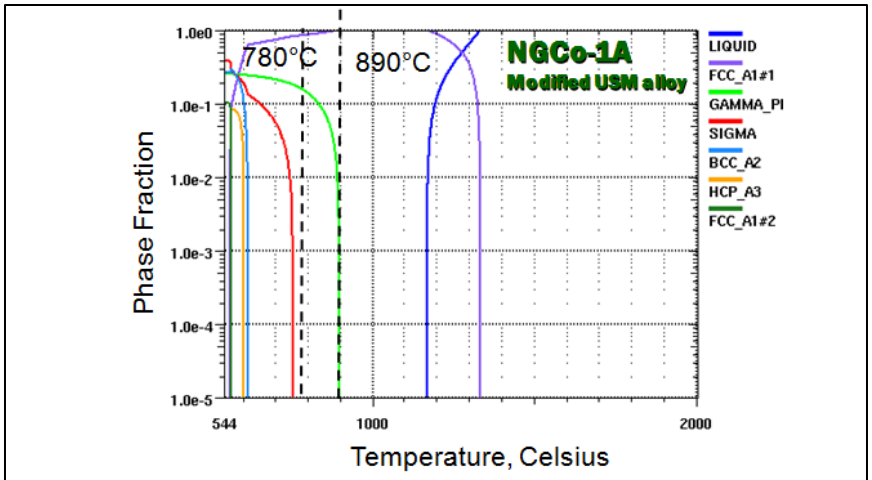

Alloy	Solvus of γ′	Phase fraction of γ′	δ (lattice misfit)	Aging Temp
QuesTek USM B86 alloy Baseline	950°C	16%	0.4%	850°C
NGCo-1A	890°C	16%	0.4%	780°C

Figure 24. Step Diagram of the NGCo-1A Design, and the Calculated Values of the Key Design Metrics

Use or disclosure of data contained on this sheet is subject to the restriction on the title page of this proposal.
Northrop Grumman Private/Proprietary Level I

2.4.2.1.1 Final NGCo-1A Alloy and Process Selection

Alloy:

- Co-Cr-Ti-Ni-Fe-V alloy
- Melt alloy at 30 lb sub-scale (SAES) – 4” VAR

Process:

- Homogenize - 1050° C/72hrs
- Grind outer layer to get 3.5” Round bar
- Extrude bar at 1000° C down to 1.0” Round (12¼: 1 reduction ratio)
- Optimize heat treatment
- Pictures below in Figure 25 provide a visual appearance of the as received NGCo-1A square round stock sections provided by QuesTek Innovations prior to the evaluation materials being shipped to the machining house.

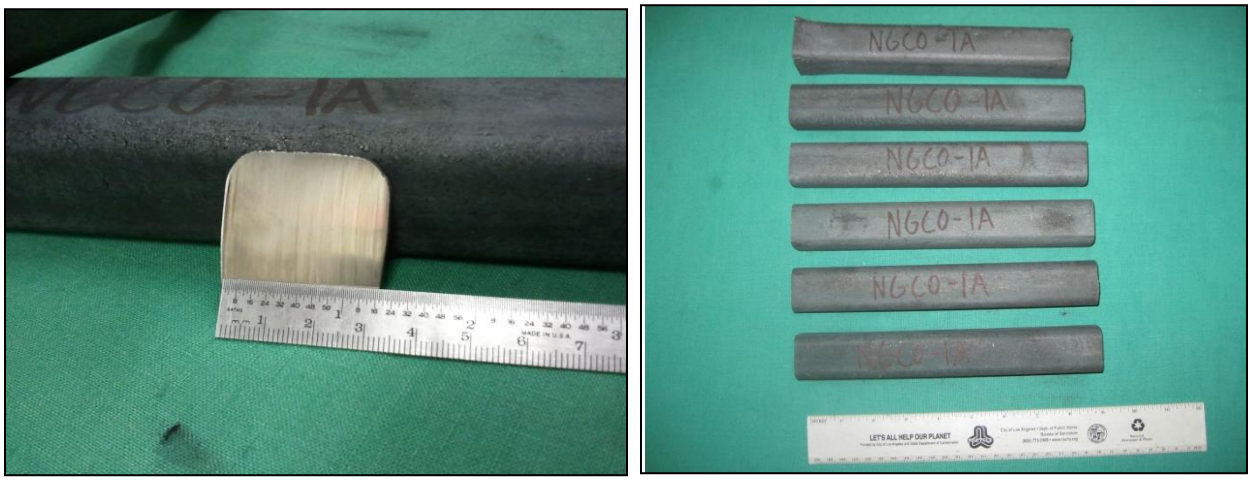

Figure 25. NGCu-1A Round Stock Evaluation Material

2.4.2.2 Design of NGCo-2A

In parallel to the temper optimization efforts, a new round of production of the same alloy design (now termed “NGCo-2A” to delineate from the first round of prototyping) was initiated at MetalWerks PMD, Inc.

Microstructural characterization of samples from the initial NGCo-1A cobalt based production batch was performed to support optimizing the material properties that had fallen short of the programs desired levels and make necessary adjustments for a larger size melt. The results analysis of the characterization fed into the 2nd round of design optimization for the Cobalt based alloy variant.

Use or disclosure of data contained on this sheet is subject to the restriction on the title page of this proposal.
Northrop Grumman Private/Proprietary Level I

The key microstructural characterization work performed was:

1. Grain-structure analysis to quantify the grain size in the alloy
2. Atom-probe analysis to resolve the nano-structure of the alloy and validate predictions
3. X-ray diffraction analysis to characterize the phases present at the gage-section of a fractured tensile specimen

Samples were analyzed using light optical microscopy both parallel (longitudinal) and perpendicular (transverse) to the rolling direction to characterize the grain-size and grain-structure.

The optical micrographs are shown in Figure 26 and Figure 27, and the estimated grain-sizes are shown in Table 5. In each direction, the grains were fairly equiaxed, with a high amount of twin-boundaries, indicative of the low stacking fault energy of the material. As expected, the grain-size is finer in the transverse direction than in the longitudinal direction.

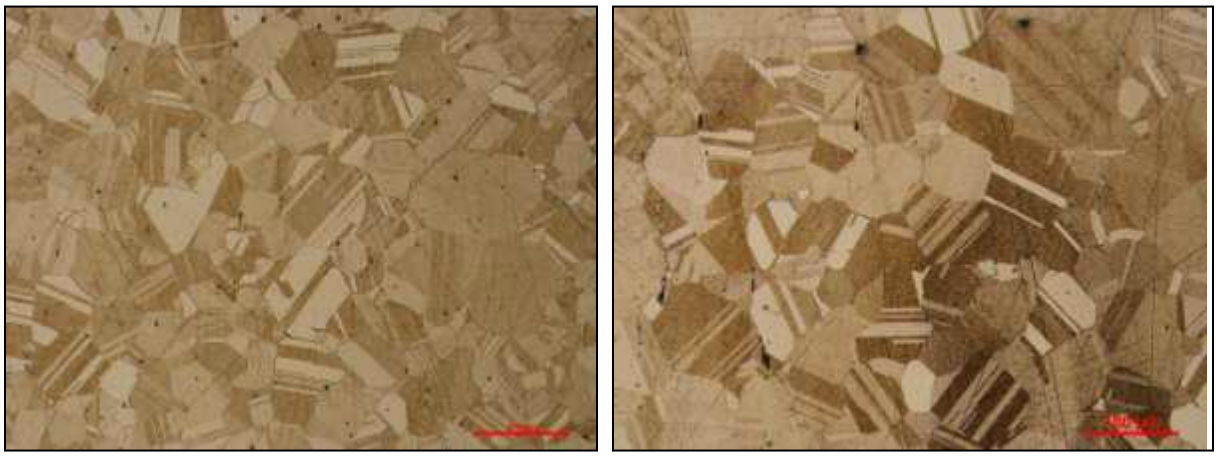

Rolling direction is from top to bottom of pictures.

Figure 26. Grain Structure Parallel to the Rolling Direction in NGCo-1A

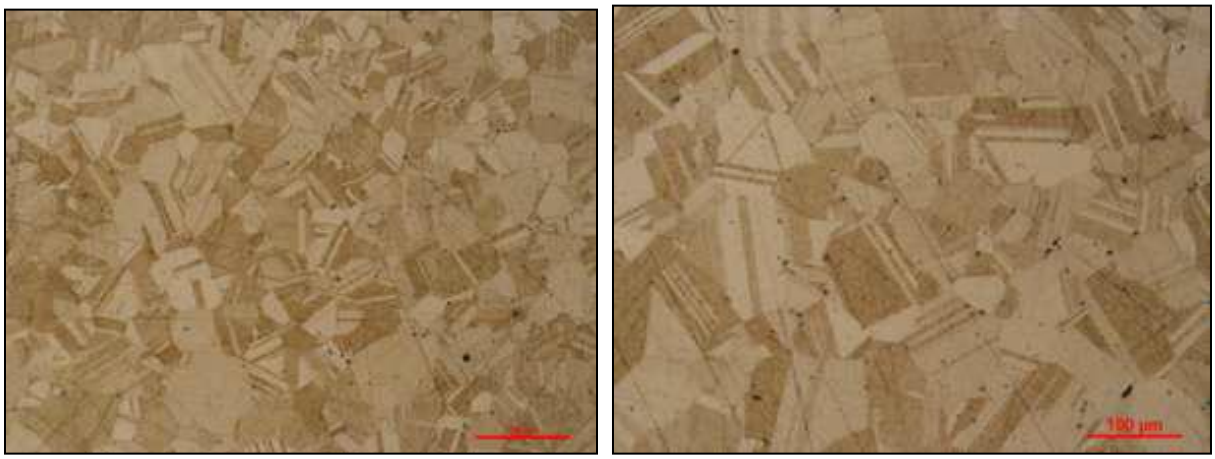

Rolling direction is perpendicular to the plane.

Figure 27. Grain Structure Perpendicular to the Rolling Direction in NGCo-1A

Use or disclosure of data contained on this sheet is subject to the restriction on the title page of this proposal.
Northrop Grumman Private/Proprietary Level I

Table 5. Grain size measurements on NGCo-1A alloy

Direction	Intercept Length (µm)	+- (µm)	ASTM Grain Size	+-
Parallel	74.2	3.6	4.2	0.1
Perpendicular	78.6	5.1	4.1	0.1

The hot-rolled NGCo-1A bar had received the following final heat-treatment:

1. Solution heat-treated at 1025º C/2hrs + water quench (WQ)
2. Aged at 780º C/24hrs + WQ

The thermodynamic step diagram for NGCo-1A alloy is shown in Figure 28:

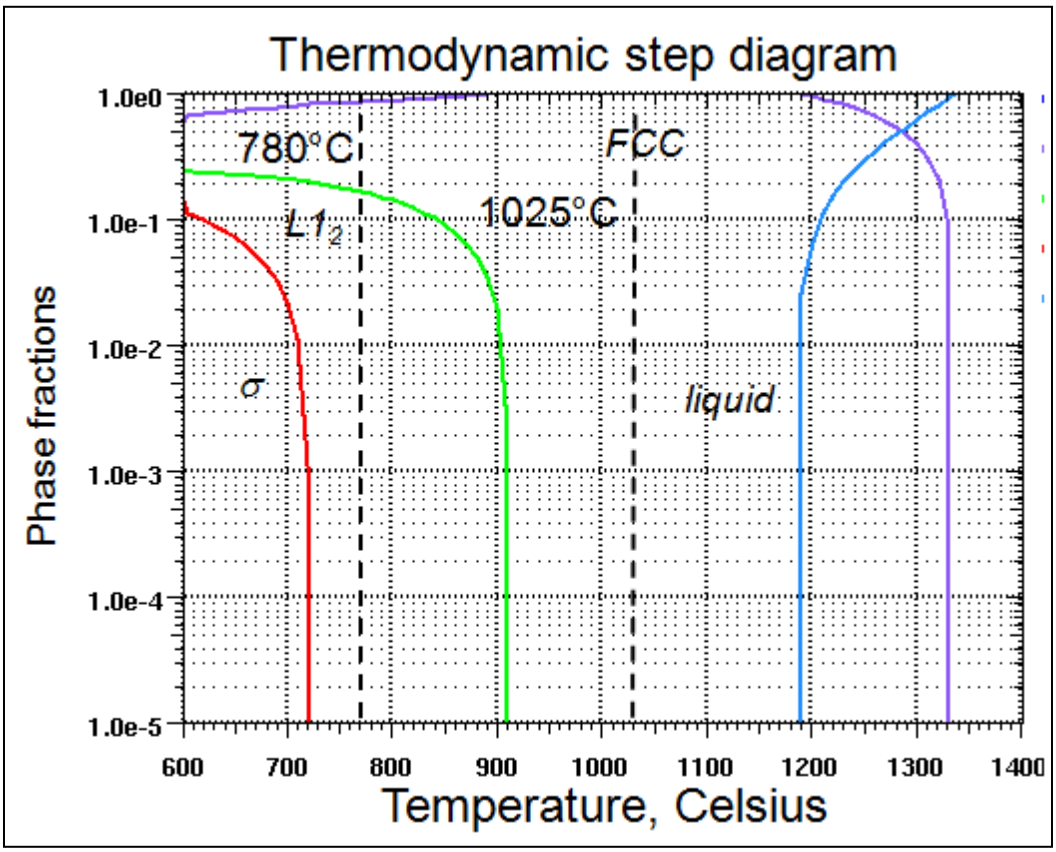

At the aging treatment of 780º C, $L1_2$ particles are predicted to form in a FCC matrix.

Figure 28. Calculated Thermodynamic Step-Diagram for NGCo-1A Alloy, Showing the Phases Present and their Equilibrium Amounts at Different Temperatures

As seen from the above diagram, at 1025º C, the system is in a 100% FCC state. After aging at 780º C for 24 hrs, the system is designed to be in a two-phase FCC+$L1_2$ phase with $L1_2$ precipitates inside an FCC matrix. Samples were analyzed on the atom-probe using a laser evaporation mode to characterize achieved precipitate structure. The atom probe extracts atom as ions from the sample and information from an identified specimen section is reconstructed so mapping of the composition can be evaluated. Two different specimens were analyzed – resulting in total runs of 21.3 million ions and 10.1 million ions respectively. The results from

Use or disclosure of data contained on this sheet is subject to the restriction on the title page of this proposal.
Northrop Grumman Private/Proprietary Level I

both runs were very similar. The atom-probe reconstruction from the longer run is shown in Figure 29.

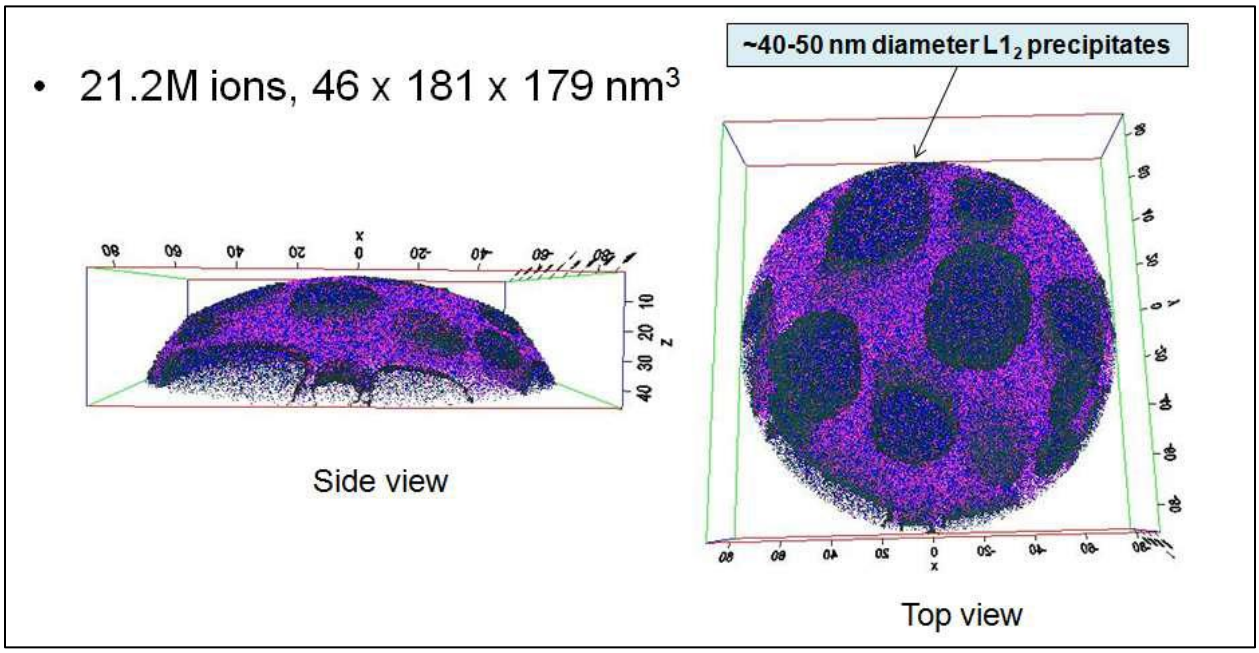

The field of view is 46nm x 181nm x 179nm. The diameter of the $L1_2$ particles is ~ 40-50nm.

Figure 29. Atom-probe Reconstruction of the NGCo-1A Alloy, Showing the Presence of $L1_2$ Particles in a FCC Matrix, as Predicted

As seen from Figure 29, the existence of the two-phase field and the presence of 40-50nm diameter $L1_2$ particles in an FCC matrix are confirmed. The particles had cuboidal morphology. The matrix and particle compositions were measured and are shown in Table 6, compared against the predicted compositions from the thermodynamic calculations:

Table 6 Comparison Between Measured and Predicted FCC and $L1_2$ Phase Compositions

Due to the excellent agreement between the predicted and measured equilibrium FCC compositions, and the accuracy of predicting the FCC+$L1_2$ two-phase field, further revision of the thermodynamic database is not deemed necessary.

Element	Measured (atom-probe)		Predicted (ThermoCalc)	
	FCC, in at%	$L1_2$, in at%	FCC, in at%	$L1_2$, in at%
Co	59.5	64.3	60.0	65.8
Cr	24.3	9.7	23.5	1.7
Fe	9.2	4.1	9.1	0.7
Ti	2.9	14.1	2.8	22.9
Ni	2.6	5.1	2.5	7.7
V	1.5	2.7	2.1	1.2

As seen from Table 6, there is excellent agreement between the measured and predicted matrix compositions. For the particle compositions, there is some discrepancy between the

Use or disclosure of data contained on this sheet is subject to the restriction on the title page of this proposal.
Northrop Grumman Private/Proprietary Level I

measured and predicted, particularly related to the Cr and Fe concentrations in the particle. The reasons for the discrepancy could be as follows:

1. The precipitates are not yet at their equilibrium composition state, and have higher non-equilibrium Cr and Fe to reduce the lattice misfit with the matrix
2. The increased Cr and Fe is an artifact from matrix overlap, due to the fine size of the precipitates.

In order to evaluate if the yield point of the NGCo-1A alloy was being controlled by FCC to -HCP transformation, an x-ray diffraction study of the gage section of a fractured tensile specimen was undertaken. The measured X-ray peaks are shown in Figure 30. One can clearly see the presence of the HCP (101) peak. X-ray diffraction of samples prior to testing showed no presence of HCP phase. This clearly proves that the HCP phase is forming during the tension testing process. However, the presence of the HCP phase by itself is not conclusive proof that the low yielding is due to the formation of the HCP phase. The HCP phase could also have been strain-induced instead of being stress-induced; i.e. it was formed after yielding occurred. In order to get a better understanding of the role that the stress plays in formation of the HCP phase, QuesTek conducted a Bolling-Richman test[4] to determine the Msσ temperature (temperature at which stress-induced HCP can form). The sample for the Bolling-Richman test was fabricated from a piece sent to QuesTek by NGC.

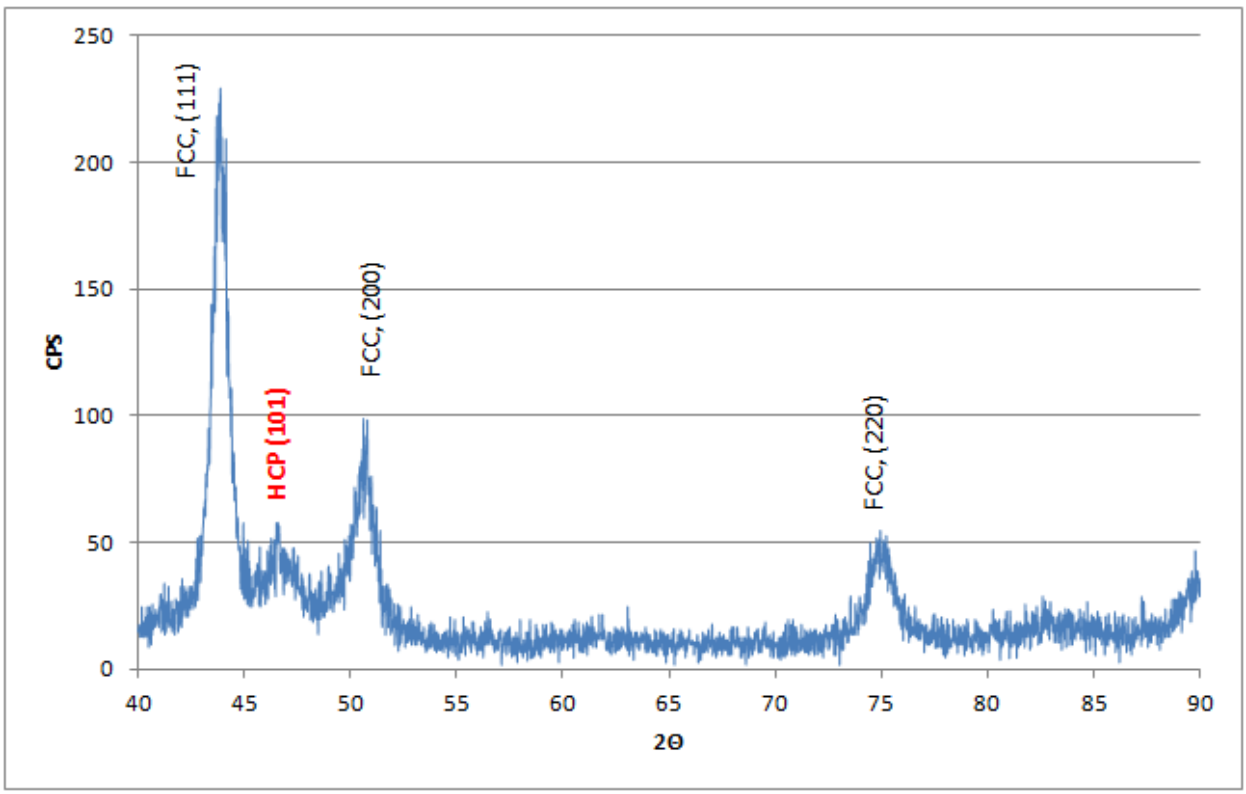

Figure 30. Measured X-ray Diffraction Peaks of the Gage-Section of a Fractured Tensile NGCo-1A Specimen, using a Cu Kα Source

To resolve the outstanding question of transformation being strain-induced (after yield) or stress-induced Bolling-Richman tests were performed on the NGCo-1A to investigate its Msσ

Use or disclosure of data contained on this sheet is subject to the restriction on the title page of this proposal.
Northrop Grumman Private/Proprietary Level I

behavior. The tests showed that the Msσ NGCo-1A was below the temperature capabilities of the instrument (i.e., below 70° C), which establishes that the yield stress of the NGCo-1A specimens were *not*, in fact transformation limited.

Based on the previous results from the 30 lb. ingot ("NGCo-1A"), a number of small adjustments to the design/specification for the 500 lb. ingot ("NGCo-2A") were made:

- The target compositional ranges for the NGCo-2A ingot were shifted slightly to reflect the *actual* compositions obtained from the NGCo-1A ingot Figure 31
- A minor addition of boron (0.005 wt.% = 50 ppm) was incorporated in the NGCo-2A specification to enhance grain boundary cohesion
- The LEAP analysis of the NGCo-1A alloy showed the expected $L1_2$ strengthening particles, but the compositional analysis of the particles indicated that the system may not yet be at equilibrium. Hardness tests indicated that NGCo-1A would see an additional strength increase if the final ageing time (at 780° C) was increased from 24 hours to 48 hours (see Figure 32).

QUESTEK INNOVATIONS LLC
1820 Ridge Avenue, Evanston, IL 60201

MATERIAL SPECIFICATION

QMS-NGCO-2A
Initial Release
Draft Date October 23, 2012

Cobalt Chrome alloy, Bars and Rods
Co -17.5Cr - 7.5Fe - 5.5Ti - 2.5Ni - 2.0V- 0.005C – 0.005B
Vacuum Induction Melted, Vacuum Arc Remelted

QUESTEK INNOVATIONS LLC

QMS- NGCO-2A **QMS- NGCO-2A**

Element	min	target	max
Carbon	0.004 (40 ppm)	0.005 (50 ppm)	0.0100 (100 ppm)
Manganese	--	--	0.002 (20 ppm)
Silicon	--	--	0.004 (40 ppm)
Phosphorus	--	--	0.002 (20 ppm)
Sulfur	--	--	0.002 (20 ppm)
Chromium	17.0	17.5	18.0
Nickel	2.3	2.5	2.7
Titanium	5.3	5.5	5.7
Iron	7.3	7.5	7.7
Vanadium	1.9	2.0	2.1
Oxygen	--	--	0.006 (60 ppm)
Nitrogen	--	--	0.0005 (5 ppm)
Boron	0.004 (40 ppm)	0.005 (50 ppm)	0.0100 (100 ppm)

Figure 31. Composition by Weight % of NGCo-2A after Minor Modifications

Use or disclosure of data contained on this sheet is subject to the restriction on the title page of this proposal.
Northrop Grumman Private/Proprietary Level I

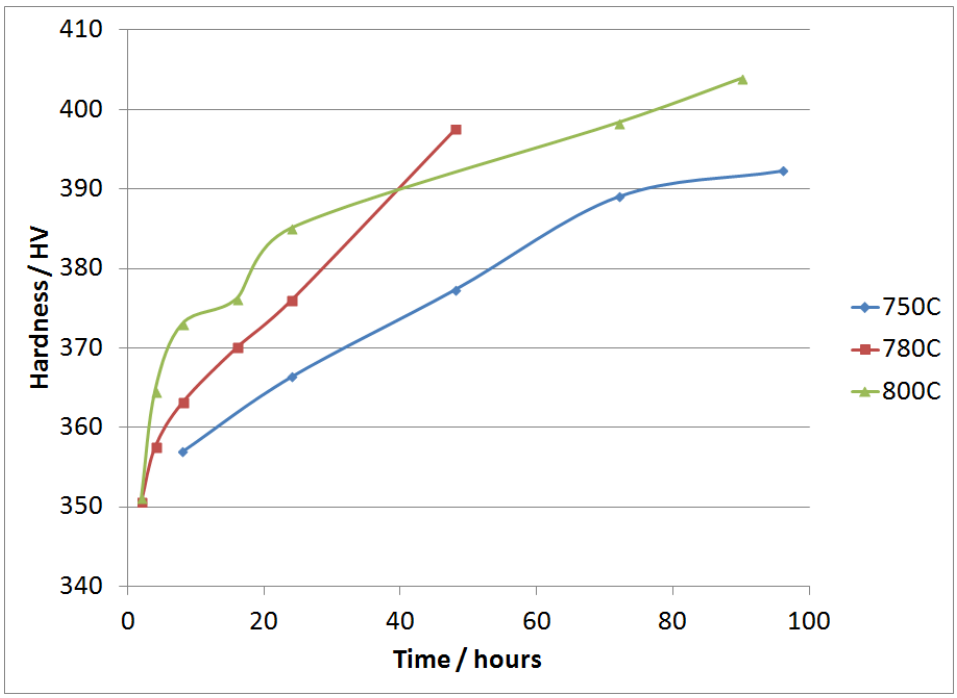

Figure 32. Temper Evaluation Shows Increased Hardness at Lower Temperature for Longer Time

QuesTek made three adjustments to achieve a target yield strength level of ~140 ksi for the NGCo-2A alloy.

The production path for the NGCo-2A alloy is shown in Figure 33. QuesTek was requested to process sufficient lengths of both ~ 4" OD and ~2" OD material in order to support characteristics comparison testing of the larger diameter product

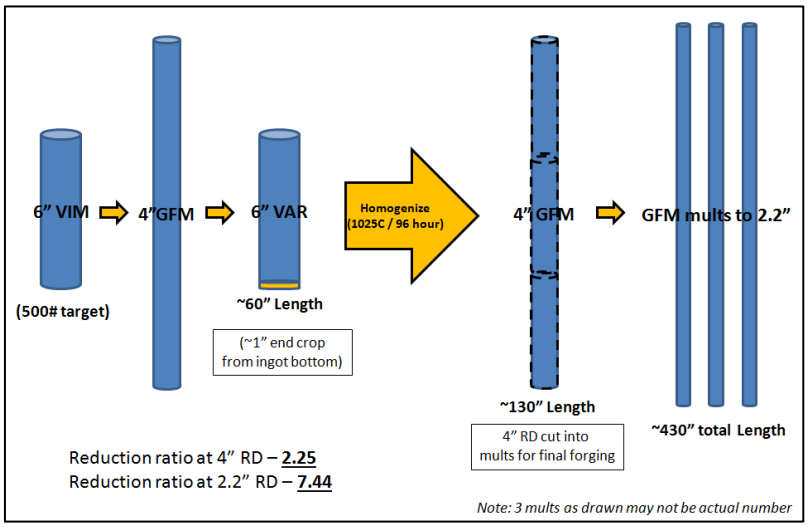

Figure 33. Production Process of NGCo-2A 2nd Generation Material

Use or disclosure of data contained on this sheet is subject to the restriction on the title page of this proposal.
Northrop Grumman Private/Proprietary Level I

During this 2nd round of prototyping the cobalt alloy encountered fracturing of the product during a forging step intermediate between VIM and VAR melting steps and broke into pieces and was declared unsuccessful. Figure 34 shows the fracturing of VIM ingot and the pieces that broke off into the machines catch area during the process.

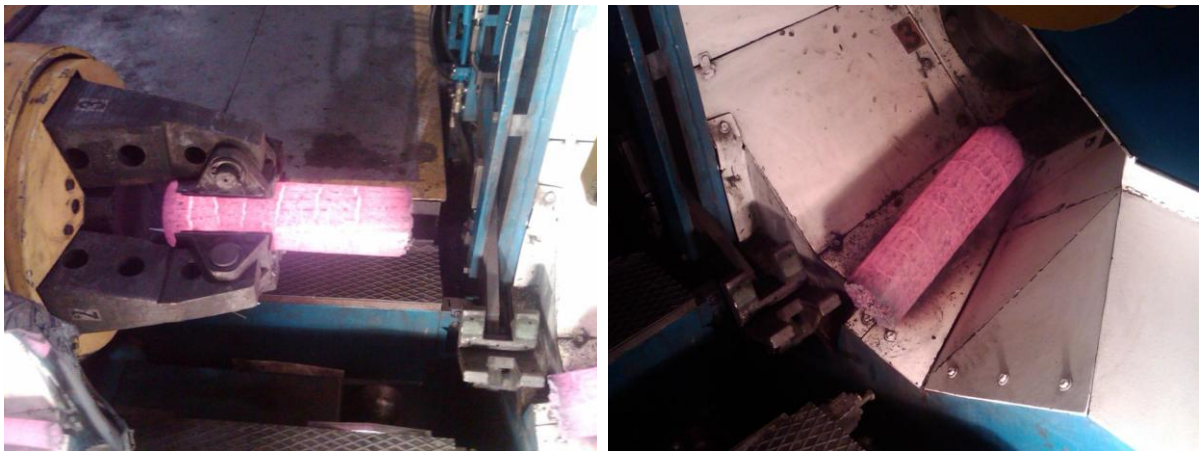

Figure 34. Forging Failure of NGCo-2A at 1175º C

Additional heat treatment optimizations of the NGCo-1A design also indicated a risk that this alloy may not achieve the program targeted yield strength goals. To reduce the risk of achieving the program targets, the alloy was redesigned, and a new round of production of the re-designed "NGCo-3A" concept alloy was initiated.

2.4.2.2.1 Final NGCo-2A Alloy and Process Selection

Alloy:

- Co-Cr-Ti-Ni-Fe-V alloy
- Melt alloy at 500 lb sub-scale – 4" VAR to 6"

Process:

- Melt alloy 6" VIM at 500 lb sub-scale (Metalwerks / Aliquippa, PA.)
- Rotary Hammer Forge (GFM) from 6" VIM to 4" Round
- VAR from 4" to 6" Round
- Homogenize at 1025º C for 96 hours
- Forge to 4" round and cool to cut mults for final forging
- Forge to 2.2" round final cleanup 2" round
- Production was unsuccessful due to processing above solvus temperature

2.4.2.3 Design of NGCo-3A Alloy

Production of a 500 lb heat of NGCo-3A was initiated at MetalWerks PMD, Inc. (Aliquippa, PA) on February 18, 2013, with a quoted lead time of 8 weeks to produce forged product. Figure

Use or disclosure of data contained on this sheet is subject to the restriction on the title page of this proposal.
Northrop Grumman Private/Proprietary Level I

35 details the production path utilized to produce the NGCo-3A prototype material. All steps from VIM to Forging were completed at MetalWerks, with final heat treatment being completed at Bodycote Santa Fe Springs, CA.

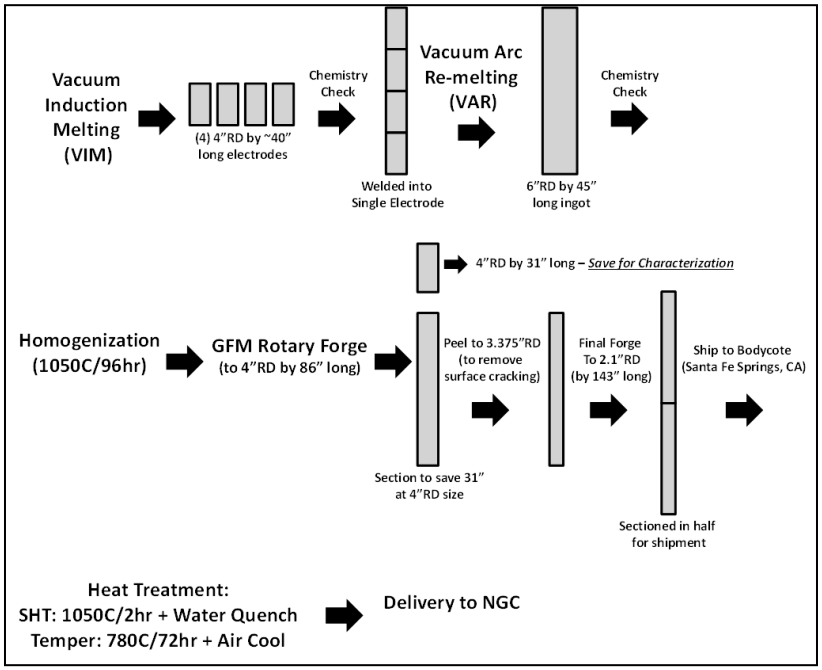

Figure 35. Schematic Detailing the MetalWerks Production Path for the NGCo-3A Alloy

MetalWerks was tasked with melting, homogenizing and forging the product, which represents all major processing steps except final heat treatment. The product was melted by Vacuum Induction Melting (VIM) at the 500 lb scale, and cast into four (4) 4 inch round by ~40 inch long bars. These bars were welded together into a single *electrode*, and Vacuum Arc Remelted (VAR) into a single 6-inch round by ~45 inch long ingot. During VIM, a portion of the melt contains excessive slag that is not cast with the rest of the product. This "*heel*", as it is referred to, was approximately 125 lb. Furthermore, the top section of the VAR ingot was removed to eliminate excessive shrinkage porosity left over from casting. Combined with the material loss during VIM, the removal of this "*hot top*" resulted in a final cast ingot weight of 315 lb.

Chemistry analysis was completed at IMR Test Labs (Lansing, NY) on both the VIM and VAR ingots, in order to verify the achieved chemistry relative to production targets. The VIM and VAR chemistry results are presented in Table 7. All results are within the target ranges, except for carbon and oxygen contents. Though only slightly below the target range, a low carbon content may be of concern with grain refinement in the alloy. Grain pinning carbides assist in maintaining a fine-grained structure through high temperature processing (homogenization, forging and solution treating), which can have a beneficial impact on mechanical properties such as static and fatigue strengths. This low carbon content may result in a less than optimal grain size, though the slight variation from the target level suggests that the impact should not be substantial. The slightly high oxygen content may lead to more than expected oxide formation, reducing the cleanliness of the microstructure. This may affect the

Use or disclosure of data contained on this sheet is subject to the restriction on the title page of this proposal.
Northrop Grumman Private/Proprietary Level I

ductility and fracture behavior (both statically and in fatigue) of the alloy by introducing stress-concentrations at inclusions. The amount of oxygen retained in the alloy is not significant, however, and the effect of this level of oxygen is expected to be minimal.

Table 7. Chemistry Results (in weight %) Measured from the VIM Electrode and the VAR Ingot of NGCo-3A, Compared against the Production Target Ranges

Element	Target (Min—Max)	VIM Chemistry	VAR Chemistry
Cr	16.6 (16.1—17.1)	16.69	16.5
Fe	7.1 (6.9—7.3)	7.15	7.1
Ti	6.3 (6.1—6.5)	6.14	6.2
Ni	2.7 (2.5—2.9)	2.75	2.8
V	2.0 (1.9—2.1)	2.02	2.0
C	0.005 (0.004—0.01)	0.0013	0.0031
B	0.005 (0.004—0.01)	0.0072	0.0085
S	-- (0.002 Max)	0.0005	<0.001
O	-- (0.006 Max)	0.0095	0.007
N	-- (0.0005 Max)	<0.0005	0.0002

Following production of the VIM/VAR ingot, the ingot was homogenized at 1050° C (+/-14° C) for 94 hours. The homogenization treatment was completed on April 9, 2013. The product was then forged directly from homogenization by a GFM rotary forging process. Figure 36 contains example images of the GFM used at MetalWerks, detailing the multi-axial forging hammers and showing an example of a product being forged in the machine.

Use or disclosure of data contained on this sheet is subject to the restriction on the title page of this proposal.
Northrop Grumman Private/Proprietary Level I

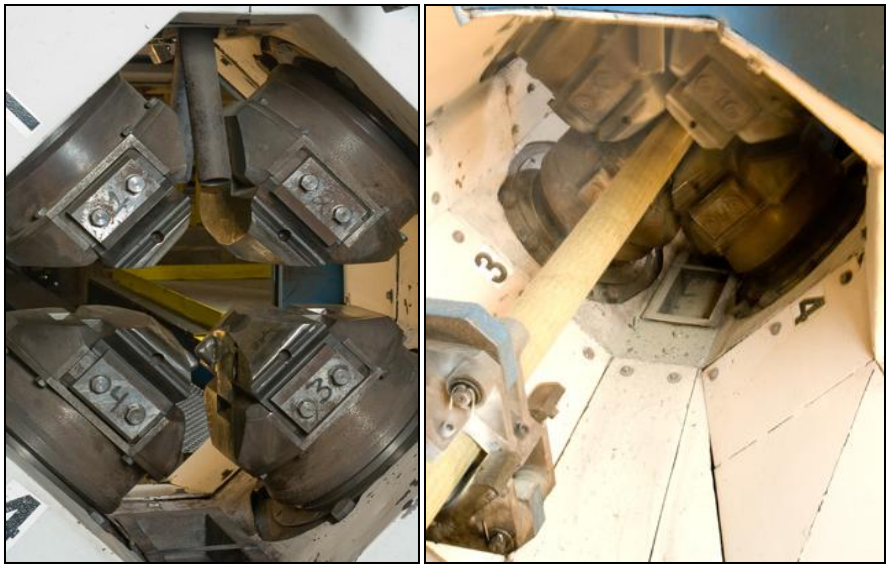

Figure on left details the multi-axial forging hammers and dies, and the figure on the right shows an example of product being forged in the machine.

Figure 36. Example images of the GFM at MetalWerks

The input billet size was 6-inches in diameter by 40 inches long. The product was forged at 8% reduction in area per pass through the GFM dies, and was forged down to 4 inches in diameter (using 9 total passes through the machine). The actual forged diameter was measured at 3.92-inches, and the total forging reduction experienced by the material at this product size was approximately 2.3. To maintain the forging temperature near 1050° C, the product was reheated for 30 minutes after 4 passes. As such, 3 reheats were needed during the initial forging of the product to 4 inch round. Forging was interrupted at the 4-inch round product size and the product was allowed to cool to room temperature, in order to cut the billet into manageable lengths for final forging to 2 inch round. The final billet length at 4-inch round was 86 inches. Figure 37 contains images of the 4-inch round product immediately after forging.

Figure 37. NGCo-3A, Immediately after Forging to the Intermediate 4 Inch Round Product Size. Total Length is 86 Inches

Use or disclosure of data contained on this sheet is subject to the restriction on the title page of this proposal.
Northrop Grumman Private/Proprietary Level I

Upon cooling to room temperature, a 31 inch length was sectioned from the bar to allow for property characterization at this product size. It is important to note that the forging reduction ratio of 2.3 at this product size is not a significant amount of forging reduction. As such, it may be expected that the mechanical properties of this product will not be as high as they would be in product that has experienced a greater forging reduction. Typically, for steel alloys, a forging reduction ratio closer to 7 is desirable to produce optimal mechanical properties, although its application to this cobalt alloy has not been investigated.

It was noted that upon cooling to room temperature, some surface cracking developed in the 4 inch product. Since these cracks would continue to propagate through the material in final forging, it was determined that the product needed to be peeled to remove the cracks. The material was peeled to a diameter of 3.875 inches to remove these surface cracks prior to final forging. Die penetrant testing was used to ensure the surface cracks were fully removed by this intermediate peeling step. Figure 38 shows an image of the 4 inch round product during dye penetrant testing, showing the extensive surface cracking in the product prior to final peeling to 3.875 inch.

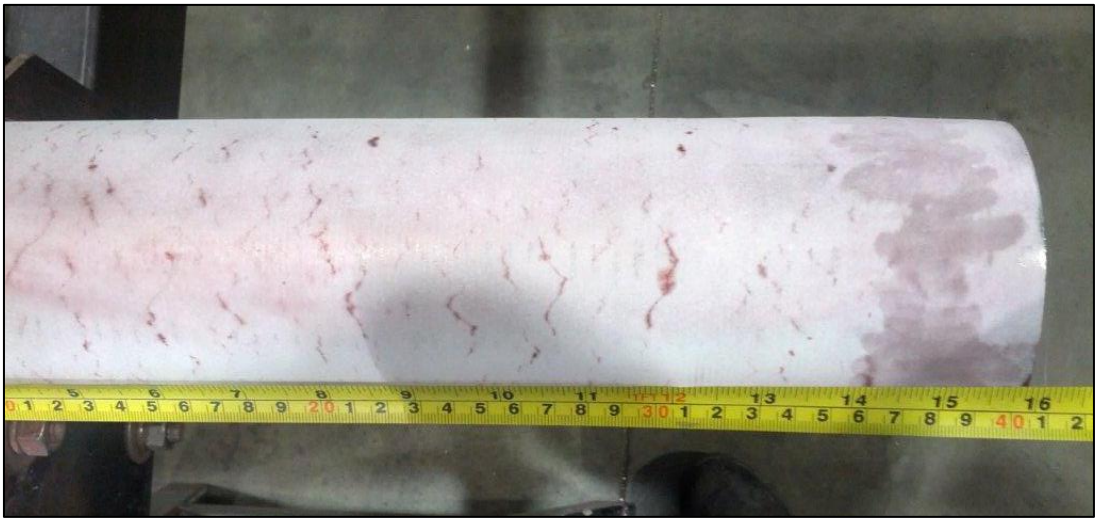

Figure 38. Example Image of NGCo-3A 4 Inch Round Product During Dye Penetrant Testing (Prior

Use or disclosure of data contained on this sheet is subject to the restriction on the title page of this proposal.
Northrop Grumman Private/Proprietary Level I

to Peeling to 3.875 Inch Diameter)

Following peeling, the remaining 55 inch long bar was forged at 1050° C to a final diameter of 2.1 inch. A final length of 143 inches of 2.1 inch round bar was produced, with a cumulative forging reduction ratio of approximately 5. Immediately after forging, the bar was wrapped in a Kaowool-type insulating wrapping to slow the cooling rate, in an effort to mitigate surface cracking due to the development of residual stresses on cooling. An image of the 2.1 inch product after forging and cooling is shown in Figure 39.

Use or disclosure of data contained on this sheet is subject to the restriction on the title page of this proposal.
Northrop Grumman Private/Proprietary Level I

Total length of the 2.2 inch diameter bar is 143 inches.

Figure 39. NGCo-3A, after Forging to the Final 2.1 Inch Round Product Size

Some surface cracking was noted in the top approximately 36 inches of the bar after cooling (far right in Figure 39). The remaining length of material was largely free of significant surface cracking. Additionally, the ends of the bar showed indications of "suck-in", an effect of the GFM process where material at the ends of the bar gets folded in. This "suck-in" effect is normal in the forging process, and it is likely to have caused entrapment of surface oxidation within the microstructure of material near these ends. This folded-in oxidation can be detrimental to mechanical properties by acting as a source for internal cracking, and so should be avoided when analyzing for mechanical properties. Approximately 7 inches of the material were removed from the top end of the bar, but the bottom end was left intact through final shipment to Northrop Grumman.

This bar was sectioned into two bars prior to shipment, each approximately 6 feet in length. Three bars in total (two at 2.1 inch by 72 inch long and one at 4 inch by 31 inch long) were shipped to QuesTek on May 6th 2013, which completed all production steps at MetalWerks.

The final production step following forging was heat treatment. An end crop from the VAR ingot had been obtained by QuesTek, homogenized in house, and used for a heat treatment response study. Mimicking the thermal processing experienced by the full product, the VAR crop material was homogenized at 1050° C for 96 hours, air cooled, then solution treated at 1050° C for 2 hours and water quenched. Individual specimens were then aged at 780° C for various times to assess the precipitation response of the alloy. As presented in Figure 40, peak hardness is achieved after aging at 780° C for 72 hours. This aging condition was used to heat treat the forged product.

Use or disclosure of data contained on this sheet is subject to the restriction on the title page of this proposal.
Northrop Grumman Private/Proprietary Level I

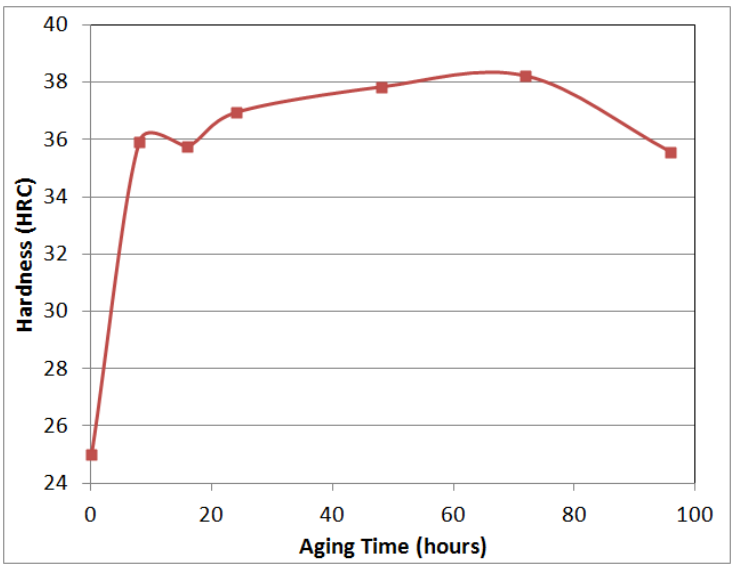

Zero hour aging time taken to be the as-solution treated hardness.

Figure 40. NGCo-3A VAR End Crop - Hardness Response Study at an Aging Temperature of 780° C

The forged product was heat treated at Bodycote, Santa Fe Springs, CA. The heat treatment schedule applied by Bodycote prior to final delivery for property characterization was:

1. Solution heat treatment at 1050° C for 2 hours + Water Quench
2. Aging (within 4 hours of quenching) at 780° C for 72 hours + Air Cool

All three bars were heat treated together as a single load. Time and temperature were controlled with a load thermocouple attached to the 4 inch product, since this product experiences the slowest heating rate. Inspection of furnace charts indicates that the prescribed heat treatment schedule was correctly applied. Upon final heat treatment, all NGCo-3A products were shipped directly to Northrop Grumman for property characterization.

Following alloy prototyping, some preliminary metallurgical characterization was completed at QuesTek to validate the results of the material processing. This included hardness microstructural evaluation of forged and heat treated material, and preliminary tensile testing with coupons heat treated at QuesTek.

Material from the NGCo-3A 2.1 inch product was heat treated at QuesTek in its full 2.1-inch diameter product form. A ~6 inch segment of material was removed from the extreme top of the bar (that is, the end of the forged piece that was the top end of the VAR ingot). Two ASTM E8 standard tensile specimens (0.25” gage diameter) were excised from the heat treated bar.

Hardness and microstructure samples were also excised from the mid-radius of the bar. Hardness was measured by both Rockwell C (HRC) and Vickers (HV) methods, taking a minimum of 12 measurements per sample. Average hardness was measured at 37.7 HRC, or 408 HV. A small slice of 2.1 inch product was also excised from the bars that were heat treated at Bodycote and sent to QuesTek for validation of the heat treatment. Hardness measurements at mid-radius of this product averaged 37.2 HRC, in good agreement with the results obtained from material heat treated at QuesTek.

Figure 41 contains detailed optical micrographs of the rotary forged and heat treated NGCo-3A 2.1 inch product microstructure. The microstructure primarily consists of equiaxed, twinned

Use or disclosure of data contained on this sheet is subject to the restriction on the title page of this proposal.
Northrop Grumman Private/Proprietary Level I

grains, with grain diameters on the order of 75-100 micrometers. Grain boundaries are largely free of cellular growth and heterogeneous precipitation, evidence that the heat treatment conditions were acceptable and that the alloying content is not too high. There are notable oxide inclusions in the micrographs, which show up as large black-colored particles drawn out in the forging direction. This microstructure sample was excised from the extreme end of the forged bar, in a region of material that is affected by "suck-in" during rotary forging. This "suck-in" effect is the folding-in of surface material at the ends of the bar during forging. This surface material includes oxide scale, which becomes trapped up internally as material is folded in. This is a typical result of the forging process, and often these "sucked-in" ends are removed prior to shipment. In an effort to save as much material as possible for mechanical property characterization, it was deemed acceptable to use this material for microstructural validation.

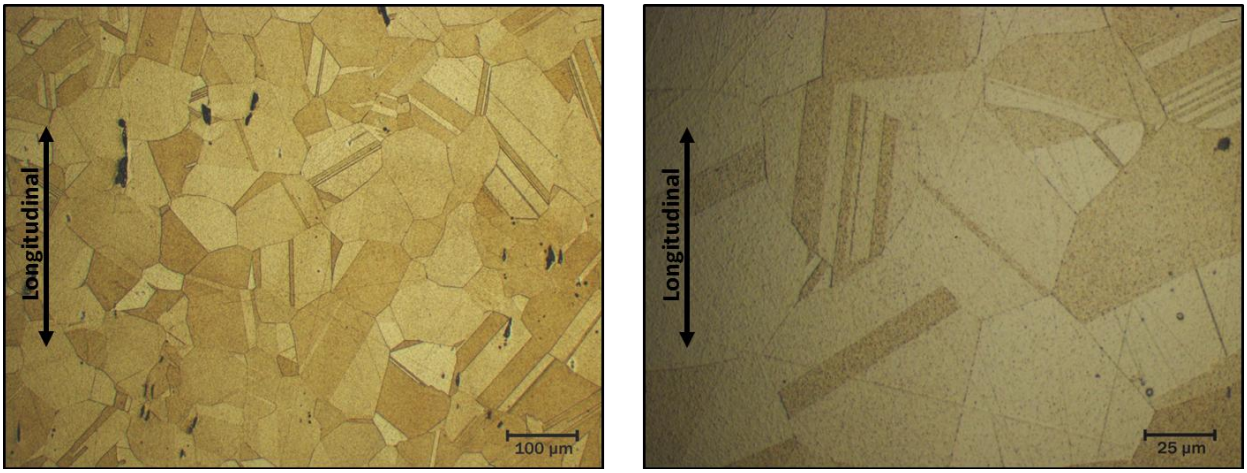

Samples were etched in a solution of 5 mL H_2O_2 + 100 mL HCl. The longitudinal direction of the bar is oriented vertically in each micrograph.

Figure 41. Optical Micrographs of Rotary Forged NGCo-3A, 2.1 Inch Product, at Different Magnifications

Table 8 presents the characterization of tensile properties for the SMF Cuprium and NGCo-3A prototypes. The Co-based NGCo-3A meets all property targets of the program except tensile yield strength. SMF Cuprium successfully achieves the target tensile yield strength, but falls short of the tensile strength and hardness goals.

Use or disclosure of data contained on this sheet is subject to the restriction on the title page of this proposal.
Northrop Grumman Private/Proprietary Level I

Table 8. Summary of Tensile Test Data Collected from the 2nd Generation Prototype Alloys
(Cuprium and NGCo-3A 2.1 inch round product), plotted against 1st generation prototype results, baseline AMS 4533 data, and the program goals.

Alloy	0.2% Offset Yield Strength (ksi)	Tensile Strength (ksi)	Elongation (%)	Hardness (HRC)	Density (lb/in^3)
Program Goals	*>140*	*>165*		*36-45*	
AMS 4533 (Baseline)	164.8	182.2	5.4	40	0.289
NGCu-1A	63.9	113.3	29.3	25	0.307
NGCo-1A	119	194	40	36	0.296
Cuprium	142	158	15	31-33	0.318
NGCo-3A	126	199	33	37-38	0.297

After evaluating the latest characteristics results obtained from both 2nd generation copper and cobalt based alternative materials an engineering decision was made to move forward with the NGCo-3A alloy as it having the best drop - in replacement potential. Materials characterization results are detailed in follow-on sections along with additional comparison characteristics evaluations performed on the down-selected NGCo-3A which support this decision.

In falling short of the program's desired tensile strength, an effort was made to obtain additional funding to further the design and development of the NGCo-3A so the materials full properties potential could be ascertained. Although the additional program funding was not available the funds remaining in the program were able to support a supplemental small scale optimization effort which is detailed below.

2.4.2.3.1 Final NGCo-3A Alloy and Process Selection

Alloy:

- Co-Cr-Ti-Ni-Fe-V alloy
- Melt alloy at 500 lb sub-scale – 4" VAR to 6"

Process:

- Melt alloy composition VIM at 500 lb sub-scale (Metalwerks / Aliquippa, PA.)
- Produce four - 4" X 40" round electrodes
- Weld into single electrode

Use or disclosure of data contained on this sheet is subject to the restriction on the title page of this proposal.
Northrop Grumman Private/Proprietary Level I

- VAR from 4” to 6” Round
  - Homogenize at 1050º C for 96 hours
  - Rotary Hammer Forge (GFM) 6” round to 4” round and cool
    - 6” round to support a higher material reduction ratio
  - Peel outer surface to cleanup surface cracking anomalies and cut mults for final forging
  - Rotary Hammer Forge to 2.1” round and final cleanup 2” round

2.4.2.4 Optimized Design of NGCo-3A

With 2nd Generation alloy NGCo-3A meeting all property goals but tensile yield strength, a follow-on effort was undertaken to assess the feasibility of improving the yield strength of the alloy through further process optimization. This follow-on effort was organized into three main tasks according to the following Gantt chart Figure 42. The effort included modeling work to identify potential modifications to the heat treatment schedule for improved strength (Task 1), an additional round of prototyping to produce material with a proper chemistry for feasibility demonstration (Task 2), and a final task of characterization of the newly produced material for its achieved strength (Task 3).

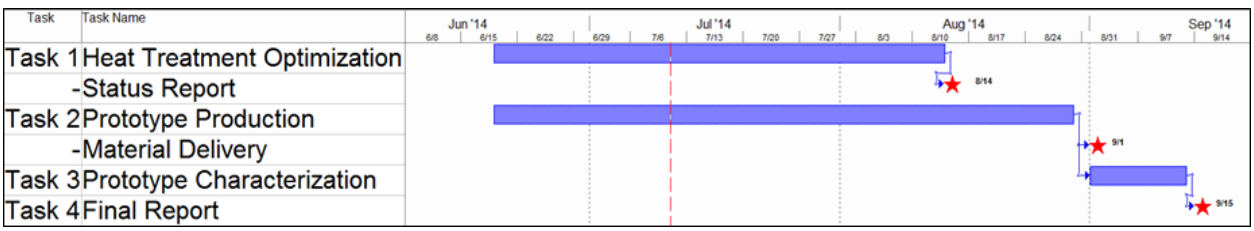

Figure 42. Gantt chart showing tasks to be performed for NGCo-3A Material Optimization

The goal of this task is to assess the feasibility of achieving higher strength in the NGCo-3A alloy through further optimization of the thermal processing. In particular, QuesTek has revisited the aging treatment to determine more efficient precipitation strengthening. Higher degrees of precipitation strengthening can be achieved through higher precipitate phase fractions or refined precipitate sizes and distributions, each of which is primarily controlled by the aging treatment (temperature and time).

QuesTek has applied its PrecipiCalc® software (commercially available as TC-Prisma through ThermoCalc®) to simulate a range of aging treatments that target higher precipitate strengthening by these means.

As this tool is rooted in the fundamental kinetics of multicomponent precipitation theory, PrecipiCalc has been successfully applied to a broad range of alloy systems including Fe, Ni, Cu, Ti, etc. The key inputs to PrecipiCalc are thermodynamic and kinetic databases, which are fundamental databases that describe phase stability and transformation kinetics within multicomponent systems. Such databases were developed by QuesTek in the Phase I of this program, since no commercial databases are currently available for cobalt alloy systems. To apply precipitation modeling to the NGCo-3A alloy design, these databases needed to be calibrated and refined using experimental data to ensure effective predictive capability. QuesTek

Use or disclosure of data contained on this sheet is subject to the restriction on the title page of this proposal.
Northrop Grumman Private/Proprietary Level I

has collected atom probe tomography (LEAP) data at three distinct aging conditions for the NGCo-3A alloy – under-aged (2 h), peak aged (72 h) and over-aged (260 h) conditions at 780° C aging temperature. From this analysis, precipitate size and fraction and accurate chemistries of the different phases is precisely measured and used to calibrate and refine the predictions made with QuesTek's thermodynamic databases. These LEAP reconstructions and corresponding phase chemistry information is presented in Figure 43. This experimental data was used to calibrate QuesTek's Co-alloy database for refined predictions of precipitate evolution during aging.

Refinement of Thermodynamic databases using new LEAP analysis of γ' particle evolution at 780°C in NGCo-3A alloy

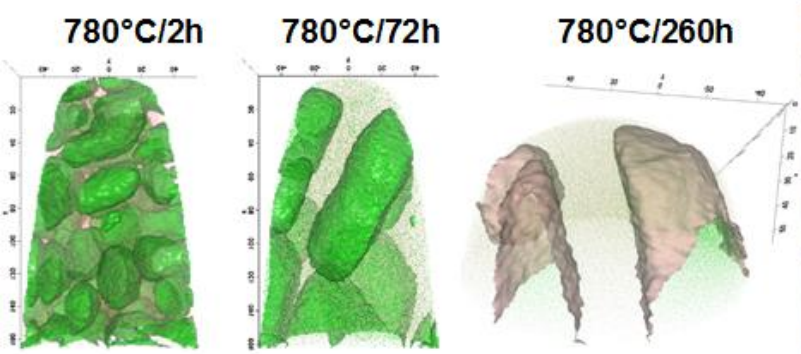

Temper Time at 780°C	2 hr	72 hr	260 hr	QT Database
Size [nm]	35	90	-	-
Vol. Frac. [%]	23.09	21.44	-	(21.76)
γ matrix [atomic%]				
Cr	24.92	25.14	24.70	22.56
Co	57.29	58.91	59.35	61.11
Ni	3.90	2.35	2.30	1.86
Ti	2.78	2.78	2.73	3.02
Fe	9.15	8.86	8.99	8.98
V	1.85	1.87	1.81	2.46
γ' precipitates [atomic%]				
Cr	10.87	10.78	10.91	1.72
Co	62.42	64.00	64.36	67.80
Ni	5.85	4.39	4.12	5.69
Ti	13.46	13.38	13.34	22.73
Fe	4.15	4.06	4.09	0.71
V	3.07	3.11	2.98	1.35

Figure 43. Experimental LEAP Analyses of the NGCo-3A used to Calibrate QuesTek's Co Thermodynamic Databases in Preparation for PrecipiCalc Simulations

Kinetic databases also needed refinement. This database assesses the diffusivities of all components in a multicomponent alloy system, and is a key input into a PrecipiCalc simulation of precipitate nucleation and growth as it provides the necessary inputs to describe the phase transformation kinetics. QuesTek has collected available literature data for diffusivities in cobalt alloys and is using this to calibrate a Co kinetic database. An example of such calibration is shown in Figure 44. This figure compares an example of the existing database of diffusivity of Cr in FCC-Co to available literature data. The database has been refined to correct for the types of discrepancies from the experimental data.

Use or disclosure of data contained on this sheet is subject to the restriction on the title page of this proposal.
Northrop Grumman Private/Proprietary Level I

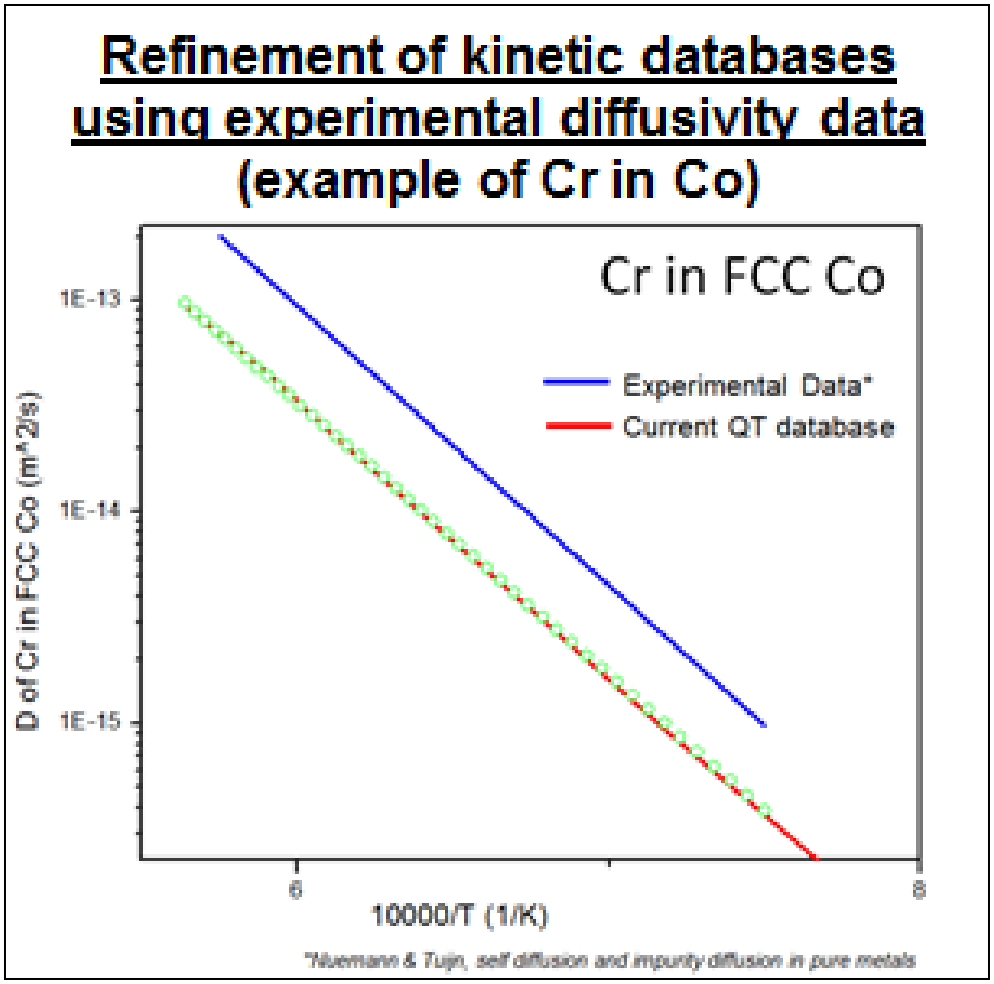

Figure 44. Example of Experimental Diffusivity Data (from literature) used to Calibrate QuesTek's Co Kinetics Databases in Preparation for PrecipiCalc Simulations

Using these refined databases; QuesTek applied its PrecipiCalc precipitation simulator to model the effect of varying aging treatments on the predicted strength of the alloy. Figure 45 plots the predicted increase in strength during aging at various temperatures (isothermal aging curves) and treatment durations (0 to 400 hours). The condition highlighted by the blue star is that applied to the Phase I material shown to have a yield strength of 126 ksi. These isothermal predictions suggest that there is minimal potential to increase the tensile yield strength much further than that already achieved through optimization of the aging treatment alone (without exceeding a 400 hour aging time, which is not economical). Two-step (non-isothermal) aging simulations were run as well, but these also did not suggest strong potential for improved yield strength either.

Use or disclosure of data contained on this sheet is subject to the restriction on the title page of this proposal.
Northrop Grumman Private/Proprietary Level I

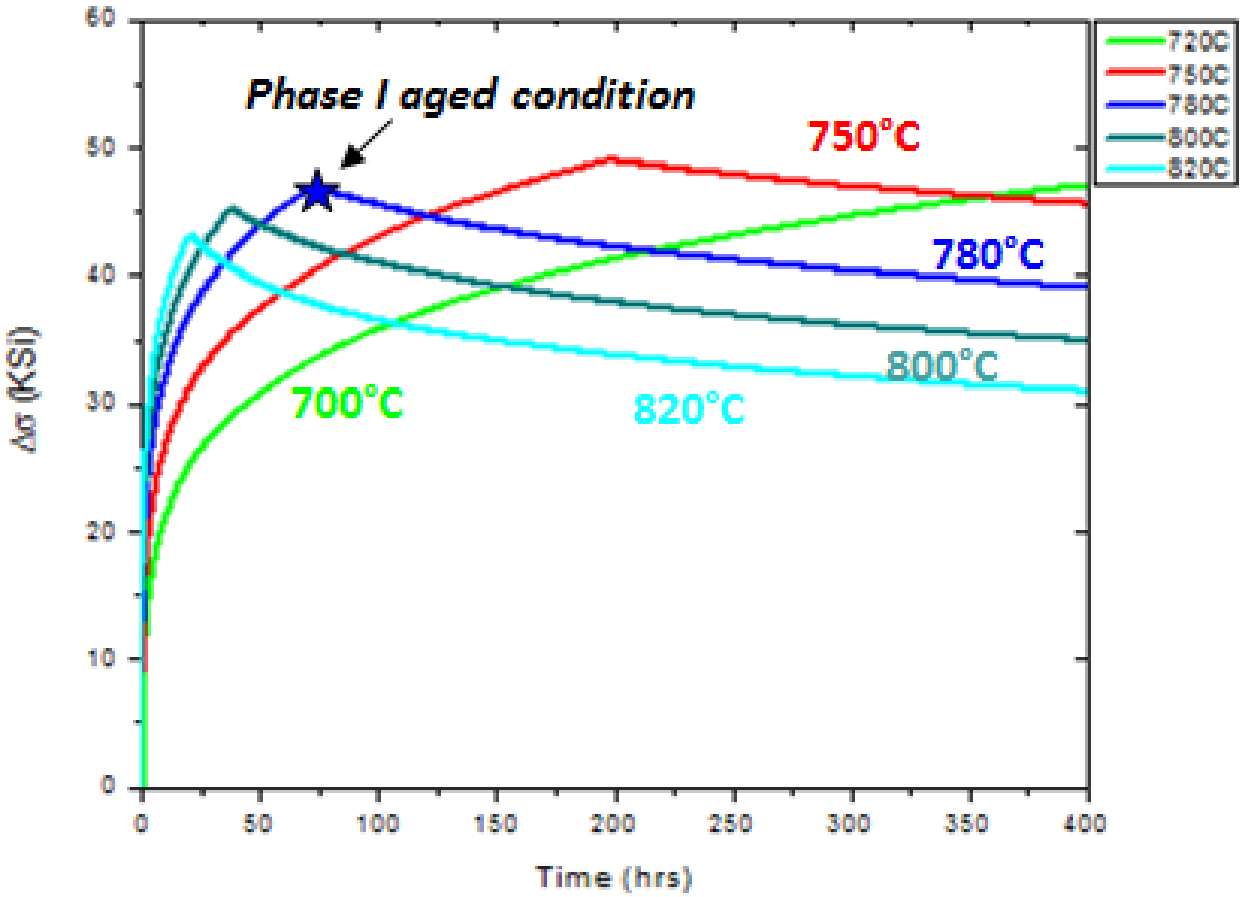

Alloy showing the predicted increment in yield strength due to precipitation of Co_3Ti during aging as a function of aging time. Note: a yield strength increment of "0" is the as-solution treated strength in the absence of precipitation hardening.

Figure 45. Calculated Isothermal Aging Curves for the NGCo-3A

To validate the model predictions, two of the most promising modified heat treatment conditions were selected from this simulation study to validate using tensile testing. Samples were excised from the longitudinal direction of the NGCo-3A 4 inch round product, re-solutionized, water quenched, and aged to three different conditions: 1) the Phase I aging condition (to serve as a baseline), 2) a new potential isothermal aging condition (750° C/196 h), and 3) a new two-step aging condition identified by the PrecipiCalc simulations as a potential treatment condition. The results of tensile yield strength are presented in Figure 46. As demonstrated, the new conditions only achieve equivalent or slightly reduced tensile yield strengths relative to the baseline (Phase I) condition. This is an expected result based on the PrecipiCalc simulation analysis.

Use or disclosure of data contained on this sheet is subject to the restriction on the title page of this proposal.
Northrop Grumman Private/Proprietary Level I

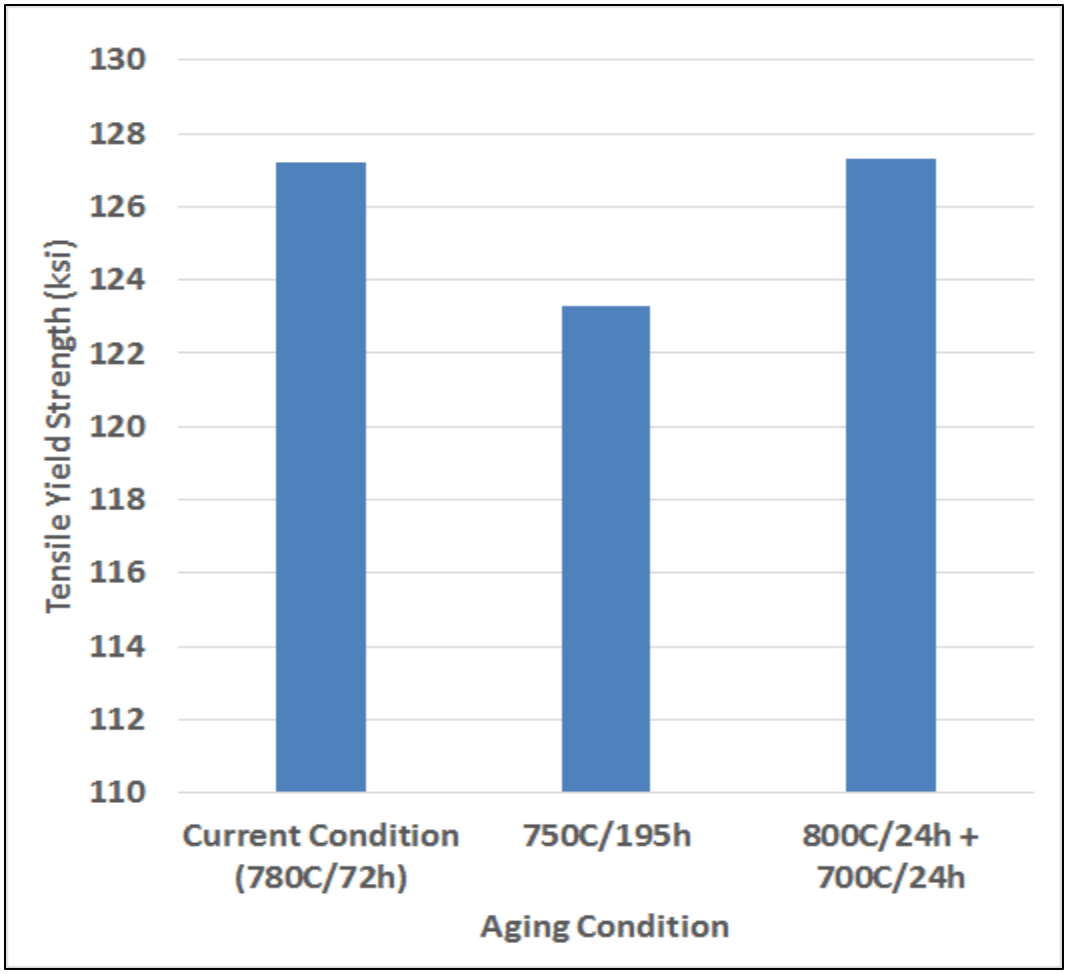

Figure 46. Tensile Yield Strength Results from Task 1 Heat Treatment Optimization Study (NGCo-3A 4" Round Material)

This result indicates that there is likely little room for improving tensile yield strength through modifications to the aging treatment alone (at least within the constraints of economical production). It is, however, expected that grain size refinement should be a more effective and higher-probability approach to improving the tensile yield strength of the alloy. The effect of grain size on yield strength is governed by the Hall-Petch relation. In the Phase I material, the grain size was found to be very coarse, on the order of 75 µm in diameter. Typical commercial production specifies average grain sizes on the order of 25-50 µm (ASTM grain size 5 – 7). The reason for such a large grain size in the prototype material is two-fold: 1) the carbon content was an order of magnitude lower than the specified target (carbon being necessary to maintaining fine grain sizes through the precipitation of a grain refining TiC dispersion), and 2) the forging reductions (RR) utilized in the prototype production were very low (RR~3, compared to typical commercial production where RR>8). The purpose of Task 2 is to produce new material that remedies each of these issues.

Use or disclosure of data contained on this sheet is subject to the restriction on the title page of this proposal.
Northrop Grumman Private/Proprietary Level I

Applying QuesTek's grain size strengthening models (based on the Hall-Petch relation, specifically calibrated for Co-based alloys), Figure 47 shows the predicted increase in strength over its current level through the refinement of grain size alone. Refining the grain structure to a typical level of 30 µm is predicted to increase tensile yield strength by ~4 ksi to ~130 ksi. Refining the grain structure to below a grain size of 7 to 10 µm (a lofty target) is predicted to result in a tensile yield strength increase of 16 ksi, or 142 ksi.

Grain Size	Current (75µm)	30 µm	20 µm	10 µm
Predicted increase in strength (ksi)	--	4	8	16

Figure 47. Predicted increase in tensile yield strength with refinement in grain size from its current level of 75 µm down to 30, 20 and 10 µm, respectively

Early in the follow-on effort QuesTek procured a new heat of the NGCo-3A alloy composition, to be used to evaluate the feasibility of improved yield strength through optimized material processing (higher forging reductions and tighter control on chemistry) and application of Task 1 heat treatment optimization. The motivation for procuring this new material is that the original round 2 material did not achieve the correct target chemistry. In particular, the carbon content was an order of magnitude lower than targeted. The carbon content is a key addition that promotes the formation of a titanium carbide phase that is present in low fractions during the forging operations. These particles act as a grain pinning dispersion that resists grain growth during high-temperature processing, thereby ensuring a fine grain structure is achieved. Also, this new production targets a higher forging reduction ratio than achieved in the Phase I, increasing from an RR of ~3 to RR>8 (which is more representative of typical commercial forging reductions).

This new heat of material was attempted to be fabricated at Special Metals (Huntington, WV) at a 30 lb, 4"RD ingot scale. The overall production path is outlined in Figure 48. Material is produced using Vacuum Induction Melting (VIM) and Vacuum Arc Remelting (VAR) processing (as is typical of high-quality aerospace alloy production). An order for the material was placed on June 23, 2014, with an estimated lead time of 8-10 weeks (delivery of end of July). The double-melted ingot was homogenized and hot worked into 1.25" RCS product (estimated forging reduction ratio of 10) before delivery to QuesTek for aging treatment.

Use or disclosure of data contained on this sheet is subject to the restriction on the title page of this proposal.
Northrop Grumman Private/Proprietary Level I

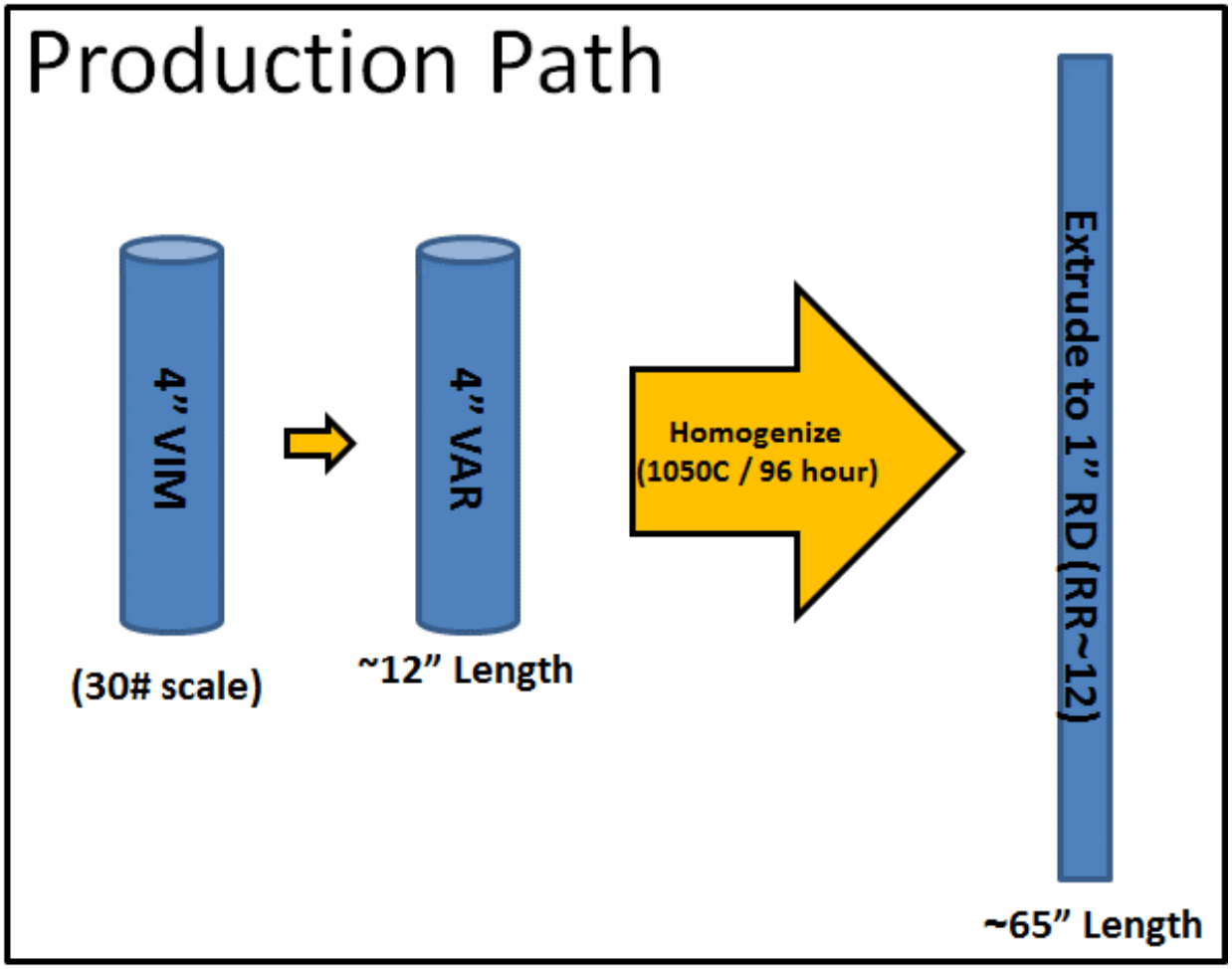

Figure 48. Schematic of Production Path for 30 lb Scale Manufacture of NGCo-3A alloy

Two initial melts of the alloy composition at Special Metals failed to meet the specified chemistry targets. In particular, the titanium content was half of the target level, and well outside the specification range. It was determined that the use of titanium shavings was the cause of this excessive alloying loss – the large surface area of the shavings results in excessive oxidation during melting. The VIM furnace at Special Metals broke down prior to the initiation of a third re-melt, and so production of the VIM/VAR ingot was shifted to a new toll manufacturer – MetalWerks. Since MetalWerks had produced this alloy at 500 lb scale in round 2, it was decided that this was a safe option to ensure timely delivery of the material within chemistry specifications. MetalWerks produced a 20 lb VIM/VAR ingot in early September 2014, and was able to achieve QuesTek's full specified chemistry targets (see Figure 49).

Use or disclosure of data contained on this sheet is subject to the restriction on the title page of this proposal.
Northrop Grumman Private/Proprietary Level I

ANALYTICAL REPORT

Alloy: QMS-NGCo-3A

Element	Concentration (wt%)	Method	Minimum (wt%)*	Maximum (wt%)*
Co	Balance			
C	0.0065	Combustion	0.0040	0.0100
Mn	<0.0020	ICP	----	0.0020
Si	<0.0040	ICP	----	0.0040
P	<0.0020	ICP	----	0.0020
S	0.0017	Combustion	----	0.0020
Cr	16.6	ICP	16.1	17.1
Ni	2.7	ICP	2.5	2.9
Ti	6.2	ICP	6.1	6.5
Fe	7.5	ICP	6.9	7.3
V	2.0	ICP	1.9	2.1
O	0.0212	IGF	----	0.0060
N	0.0005	IGF	----	0.0005
B	0.0073	ICP	0.0040	0.0100

Figure 49. Chemistry Analysis of the Round 3 Production of NGCo-3A at MetalWerks

This new material was delivered to Special Metals for the remaining processes of homogenization and hot rolling. A QuesTek representative was onsite to witness the hot rolling into 1.25" RCS, as this was deemed a technical risk due to issues in prior prototyping rounds. Material was homogenized per QuesTek's instructions (1050° C for 96 hours), and hot rolled directly from homogenization. The ingot successfully made it through an initial pass through the hot rollers (the initial pass is intended to square up the round ingot into a rounded-corner square shape). During a second pass through (at which point the working force on the material begins to increase), the ingot cracked directly in half. Close inspection of the fractured faces (Figure 50) reveals a large amount of porosity in the center of the ingot, likely a casting defect left over from the VAR process. This fracture rendered the material unsalvageable, and the hot working processes were suspended. With no hot work put into the homogenized material, the prototype material will not achieve the technical goals of the follow-on effort, and so no further characterization work was pursued at this time.

Both Northrop Grumman Corporation and QuesTek Innovations have an interest in seeing this final optimized product processing through so the NGCo-3A alloys potential performance can be identified. QuesTek continues to pursue this optimization material production effort with funding provided by the National Institute of Standards and Technology (NIST) program. If progress information on this effort becomes available prior to the end of this program it will be provided as an addendum for this report. This information would support a conclusion to the NGCo-3A materials final performance characteristics in meeting the programs desired tensile yield strength.

Use or disclosure of data contained on this sheet is subject to the restriction on the title page of this proposal.
Northrop Grumman Private/Proprietary Level I

Upper left – reconstructed ingot showing the original shape of the billet; Upper right – fractured faces of the billet which are shown at higher magnification in lower images.

Figure 50. Images of the Round 3 NGCo-3A Prototype Ingot after Fracturing During Hot Rolling

3.0 ALLOY CHARACTERIZATION AND DISCUSSION

After alloy design and fabrication the alternative material testing and characteristic evaluation was performed. The ultimate program goal is to design and develop materials that would be capable of replacing Cu-Be alloys currently used on military platforms. Alternative materials to be developed shall meet the following requirements:

- Tensile strength greater than 165,000 psi
- Yield strength at 0.2% offset greater than 140,000 psi
- Hardness of 36 to 45 Rockwell C (HRC)

Alternative materials must also meet or exceed the performance of Cu-Be alloys in terms of friction coefficient in dry sliding conditions against low-alloy steels, wear resistance, resistance to galling and spalling, axial fatigue, and rolling contact fatigue.

Use or disclosure of data contained on this sheet is subject to the restriction on the title page of this proposal.
Northrop Grumman Private/Proprietary Level I

As a result of the alternative alloy design and process modeling task, six alloy variations were designed, fabricated and tested. These alternative alloys were comprised of three copper based and three cobalt based systems as described below:

1. Copper-based alloys (NGCu-1A)
   a. NGCu-1A was Sn-free – lower fabrication risk; higher risk in achieving required properties
2. Copper-based alloy (NGCu-1B)
   a. NGCu-1B with Sn – higher fabrication risk; lower risk in achieving required properties
3. Copper-based alloys (Cuprium)
   a. Cuprium with Sn is spray metal formed to lower both fabrication risk and ability to achieve required properties
4. One Cobalt-based alloy (NGCo-1A)
   a. Modification of an alloy that QuesTek had designed for the US Marine Corps
   b. Modification was necessary to improve the quench suppressibility of the alloy
5. Cobalt-based alloys (NGCo-2A)
   a. Modified slightly for larger size melt
6. Cobalt-based alloys (NGCo-3A)
   a. Modified for higher strength and grain reduction

To evaluate the performance of these potential alternatives the alloy Evaluation\Characterization task was performed. In doing so, baseline AMS 4533 material was tested along with the newly designed alloys to provide comparison data and characteristic validation for the various tests identified.

3.1 CHARACTERIZATION TESTING PERFORMED AND RESULTS

Alternative alloy development materials manufactured by QuesTek were processed and sent to NGAS. Ingot materials were received and redirected to the machining houses; X5 Manufacturing, Element Materials and our own in house machining at the Space Park location. Material from the initial round of alloy development were all machined at X5 Manufacturing and the second round of alloy development material were machined at Element Materials and Northrop Grumman Corp-Space Park machine shop to support the testing coupons required for characterization. All machining samples were prepared and ASTM dimensions and surface finishes measured to validate the machining house capabilities in producing ASTM quality test coupons.

Four ASTM tests were targeted in evaluating the initial alternative alloy materials characteristics:

1. Tension ASTM E8
2. Compression ASTM E9
3. Wear Testing Pin on Disk ASTM G99
4. Reciprocating Ball on Flat ASTM G133

Coupons prepared were made per the ASTM specifications paying close attention to dimensional geometry and surface finishing aspects to avoid any variables that could cause a

Use or disclosure of data contained on this sheet is subject to the restriction on the title page of this proposal.
Northrop Grumman Private/Proprietary Level I

potential disparity in the results. Coupon machining of the alloys was performed and samples were shipped via Northrop Grumman to test houses for testing. EP Laboratories Inc., Irvine, CA. - performed (ASTM G99, ASTM G133) coupons, Element Materials Technology, Huntington Beach, CA. - performed (ASTM E8, ASTM E9 and ASTM E606) coupons and Wear and Friction Resources Tomball, TX. – performed (ASTM G98) coupons. These three testing houses were awarded the statements of work for performing the identified ASTM tests.

3.1.1 Tension Test Results of Evaluation Materials

Element Materials Technology Labs performed the ASTM E8 tension testing for all alloys and baseline material. Configuration of test specimen is shown in Figure 51.

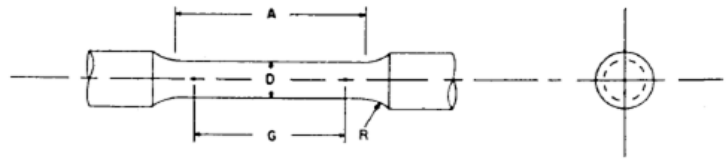

Dimensions, mm [in.]
For Test Specimens with Gage Length Four times the Diameter [E8]

Small-Size Specimens Proportional to Standard

	Specimen 3
G—Gage length	24.0 ± 0.1 [1.000 ± 0.005]
D—Diameter (Note 1)	6.0 ± 0.1 [0.250 ± 0.005]
R—Radius of fillet, min	6 [0.188]
A—Length of reduced section, min (Note 2)	30 [1.25]

NOTE 1—The reduced section may have a gradual taper from the ends toward the center, with the ends not more than 1 % larger in diameter than the center (controlling dimension).

NOTE 2—If desired, the length of the reduced section may be increased to accommodate an extensometer of any convenient gage length. Reference marks for the measurement of elongation should, nevertheless, be spaced at the indicated gage length.

Figure 51. Configuration of Tensile Specimen per ASTM E8

Tension measurements provide a few different types of associated characteristics such as yield strength, plastic strain, elastic deformation and ductility. Ductile fracture features of a cup cone type are evident in the broken specimen. Typical test specimens are shown in Figure 52 and results are shown in Figure 53.

Use or disclosure of data contained on this sheet is subject to the restriction on the title page of this proposal.
Northrop Grumman Private/Proprietary Level I

Figure 52. Typical ASTM E8 Tensile Test Fixture and Tensile Specimen

Use or disclosure of data contained on this sheet is subject to the restriction on the title page of this proposal.
Northrop Grumman Private/Proprietary Level I

element

Element Materials Technology
15062 Bolsa Chica
Huntington Beach, CA
92649-1023 USA

P 714 892 1961
F 714 892 8159
T 888 786 7555
info.hb@element.com
element.com

Contact: George Pelzl
Northrop Grumman Corp. - Aircr
One Hornet Way
Dept. Qg40/W5Ma
EL SEGUNDO, CA 90245-2804

TEST CERTIFICATE — ITAR-CONTROLLED DATA

Date: 7/19/2012
Purchase Order Number: 2814728
Work Order Number NOR149-07-02-84557-5

Description:	CU 1 ASMT E8 TEST COUPONS
Specification:	FOR INFORMATION ONLY
Priority Rating:	DO-A1
Project ID:	PID1Q

TENSILE						
Test Method:	ASTM E8-11					
Sample No.	**Tensile Strength**	**Yield Strength At 0.2% Offset**	**Elongation in 4D**	**Reduction of Area**	**Diameter**	**Area**
	Min (ksi)	**Min. (ksi)**	**Min. (%)**	**Min. (%)**	**(in)**	**(in^2)**
Requirements :	**N/S**	**N/S**	**N/S**	**N/S**		
CU 1 – 1	113	63.5	30.0	39	0.2520	0.0499
CU 1 – 2	113	64.0	31.0	40	0.2510	0.0495
CU 1 – 3	114	64.0	29.0	42	0.2520	0.0499
CU 1 – 4	113	64.0	28.0	35	0.2510	0.0495
CU 1 – 5	112	63.0	28.0	31	0.2520	0.0499
CU 1 – 6	115	65.0	30.0	42	0.2520	0.0499

FOR INFORMATION ONLY

This document contains technical data whose export and re-export/re-transfer is subject to control by the U.S. Department of State under the Arms Export Control Act and the International Traffic in Arms Regulations. The Department of State's prior written approval is required for the export or re-export/re-transfer of such technical data to any foreign person, foreign entity or foreign organization whether in the United States or abroad.

Respectfully submitted

15062 Bolsa Chica, Huntington Beach, CA 92649
(714) 892-1961 ph • (714) 892-8159 fax www.element.com

Dercy Urrea
Quality Administrator

The information contained in this certification represents only the material submitted and is certified only for the quantities tested. Reproduction except in full is reserved pending written approval. The recording of false, fictitious, or fraudulent statements or entries on the certificate may be punishable as a felony under federal law. All testing was performed in a mercury free environment. **All testing performed in accordance with the latest edition of the applicable ASTM, or other Federal Test Method in effect at the time of test.**

Page 1 of 1

Figure 53. Typical Tension Test Results

Review of the alternative alloys will be mainly dependent on the comparison to the baseline because they are being modeled and designed after the performance characteristics of the standard AMS 4533 Copper Beryllium. Five or more samples were tested per alloy and average results provided below. Six measurements are recorded for each material provided:

Use or disclosure of data contained on this sheet is subject to the restriction on the title page of this proposal.
Northrop Grumman Private/Proprietary Level I

Baseline Copper Beryllium:
- Tensile Strength Min – (182 ksi)
- Yield Strength @ 2% Offset Min – (164.8 ksi)
- Elongation in 4D Min – (5.4%)
- Reduction of area Min – (11.7%)
- Diameter in – (.2500”)
- Area – (.0491 sq.in.)

NGCu-1A:
- Tensile Strength Min – (113.3 ksi)
- Yield Strength @ 2% Offset Min – (63.9 ksi)
- Elongation in 4D Min – (29.3%)
- Reduction of area Min – (38.2%)
- Diameter in – (.2516”)
- Area – (0.0497 sq.in.)

Cuprium:
- Tensile Strength Min – (157.8 ksi)
- Yield Strength @ 2% Offset Min – (141.6 ksi)
- Elongation in 4D Min – (14.5%)
- Reduction of area Min – (16.2%)
- Diameter in – (0.1132”)
- Area – (0.0 101 sq.in.)

NGCo-1A:
- Tensile Strength Min – (194 ksi)
- Yield Strength @ 2% Offset Min – (119 ksi)
- Elongation in 4D Min – (40%)
- Reduction of area Min – (51%)
- Diameter in – (0.2520”)
- Area – (0.0499 sq.in.)

NGCo-3A (2”dia.):
- Tensile Strength Min – (200 ksi)
- Yield Strength @ 2% Offset Min – (126.1 ksi)
- Elongation in 4D Min – (32.9%)
- Reduction of area Min – (27.9%)
- Diameter in – (0.2525”)
- Area – (0.0500 sq.in.)

NGCo-3A (4”dia.):
- Tensile Strength Min – (202ksi)
- Yield Strength @ 2% Offset Min – (127.2ksi)
- Elongation in 4D Min – (30.3%)
- Reduction of area Min – (39%)
- Diameter in – (0.2505”)
- Area – (0.0492 sq.in.)

Use or disclosure of data contained on this sheet is subject to the restriction on the title page of this proposal.
Northrop Grumman Private/Proprietary Level I

When comparing the performance results it is noted that the Tensile strength of the NGCo-3A alloy rates the highest although in yield strength the baseline performs highest among the three alloys. Both the elongation and the reduction area of the NGCo-3A are higher than the baseline material. This information was shared and reviewed with QuesTek Innovations to provide them with physical testing performance properties required during the design phases to support next generation alternative alloy development. All tensile evaluation test results/reports are located in Appendix A.

3.1.2 Compression Test Results of Evaluation Materials

Element Materials Technology Labs also performed the ASTM E9 compression testing on the alternative alloys and baseline material. Configuration of compression specimen is shown in Figure 54. Typical machined compression specimen is shown in Figure 55.

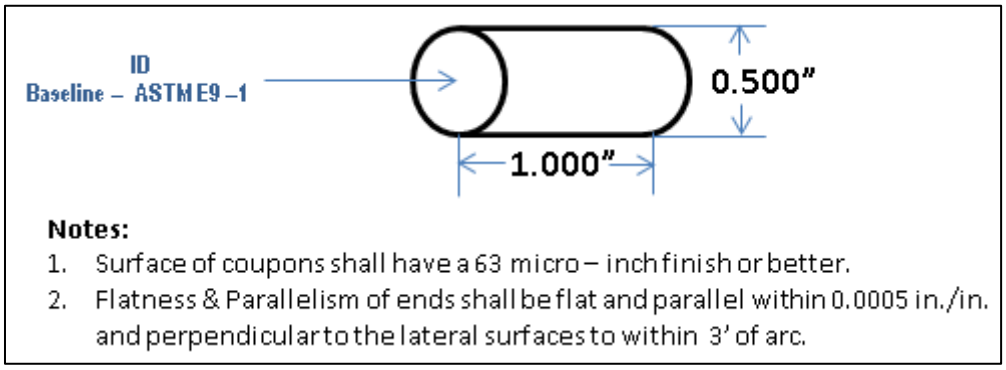

Figure 54. Configuration of Compression Specimen per ASTM E9

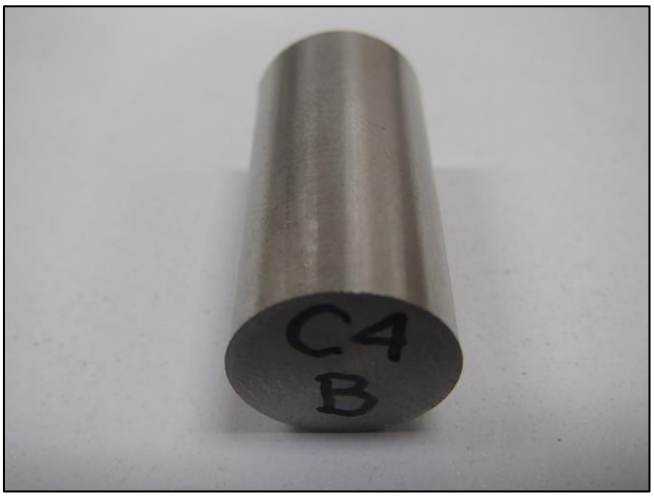

Figure 55. Typical ASTM E9 Machined Compression Specimen

Use or disclosure of data contained on this sheet is subject to the restriction on the title page of this proposal.
Northrop Grumman Private/Proprietary Level I

Typical test results are shown in Figure 56.

element

Element Materials Technology
15062 Bolsa Chica
Huntington Beach, CA
92649-1023 USA

P 714 892 1961
F 714 892 8159
T 888 786 7555
info.hb@element.com
element.com

Contact: George Pelzl
Northrop Grumman Corp. - Aircr
One Hornet Way
Dept. Qg40/W5Ma
EL SEGUNDO, CA 90245-2804

TEST CERTIFICATE — ITAR-CONTROLLED DATA

Date: 7/19/2012
Purchase Order Number: 2814728
Work Order Number NOR149-07-02-84557-1

Description:	CO 1 ASMT E9 TEST COUPONS
Specification:	FOR INFORMATION ONLY
Priority Rating:	DO-A1
Project ID:	PID1Q

COMPRESSION TEST

Test Method:		**ASTM E9-09**		
Serial No.	**Diameter**	**Area**	**Yield Load At 0.2% Offset**	**Yield Strength At 0.2% Offset**
			(lbs.)	**(ksi)**
CO1-1	0.500	0.1963	23,392	119.1
CO1-2	0.500	0.1963	23,307	118.7
CO1-3	0.499	0.1956	23,713	121.3
CO1-4	0.500	0.1963	23,679	120.6
CO1-5	0.500	0.1963	23,368	119.0
CO1-6	0.500	0.1963	23,450	119.4
CO1-7	0.500	0.1963	23,548	119.9
CO1-8	0.500	0.1963	23,643	120.4
Requirements:			**-**	**For Info**

FOR INFORMATION ONLY

This document contains technical data whose export and re-export/re-transfer is subject to control by the U.S. Department of State under the Arms Export Control Act and the International Traffic in Arms Regulations. The Department of State's prior written approval is required for the export or re-export/re-transfer of such technical data to any foreign person, foreign entity or foreign organization whether in the United States or abroad.

Respectfully submitted

15062 Bolsa Chica, Huntington Beach, CA 92649
(714) 892-1961 ph • (714) 892-8159 fax www.element.com

Darcy Urrea
Quality Administrator

The information contained in this certification represents only the material submitted and is certified only for the quantities tested. Reproduction except in full is reserved pending written approval. The recording of false, fictitious, or fraudulent statements or entries on the certificate may be punishable as a felony under federal law. All testing was performed in a mercury free environment. **All testing performed in accordance with the latest edition of the applicable ASTM, or other Federal Test Method in effect at the time of test.**

Page 1 of 1

Figure 56. Typical Compression Test Results

Axial compression testing provides a useful method for measuring the plastic flow behavior and ductile fracture limits of the materials. Plotted stress and strain curves will provide elastic

Use or disclosure of data contained on this sheet is subject to the restriction on the title page of this proposal.
Northrop Grumman Private/Proprietary Level I

limit, proportional limit, yield point, yield strength and compressive strength. Again the testing evaluation of the material alloys will be mainly dependent on the comparison to the baseline because the alternative alloys are being modeled and designed after those performance characteristics of the Copper Beryllium. Ten samples (total or per alloy) were tested and an average resultant is provided below. Four measurement types are recorded for each material provided:

Baseline Copper Beryllium:
- Diameter – (0.5000”)
- Area – (0.1963 sq.in.)
- Yield Load at 2% Offset – (33,120 lbs)
- Yield Strength at 2% Offset – (168.7 ksi)

NGCu-1A:
- Diameter – (0.4994”)
- Area – (0.1959 sq.in.)
- Yield Load at 2% Offset – (12,592 lbs)
- Yield Strength at 2% Offset – (64.3 ksi)

NGCo-1A:
- Diameter – (0.4998”)
- Area – (0.1962 sq.in.)
- Yield Load at 2% Offset – (23,513 lbs)
- Yield Strength at 2% Offset – (119.8 ksi)

NGCo-3A (2”):
- Diameter – (0.499”)
- Area – (0.196 sq.in.)
- Yield Load at 2% Offset – (25,365 lbs)
- Yield Strength at 2% Offset – (129.8 ksi)

NGCo-3A (4”):
- Diameter – (0.499”)
- Area – (0.196 sq.in.)
- Yield Load at 2% Offset – (25,803 lbs)
- Yield Strength at 2% Offset – (132.0 ksi)

In reviewing the compression data it is noted that the alternative alloys have lower yield strength than the baseline. The yield strength of the NGCo-3A alloy is lower than the baseline although much better in relation to the NGCu-1A or NGCu-1B materials. All compression test results/reports are located in Appendix A.

3.1.3 Pin-on-Disk Wear Testing Results of Evaluation Materials

EP Laboratories performed the ASTM G99 wear testing of the pin-on-disk for the two alloys and the baseline material. Pin-on-disk specimen configuration is shown in Figure 57. Typical machined pin-on-disk specimen is shown in Figure 58.

Use or disclosure of data contained on this sheet is subject to the restriction on the title page of this proposal.
Northrop Grumman Private/Proprietary Level I

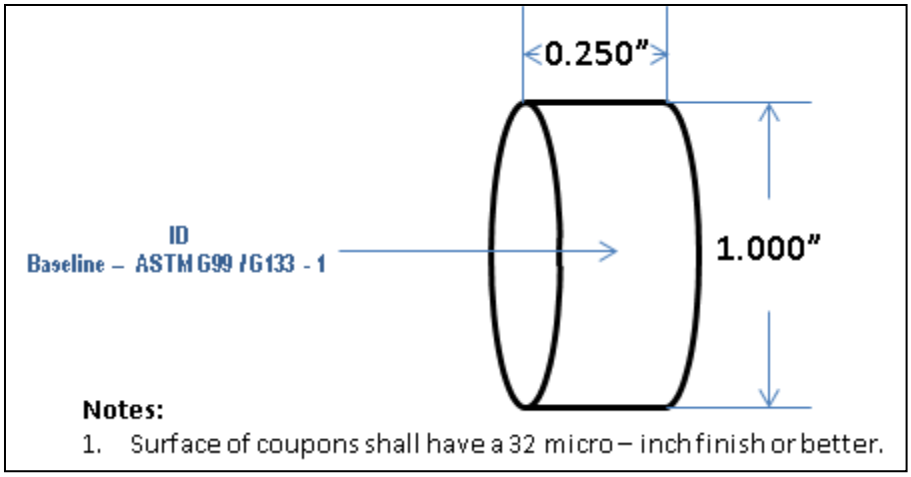

Figure 57. Configuration of Pin-on-Disk Specimen

Figure 58. Typical ASTM G99 Machined Pin-on-Disk Wear Specimen

The pin-on-disk wear test provides wear and friction coefficients, factors and rates for both the pin and disk specimens. This testing method facilitates the determination and study of friction and wear behavior of alloy solid state material combination, with varying time, contact pressure and velocity. Schematic illustration of wear test arrangement is shown in Figure 59.

Use or disclosure of data contained on this sheet is subject to the restriction on the title page of this proposal.
Northrop Grumman Private/Proprietary Level I

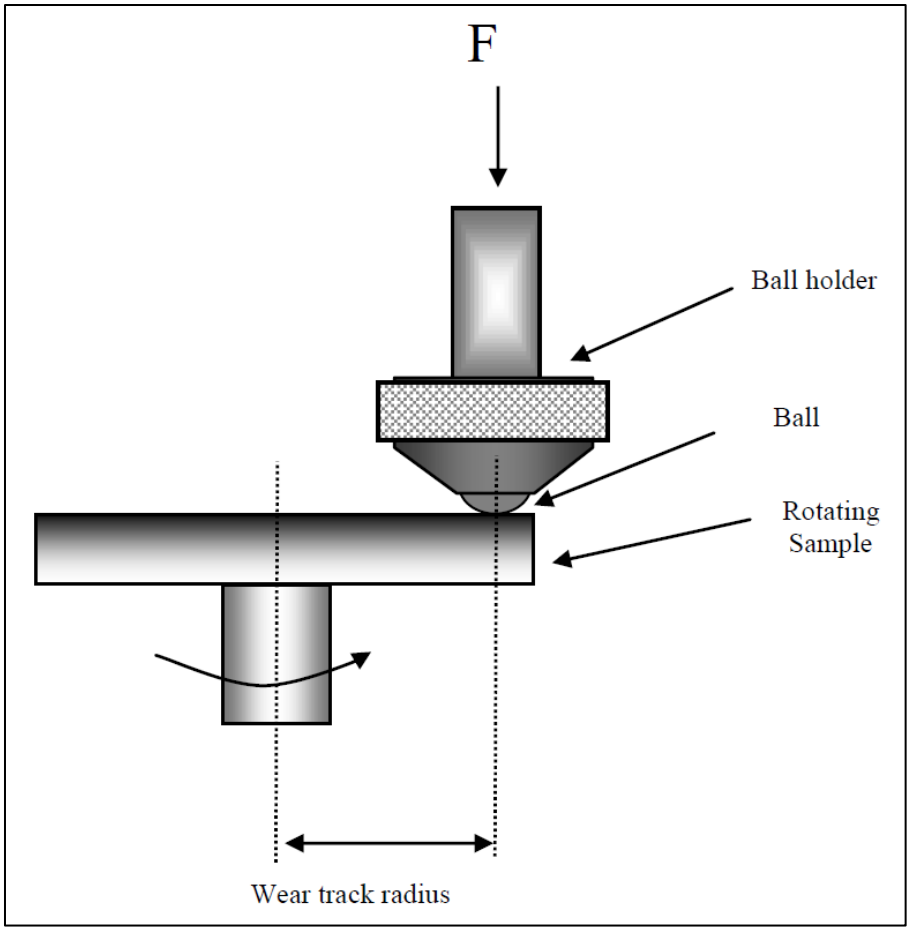

Figure 59 - Schematic Illustration of Pin-on-Disk Wear Test Setup

Several samples were tested from each alloy and the average results with the standard deviations are provided below:

Baseline CuBe:
Initial μ - (.181 ± 0.022)
Average μ - (0.785 ± 0.016)

NGCu-1A:
Initial μ - (0.219 ± 0.016)
Average μ - (0.871 ± 0.005)

NGCo-1A:
Initial μ - (.181 ± 0.007)
Average μ - (0.511 ± 0.046)

NGCo-3A (2”):
Initial μ - (0.206 ± 0.015)
Average μ - (0.513 ± 0.044)

NGCo-3A (4”):
Initial μ - (0.203 ± 0.006)
Average μ - (0.503 ± 0.039)

Use or disclosure of data contained on this sheet is subject to the restriction on the title page of this proposal.
Northrop Grumman Private/Proprietary Level I

EP laboratories provided the following comments based on the 1st round samples (Baseline, NGCu-1A and NGCo-1A) evaluated per alloy:

1. Observations – Ball (static partner)
   a. Material transfer was observed for “Baseline” and “NGCo-1A”
   b. A flat worn cap was noted for NGCo-1A
2. Observations – Disk (Coupon)
   a. “Baseline”: uneven track.
   b. NGCu-1A: Discoloration was observed on most coupons
3. Results suggest that
   a. NGCo-1A coupons have a better wear property than Baseline and NGCu-1A
   b. NGCu-1A coupons have worse wear properties than Baseline and NGCo-1A

EP laboratories provided the following comments based on the 2nd round of samples evaluated for the 5 five - 2” material specimens and the three - 4” material specimens from the NGCo-3A cobalt based alloy:

1. Observations – Ball (static partner)
   a. A lot of material transfer was observed for all samples except as follows: a little on 3A-4” no1, 3A-2” no3, and 3A-2” no5.
   b. A flat worn cap was observed for: 3A-4” no1, 3A-2” no3, and 3A-2” no5.
2. Observations – Disk (Coupon)
   a. Debris/material transfer was observed for all samples

This materials characteristic testing performance information for the coefficient of friction was shared and reviewed with QuesTek Innovations in support of improved properties development efforts. All pin-on-disk evaluation test results/reports are located in Appendix A.

The initial set of pictures below in Figure 60 show the disk and ball visual wear test results of the first wear track for the baseline AMS 4533 Cu-Be, NGCu-1A, NGCo-1A, NGCo-3A (2”) and NGCo-3A (4”) alloys.

Use or disclosure of data contained on this sheet is subject to the restriction on the title page of this proposal.
Northrop Grumman Private/Proprietary Level I

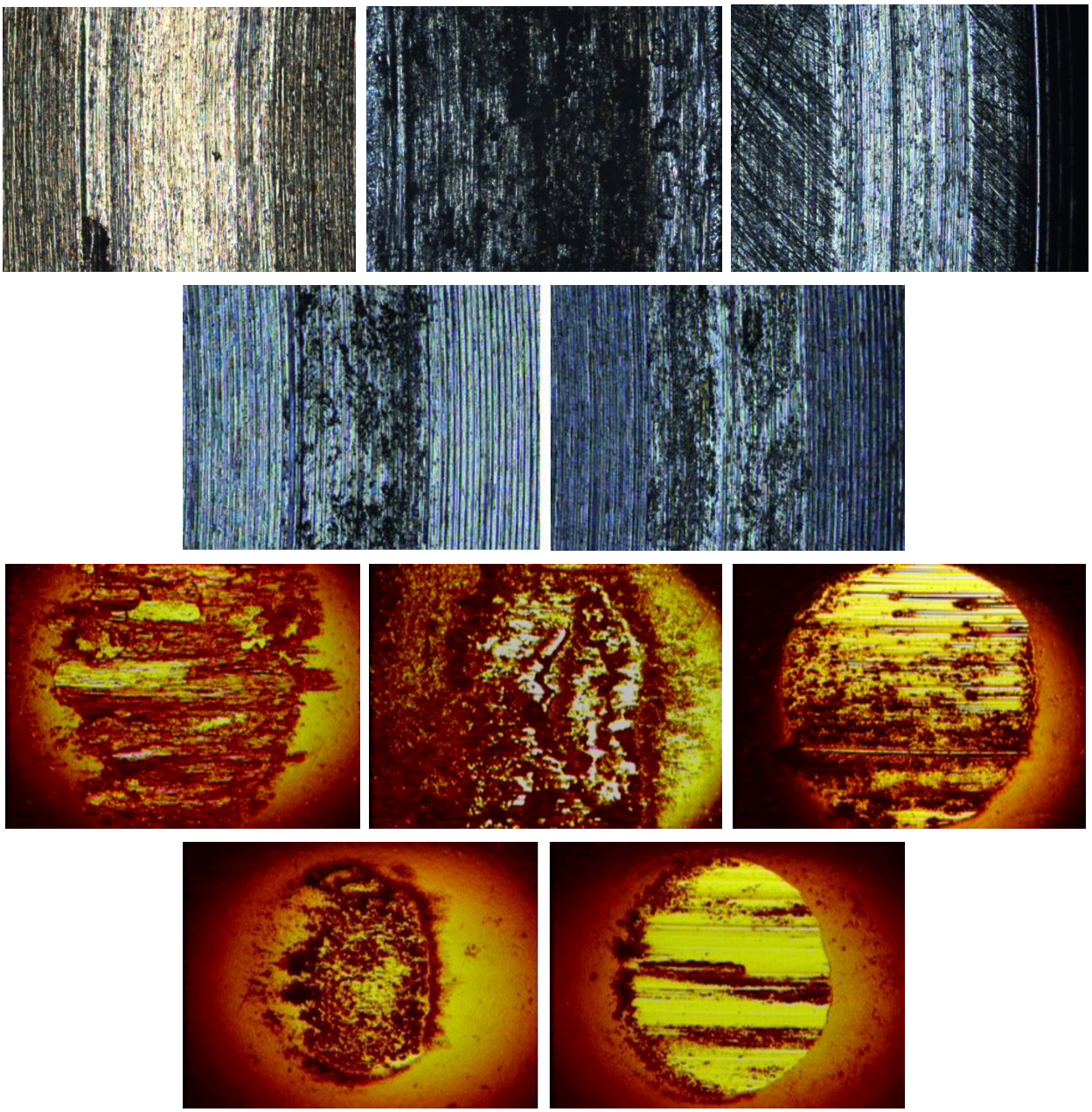

Figure 60. Visual Wear of Track # 1 of the Disk and Associated 440C Steel Ball for AMS 4533 Cu-Be, NGCu-1A, NGCo-1A, NGCo-3A (2”) and NGCo-3A (4”) Respectfully

This next set of pictures below in Figure 61 show the disk and ball visual wear test results after the 10th wear track for the baseline AMS 4533 Cu-Be, NGCu-1A, and NGCo-1A alloys. Pictures were not taken of 10th wear track for the NGCo-3A (2”) and NGCo-3A (4”) alloys in the second round of evaluations.

Use or disclosure of data contained on this sheet is subject to the restriction on the title page of this proposal.
Northrop Grumman Private/Proprietary Level I

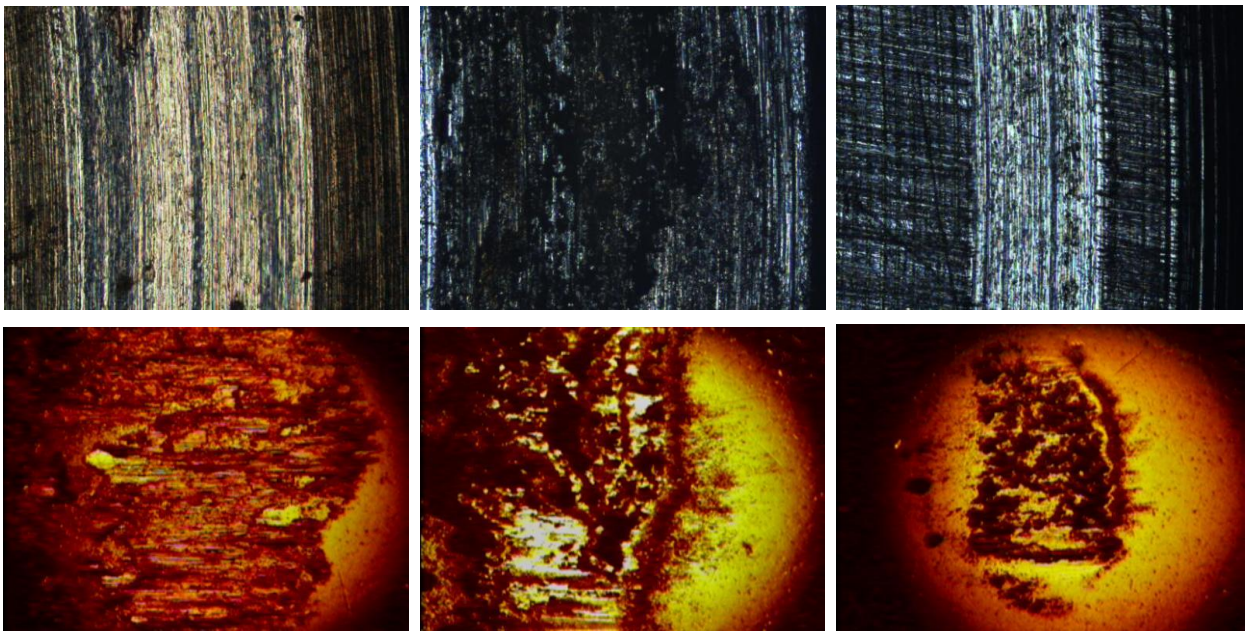

Figure 61. Visual Wear of Track # 10 of the Disk and on the Associated 440C Steel Ball for AMS 4533 Cu-Be, NGCu-1A and NGCo-1A Respectfully

The cobalt based evaluation material has the best visual appearance and shows the least amount of wear on both the disk and the ball for the respective wear travel/distance.

3.1.4 Reciprocating-Ball-on-Flat Test Results of Evaluation Materials

EP Laboratories also performed the ASTM G133 wear testing for the two alternative alloys and the baseline material. Configuration of the test specimen is shown in Figure 62. Typical machined specimens are shown in Figure 63.

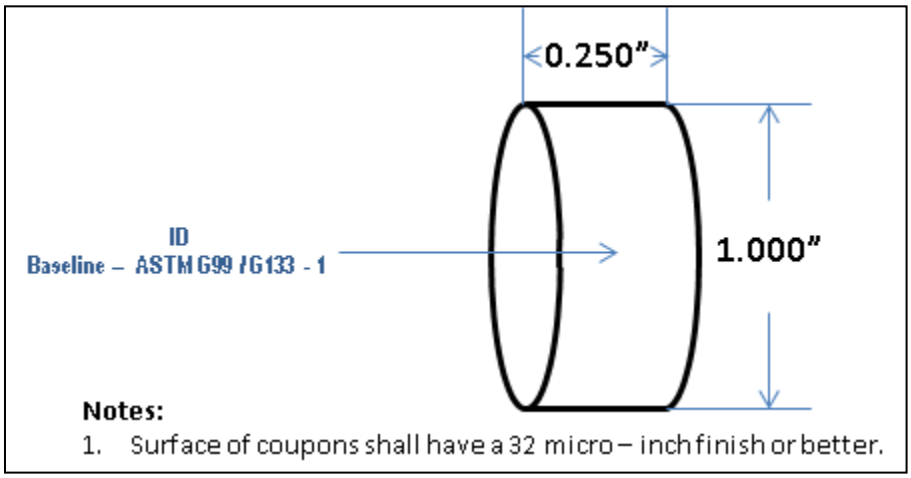

Figure 62. Configuration of Wear Testing Reciprocating-Ball-on-Flat Test Specimen

Use or disclosure of data contained on this sheet is subject to the restriction on the title page of this proposal.
Northrop Grumman Private/Proprietary Level I

Figure 63. Typical ASTM G133 Machined Reciprocating-Ball-on-Flat Specimens

The reciprocating-ball-on-flat test provides wear volumes and wear rates of the contacting ball and flat specimen materials. The volume and rates are calculated from the dimensional changes for both the ball and flat specimens. Schematic Illustration of the Reciprocating-Ball-on-Flat Wear Testing machine is shown in Figure 64.

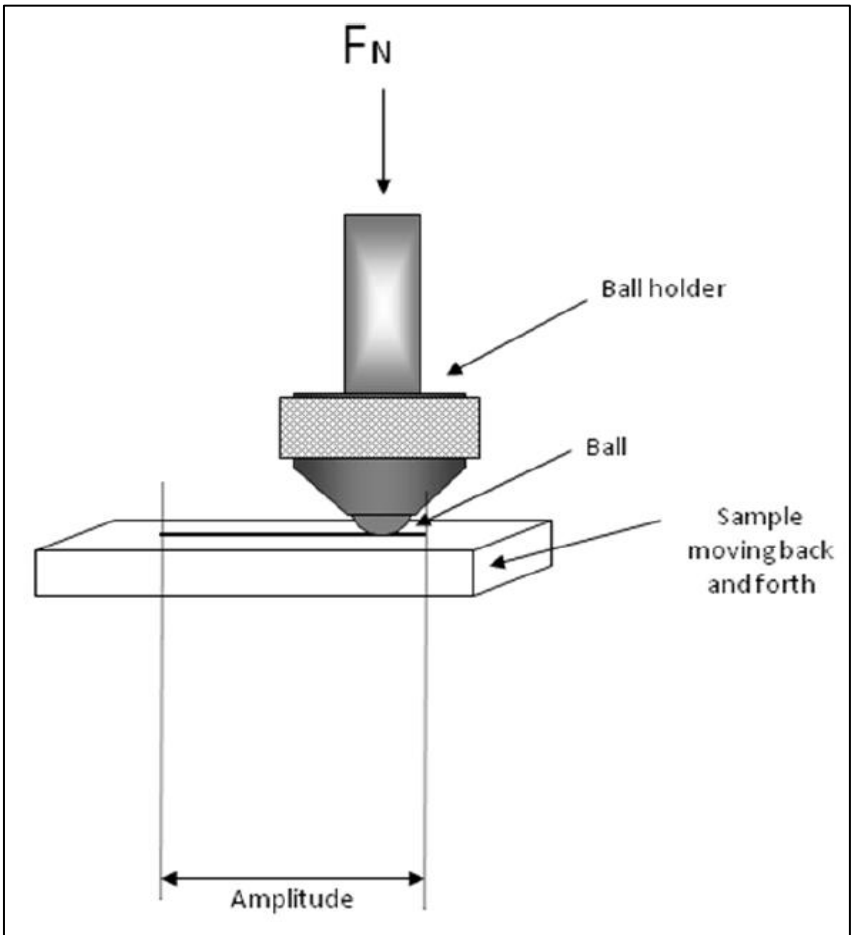

Figure 64. Schematic Illustration of Reciprocating-Ball-on-Flat Wear Test Setup

Use or disclosure of data contained on this sheet is subject to the restriction on the title page of this proposal.
Northrop Grumman Private/Proprietary Level I

Some non-standard testing conditions were performed to produce more detailed level material characteristics values to help support representative performance characteristics desired and are noted in the test report. Several samples were tested from each alloy and average results with the standard deviation are provided below:

Baseline CuBe:
Initial μ - (0.145 ± 0.030)
Average μ (2 way extraction) – (0.647 ± 0.057)

NGCu-1A
Initial μ - (0.194 ± 0.012)
Average μ (2 way extraction) - (0.625 ± 0.012)

NGCo-1A
Initial μ - (0.161 ± 0.011)
Average μ (2 way extraction) - (0.240 ± 0.006)

NGCo-3A (2”dia)
Initial μ - (0.137 ± 0.035)
Average μ (2 way extraction) - (0.301 ± 0.020)

NGCo-3A (4”dia)
Initial μ - (0.133 ± 0.054)
Average μ (2 way extraction) - (0.288 ± 0.021)

EP laboratories provided the following comments based on the 1st round samples (Baseline, NGCu-1A and NGCo-1A) evaluated per alloy:

1. Observations – Ball (static partner)
   a. Material transfer was observed for “Baseline” and “NGCu-1A”
   b. Light abrasion/wear was observed for “NGCo-1A”
2. Observations – Disk (Coupon)
   a. “NGCo-1A”: Uneven track on some specimens
   b. “NGCu-1A”: Discoloration was observed on most specimens
3. Results suggest that
   a. “NGCo-1A”: Specimens have better wear property than Baseline and NGCu-1A
   b. “NGCu-1A”: Specimens have worse wear properties than Baseline and NGCo-1A

EP laboratories provided the following comments based on the 2nd round of samples evaluated for the 5 five - 2” material specimens and the three - 4” material specimens from the NGCo-3A cobalt based alloy:

1. Observations – Ball (static partner)
   a. Slight material transfer was observed for all specimens.
   b. Light abrasion/wear was observed for all specimens. However, damaged area didn’t appear to be flat.
2. Observations – Disk (Coupon)
   a. The NGCo-3A(4”) specimens seemed to have a more even wear track.
   b. Some material transfer/debris was observed
      i. The uneven surface finish affected the uniformity of the track

Use or disclosure of data contained on this sheet is subject to the restriction on the title page of this proposal.
Northrop Grumman Private/Proprietary Level I

This materials characteristic testing performance information for the coefficient of friction was shared and reviewed with QuesTek Innovations in support of improved properties development efforts. All reciprocating-ball-on-flat evaluation test results/reports are located in Appendix A.

The set of pictures below in Figure 65 show some of the visual results of the reciprocating-ball-on-flat test. This initial group shows the first wear track results of the disk and associated ball for the baseline AMS 4533 Cu-Be, NGCu-1A and NGCo-1A, NGCo-3A (2”) and NGCo-3A (4”) alloys. Some material build-up is noted on the NGCu-1A sample.

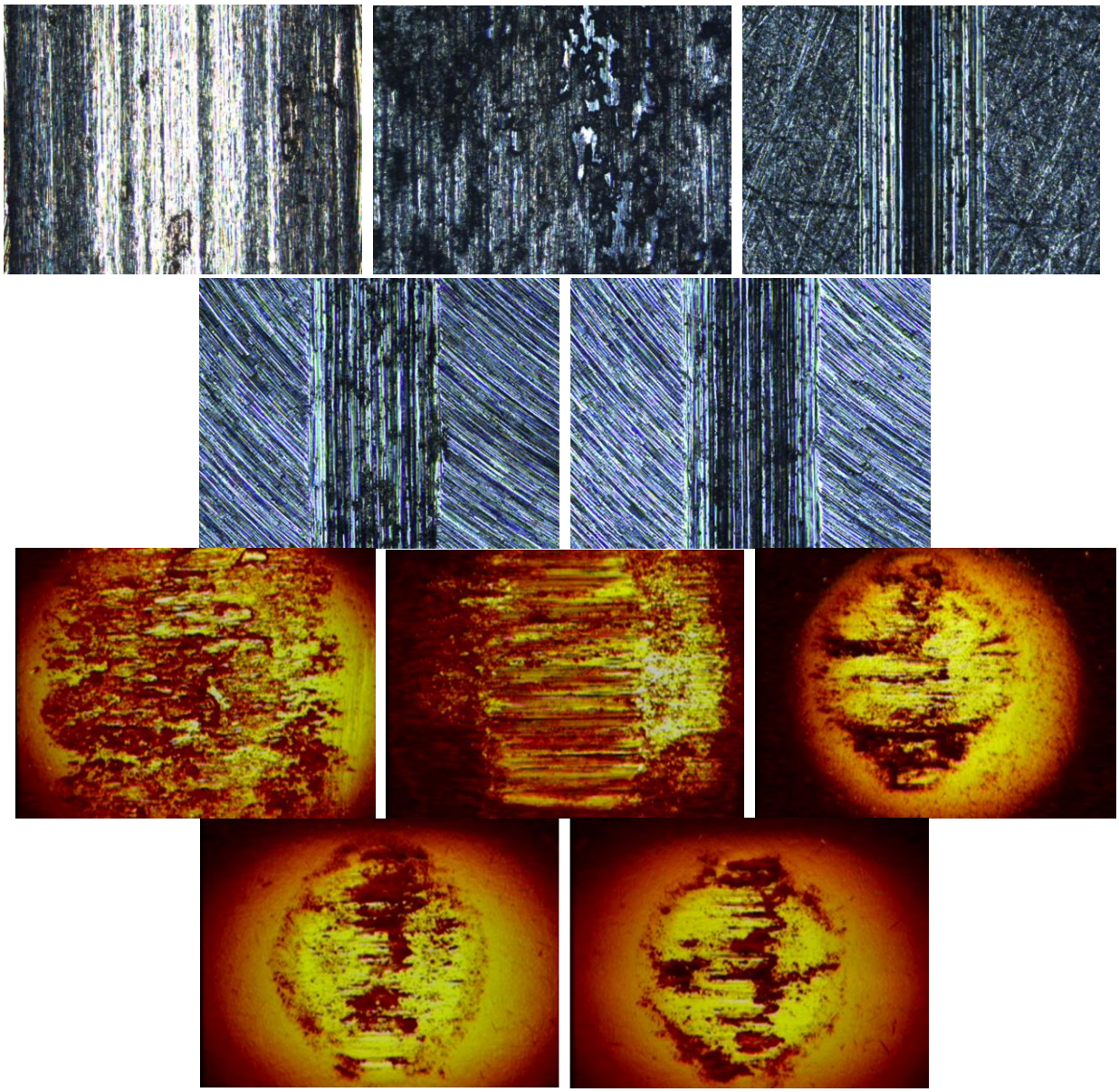

Pictured is the disk and associated 440C Steel Ball for AMS 4533 Cu-Be, NGCu-1A and NGCo-1A, NGCo-3A (2”) and NGCo-3A (4”) alloys respectively.

Figure 65. Visual Wear of Track #1 of Reciprocating-Ball-on-Flat Wear Test

Use or disclosure of data contained on this sheet is subject to the restriction on the title page of this proposal.
Northrop Grumman Private/Proprietary Level I

The following set of pictures in Figure 66 below shows the visual results of the reciprocating-ball-on-flat test upon the tenth wear track of the disk and associated ball for the baseline AMS 4533 Cu-Be, NGCu-1A and NGCo-1A alloys. No pictures of the tenth wear track were taken for the NGCo-3A (2”) and NGCo-3A (4”) specimens so comparisons are not shown below. A wider spread and slightly more pronounced material build up is noted in the tracking area on the NGCu-1A sample. Both the baseline AMS 4533 Cu-Be and the Cobalt based alloys show additional wear but look much the same as track 1 wear appearance even though they were all subjected to the greater amount of travel of the ball upon the flat disk.

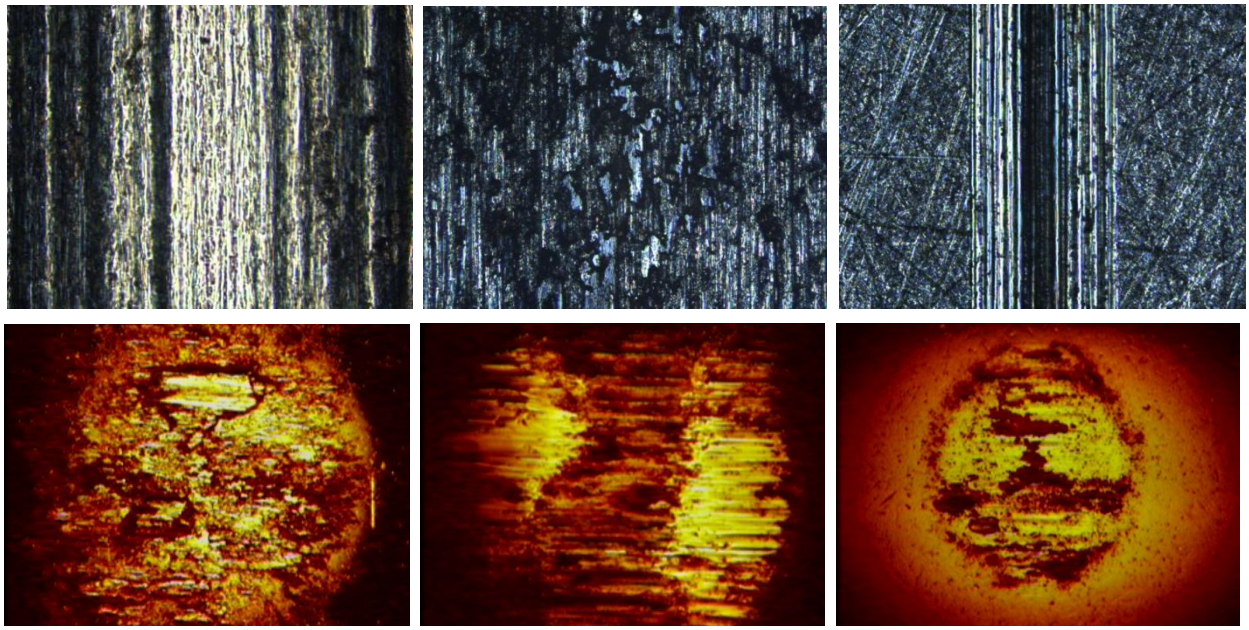

Pictured is the disk and associated 440C Steel Ball for AMS 4533 Cu-Be, NGCu-1A and NGCo-1A respectively.

Figure 66. Visual Wear of Track # 10 of Reciprocating-Ball-on-Flat Wear Test

The cobalt based evaluation material has the best visual appearance and shows the least amount of wear on both the disk and the ball for the respective wear travel/distance.

3.1.5 Alternative Alloys Testing Evaluation & Material Down-Selection

Data results from the typical performance characteristics testing suite, that includes Tensile, Compression, Pin-on-Disk, and Reciprocating-Ball-on-Flat, was gathered and charted for the two alternative alloys and the baseline materials.

Alloy tensile characteristics chart in Figure 67 displays results of the various developmental materials that have been produced and tested during the duration of the program. Again the testing evaluation of the material alloys will be mainly dependent on the comparison to the baseline because the alternative alloys are being modeled and designed after those performance characteristics of the Copper Beryllium. Four performance properties of the alloys; tensile strength, tensile yield strength, percent elongation, and percent of reduction in area are all presented in the chart for each alloy supporting a comparison to the baseline. The ASTM E8 tensile data results carry a lot of weight in the alternative alloy material down selection decision process.

Use or disclosure of data contained on this sheet is subject to the restriction on the title page of this proposal.
Northrop Grumman Private/Proprietary Level I

The tin-free copper based alloy identified as (NGCo-1A) shows the lowest tensile strength and tensile yield values within the group and hence was targeted for elimination. These low values were predicted when performing the design and development of this alloy and now have been validated. The copper based alloy with tin identified as Cuprium [the (SMF) alloy] has performed very well and presents a tensile yield strength value that meets the desired program level although it falls slightly short on the other desired properties. This outcome of the Cuprium alloy had also been predicted in the design and development phase which had foreseen that the manufacturing process in producing consistent homogeneity throughout the ingot would be its greatest hurdle in obtaining the program level values. The unique spray metal forming (SMF) process proved to be a viable method in producing the high level of homogeneity required and the performance supports the unique systems approach. Percent elongation and percent reduction in area values for the Cuprium were slightly lower than desired in pursuing any further enhancement in the alloy and hence the Cuprium was also targeted for elimination from the alternative alloy material down-selection.

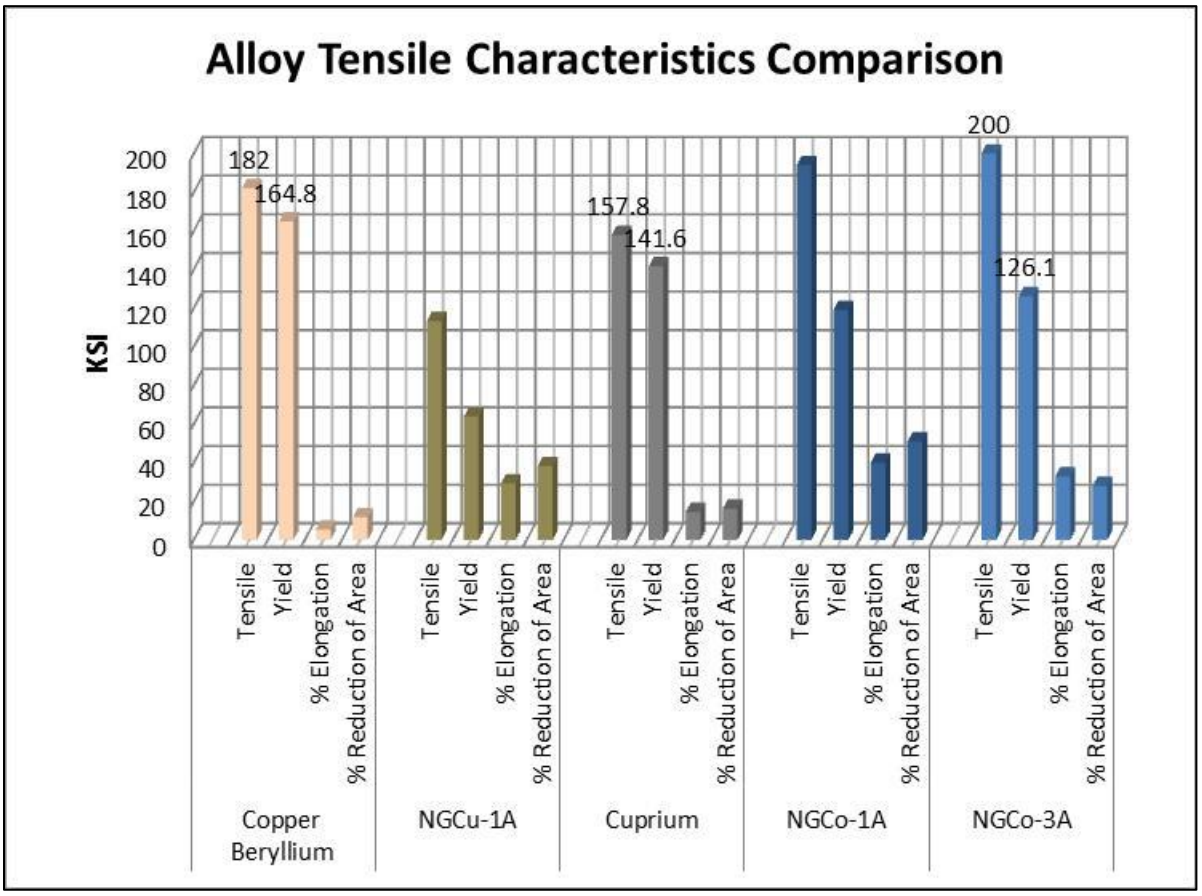

Figure 67. Alloy Tensile Characteristics Comparison Chart

Cobalt based alloy materials identified with NGCo-1A and NGCo-3A designations produced the highest tensile strength and hardness values although fell slightly short in obtaining the program goal for the tensile yield strength property. Both the percent elongation and the percent reduction in area values of the cobalt 1st and 2nd round development material present further enhancement potential. A well noted observation in this chart is the improved tensile strength presented in the 2nd round of the NGCo-3A development material and the reduction effects on

Use or disclosure of data contained on this sheet is subject to the restriction on the title page of this proposal.
Northrop Grumman Private/Proprietary Level I

the values of the percent elongation and percent reduction of area. Although these values present reductions, their levels are still great enough to support the potential for further material enhancement in capturing the desired program tensile yield strength values.

Although the tensile characteristics play a large role in the down-selection process the other performance characterisics that are being evaluated also weigh in on the final material down selection. Another characteristic tested within the suite of evaluation tests is the compression yield strength. This test typically produces similar strength values to those produced in the tensile testing. Figure 68 presents the data comparison of the NGCo-3A alternative alloy to that of the copper beryllium baseline material. The NGCu-1A results were not presented because levels were considerably lower than the program goal. As for the Cuprium it is unfortunate that there was not enough experimental material produced to support the further testing.

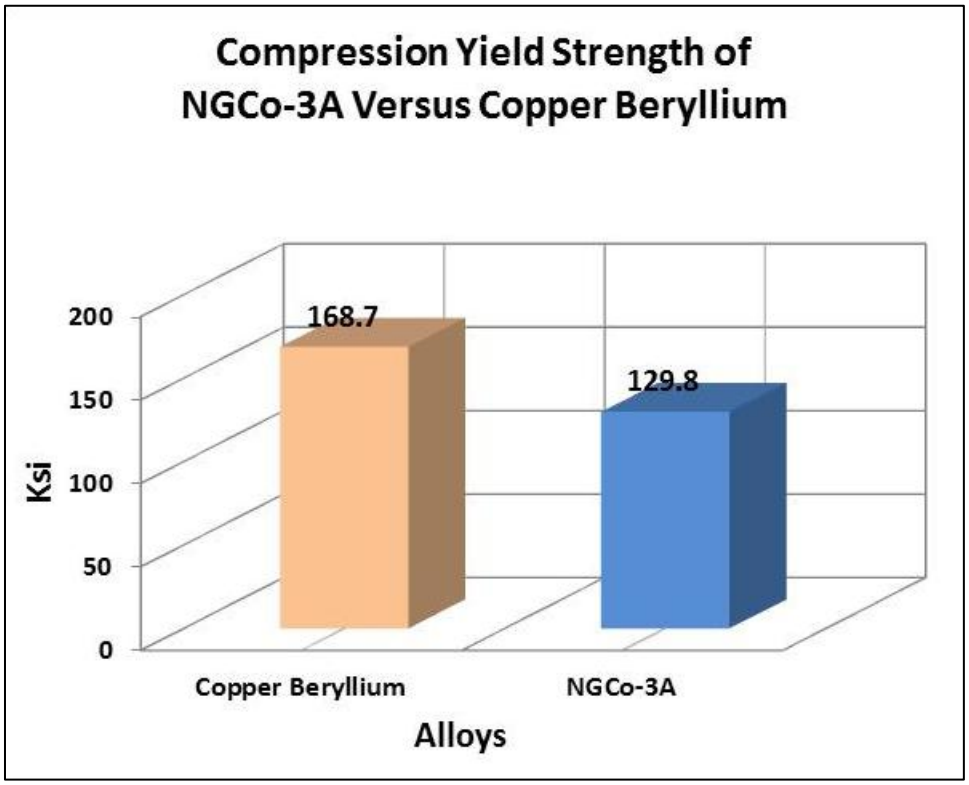

Figure 68. Compression Yield Strength Comparison of NGCo-3A & Copper Beryllium

The compression yield test chart shows the NGCo-3A material producing a slightly higher compression value then that of the tensile yield strength value shown in the previous chart but compare in value very closely. Because the value of the NGCu-1A was considerably lower and no test material or data was availble for the Cuprium, the NGCo-3A material was the down-selected alternative candidate of choice for the compression yield stress evaluation. The NGCo-3A yields a lower compression value than the copper beryllium standard.

The next set of tests focuses on wear and friction properties that produce coefficient of friction and material removal values for evaluation. Material data results for the NGCu-1A and Cuprium are not presented in the following charts for the same justifications that were no materials to perform the tests. Figure 69 presents the pin on disk and reciprocating ball on flat

Use or disclosure of data contained on this sheet is subject to the restriction on the title page of this proposal.
Northrop Grumman Private/Proprietary Level I

coefficient of friction values for the NGCo-3A cobalt based and the copper beryllium baseline material. The comparison shows that the NGCo-3A material is superior in property performance to the baseline in producing lower coefficient of friction values for both wear tests performed. Cobalt based materials are well known for their low sliding resistance and here it can be seen in the alternative alloy materials comparison presented.

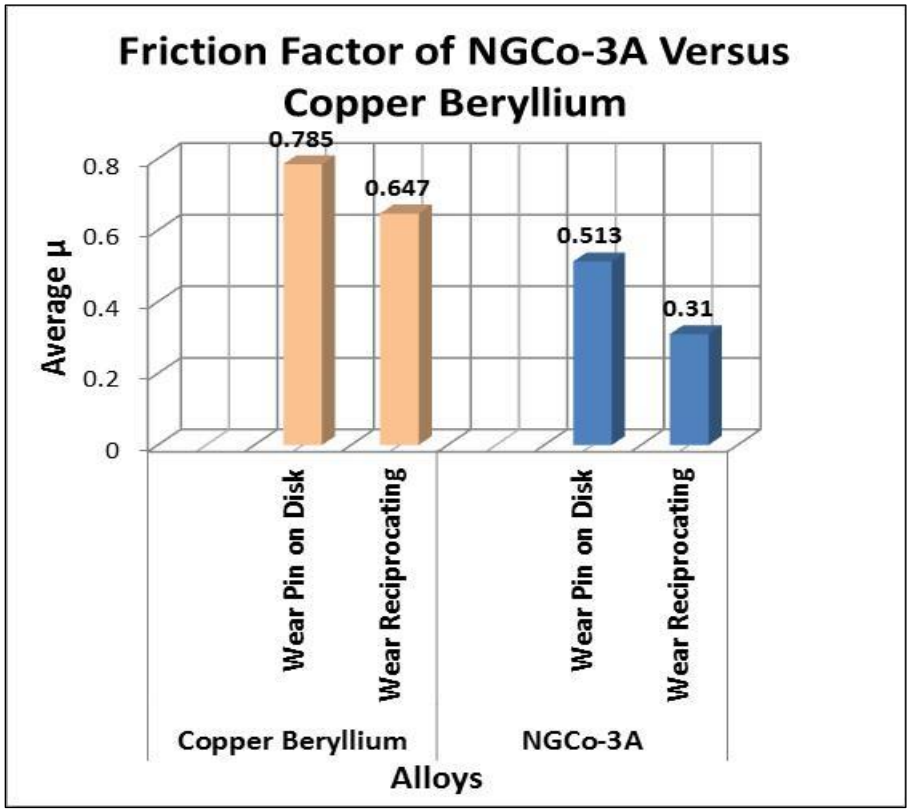

Figure 69. Friction Factor Comparison of NGCo-3A and Baseline Copper Beryllium

The ASTM G99 and G133 wear and friction tests are the last of the tests to be performed form the standard set of testing. The results presented from this standard suite of characterization tests identify the NGCo-3A alternative alloy as being the best in performance and having the most potential for further properties enhancement in both meeting the programs desired level of performance and producing a drop-in replacement for the copper beryllium. Further characteristics testing for galling and stress-life were held off till the alternative alloy material down selection was concluded to both reduce testing and associated costs. The results for these final characterization tests are detailed in the following sections.

3.1.6 Galling Test Results of Evaluation Materials

Wear and Friction Resources in Tomball, Texas performed the ASTM G98 testing and provided the data results for the galling of the NGCo-3A (2" and 4" diameter materials) and AMS 4533 copper beryllium baseline material. Configuration of galling test specimen is shown in Figure 70. All samples were machined at Northrop Grumman Space Park machining center. Images of the machined (button) samples are presented in Figure 71. Several samples were

Use or disclosure of data contained on this sheet is subject to the restriction on the title page of this proposal.
Northrop Grumman Private/Proprietary Level I

produced to support the various loading intervals required to reveal the alloy materials initiation of galling.

The galling test provides the load value at the point in which a material begins to gall. Galling threshold testing was conducted per ASTM Standard Test Method for Galling Resistance of Materials. The test materials were the NGCo-3A (from a 2” diameter ingot), the NGCo-3A (from a 4” diameter ingot) along with the AMS 4533 copper beryllium standard material. The opposing sample, the block, was a PH13-8Mo stainless steel, H1000 condition.

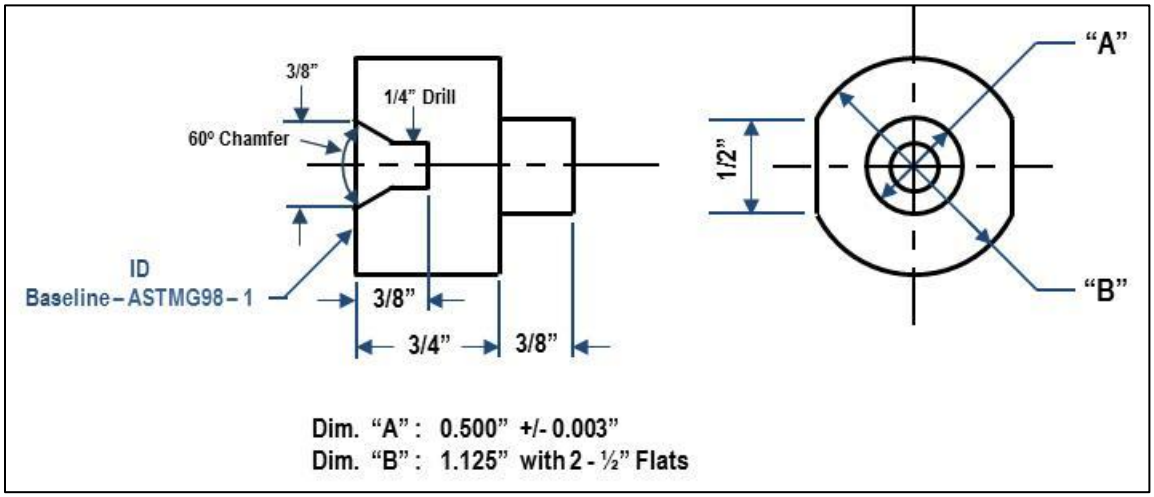

Figure 70. Configuration of ASTM G98 Galling Test Specimen

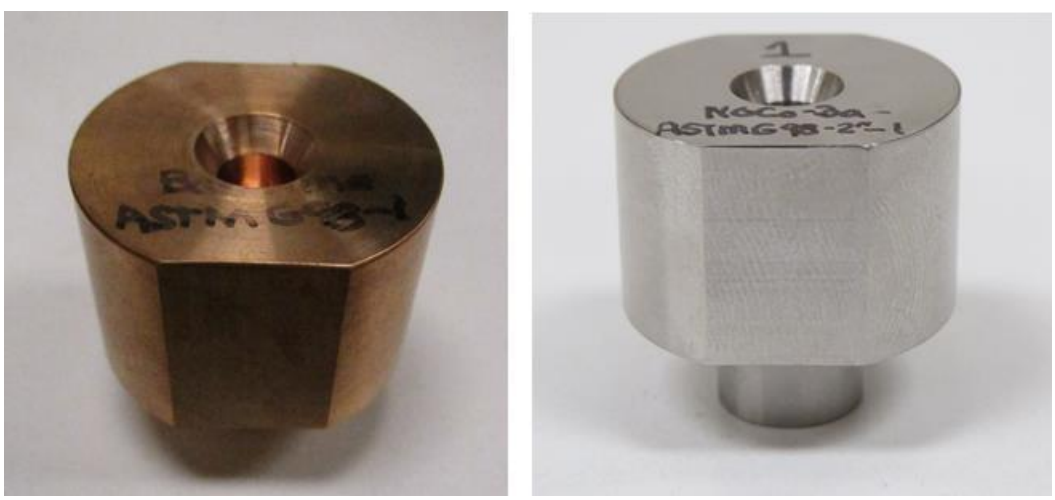

Figure 71. Typical ASTM G98 Machined Galling Button Specimens

This standard galling test utilizes one specimen, called a button, and a mating specimen, called a block, that are compressively loaded to a given contact pressure then turned relative to each other for one full, 360º turn within an elapsed time between 3 and 20 seconds. The contacting surfaces are then examined without magnification for permanent damage to the surfaces. If damage occurred the test is repeated at a lower load until no galling is found and vice versa if no damage occurred in the first test. The equipment consists of a load frame, a stationary

Use or disclosure of data contained on this sheet is subject to the restriction on the title page of this proposal.
Northrop Grumman Private/Proprietary Level I

fixture to hold one specimen, and a second fixture with a means to spin the moveable sample. Figure 72 shows the test fixture used in performing the ASTM G98 galling tests.

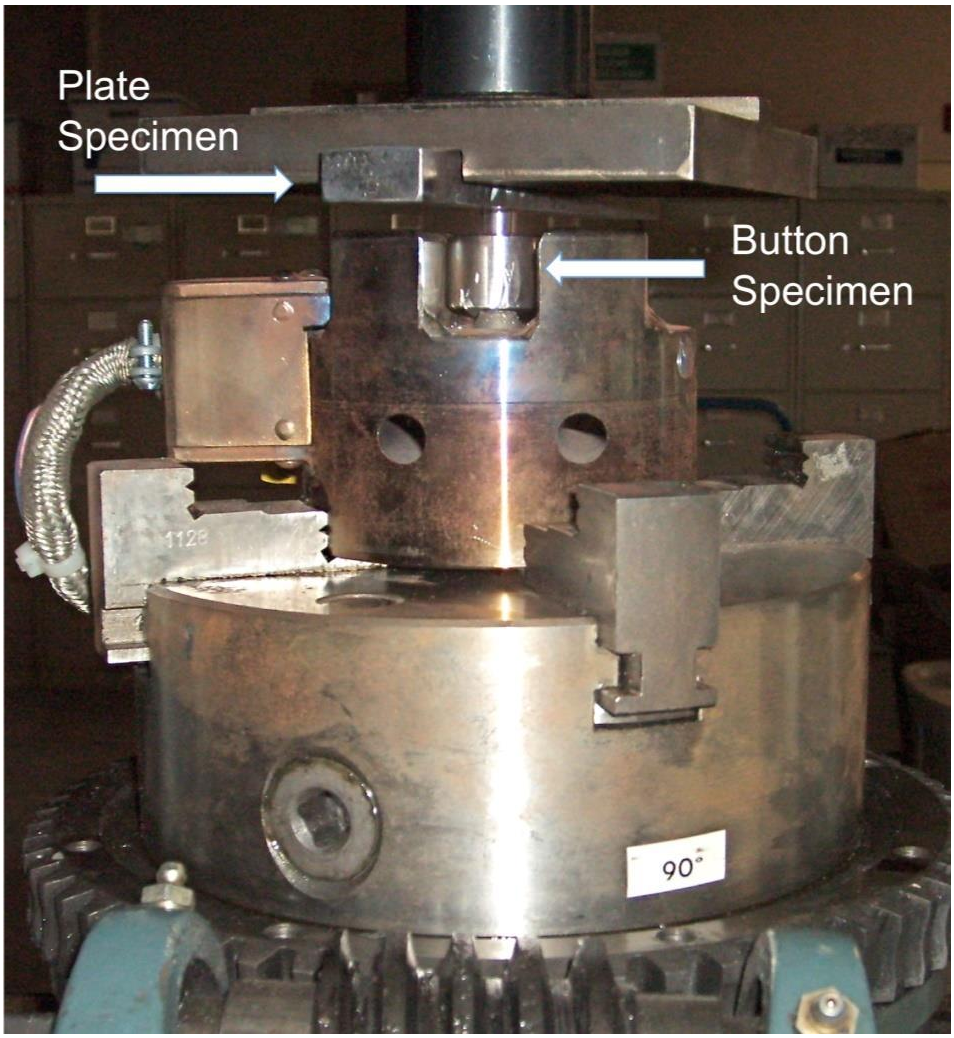

Figure 72. Typical ASTM G98 Test Setup Fixture

It was found that the galling threshold of both alloys was greater than 114,100 psi. There was no measureable difference in the threshold among the three specimens. The contact pressures achieved in the galling tests are probably lower than the theoretical yield strength of the alloys because G98 specimens typically experience unequal loading across the face of the button with the outer periphery experiencing higher loads than the center. The contact pressure was increased incrementally up to the point the buttons deformed during rotation. In all three material combinations no galling was observed. A summary of the galling test results is provided in Table 9. The tested surfaces of the buttons and blocks are in Figures 73 through 75.

Use or disclosure of data contained on this sheet is subject to the restriction on the title page of this proposal.
Northrop Grumman Private/Proprietary Level I

Table 9. Summary of ASTM G98 Galling Test Results

Summary of Galling Threshold Testing

Sample	Load (pounds)	Contact Pressure (psi)	Galling?
Cu-Be	13,998	71,300	No
Cu-Be	16,798	85,600	No
Cu-Be	19,597	99,900	No
Cu-Be *	22,397	114,100	No
NGCo-3A (2")	4,199	21,398	No
NGCo-3A (2")	7,838	39,943	No
NGCo-3A (2")	13,998	71,327	No
NGCo-3A (2") *	22,397	114,124	No
NGCo-3A (4")	16,797	85,593	No
NGCo-3A (4")	19,597	99,858	No
NGCo-3A (4") *	22,396	114,124	No

* Note: Button specimen deformed after approximately 180 degrees of rotation.

Hardness's for the four alloys measured 38, 38, 39 and 44 Rc for the Cu-Be, NGCo-3A (2"), NGCo-3A (4") and PH13-8Mo H1000 condition stainless blocks respectively.

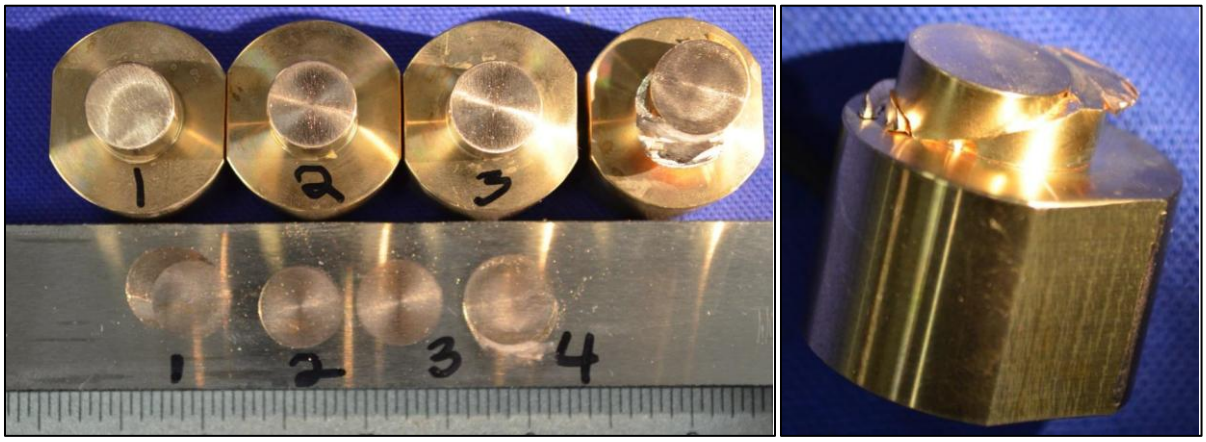

Figure 73. ASTM G98 CuBe Test Specimens with Highest Loaded Specimen

Use or disclosure of data contained on this sheet is subject to the restriction on the title page of this proposal.
Northrop Grumman Private/Proprietary Level I

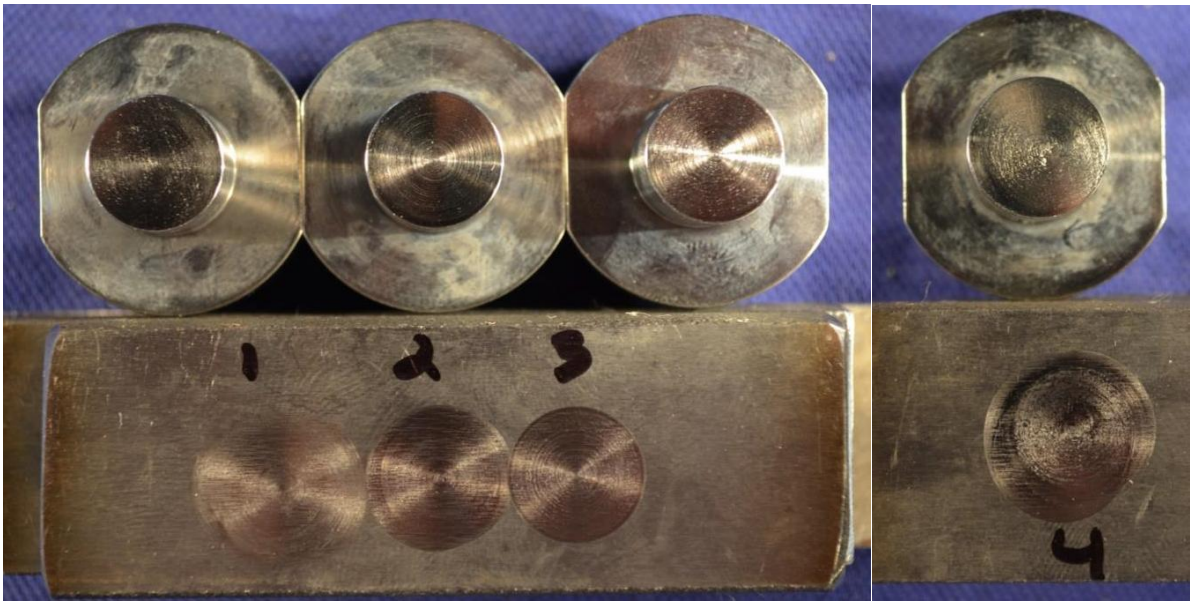

Figure 74. ASTM G98 NGCo-3A (2”) Test Specimens along with Highest Loaded Specimen

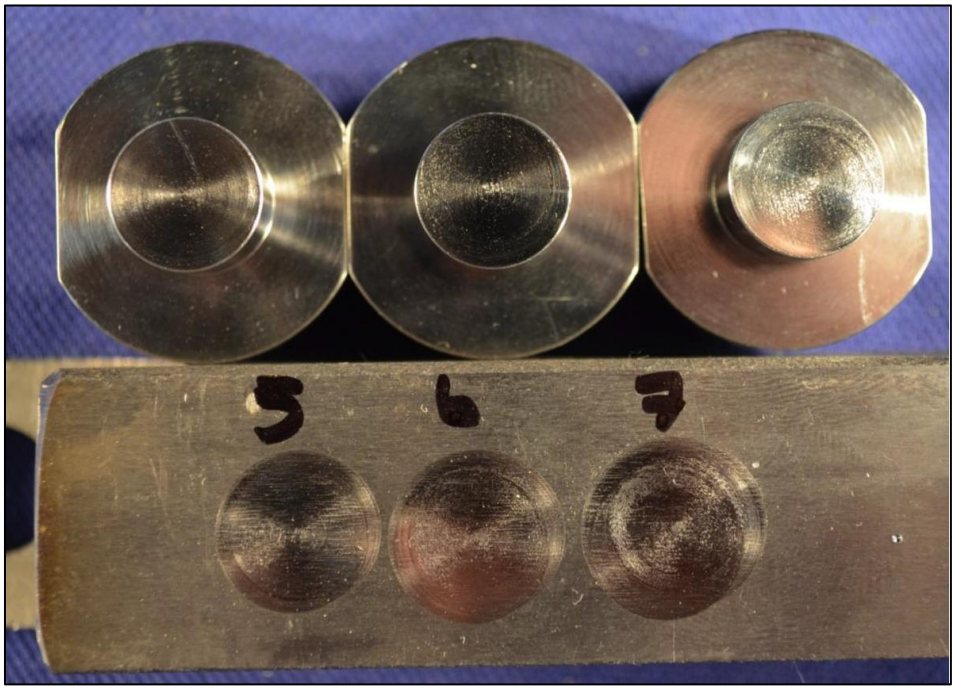

Figure 75. ASTM G98 NGCo-3A (4”) Test Specimens along with Highest Loaded Specimen

Conclusion:

1. The galling thresholds of the two tested alloys against PH13-8Mo H1000 condition stainless were greater than 114,100 psi.
2. There was no measureable difference in the galling thresholds among the three specimen groups.
3. Based on the permanent deformation that took place in the button specimens, localized loads were approaching the materials’ yield strengths.

Use or disclosure of data contained on this sheet is subject to the restriction on the title page of this proposal.
Northrop Grumman Private/Proprietary Level I

Comparison result validate that the NGCo-3A alternative alloy is as good as the incumbent alloy for galling.

3.1.7 Fatigue Life Cycle Test Results of Evaluation Materials

Element Materials Technologies in Huntington Beach, CA., performed the ASTM E606 strain life fatigue cycle testing on both NGCo-3A alloy (from the 2” billet) and the NGCo-3A alloy (from the 4” billet) along with the baseline material and provided the data results.

Configuration of ASTM E606 test sample is shown in Figure 76. All fatigue life test samples were machined at Northrop Grumman Space Park machining center. Sample measurements verification and surface finish checks were performed to support consistent sample replication. Images of the machined (fatigue life) samples are shown in Figure 77. Several samples were produced from the alloys to support the various stress loading conditions in creating the alloy fatigue life stress materials comparison curves.

This testing will provide the strain-life cycle comparison of the alternative NGCo-3A alloy to the baseline for various strain and load ratio conditions. Strain-life curves developed from the testing were plotted so evaluation results could be easily evaluated. Data results from both the 2” and 4” NGCo-3A material billets were used in producing the fatigue life curves for the NGCo-3A alloy.

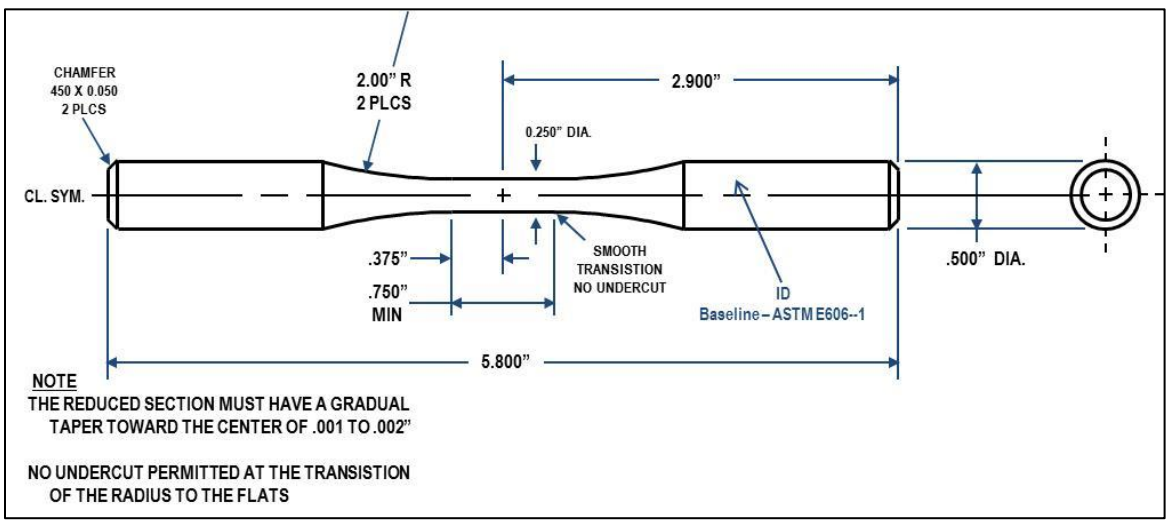

Figure 76. ASTM E606 Fatigue-Life Cycle Specimen Details

Use or disclosure of data contained on this sheet is subject to the restriction on the title page of this proposal.
Northrop Grumman Private/Proprietary Level I

Figure 77. Typical ASTM E606 Machined Fatigue-Life Specimens (NGCo-3A and Copper Beryllium)

Two cyclic conditions were performed to evaluate the materials under these varying conditions. Both the R = (0) and the R= (-1) conditions were tested. This side by side comparison is presented in Figure 78. The strain controlled fatigue life tests at the various stress loading conditions provides cyclic fatigue performance characteristics of the evaluation materials.

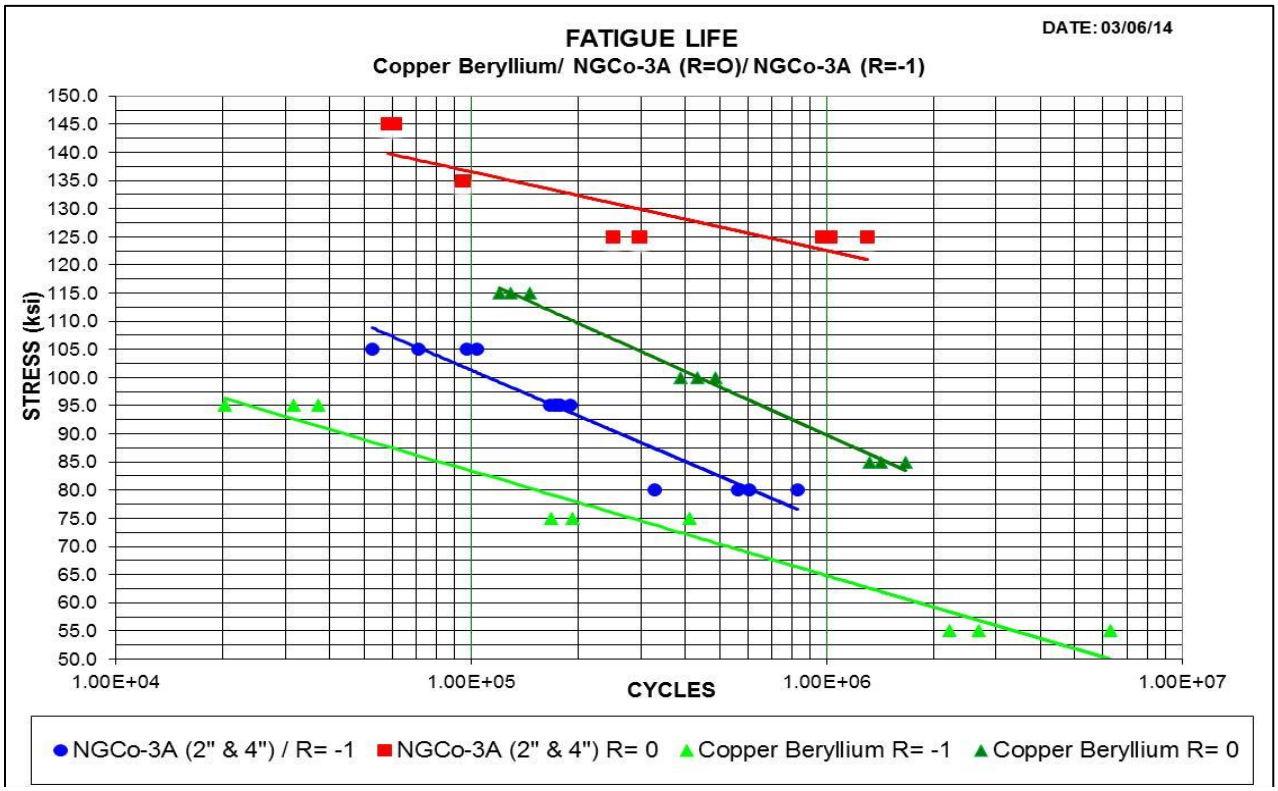

Figure 78. Fatigue Life Cycle Comparison Test Results of the NGCo-3A Alternative and the Standard CuBe Alloy

Use or disclosure of data contained on this sheet is subject to the restriction on the title page of this proposal.
Northrop Grumman Private/Proprietary Level I

Results of both the R = (0) and R = (-1) at the various load conditions show that the NGCo-3A has superior load and cyclic fatigue performance behavior over the baseline alloy material. A majority of the characteristic testing results have demonstrated an as good or better performance level from the NGCo-3A alternative alloy as compared to the baseline material supporting the potential for the alternative material to become a drop in replacement material.

4.0 ENHANCED BUSHING DEVELOPMENT EVALUATION

Extensive research has been conducted to study the complex mechanical behavior of metal alloy under complicated loading conditions numerically and experimentally.

For wear and contact studies, Teisanu et al.[7] performed both experimental and Finite Element Analysis (FEA) for the Powder Metallurgy iron based bearing bush isolated from the spindle and loaded with variable friction forces. The equivalent Von Mises stresses distribution and the elastic deformations' distribution were determined. Molinari et al.[8] [MORR-01] formulated a Lagrangian finite element framework capable of accounting for large plastic deformations and history-dependent material behavior of dry sliding wear in metals. The model is validated against a conventional test configuration consisting of a brass pin rubbing against a rotating steel plate. Kim et al.[9] [KWBH-05] used a numerical approach to simulate the progressive accumulation of wear in oscillating metal on metal contacts. The approach used a reciprocating pin-on-disk tribometer to measure a wear rate for the material pair of interest. This wear rate is an input to a FEA that simulates a block-on-ring experiment. After the simulation, two block-on-ring experiments were performed with the same materials that were studied in the reciprocating pin-on-disk experiments.

The goal of the Finite Element Analysis is to mimic the bushing experimental test and to perform parametric studies of the bushing stresses. The fatigue life of the proposed new type of alloy materials which will replace the Cu-Be alloy bushing can be predicted based on the simulation results.

Various parametric of FEA studies will be performed. It is emphasized that the trends, instead of exact predictions, of the mechanical behaviors due to various parameters will be presented.

4.1 FINITE ELEMENT SIMULATION TOOLS

There are several software packages on the market for Finite Element Analysis:

- Siemens NX
- ABAQUS
- Pro/Mechanica
- ANSYS WORKBENCH
- Others.

While NX at the moment only handles linear analyses, ABAQUS is being recommended by most experts as the preferable program, especially for a contact and non-lineal analysis. ABAQUS/CAE has a very intuitive interface and is very powerful. ABAQUS does a good job of handling contact, plasticity, and other non-linear problems. In addition to their ABAQUS/Standard solver, they offer an explicit solver for dynamic problems. ABAQUS also

Use or disclosure of data contained on this sheet is subject to the restriction on the title page of this proposal.
Northrop Grumman Private/Proprietary Level I

has the ability to incorporate Python scripting[8] into a model which gives the user a lot of flexibility in their analysis.

4.2 GENERAL PROPERTIES

The general bushing geometries considered in the simulations include: (a) 1/4" width bushing (Figure 80) and (b) 1" width bushing (Figure 81). The impact of inner and outer chamfers will be analyzed (Figure 82). The model utilizes three parts: a shaft, a bushing, and a loading plate. The dimensions are listed in Table 10. The parts are arranged to match the testing setup, with all parts centered with each other (Figure 79). The general interaction properties and boundary conditions (BCs) are specified as follows. ABAQUS/ Standard Version 6.10 of ABAQUS Inc.[10], dynamic/implicit analysis with Full Newton solution technique, is used to solve the contact problem.

Interaction Properties

The general objective is to ensure the bushing does not rotate in the plate (In ABAQUS called "sticking") while the shaft rotates, utilizing these contact properties:

Tangential Direction: $\mu = 0.75$ (static coefficient of friction) between the bushing and the shaft, $\mu = 1.2$ (static coefficient of friction) between the bushing and the plate. Penalty friction formulation is used to model a modified Coulomb friction by introducing the elastic slip in the sticking phase (Simulating ideal friction behavior can be very difficult; therefore, by default in most cases, ABAQUS uses a penalty friction formulation with an allowable "elastic slip." The "elastic slip" is the small amount of relative motion between the surfaces that occurs when the surfaces should be sticking. Abaqus automatically chooses the penalty stiffness so that this allowable "elastic slip" is a very small fraction of the characteristic element length.)

Normal Direction: hard contact.

The part geometry provides a 0.001" clearance at both the shaft/bushing and the bushing/plate interactions.

Boundary and Loading Conditions

As shown in **Figure 79**,

- Bottom face of plate is fixed (U1=U2=U3=UR1=UR2=UR3=0).
- Shaft is constrained along the Z-direction to prevent movement (U3=0). Two different boundary conditions of the shaft will be considered: (1) a "long" shaft that is free to rotate at the ends (as a simply supported beam, no rotational boundary conditions) and (2) a "short" shaft that cannot rotate at the ends (as a fixed beam, UR1=UR2=UR3=0).
- Concentrated static loads are applied symmetrically at both ends of the shaft along the positive Y-direction. This is equivalent to the total concentrated loads applied on the center of the plate in the modeled setup. Unless otherwise noted, this load is either progressive (2000; 4000; 6000; 8000; 10,000 lbs.), or a single-step load of 10,000 lbs. These loads are applied with a small initial ramp-up period to minimize inertial impact effects.
- Prior to applying the concentrated loads to the shaft, the shaft rotates at specified values in radian/sec. The shaft rotational velocity is applied from either one side (one-sided/asymmetric rotation) or both sides (symmetric rotation) of the shaft. These two

Use or disclosure of data contained on this sheet is subject to the restriction on the title page of this proposal.
Northrop Grumman Private/Proprietary Level I

conditions will cause different stress distributions on the shaft as will be discussed in chapter 6.3 Parametric Case Studies.

Elements

- Linear hexahedron, type C3D8R. Three-dimensional solid continuum, linear, reduced-integration, brick elements with 8 nodes.

Geometry:

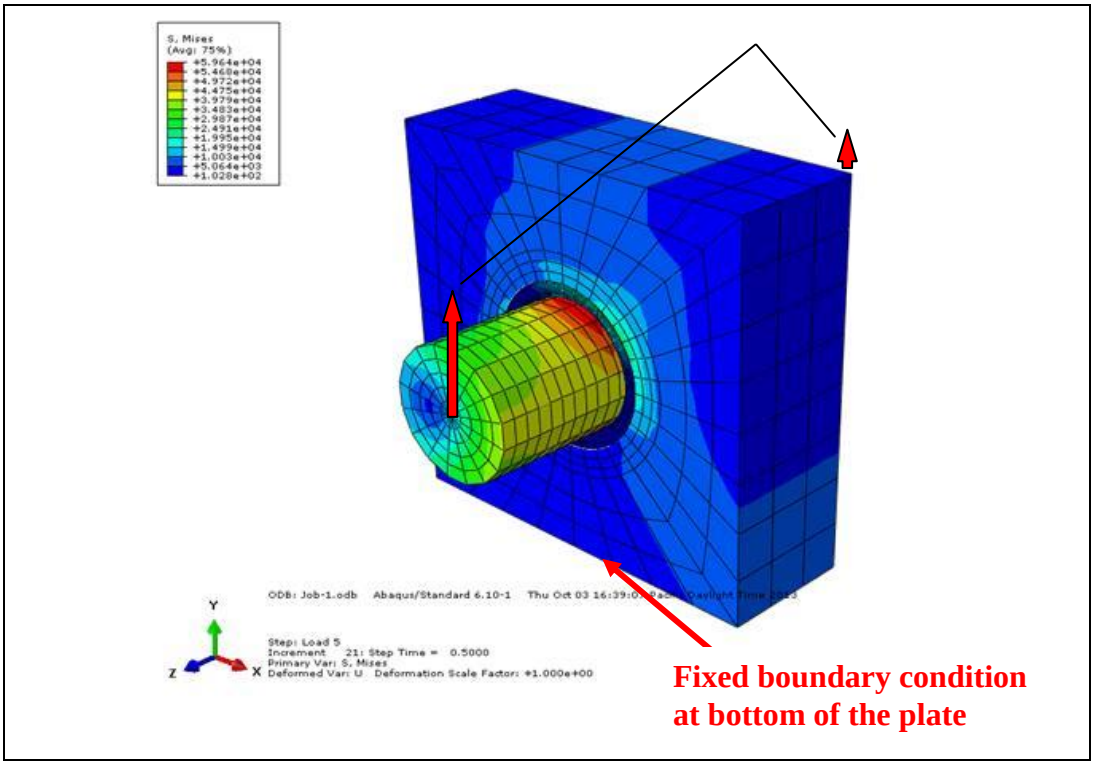

Figure 79. General Mesh of the 1" Width Bushing Showing the Bushing, Shaft, and Plate Geometry

Use or disclosure of data contained on this sheet is subject to the restriction on the title page of this proposal.
Northrop Grumman Private/Proprietary Level I

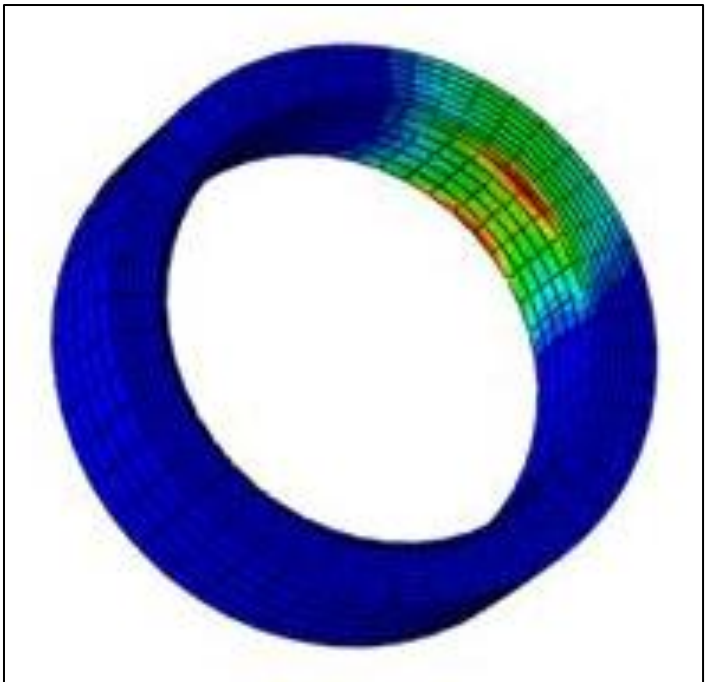

Figure 80. General Mesh for 1/4" Width Bushing

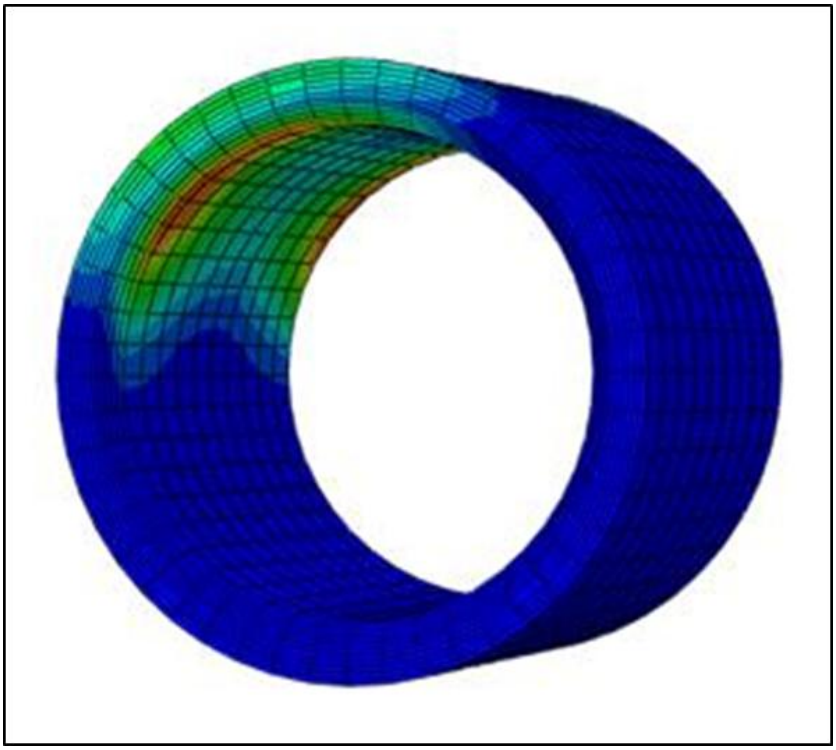

Figure 81. General Mesh for 1" Width Bushing

Use or disclosure of data contained on this sheet is subject to the restriction on the title page of this proposal.
Northrop Grumman Private/Proprietary Level I

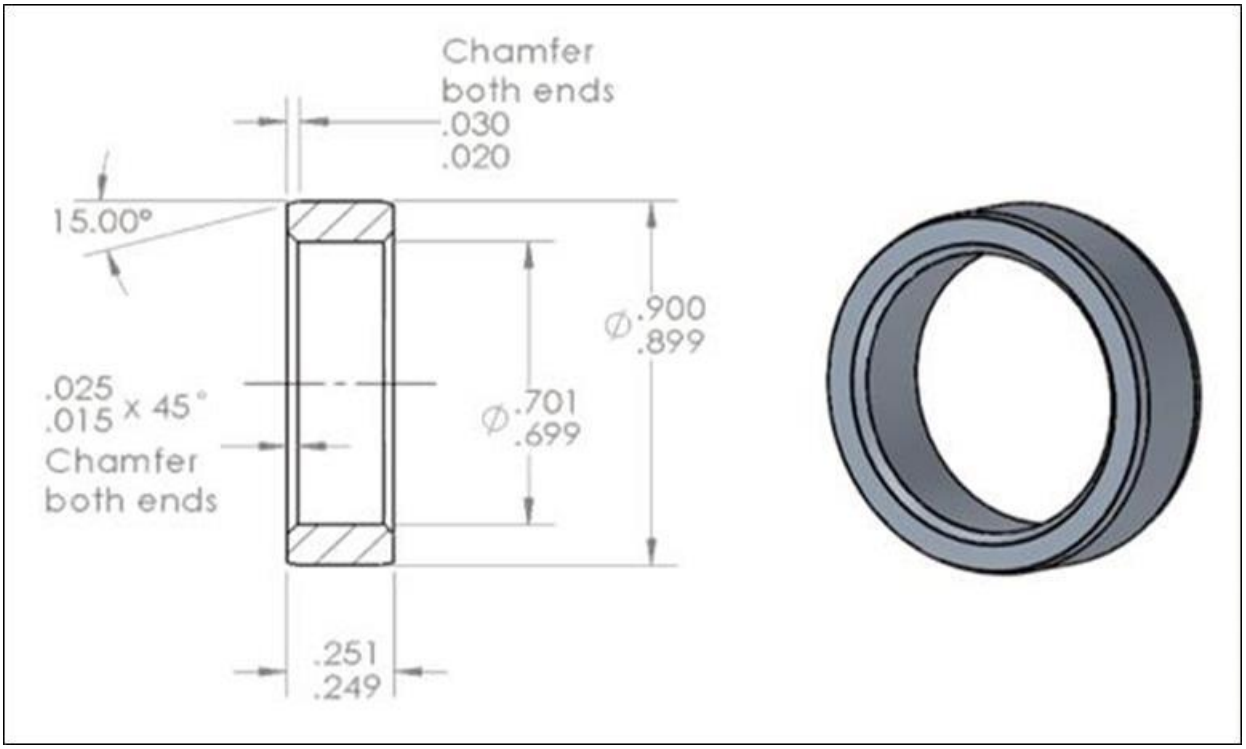

Figure 82. Geometry of the 1/4" Width Bushing with Chamfer

Table 10. General Geometric Properties of Bushing, Shaft and Plate

Part	Inner Diameter (in)	Outer Diameter (in)	Length (in)	Thickness (in)	Inner Chamfer (in)
1" Bushing	0.999	1.5	1	0.249	0.05
¼" Bushing	0.699	0.9	0.25	0.099	0.02
1" Shaft	N/A	1	3	N/A	N/A
0.7" Shaft	N/A	0.7	3	N/A	N/A
	Width (in)	**Height (in)**	**Thickness (in)**		
Plate	3	3	1		

4.3 PARAMETRIC CASE STUDIES

Various parametric studies are performed and presented in the following sections.

4.3.1 CASE 1: Increasing Load

This case study investigates the relation between applied loading and bushing stresses. The rotational velocity of 0.35 rad/sec is the approximate rotational speed for a shaft going through one -15°/+15° cycle every 3 seconds. Since a full cycle will go from 0 to +15° to 0 to -15° to 0 within 3 seconds, the total rotational angle is 60° in 3 seconds. A unidirectional velocity is chosen for simplicity. Model properties of case 1 are listed in Table 11.

Use or disclosure of data contained on this sheet is subject to the restriction on the title page of this proposal.
Northrop Grumman Private/Proprietary Level I

Table 11. Model Properties for Case Study 1 (Increasing Load)

Loading	Progressive (1000 lb increments), symmetric
Rotation	0.35 rad/sec, one-sided rotation
Shaft BCs	Long shaft (U3=0)
Bushing Geometry	1" bushing
Material	Cu-Be TF-00

Results:

Symmetric loading appears to have a roughly linear effect on the bushing contact pressure (Figure 83). The bushing maximum Von Mises stress follows the same pattern (usually within 200 psi of the contact pressure). With this bushing geometry, the internal stresses do not approach yielding even at 20 kips of loading. Thus, this response is characteristic of linear elastic behavior.

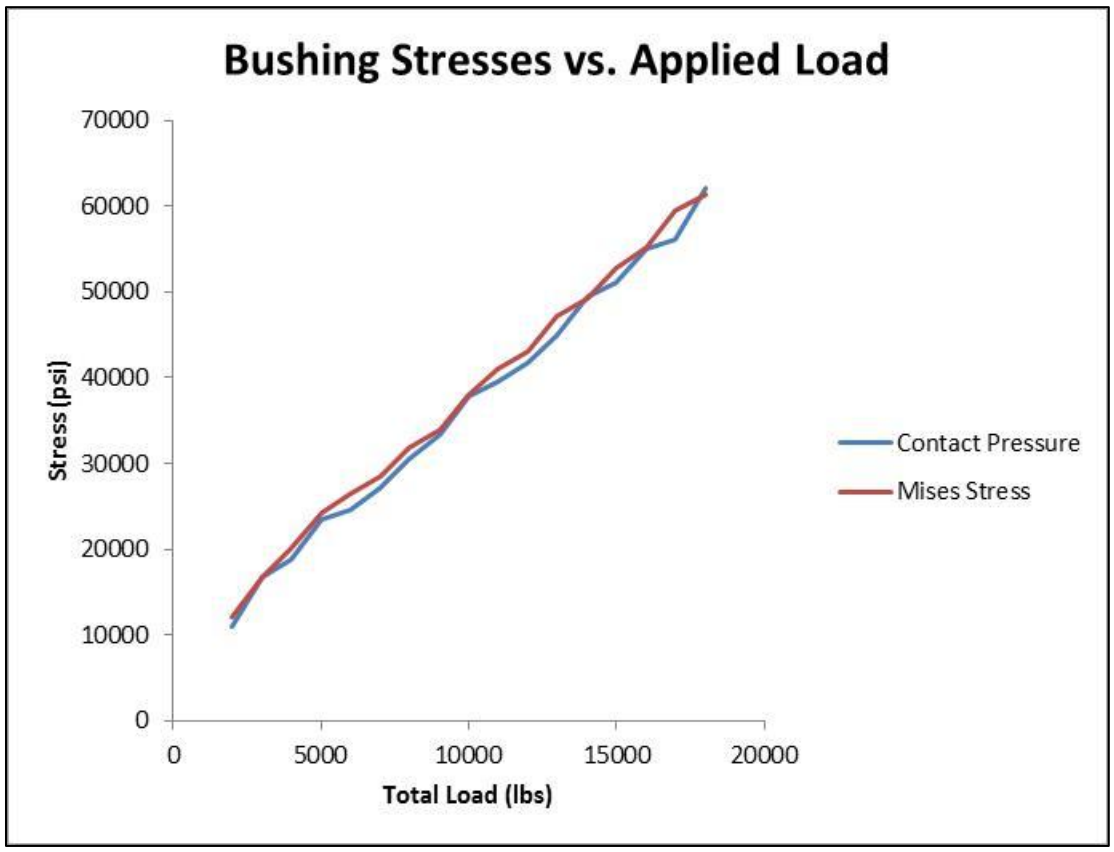

Figure 83. Bushing Stresses Versus Applied Load

4.3.2 CASE 2: Shaft Rotational Velocity

This case study investigates the effect of the shaft's rotational velocity on the bushing stresses. The rotational velocity is unidirectional for simplicity, and is steadily increased across each time step. Unlike the other case studies, the load is applied prior to any applied rotation. Model properties of case 2 are listed in Table 12.

Use or disclosure of data contained on this sheet is subject to the restriction on the title page of this proposal.
Northrop Grumman Private/Proprietary Level I

Table 12. Model Properties for Case Study 2 (Shaft Rotational Velocity)

Loading	Single-step (10,000 lbs), symmetric
Rotation	Progressive, 0.1 rad/sec increments, one-sided rotation
Shaft BCs	Long shaft (U3=0)
Bushing Geometry	1" bushing
Material	Cu-Be TF-00

Results:

Because this is a quasi-static analysis, varying the rotation speed appears to have little effect (Figure 84). The only change is when rotation first initiates from zero, where the stress appears to shift from the bushing to the shaft, as the drop of bushing stresses. This is mainly due to the dynamic effect for the transfer of stresses from the bushing to the shaft. Once the shaft is rotating, increasing the speed will release additional energy through heat and wear/fatigue, neither of which are considered in this model.

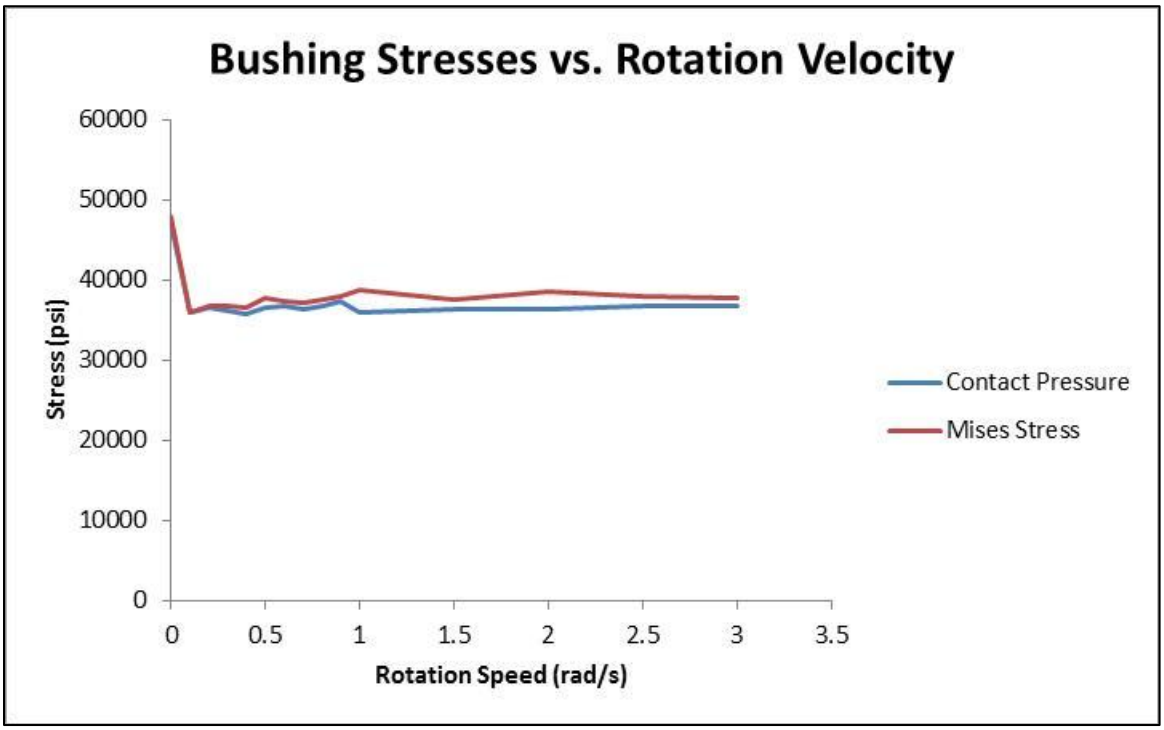

Figure 84. Bushing Stresses versus Rotation Velocity

4.3.3 CASE 3: Coefficient of Friction

This case study investigates the effect of the bushing's coefficient of friction on the bushing stresses. To ensure no slip between the bushing and plate, that surface interaction is assigned a coefficient of friction of $\mu = 2.0$. The bushing/shaft interaction is then assigned a progressively larger coefficient of friction. Model properties of case 3 are listed in Table 13.

Use or disclosure of data contained on this sheet is subject to the restriction on the title page of this proposal.
Northrop Grumman Private/Proprietary Level I

Table 13. Model properties for case study 3 (coefficient of friction)

Loading	Single-step (10,000 lbs), symmetric
Rotation	0.35 rad/sec, one-sided rotation
Shaft BCs	Long shaft (U3=0)
Bushing Geometry	1" bushing
Material	Cu-Be TF-00

Results:

The Von Mises stresses increase fairly steadily with increased μ (static coefficient of friction), and the shaft experiences noticeably higher stresses than the bushing (Figure 85). However the shaft and the bushing contact pressures are fairly even, which makes sense as they are directly interacting (Figure 86). Interestingly, contact pressure appears to decrease with greater μ. This may be explained by the increasing contact shear stress shown in Figure 87. Increasing μ may be diverting strain energy from normal pressure to shear. These results can provide insight into fatigue behavior if additional data relating fatigue damage to coefficient of friction is obtained.

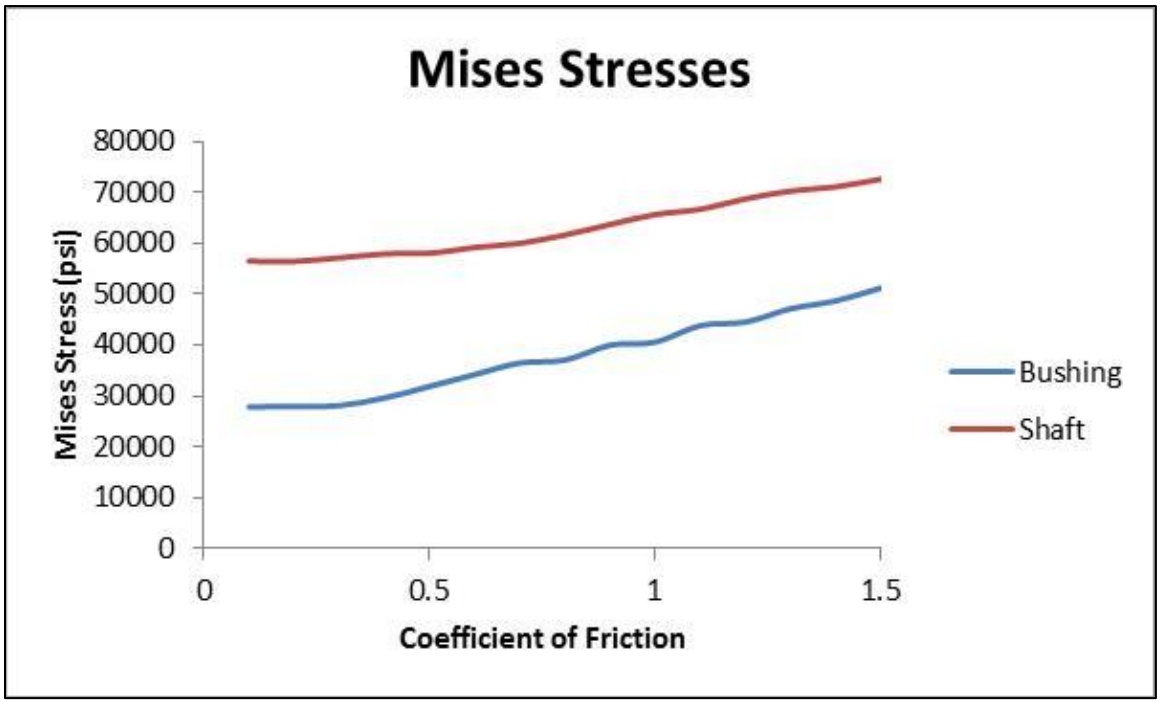

Figure 85. Bushing and Shaft Von Mises Stresses versus Static Coefficient of Friction

Use or disclosure of data contained on this sheet is subject to the restriction on the title page of this proposal.
Northrop Grumman Private/Proprietary Level I

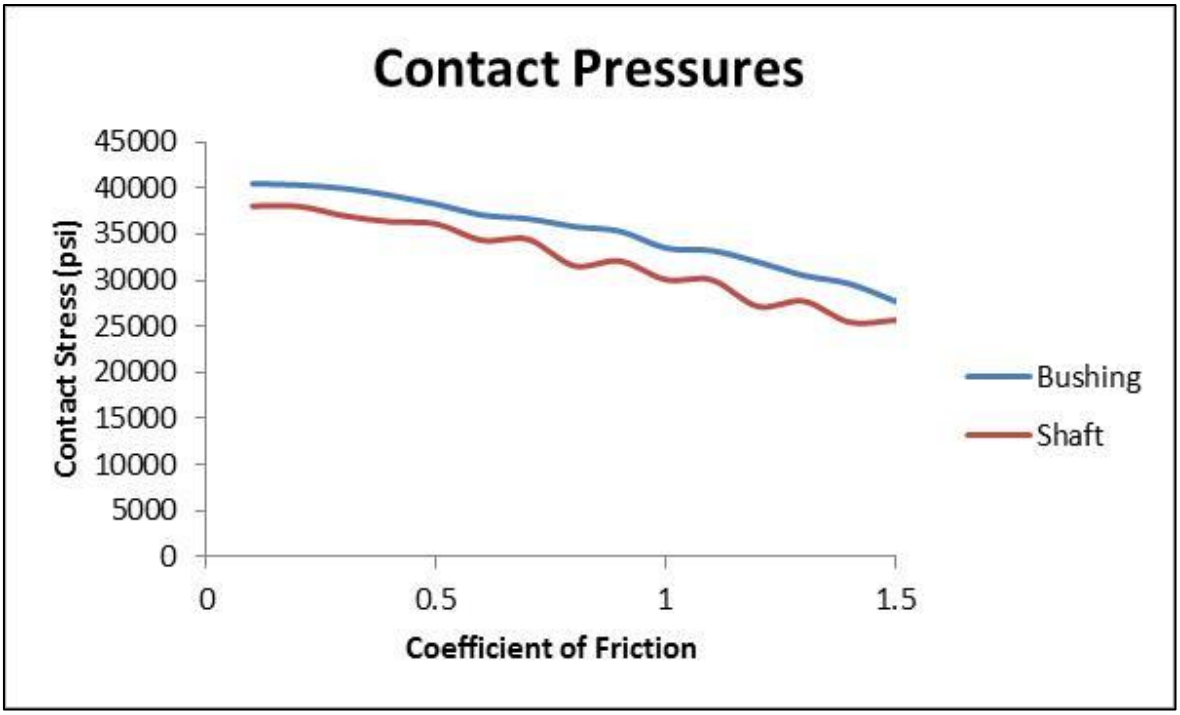

Figure 86. Bushing and Shaft Contact Pressures versus Static Coefficient of Friction

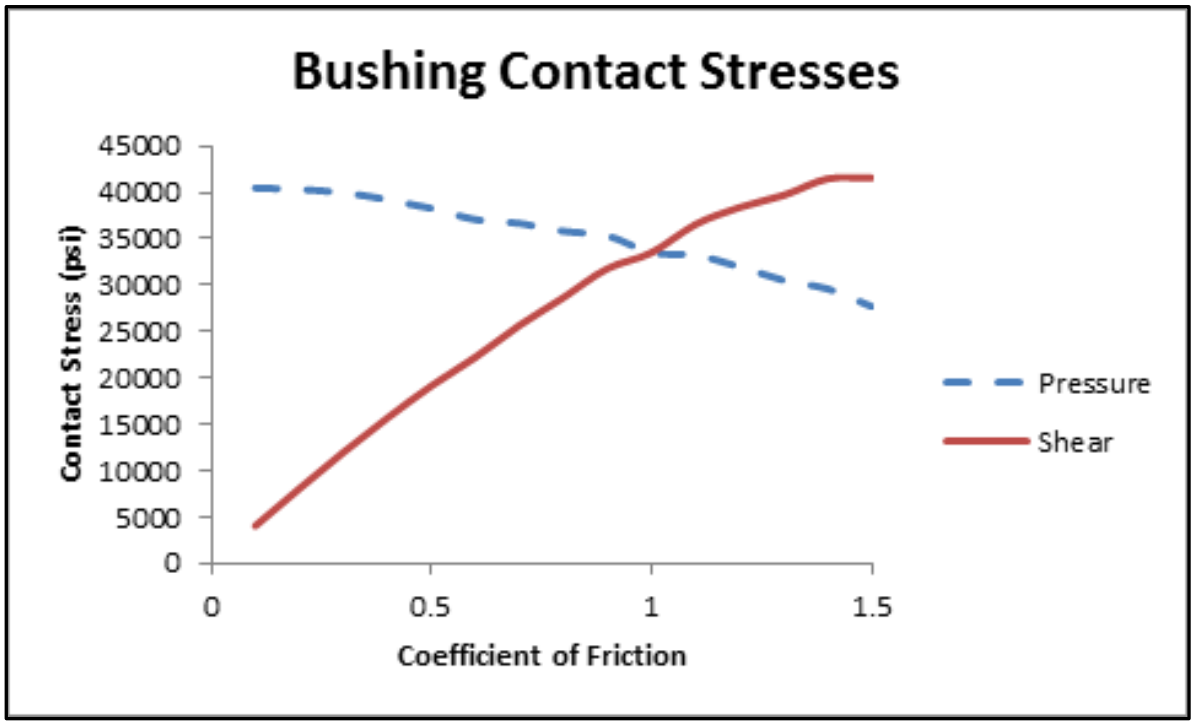

Figure 87: Bushing Contact Pressures & Contact Shear Stress versus Static Coefficient of Friction

Use or disclosure of data contained on this sheet is subject to the restriction on the title page of this proposal.
Northrop Grumman Private/Proprietary Level I

4.3.4 CASE 4: Shaft Boundary Conditions, Loading Conditions, and Tilt

This case study investigates the effect of various shaft boundary conditions on the bushing stresses. The rotational velocity is set to 0.58 rad/sec, equivalent in speed to a +25°/-25° cycle every 3 seconds. Since a full cycle will go from 0 to +25° to 0 to -25° to 0 within 3 seconds, the total rotational angle is 100° in 3 seconds. The variables considered will be the shaft boundary conditions (long or short shaft), applied rotation (symmetric or asymmetric), shaft tilt, and applied load direction (aligned with the tilted shaft vs aligned with the loading plate). The shaft tilt can represent a manufacturing error that causes a connection to be misaligned. For reference, "CPRESS" refers to contact pressure, while "CSHEAR1" is the contact shear stress in the rotational direction.

Shaft is constrained along the Z-direction to prevent movement (U3=0). Two different boundary conditions of the shaft will be considered: (1) a "long" shaft that is free to rotate at the ends (as a simply supported beam, no rotational boundary conditions) and (2) a "short" shaft that cannot rotate at the ends (as a fixed beam, UR1=UR2=UR3=0).

Prior to applying the concentrated loads to the shaft, the shaft rotates at specified values in radian/sec. The shaft rotational velocity is applied from either one side (one-sided/asymmetric rotation) or both sides (symmetric rotation) of the shaft. These two conditions will cause different stress distributions on the shaft as will be discussed herein. Model properties of Case 4 are listed in Table 14.

Table 14. Model Properties for Case Study 4 (shaft Boundary Conditions, Loading Conditions, & Tilt)

Loading	Single-step (10,000 lbs), symmetric
Rotation	0.58 rad/sec, asymmetric or symmetric rotation
Shaft BCs	Long shaft (U3=0) or Short shaft (U3=UR1=UR2=UR3=0)
Bushing Geometry	1" Width bushing
Material	Cu-Be TF-00

Table 15. Effects of Tilt and Boundary Conditions with Non-Tilting Load and Asymmetric Rotation

Shaft Tilt	Bushing Von Mises Stress (psi)	Bushing CPRESS (psi)	Bushing CSHEAR1 (psi)	Shaft Von Mises Stress (psi)	Shaft CPRESS (psi)	Shaft CSHEAR1 (psi)
0 ("long" shaft)	53880	41270	30950	58910	46330	34750
0 ("short" shaft)	44000	34330	25750	46650	35990	26990
0.11 ("short" shaft)	52600	40620	30470	45940	45710	34280
% Change	19.55%	18.32%	18.33%	-1.52%	27.01%	27.01%

Table 16. Effects of Shaft Tilt with Tilting Load Asymmetric Rotation

Shaft Tilt	Bushing Von Mises Stress (psi)	Bushing CPRESS (psi)	Bushing CSHEAR1 (psi)	Shaft Von Mises Stress (psi)	Shaft CPRESS (psi)	Shaft CSHEAR1 (psi)
0 ("short" shaft)	44000	34330	25750	46650	35990	26990
0.11 ("short" shaft)	55530	43230	32420	45500	47120	35340
% Change	26.20%	25.92%	25.90%	-2.47%	30.93%	30.94%

Use or disclosure of data contained on this sheet is subject to the restriction on the title page of this proposal.
Northrop Grumman Private/Proprietary Level I

Table 17. Effect of Shaft Tilt with Tilting Load and Symmetric Rotation

Shaft Tilt	Bushing Von Mises Stress (psi)	Bushing CPRESS (psi)	Bushing CSHEAR1 (psi)	Shaft Von Mises Stress (psi)	Shaft CPRESS (psi)	Shaft CSHEAR1 (psi)
0 (“short” shaft)	43870	34220	25660	35020	35740	26810
0.11 (“short” shaft)	55270	43070	32300	37970	47060	35290
% Change	25.99%	25.86%	25.88%	8.42%	31.67%	31.63%

Results:

Results are presented in from Table 15 to Table 17:

1. Applying a shaft tilt will, in general, increase the stresses and contact pressures in both the shaft and bushing (~25% in this test) (Figure 89). However, enforcing the minute rotation (“short” shaft) required additional boundary conditions, which actually reduced the stresses and contact pressures by itself as shown in Table 11 (“long” shaft vs. “short” shaft at 0 degree tilt). The previous models assumed a “long” shaft which allowed the ends of our model's shaft to rotate and deform freely, like a pinned support. In the “long” shaft system, a small tilt will have little to no effect because the shaft will simply deform to straighten out. Thus, it must be treated as a short shaft, which may in fact be more realistic depending on the particular application. This makes the shaft itself much stiffer, so a lot of the load is absorbed and more evenly distributed throughout the shaft (Figure 88). The additional boundary conditions reduce the maximum stresses by about 20%.
2. Changing the loading direction to match the shaft (normal to the shaft's axis when tilted) will increase the contact pressures slightly.
3. Von Mises stresses in the shaft are focused on the end that applied the rotation under the short shaft BCs. These are probably caused by a constant warping of the bent beam as it rotates (the bushing enforces a set position). To compensate and compare, the shaft rotation is applied on both sides of the shaft, and got much cleaner Von Mises stress fields (Figure 90). However, while the shaft stresses are more evenly distributed (~33% reduction in maximum Von Mises stress), the bushing stresses are relatively unaffected.

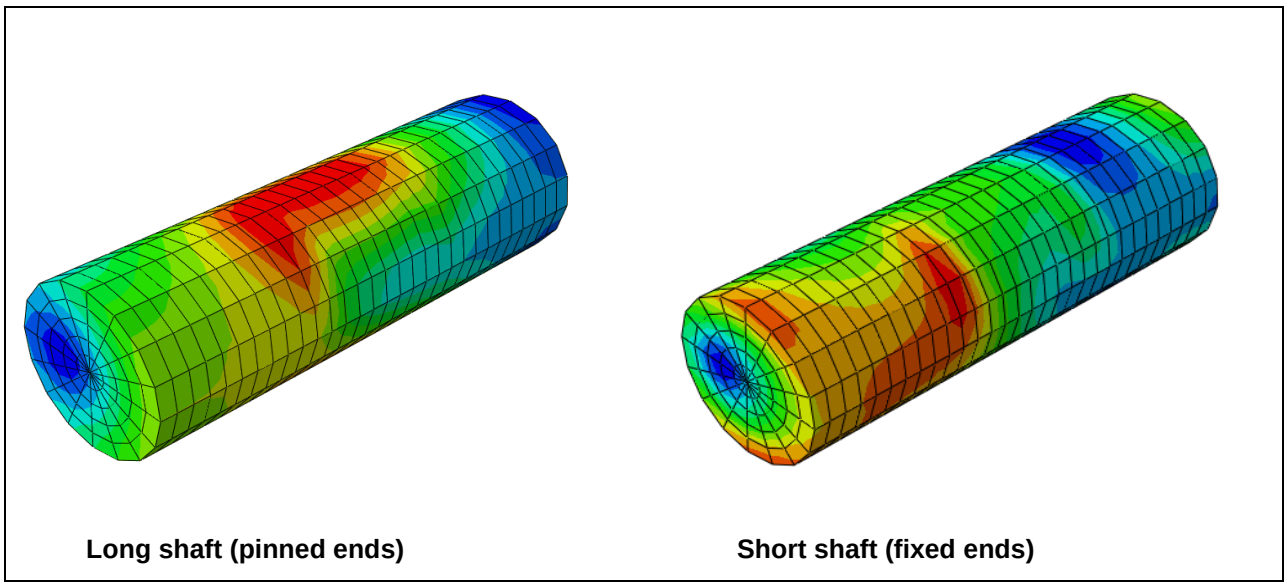

Figure 88. Shaft Stresses versus Boundary Conditions (with Asymmetric Rotation)

Use or disclosure of data contained on this sheet is subject to the restriction on the title page of this proposal.
Northrop Grumman Private/Proprietary Level I

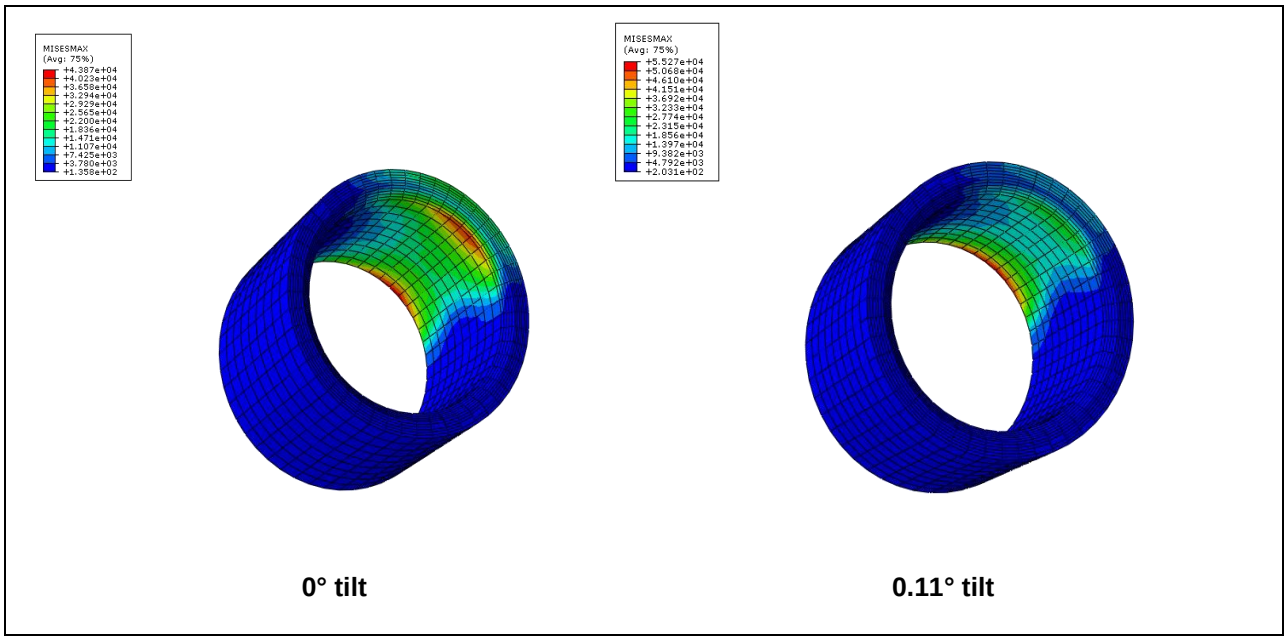

Figure 89. Bushing Stress Distribution versus Shaft Tilt

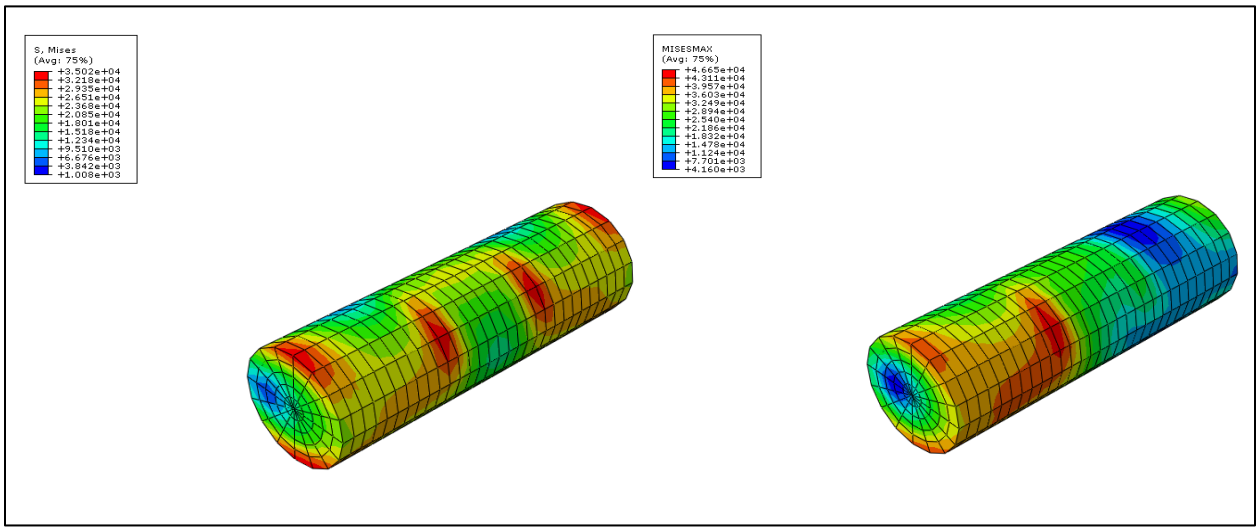

Figure 90. Shaft Stresses as Affected by Symmetric or Asymmetric Rotation

4.3.5 CASE 5: Bushing Yield Stress

This case study investigates the effects of bushing yield stress on the failure behavior of the bushing. Model properties case 5 are listed in Table 18.

Table 18. Model Properties for Case Study 12 (Bushing Yield Stress)

Loading	Progressive (2,000-10,000 lbs), symmetric
Rotation	0.58 rad/sec, symmetric rotation
Shaft BCs	Short shaft (U3=UR1=UR2=UR3=0)
Bushing Geometry	0.25” bushing
Material	Cu-Be TF-00

Use or disclosure of data contained on this sheet is subject to the restriction on the title page of this proposal.
Northrop Grumman Private/Proprietary Level I

Results:

At lower yield stresses, the bushing experienced significant deformation under full load (Figure 92 to Figure 94). Additionally, yielding began much earlier for the lower yield stress bushings. After about 140 ksi, the bushing started experiencing minimal plastic deformations, and initial yielding both occurred later and to a lower degree than the lower yield stress bushings (Figure 91).

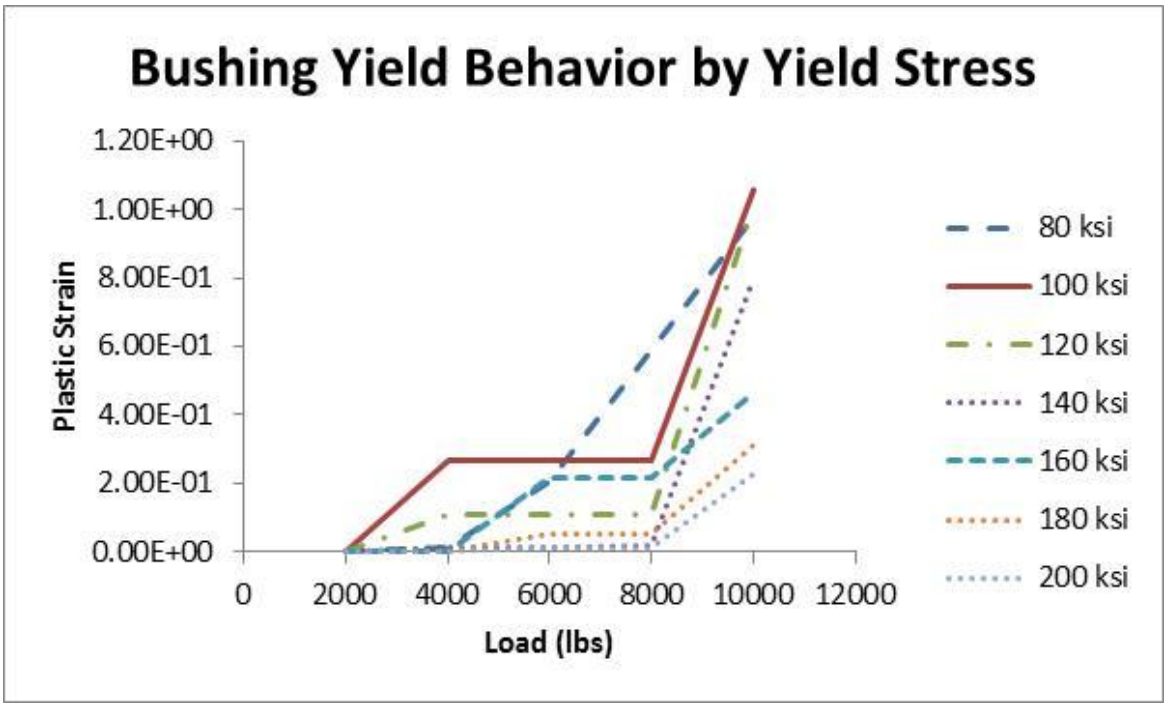

Figure 91. Load vs. Strain for Different Yield Stresses

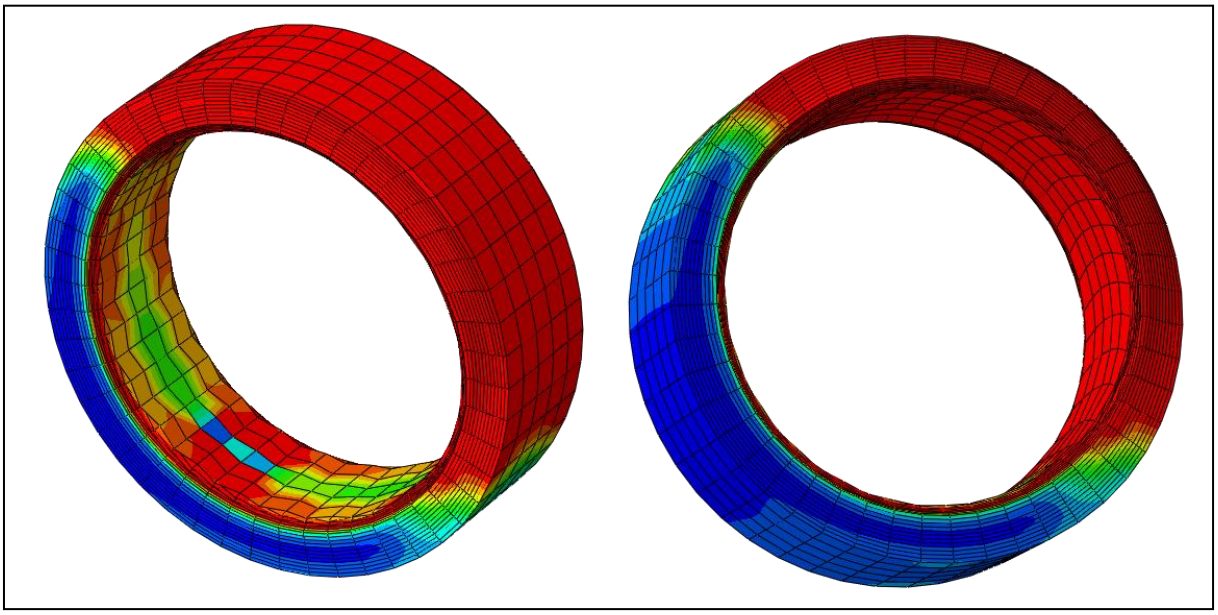

Figure 92. Von Mises Stresses Under 10 kips of Load for 80 ksi Yield Strength Bushing

Use or disclosure of data contained on this sheet is subject to the restriction on the title page of this proposal.
Northrop Grumman Private/Proprietary Level I

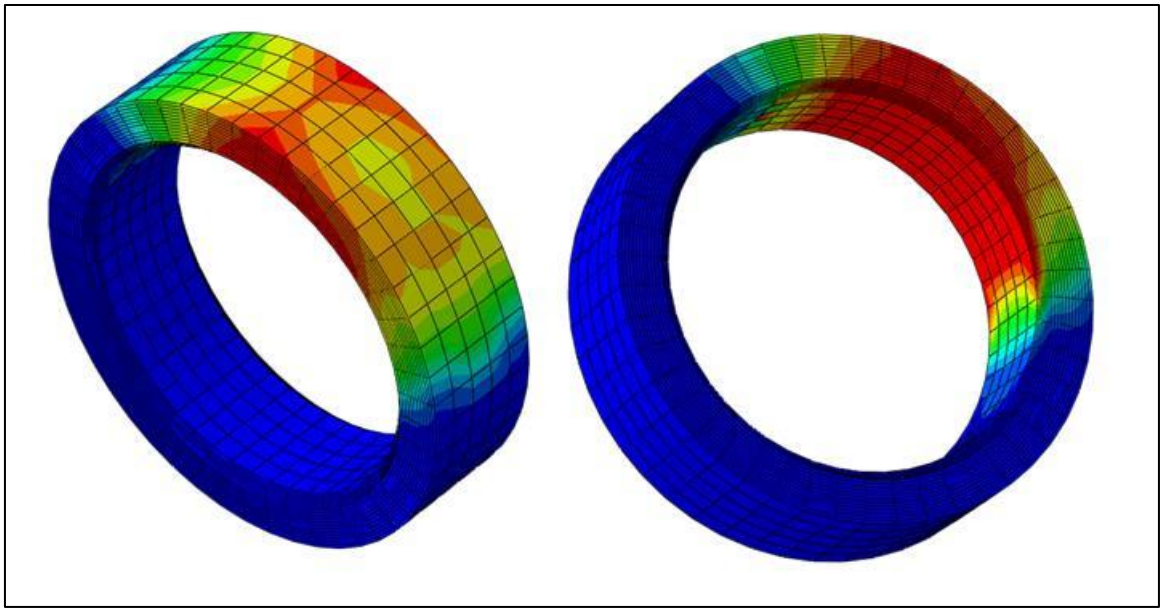

Figure 93. Von Mises Stresses Under 10 kips of Load for 140 ksi Yield Strength Bushing

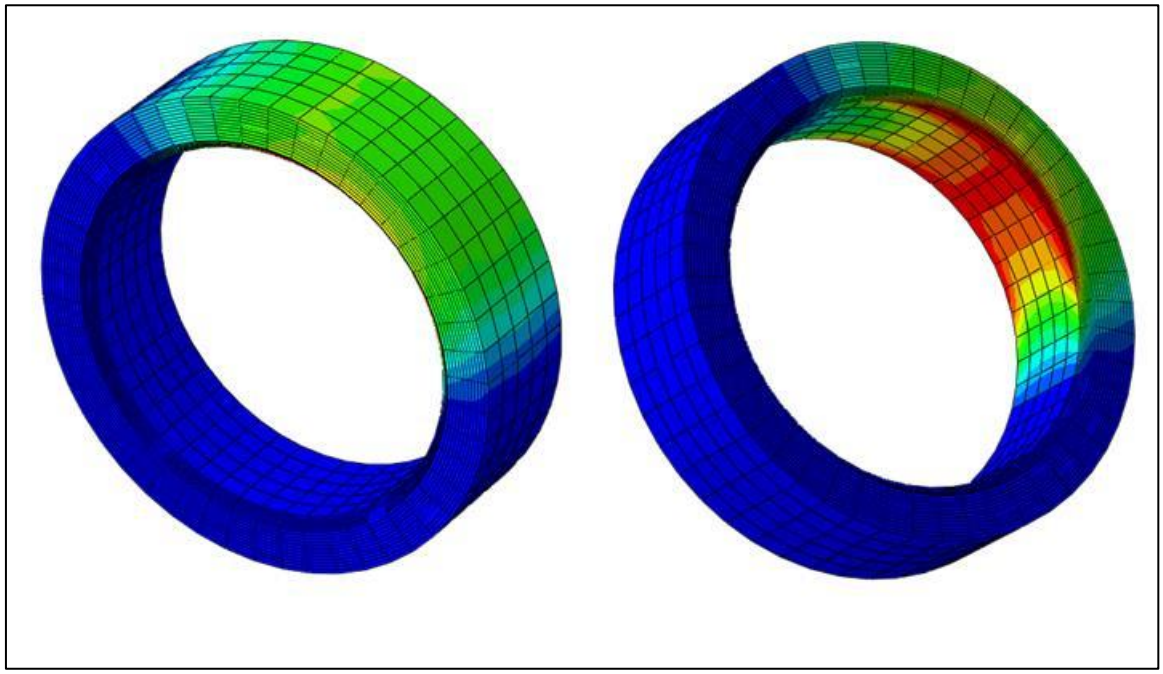

Figure 94. Von Mises Stresses Under 10 kips of Load for 200 ksi Yield Strength Bushing

Use or disclosure of data contained on this sheet is subject to the restriction on the title page of this proposal.
Northrop Grumman Private/Proprietary Level I

4.3.6 CASE 6: Effect of Bushing/Shaft Tolerance

All the preceding case studies have assumed a tolerance of 0.001" between the bushing and shaft. However, the final testing setup actually has a 0.01" tolerance between the bushing and shaft, a fairly significant difference. To check compatibility between the preceding case studies and the physical test, this case study will investigate the effects of modifying the bushing/shaft tolerance on the bushing responses. Model properties of case 6 are listed in Table 19.

Table 19. Model Properties for Case Study 6 (Effect of Bushing/Shaft Tolerance)

Loading	Progressive (2,000-10,000 lbs.), symmetric
Rotation	0.58 rad/sec, symmetric rotation
Shaft BCs	Short shaft (U3=UR1=UR2=UR3=0)
Bushing Geometry	0.25" bushing
Material	Cu-Be TF-00

Results:

As shown in Figure 95 and Figure 96, increasing the bushing/shaft tolerance leads to an increase in both stress and plastic strain. This difference primarily occurs early on during the loading phase, with the values at max load approximately equal to each other. These results indicate while these case studies may be valid for establishing trends, they should not be expected to agree precisely with the experimental results.

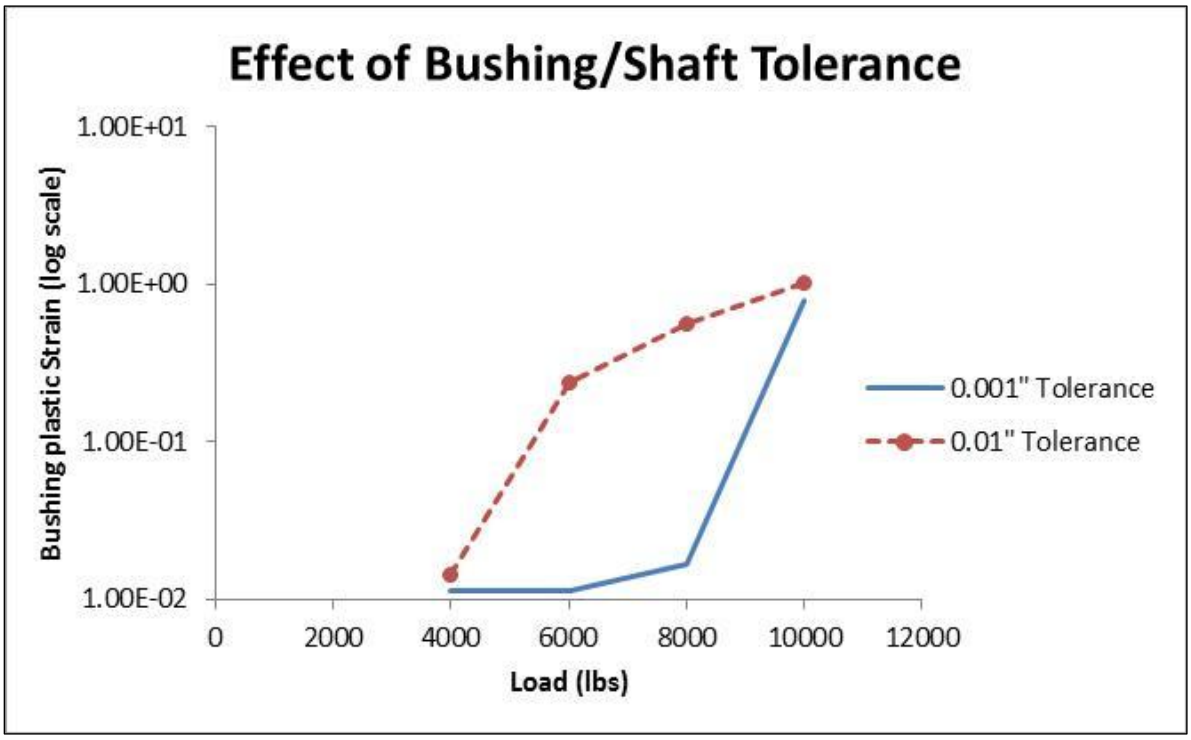

Figure 95. Effect on Strain from Bushing/Shaft Tolerance

Use or disclosure of data contained on this sheet is subject to the restriction on the title page of this proposal.
Northrop Grumman Private/Proprietary Level I

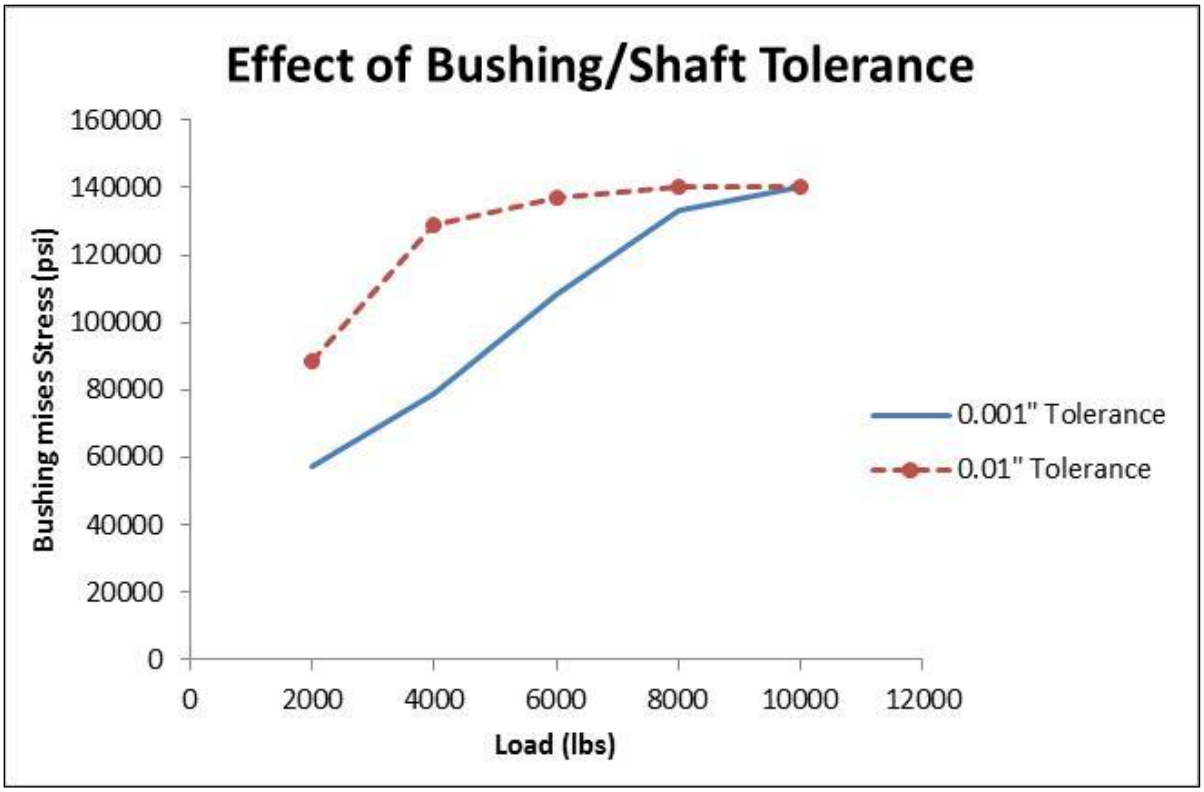

Figure 96. Effect on Bushing Stress from Bushing/Shaft Tolerance

4.4 SUMMARY AND CONCLUSIONS OF MODELING EVALUATION

The objective of the FEM analysis was to study the complex mechanical behavior of bushing under complicated loading condition numerically. The computer simulation provides a broad and important understanding of general behavior and the impact of boundary conditions and configurations on working conditions of different bushing designs.

In this section, the properties of existing materials and working condition were documented. Using the data, the finite element analysis performed the parametric analysis of the bushing parameters.

In first study, the relationship between applied loading and bushing stress was evaluated. Symmetrical loading appears to have roughly linear effect on bushing contact pressure and maximum Von Mises stress. In second study, impact of shaft rotational velocity on stress was evaluated. It was found that the varying rotation speed has little effect on contact pressure and maximum Von Mises stress. In third study, the effect of bushing's coefficient of friction on stresses was investigated. The Von Mises stresses increase fairly steadily with increasing coefficient of friction. However, the contact pressure decreases with increasing coefficient of friction. In forth study, the effect of various shaft boundary conditions such as tilt on the bushing stresses was calculated. Applying shaft tilt will in general increases the stress and contact pressure in shaft and bushing. In fifth study, the effect of bushing yield stress on failure behavior of the bushing was evaluated. It was found that at lower yield stresses, the bushing experienced significant deformation under load. For materials with the yield strength higher than 140ksi, the bushing experiencing minimum plastic deformation up to 8000lbs load. In last study, the effect

Use or disclosure of data contained on this sheet is subject to the restriction on the title page of this proposal.
Northrop Grumman Private/Proprietary Level I

of tolerance on plastic strain was investigated. It was found that the increasing bushing/shaft tolerance leads to an increase in both stress and plastic strain. The impact decreases at higher loads. This enhanced bushing development summary was prepared from information's that was provided in the Alternative Copper Beryllium Alloys Development research project report prepared by Dr. Christiane Beyer and is attached in the appendix.

5.0 FULL SCALE ENVIRONMENTAL BUSHING TESTING

Material characteristic data provides a great deal of insight into the performance that a material is expected to represent however when you can also include real life testing conditions that emulate the typical uses of the evaluation material the data obtained become much more value added and systematically it reinforces the alloy materials evaluation. In support of one of this programs task the testing of sub-component and full scale bushings was performed so that real life comparison testing could substantiate the alloy evaluation package and provide further results in defining the alternative alloys performance. Full-scale bushing testing similar to SAE AS81820 was conducted to demonstrate comparison alloy performance under high loading conditions identified in requirement definitions task at the onset of the program.

Bushing test methods utilized in a previous alternative alloy bushing material evaluations program were developed and performed by Lockheed Martin Aeronautics (LMA). These test methods were closely followed in this programs effort so that the new alloys performance results can be directly compared with previous testing results to support a quick indication of the newly developed alternative alloys performance. Two bushing test methods were established that emulate typical bushing usage; (1) Threshold – A high load low speed oscillation test, (2) Endurance – Constant load with constant 360º pin rotation speed test.

These unique bushing tests were performed by Metcut Research Inc. The tests were to utilize a unique test system identified in the MIL-B-81820 specification and to follow methods which had been uniquely modified to the desired loads previously utilized in the LMA alternative alloy testing. The test system rigging utilized by Metcut was a bit different than that which had been used by LMA but had similar load dynamics that was applied to the bushings. Photo images of the Metcut Research test system is shown in Figure 97.

The bushing drawings in Figure 98 provides the configuration details of the chamfered (standard) and enhanced radius bushing design utilized for testing. Test bushings were machined at Northrop Grumman's Space Park machining center from the down-selected cobalt NGCo-3A alternative alloy and the standard AMS 4533 copper beryllium. A total of 18 bushings were machined: Seven CuBe bushings with a chamfer along with eleven NGCo-3A bushings which consisted of seven with a chamfer, two with a radius, and two with no geometric detail to the bushings inner diameter. The test pins were also produced in house utilizing MP35N material heat treated to AMS-5845 and machined to the configuration presented in Figure 99.

Use or disclosure of data contained on this sheet is subject to the restriction on the title page of this proposal.
Northrop Grumman Private/Proprietary Level I

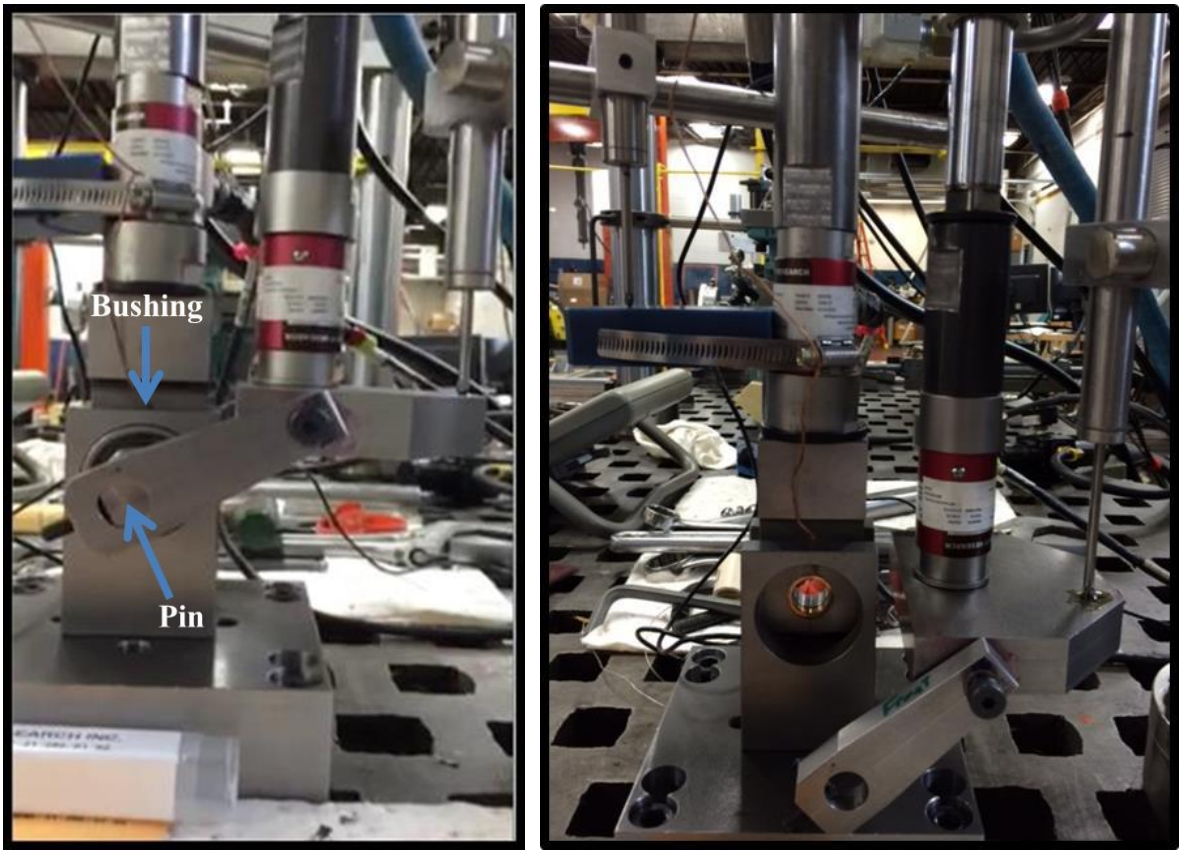

Figure 97. Images of Bushing Test System Rigging

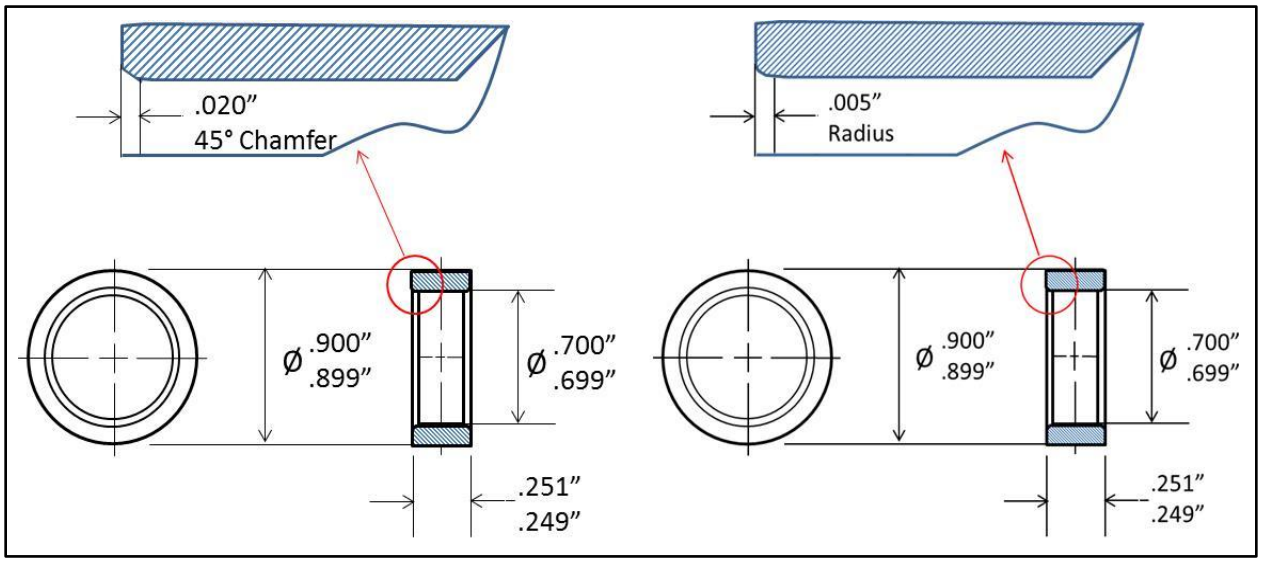

Figure 98. Configuration of Chamfer and Radius Type Bushing Specimens

Use or disclosure of data contained on this sheet is subject to the restriction on the title page of this proposal.
Northrop Grumman Private/Proprietary Level I

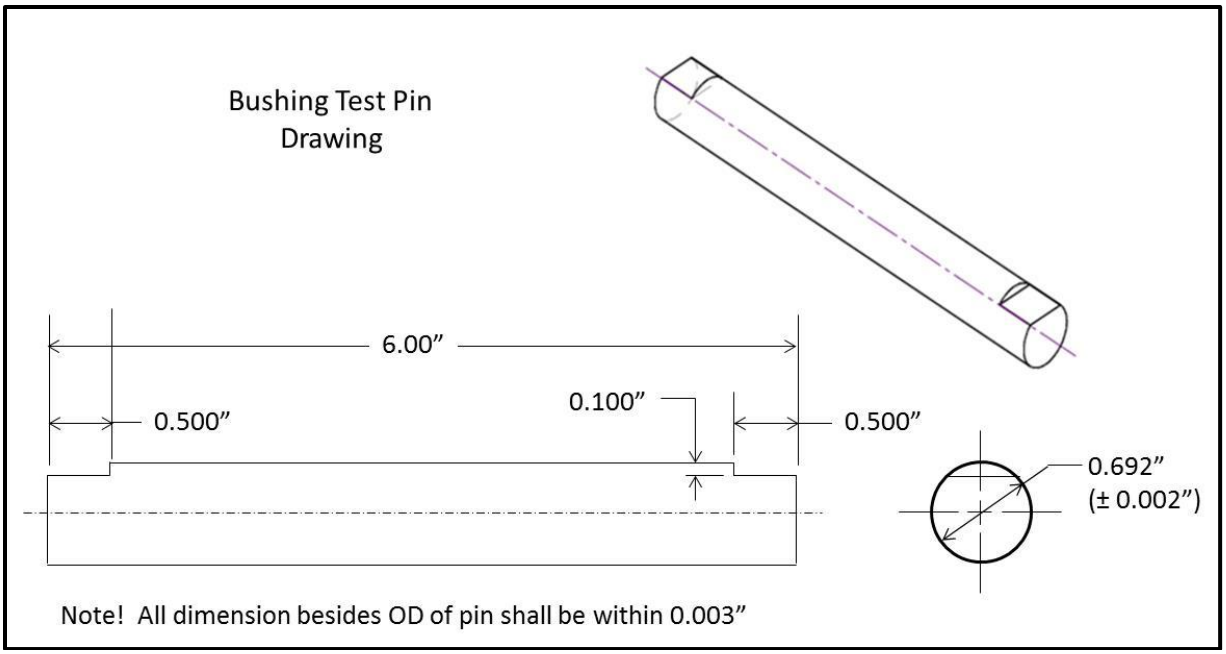

Figure 99. Configuration of the Test Pin made from MP35N Material

Sample dimensions and surface finish was inspected to ensure consistent sample preparation was controlled to reduce potential inconsistencies in performance results. A test matrix in Table 20 was prepared to support a total of 16 tests that consisted of 8 Threshold tests and 8 Endurance tests with the chamfer and radius variants as listed.

Table 20. Full Scale Bushing Test Matrix for Alloy Performance Comparison

Bushing Test Matrix				
Test	**Copper Beryllium (Chamfer)**	**NGCo-3A (Chamfer)**	**NGCo-3A No Chamfer**	**NGCo-3A Radius**
Threshold	4 bushings	3 bushings		1 bushing
Endurance	2 bushings	1 bushings		1 bushing

Metcut was provided the test samples and testing was performed. Prior to Metcut installing a test bushing into the fixture an orientation reference mark was applied to edge face of bushing to accommodate measurement and positioning location. Measurements were taken of the bushing ID before and after installation to validate the bushing to pin clearance. The bushing was inserted into the fixture with reference mark at a 12 o’clock position (normal force) to identify the point of contact load location on the bushing. The reference was also used in monitoring any bushing rotation (slipping) within the fixture. A thermocouple was tacked to the bushing at the 12 o’clock position to capture bushing temperature during testing. Two position sensors (LVDT types) were utilized in capturing data from the testing: (1) One to monitor the bushing wear displacement. (2) One to measure the reciprocating angle of rotation.

Use or disclosure of data contained on this sheet is subject to the restriction on the title page of this proposal.
Northrop Grumman Private/Proprietary Level I

5.1 BUSHING THRESHOLD TEST AND EVALUATION

Testing procedure upon completing the bushing and pin installation was to initiate the oscillation rotation of the pin in the bushing with an initial static load of 2000 lbs. The oscillation initiates at 0º, pin rotates 25º in one direction and stops, pin reverses direction and rotates 50º in the opposite direction through zero and stops, pin reverse direction again for 25º back to zero completing one cycle. The oscillation is performed for 100 cycles and then an additional 500 lb load is applied for the next 100 cycles. This is repeated till the last 100 cycles at 10,000 lbs is completed or until failure occurs to the bushing that requires the test to be terminated. The data results were plotted from the initial threshold test and presented in Figure 100. Photos of the visual inspection showing the bushing and the pin are in Figure 101.

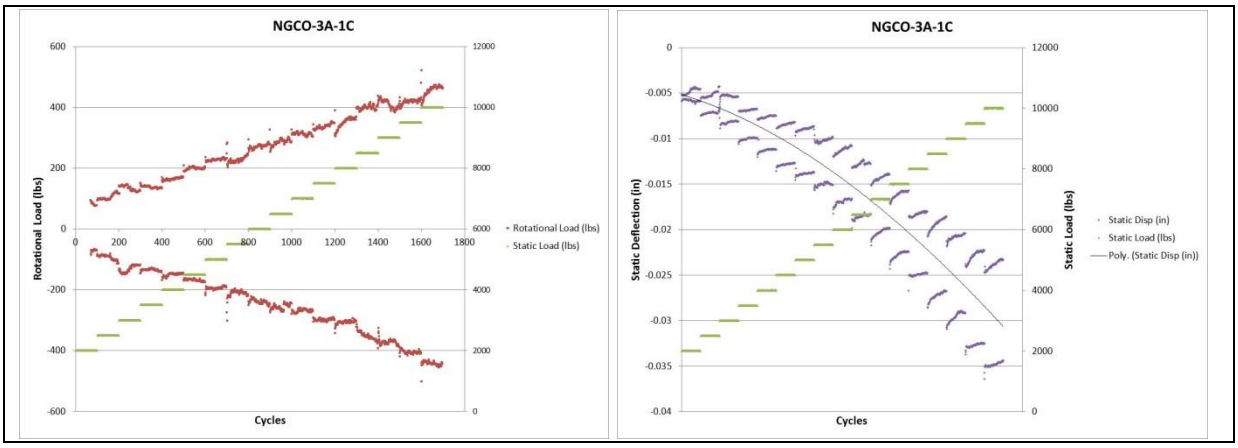

Figure 100. NGCo-3A-1C Bushing Threshold Test Result Plotted

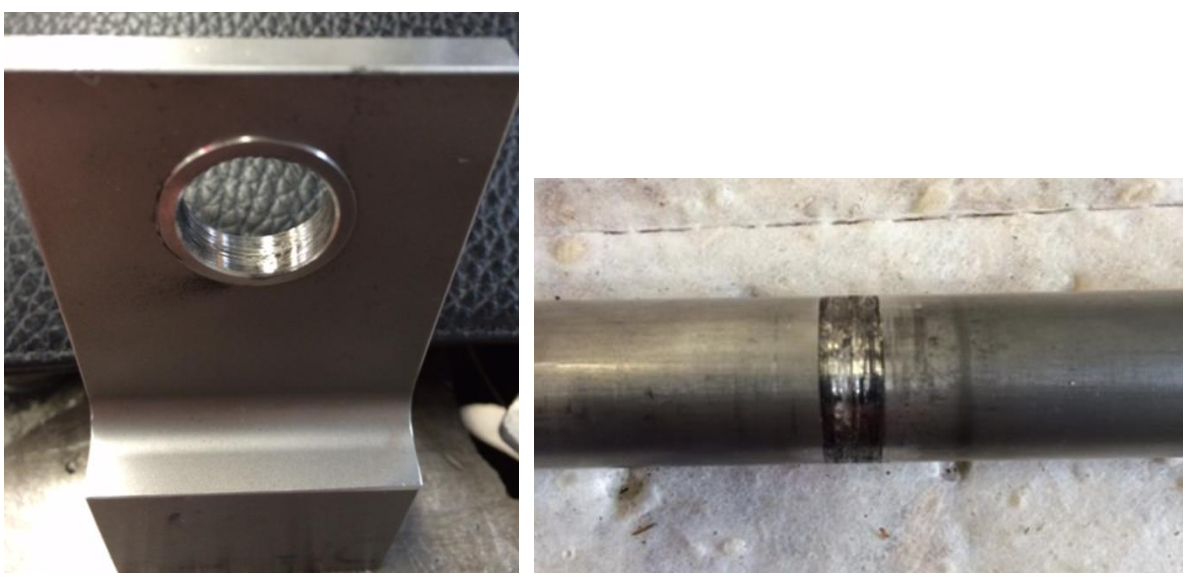

Figure 101. Photos of NGCo-3A-1C Bushing and Pin Inspection Post Threshold Test

Results of the NGCo-3A-1C shows wear displacement in the range of about 0.025”. This minimal wear is similar to results noted in the LMA evaluation. Temperature data for this bushing was not captured as it was forgotten to be installed when the system setup for this

Use or disclosure of data contained on this sheet is subject to the restriction on the title page of this proposal.
Northrop Grumman Private/Proprietary Level I

bushing was performed. Photos support visual indications that galling had occurred during the test but data results do not provide any details that point to when the initiation of galling occurred. Upon evaluating the results it was decided that identifying the initiation of galling was a necessary characteristic in determining the side by side performance comparison of the alloys.

So test conditions were changed slightly on the second threshold test in an attempt to capture the initiation of galling. A new NGCo-3A bushing was installed into the system test setup in preparation for testing. For the second test the static load of 2,000 lbs remained the same but it was requested that the system be turned off after the first 100 cycles so a visual inspection could be performed to determine if galling had occurred. All other test conditions remained the same. The results of 2nd Threshold test are presented in Figure 102.

Results show data points that were captured for the second threshold test. Just the initial and final data values were captured for this test. The only data that really stands out in the plots is the increased temperature value that starts out at around 107º F and toward the end of the test it finishes around 130º F. The system was disassembled and a visual inspection did indicate that galling had occurred. The visual photos are presented in Figure 103.

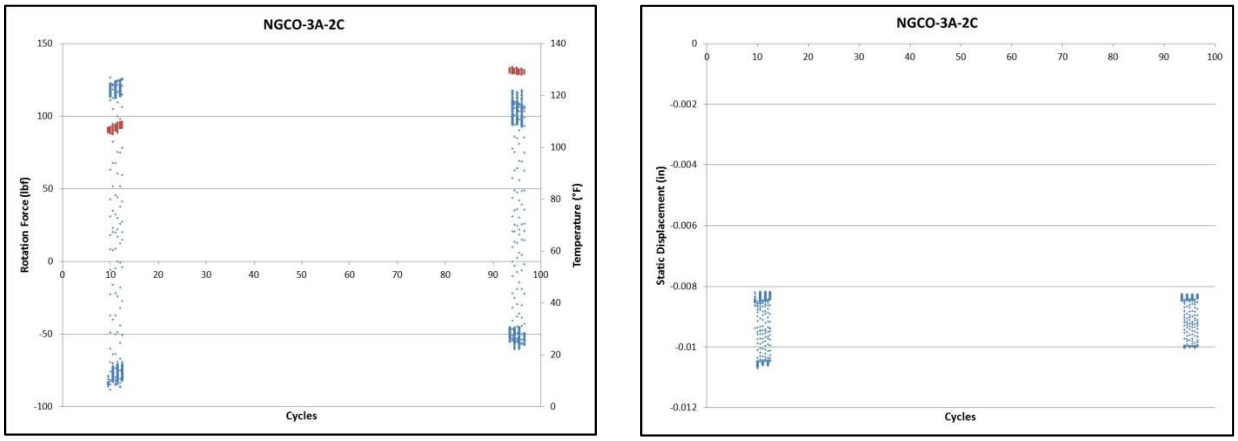

Figure 102. NGCo-3A- 2C Bushing Threshold Test Result Plotted 2,000 lb Load for 100 Cycles

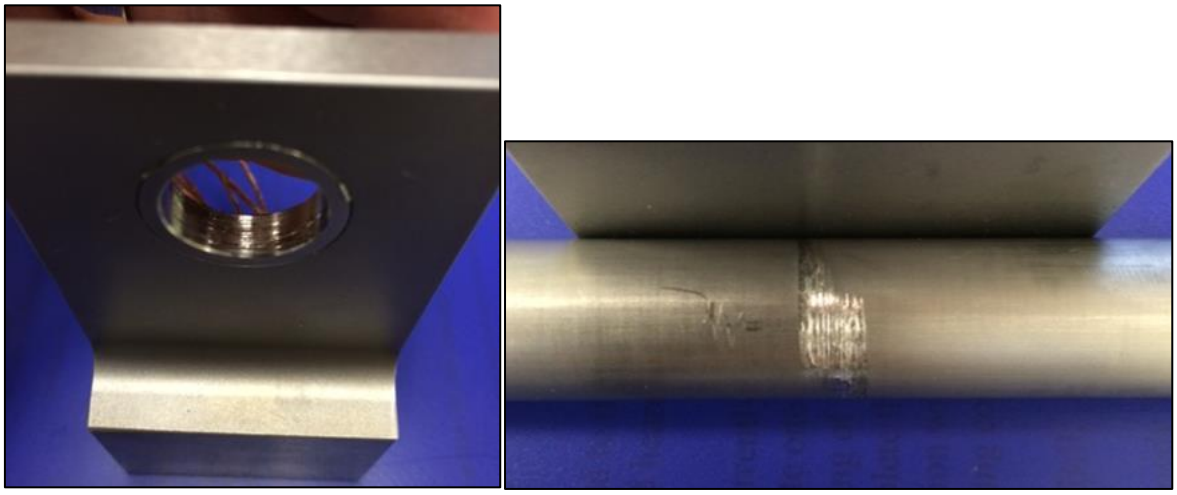

Figure 103. Photos of Bushing and Pin Post NGCo-3A-2CThreshold Test 2,000 lb Load for 100 Cycles

Use or disclosure of data contained on this sheet is subject to the restriction on the title page of this proposal.
Northrop Grumman Private/Proprietary Level I

With the results for the NGCo-3A-2C bushing still visually indicating some small material transfer after reducing the cyclic exposure there was another testing decision made to change to the copper beryllium alloy bushing to see if similar results were obtained.

For the 3rd threshold test the testing conditions remained the same as the previous test and the only change would entail the use of a copper beryllium bushing. A CuBe-1C bushing was installed into the system test setup and tested. Upon the completion of the 100 cycles the test system was dismantled and the bushing and pin was visually inspected. Similar material transfer was identified in the CuBe-1C sample as to that identified with the NGCo-3A-2C bushing. There was further evaluation interest to see how the bushing would respond to an additional 500-lb load so the system was reassembled and tested at a 2500 lb load for another 100 cycles using the same CuBe bushing. Upon completion of the additional 100 cycles the systems was dismantled again to visually evaluate the results. Additional material transfer was identified in the evaluation but still no severe galling was apparent so further interest to continue with yet another additional 500-lb load was performed. At about 80 cycles into the third trial evaluation the CuBe-1C bushing was ejected from the holding fixture and the test was stopped.

Results of the third threshold test with the extended evaluation of the CuBe-1C bushing are presented in Figure 104. Photos taken of the CuBe-1C bushing at the various visual inspections of extended bushing testing are presented in Figure 105a & b.

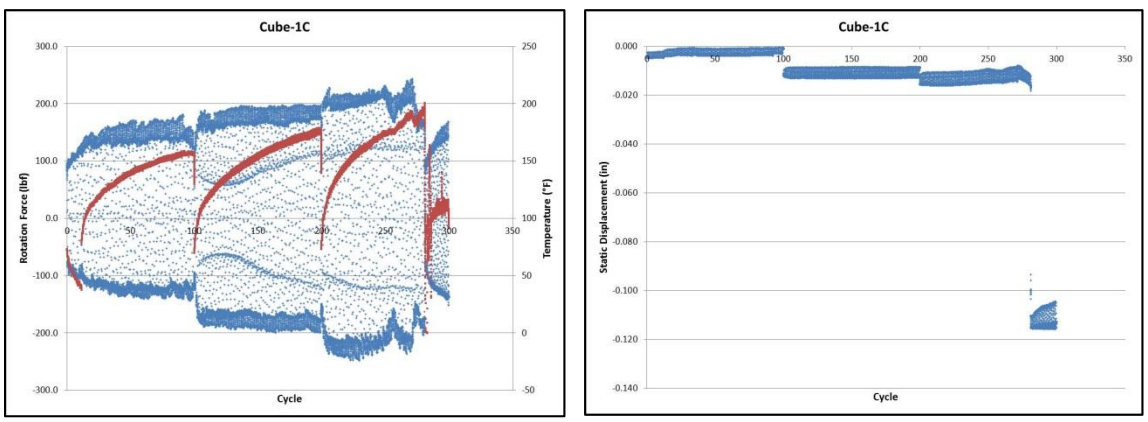

Figure 104. CuBe-1C Bushing Threshold Tests (1, 2 & 3) Result Plotted

Use or disclosure of data contained on this sheet is subject to the restriction on the title page of this proposal.
Northrop Grumman Private/Proprietary Level I

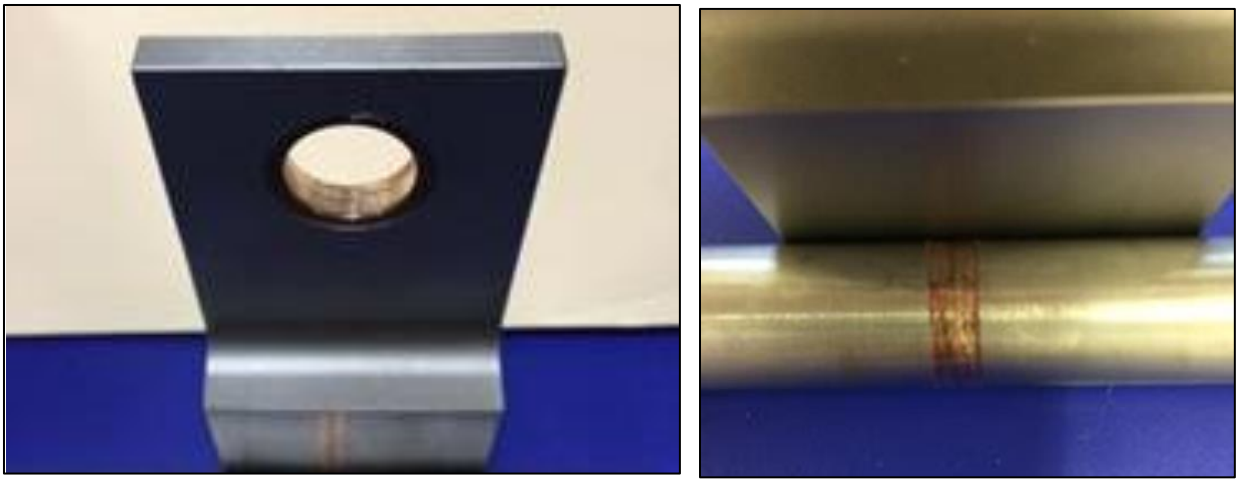

Figure 105a. Photos of CuBe-1C Bushing and Test Pin Post Initial Test of 2,000 lb Load & 100 Cycles

Figure 105b. Photo of CuBe-1C Bushing & Test Pin Post Threshold Tests (1, 2, & 3)

An evident amount of material transfer from both the NGCo-3A-2C and the CuBe-1C alloy samples suggests that further testing is still required in identifying the initiation of galling. For the fourth threshold test the load was again lowered, this time a significant amount, down to a 500 lb load in hopes that the reduction in load would be adequate enough to reduce the dynamic effect low enough so that the mechanism of galling could then be crept up on. A new bushing CuBe-2C was installed in the system and the test was initiated. Upon completion of the first 100 cycles the CuBe-2C bushing was removed from the system and a visual evaluation was performed. The bushing did have signs of slight material transfer but not enough to be considered galling so the bushing was reinstalled into the system and another 100-cycle test was performed at the 500 lb load. System disassembly was again performed after the additional 100-cycles were completed and this time visual inspection of the material transfer was identified as galling. Results of the CuBe-2C bushing test runs with 500 lb load for 100 cycles and follow on

Use or disclosure of data contained on this sheet is subject to the restriction on the title page of this proposal.
Northrop Grumman Private/Proprietary Level I

additional 100 cycles is presented in Figure 106. Photos of the bushings after the initial 100 cycles and after the final 100 cycles are shown in Figure 107.

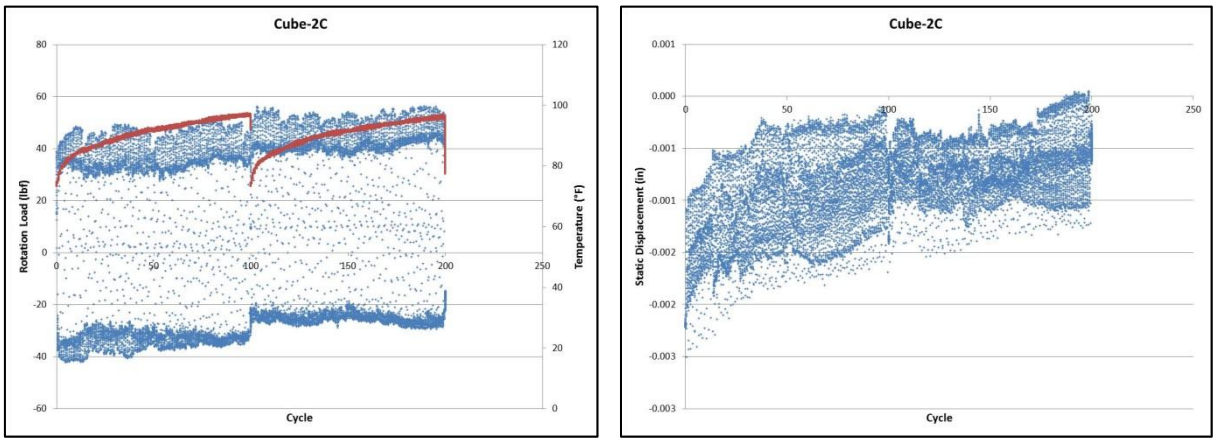

Figure 106. CuBe-2C Bushing Threshold Test (1 & 2) Results Plotted

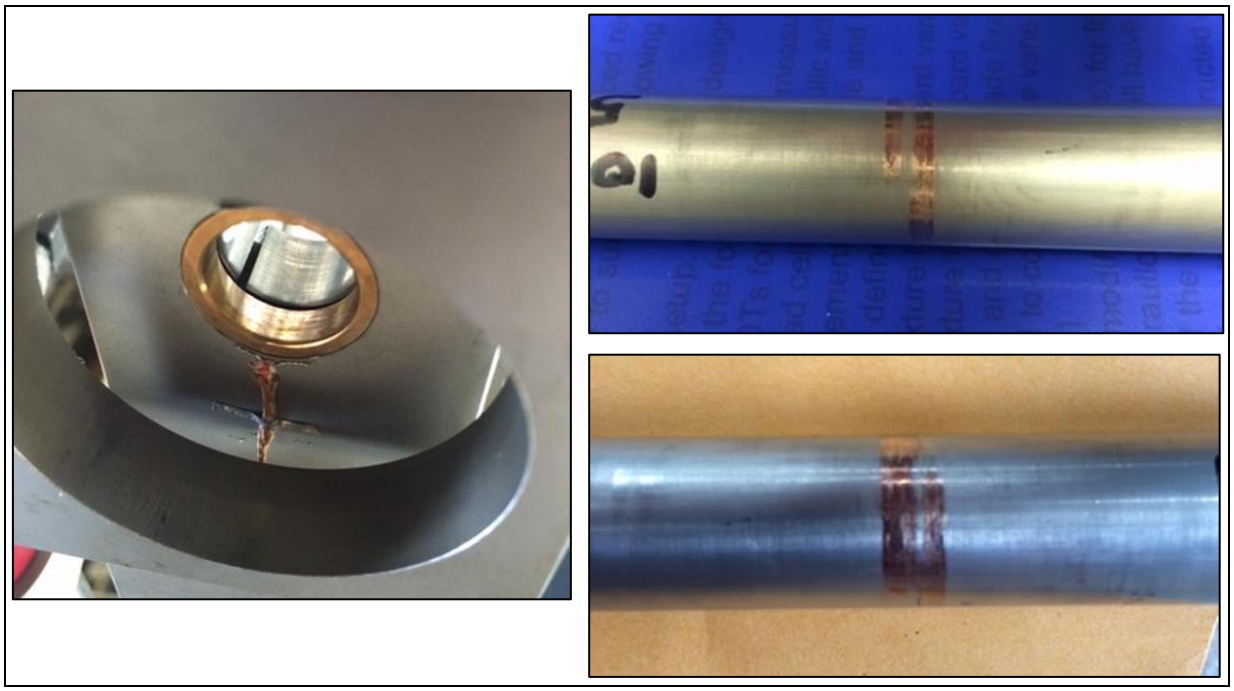

Figure 107. Photos of CuBe-2C Bushing & Pin Post Threshold Tests (1 &2)

With the initiation of galling identified for the copper beryllium alloy bushing the same test conditions were performed on the NGCo-3A alloy to evaluate the comparison. A new NGCo-3A-3C bushing was installed in the test system and testing performed with the same 500 lb static load for 100 cycles and removed for visual inspection. Result for the initial 100 cycles run produced very slight material transfer superior to the standard copper beryllium. The bushing was re-installed in the test system and tested for another 100 cycles. Results of the second test were only slightly different and still superior in comparison to the baseline. The bushing was reinstalled and tested three more times before a significant amount of wear was identified and the

Use or disclosure of data contained on this sheet is subject to the restriction on the title page of this proposal.
Northrop Grumman Private/Proprietary Level I

testing was stopped. Results of the 5 testes performed on NGCo-3A-3C are presented in Figure 108. Photos of the visual inspections identifying the wear follow in Figure 109.

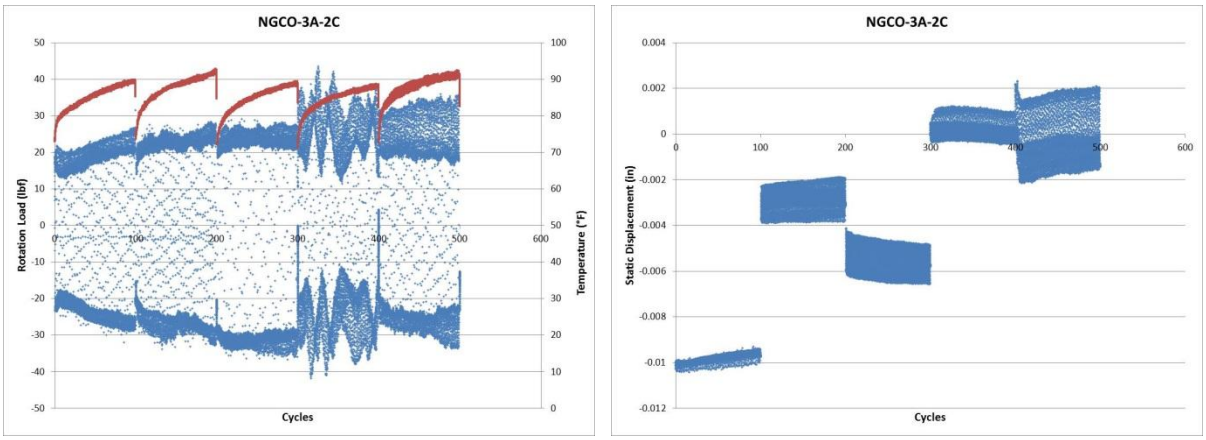

Figure 108. NGCo-3A-3C Bushing Threshold Test (1, 2, 3, 4 & 5) Result Plotted

Use or disclosure of data contained on this sheet is subject to the restriction on the title page of this proposal.
Northrop Grumman Private/Proprietary Level I

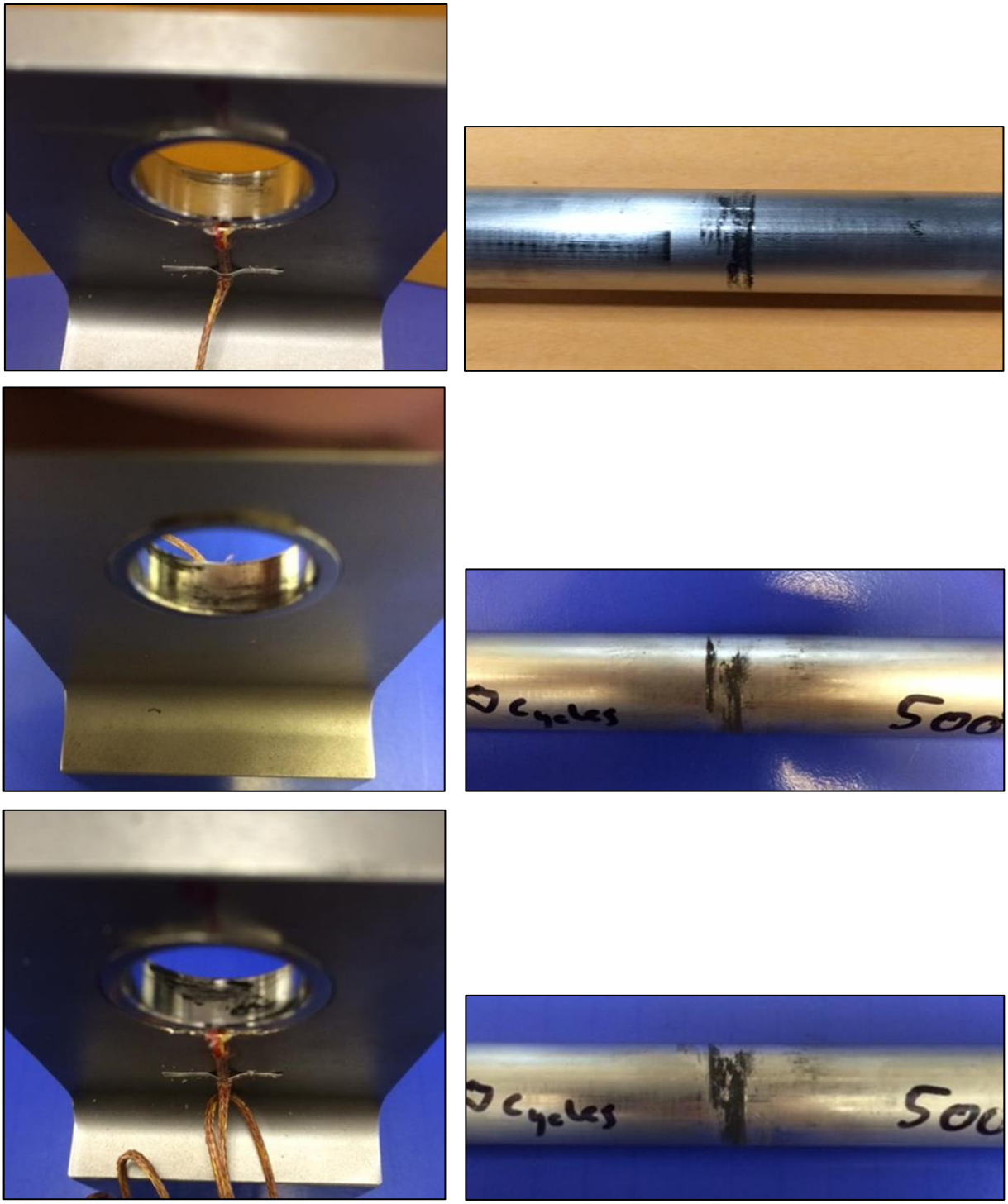

Figure 109. Photo Sets of NGCo-3A-3C Visual Inspection Results of Bushing & Pin for 0-100 Cycles, 200-300 Cycles and 400-500 Cycles Respectively All at 500 lb Static Load

Use or disclosure of data contained on this sheet is subject to the restriction on the title page of this proposal.
Northrop Grumman Private/Proprietary Level I

Initiation of galling was captured for both the NGCo-3A alternative alloy and the standard copper beryllium. As a validation of this initiation of galling characteristic repeatability tests were performed. Threshold tests were repeated for both the NCCo-3A and the CuBe alloy bushings to confirm initiation results. Testing results for comparison and repeatability of both alloys at the 500 lb static load and the results performed at each 100 cycle test interval (0-100, 100-200 and 200-300) are presented in Figure 110. Photos of both the NGCo-3A-4C and CuBe-3C with pins for the 0-100 cycles and 200-300 cycles visual inspections are presented in sequence in Figure 111.

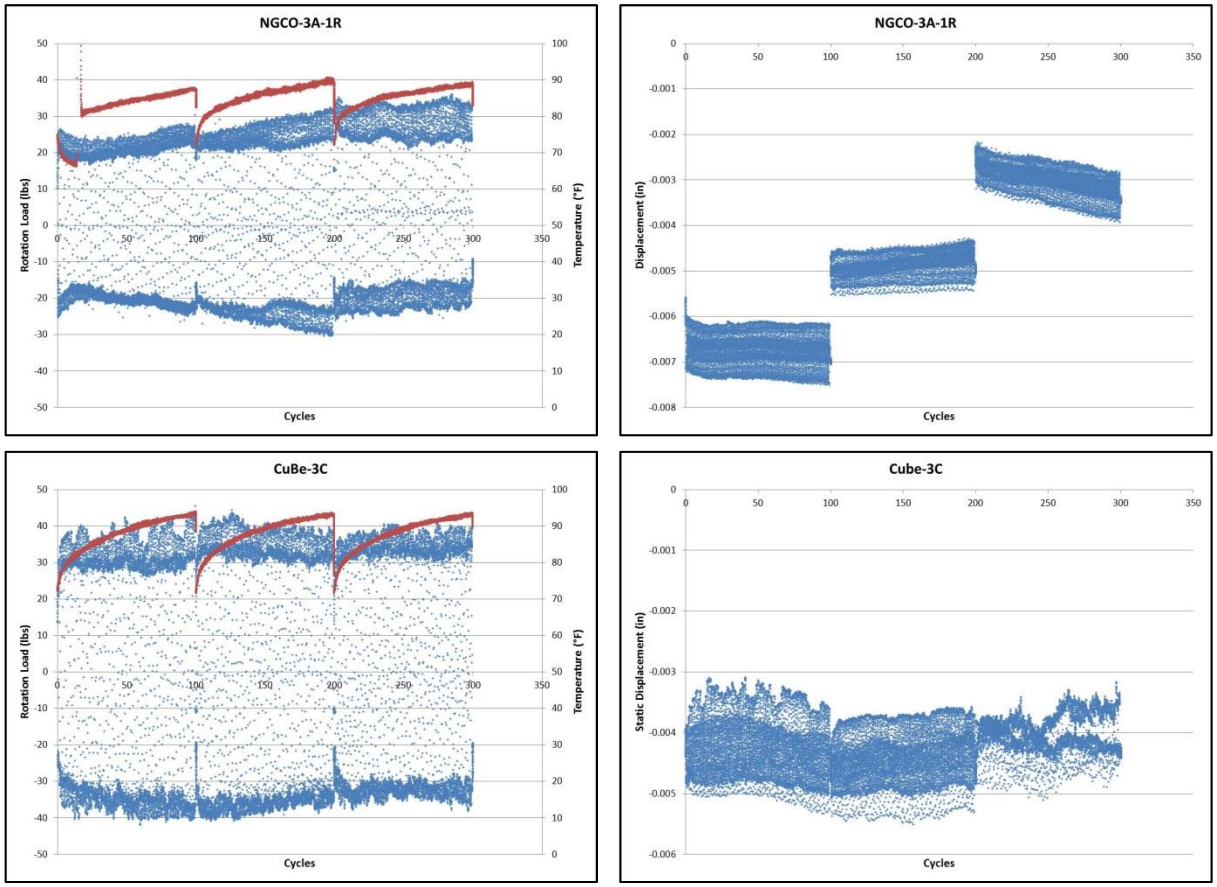

Figure 110. NGCo-3A-1R and CuBe-3C Bushing Threshold Test (1, 2, & 3) Result Plotted

Use or disclosure of data contained on this sheet is subject to the restriction on the title page of this proposal.
Northrop Grumman Private/Proprietary Level I

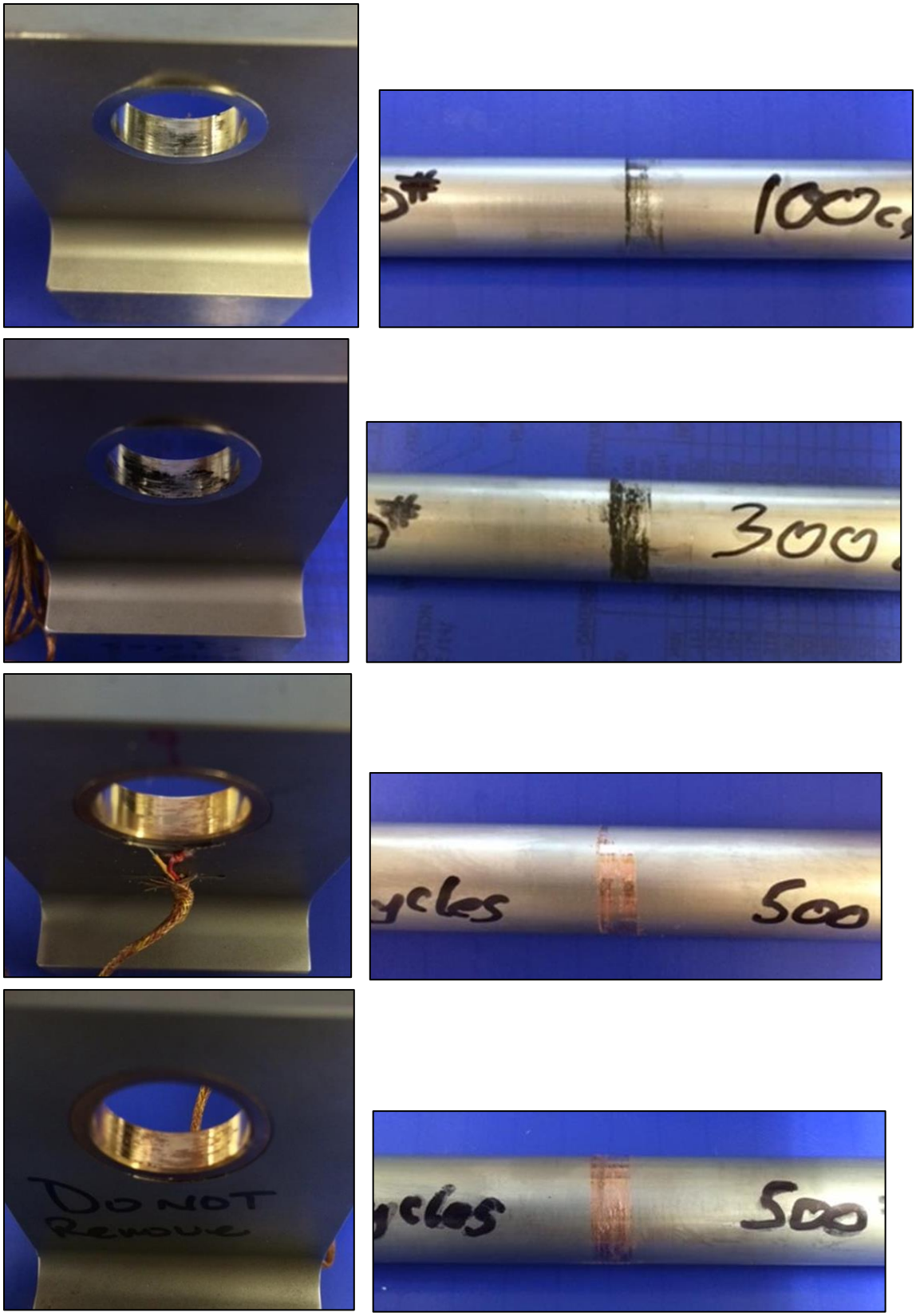

Figure 111. Results of Initiation of Galling Repeatability of NGCo-3A-1R 100 Cycles and 300 Cycles Followed by CuBe 100 Cycles and 300 Cycles Visual Inspections

Use or disclosure of data contained on this sheet is subject to the restriction on the title page of this proposal.
Northrop Grumman Private/Proprietary Level I

The repeatability tests show the superior performance of the NGCo-3A material over the CuBe standard after being exposed to the same test conditions producing lower temperature, lower rotational load and similar wear properties.

As a final threshold test the CuBe-4C bushing was exposed to the same conditions as the initial NGCo-3A-1C bushing. Those conditions were an initial 2,000 lb static load for the initial 100 cycles followed by an additional 500 lb increment every 100 cycles thereafter until 10,000 lbs or failure occurred. Figure 112 presents the results of the high-load low-frequency oscillation of the CuBe-4C test performed out to 10,000 lbs and 1,700 cycles.

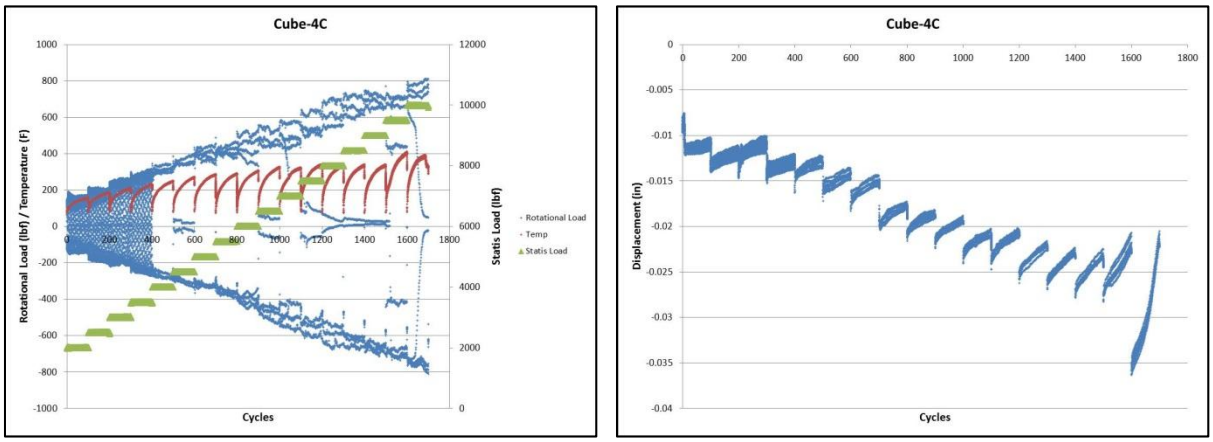

Figure 112. Results of CuBe-4C Bushing Being Incrementally Loaded with 500 lb Increase Every 100 Cycles out to 10,000 lbs.

Visual inspection comparison of the CuBe-4C bushing to that of the NGCo-3A-1C previously tested using the same testing conditions shows very similar results. The visual inspections performed on both alloy bushings indicate metal transfer and show galling. The copper beryllium displays a smoother surface galling appearance in comparison to that of the surface finish of the NGCo-3A bushing that has a courser surface appearance. Visual inspection photos of the CuBe-4C bushing and pin are presented in Figure 113.

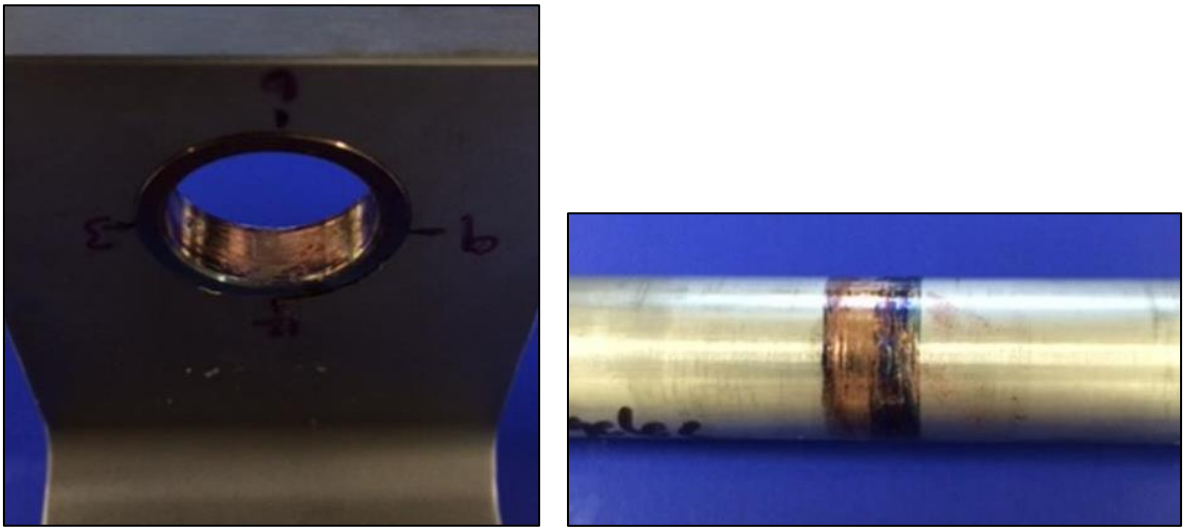

Figure 113. Results of Visual Inspection of CuBe-4C Tested Out to 1,700 Cycles and 10,000 lbs

Use or disclosure of data contained on this sheet is subject to the restriction on the title page of this proposal.
Northrop Grumman Private/Proprietary Level I

The instrumentation readings for the displacement and load support both a lower value of wear for the NGCo-3A material and a lower rotational load reading indicating only about half the force is produced in comparison to the CuBe. These superior characteristics are indications that support the NGCo-3A alloy as a viable alternative for the standard copper beryllium.

The threshold bushing test data was collected and put into an all up summary of the result that are presented in Table 21.

Table 21. Summary of Threshold Test Conditions and Visual Inspection Notes

Threshold Bushing Test Summary						
Test #	Alloy	Bushing Geometry 0.09" X 0.07"	Applied Loading (Lbs)	Cycles (0º/+25º/-25º/0º)	MaxLoad (Lbs)	Notes
1	NGCo-3A -1C	Chamfer	2,000 initial - ↑500Lb every 100 cycles	0-1,700	10,000	Galling Identified
2	NGCo-3A-2C	Chamfer	2,000	0-100	2,000	Galling Identified
3	CuBe-1C	Chamfer	2,000	0-100	2,000	Mild Material Transfer
3a	CuBe -1C	Chamfer	2,500	100-200	2,500	Slight Galling Identified
3b	CuBe -1C	Chamfer	3,000	200-280	3,000	Bushing Ejected
4	CuBe -2C	Chamfer	500	0-100	500	Mild Material Transfer
4a	CuBe -2C	Chamfer	500	100-200	500	Galling Identified
5	NGCo-3A-3C	Chamfer	500	0-100	500	Slight Material Transfer
5a	NGCo-3A-3C	Chamfer	500	100-200	500	Mild Material Transfer
5b	NGCo-3A-3C	Chamfer	500	200-300	500	Mild Material Transfer
5c	NGCo-3A-3C	Chamfer	500	300-400	500	Slight Galling Identified
5d	NGCo-3A-3C	Chamfer	500	400-500	500	Galling
6	CuBe-3C	Chamfer	500	0-100	500	Slight Material Transfer
6a	CuBe-3C	Chamfer	500	100-200	500	Mild Material Transfer
6b	CuBe-3C	Chamfer	500	200-300	500	Galling Identified
7	NGCo-3A-1R	Radius	500	0-100	500	Slight Material Transfer
7a	NGCo-3A-1R	Radius	500	100-200	500	Mild Material Transfer
7b	NGCo-3A-1R	Radius	500	200-300	500	Galling Identified
8	CuBe-4C	Chamfer	2,000 initial - increase 500Lb every 100 cycles	0-1,700	10,000	Galling Identified

5.2 BUSHING ENDURANCE TEST AND EVALUATION

Endurance testing took on a similar approach as that of the threshold testing in determining the initiation of galling by starting with an identified load and performing trials till initiation of galling is identified.

Use or disclosure of data contained on this sheet is subject to the restriction on the title page of this proposal.
Northrop Grumman Private/Proprietary Level I

Test processing for the endurance testing is slightly different in that now instead of an oscillating rotation being applied to the pin it changes to full 360º multiple revolution motion in a single direction. Rotational speed for all endurance testing was set at a constant speed of approximately 30 rotations per minute (rpm). The static load was held constant during each test but in the effort to identify the onset of galling the load was varied from test to test until the initiation of galling was indicated.

The test system utilized the same rigging except the shaft was connected to a continuous revolving source. A new test bushing was mounted into the fixture and installed into the system. The first endurance test began with an NGCo-3A-4C bushing that was run at a static load of 500 lbs for 100 full rotations (cycles) to keep testing conditions constant with those performed on the threshold testing. After completing the 100 cycles the system was dismantled and the bushing was visually inspected. The data results are presented in Figure 114. A visual inspection was performed and galling was identified. Photos of the NGCo-3A-4C bushing are shown in Figure 115.

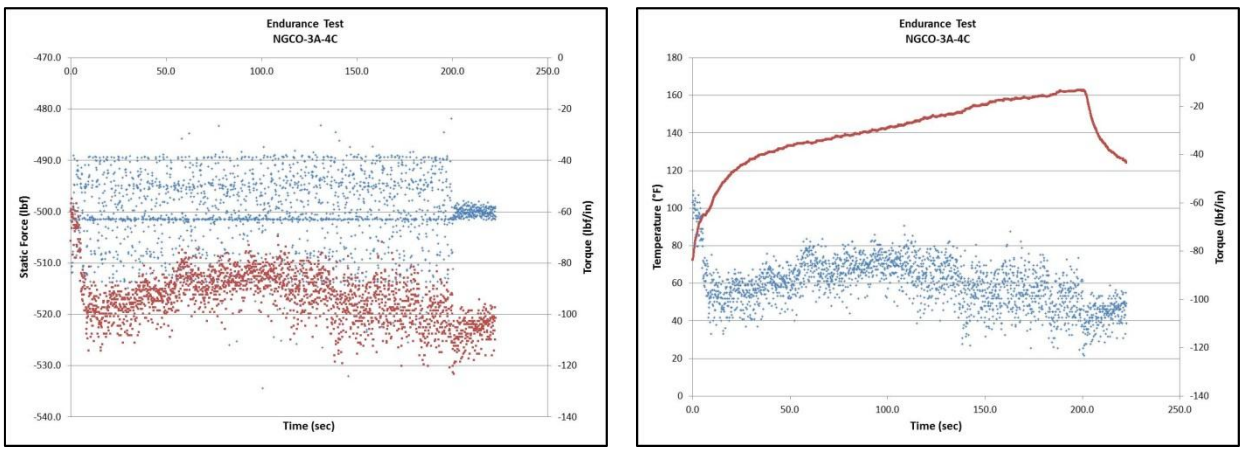

Figure 114. Results of Initial NGCo-3A-4C Endurance Test at 500 lb Load for 100 Cycles

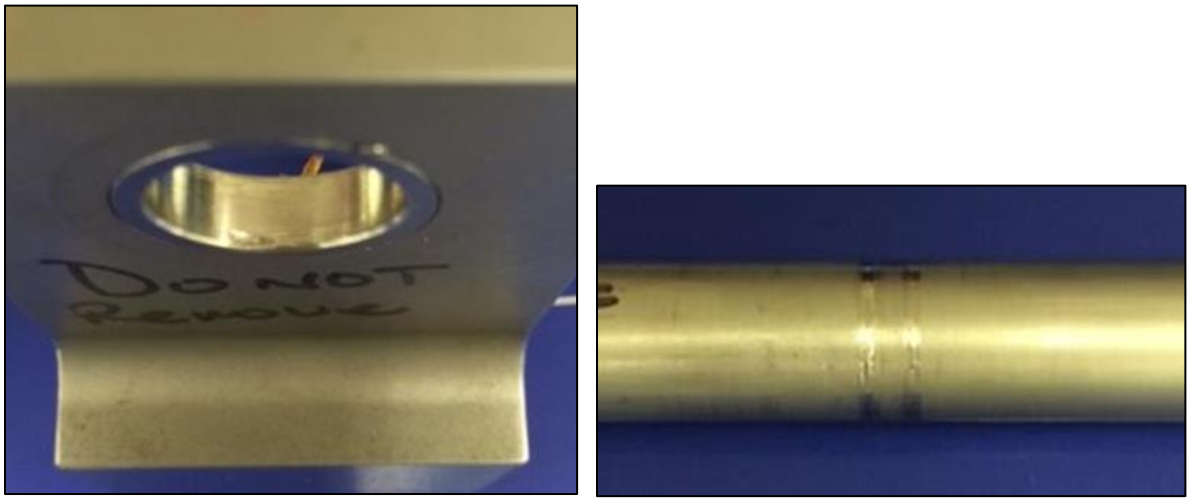

Figure 115. Visual Inspection results of NGCo-3A-4C at 500 lb load 100 Cycles

A new NGCo-3A-5C bushing was installed and the system was reassembled in preparation for the performing the next endurance. The static load for this next test was reduced to 250 lbs in

Use or disclosure of data contained on this sheet is subject to the restriction on the title page of this proposal.
Northrop Grumman Private/Proprietary Level I

an effort to capture the galling initiation. The test was performed and the data results are presented in Figure 116 with visual inspection photos in Figure 117.

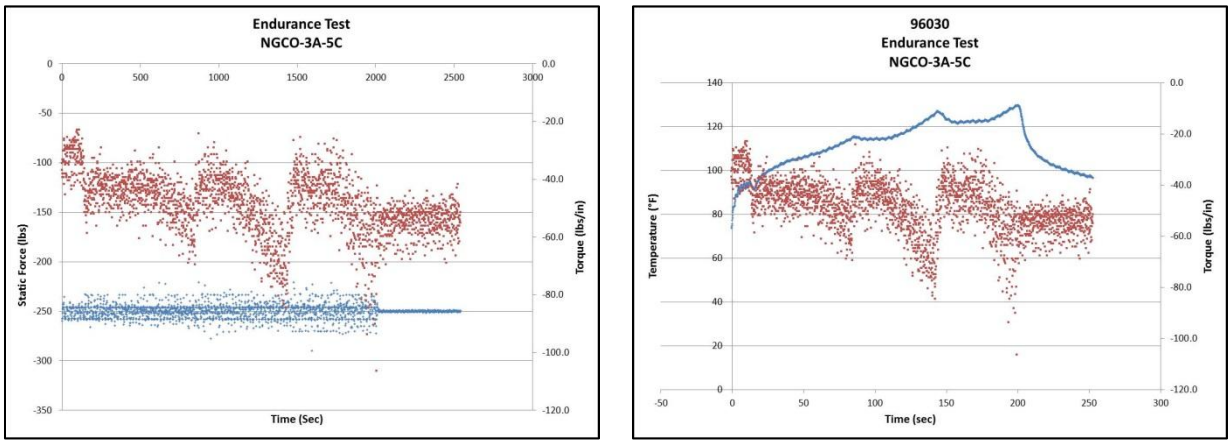

Figure 116. Results of NGCo-3A-5C Endurance Test at 250 lb Load for 100 Cycles

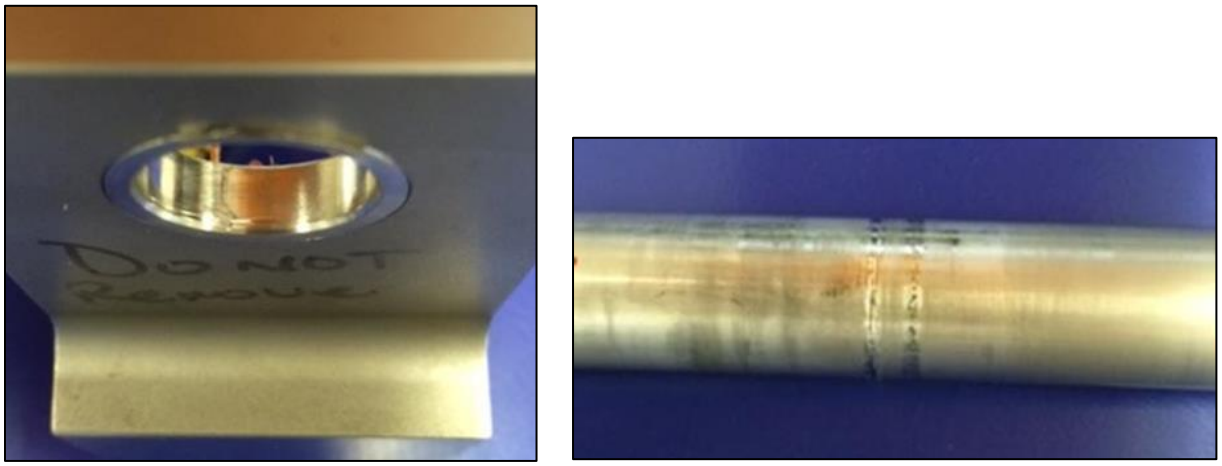

Figure 117. Results of NGCo-3A-5C Visual Inspection of 250 lb Load for 100 Cycles

With apparent galling still being produced at the present conditions the decision to change to the copper beryllium bushing was made to see if similar results would be obtained. A new CuBe-5C bushing was installed and the system was reassembled. This test will use the same conditions as the previous one with the only change being the bushing. The test was performed and the data results are plotted and presented in the Figure 118. Visual inspection photos are presented in Figure 119.

Use or disclosure of data contained on this sheet is subject to the restriction on the title page of this proposal.
Northrop Grumman Private/Proprietary Level I

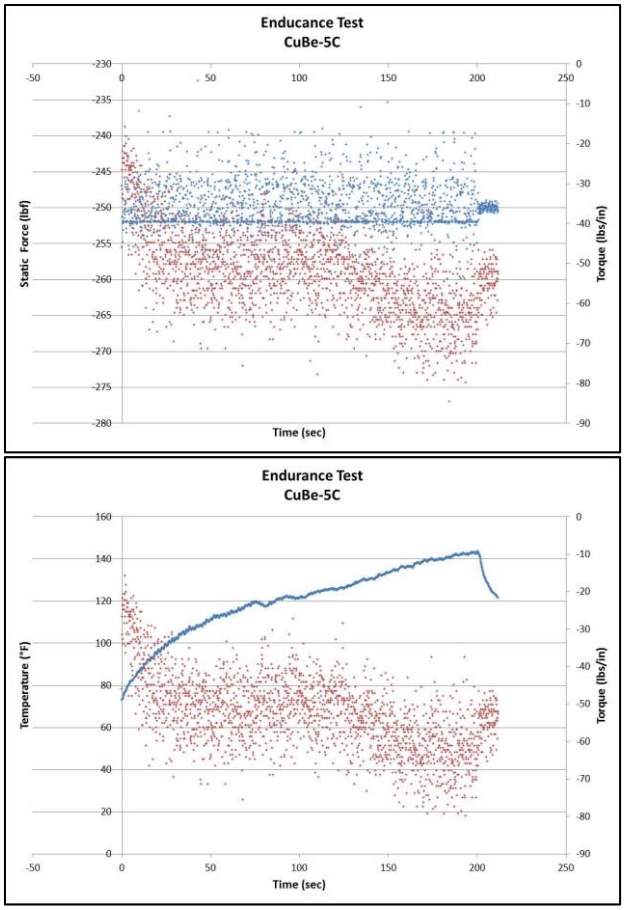

Figure 118. Results of CuBe-5C Endurance Test at 250 lb Load for 100 Cycles

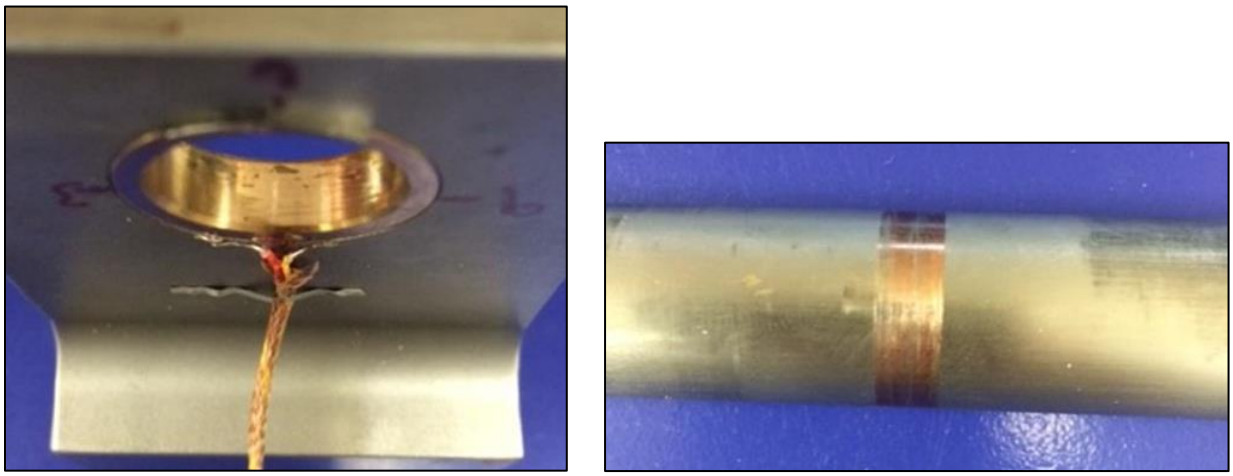

Figure 119. Results of CuBe-5C Visual Inspection of 250 lb Load for 100 Cycles

Galling was evident in the CuBe-5C copper beryllium standard bushing as well and so the bushing was removed and a new CuBe-6C bushing was installed into the fixture and the system reassembled. So again the static load was lowered this time to a 100 lb load and the test was performed. The result of the visual inspection for this test did not indicate any galling so the

Use or disclosure of data contained on this sheet is subject to the restriction on the title page of this proposal.
Northrop Grumman Private/Proprietary Level I

system was reassembled and ran for another 100 cycles. The data results were plotted and are presented Figure 120. Visual inspection did identify galling after running the second 100 cycles at the 100 lbs static load and the results are presented in Figure 121.

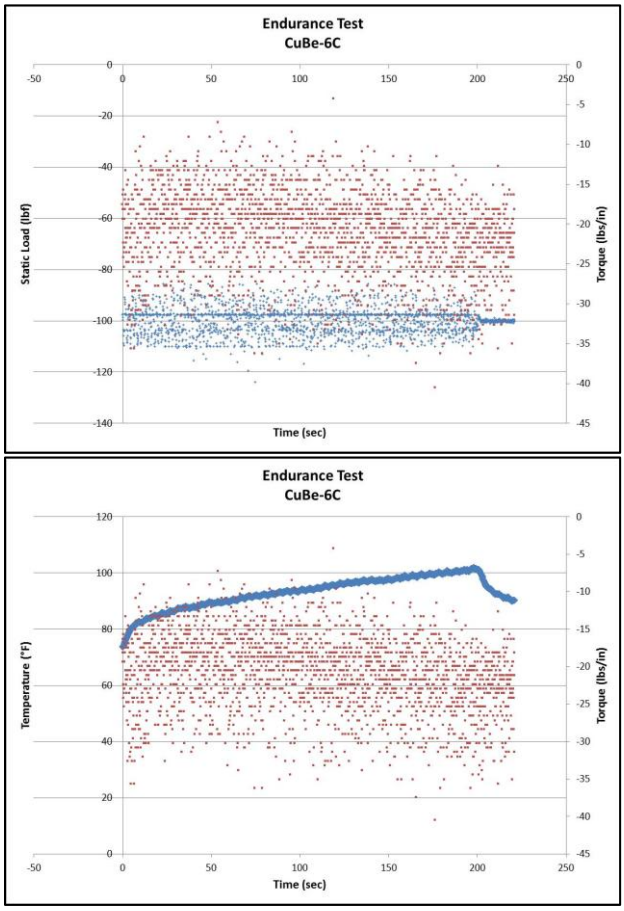

Figure 120. Results of CuBe-6C Endurance Test at 100 lb Load for 100 Cycles

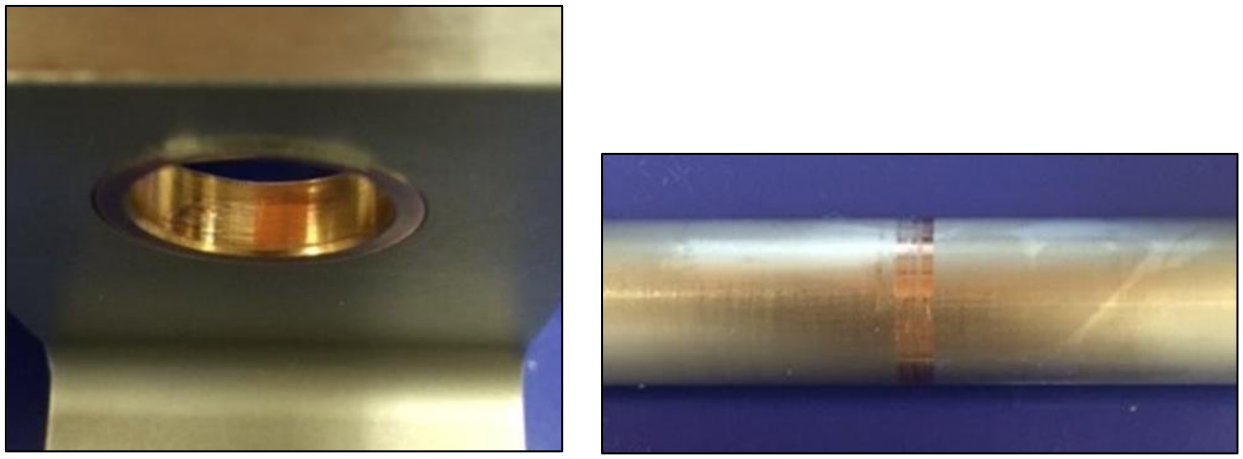

Figure 121. Results of CuBe-6C Visual Inspection of 100 lb Load for 100 Cycles

With galling initiation being identified for the CuBe bushing it was removed and now a new NGCo-3A-6C bushing was installed into the testing fixture. The 100-lb loading condition was

Use or disclosure of data contained on this sheet is subject to the restriction on the title page of this proposal.
Northrop Grumman Private/Proprietary Level I

not changed and the test was performed for the same 100 cycles. The bushing was removed from the fixture and the visual evaluation identified slight galling after the first 100 cycles at the 100 lb load. The test results were plotted and are shown in Figure 122. The visual inspections photos for the NGCo-3A-6C bushing and the pin are shown in Figure 123.

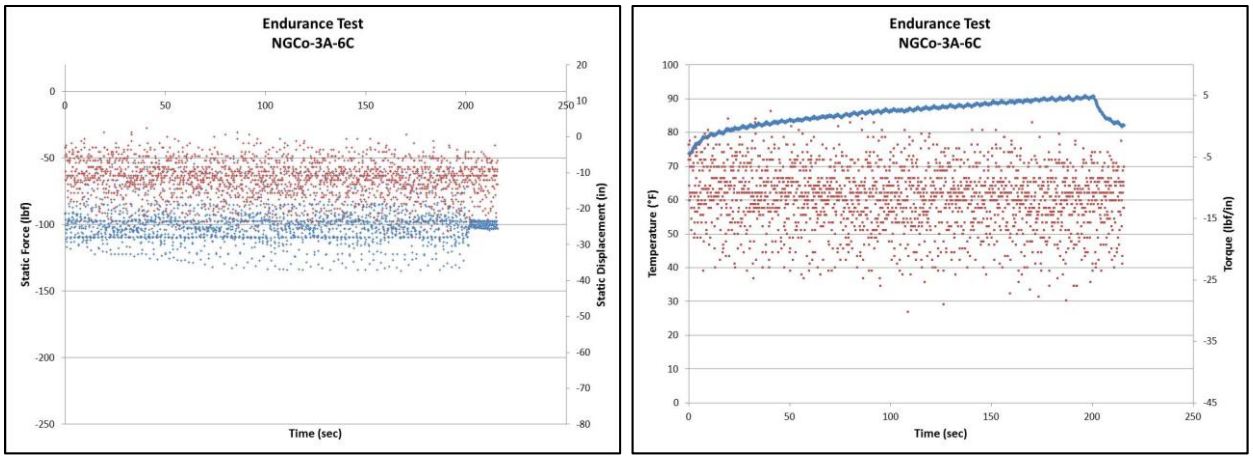

Figure 122. Results of NGCo-3A-6C Endurance Test at 100 lb Load 0-100 Cycle

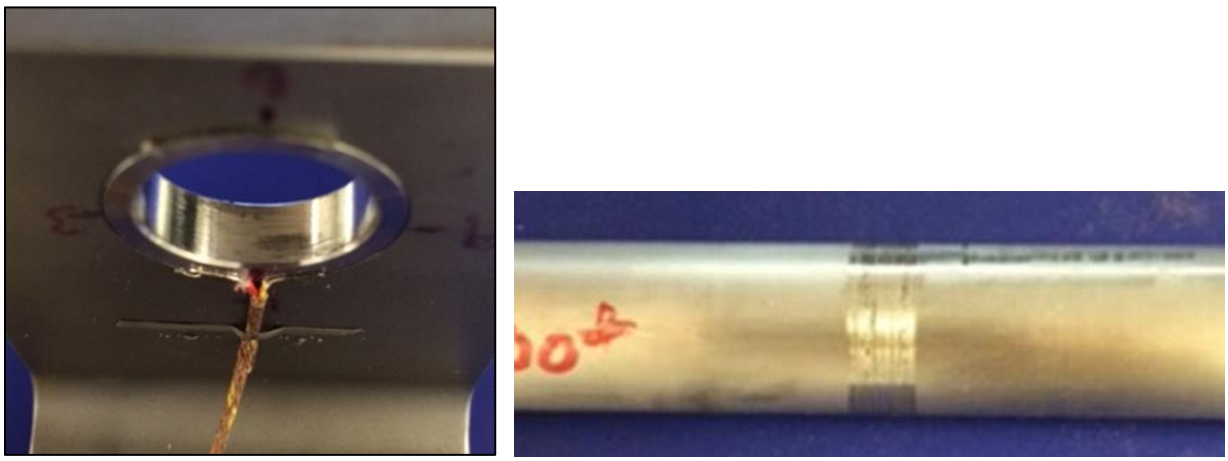

Figure 123. Results of NGCo-3A-6C Visual Inspection of 100 lb Load for 100 Cycles

To confirm the galling results of the NGCo-3A-6C alternative alloy a repeatability test was performed. The NGCo-3A-6C bushing was removed from the bushing support plate and the new NGCo-3A-7C bushing installed and then the test system was reassembled. Testing conditions of 100 lb static load for 100 cycles was performed. The bushing was removed and visually inspected and there were some indications of material transfer on the pin but no galling was identified. With no galling being identified the visual inspection photos were taken and then the bushing was re-installed into the test system and an additional 100 cycles at the 100 lb static load was performed. Again the bushing was removed and a visual inspection performed in which the indication of galling was identified. The test results were plotted and are shown in Figure 124. The visual inspections photos for the NGCo-3A-7C bushing and the pin for the 0-100 cycles and 100-200 cycles at 100 lb load are shown in Figure 125.

Use or disclosure of data contained on this sheet is subject to the restriction on the title page of this proposal.
Northrop Grumman Private/Proprietary Level I

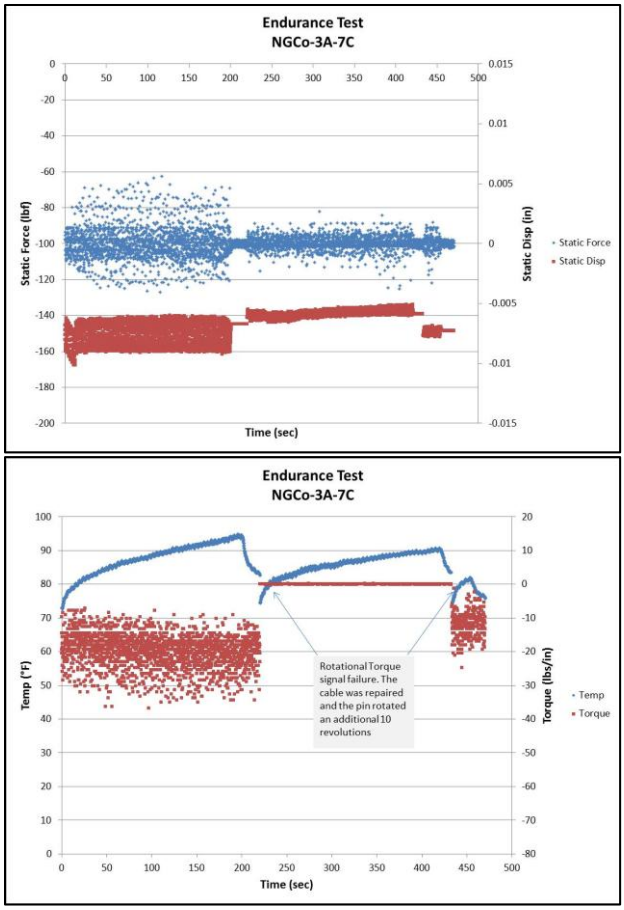

Figure 124. Results of NGCo-3A-7C Endurance Test at 100 lb Load 0-100 & 100-200 Cycles

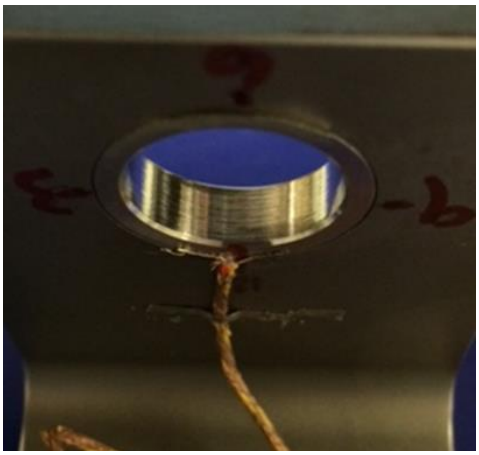

Use or disclosure of data contained on this sheet is subject to the restriction on the title page of this proposal.
Northrop Grumman Private/Proprietary Level I

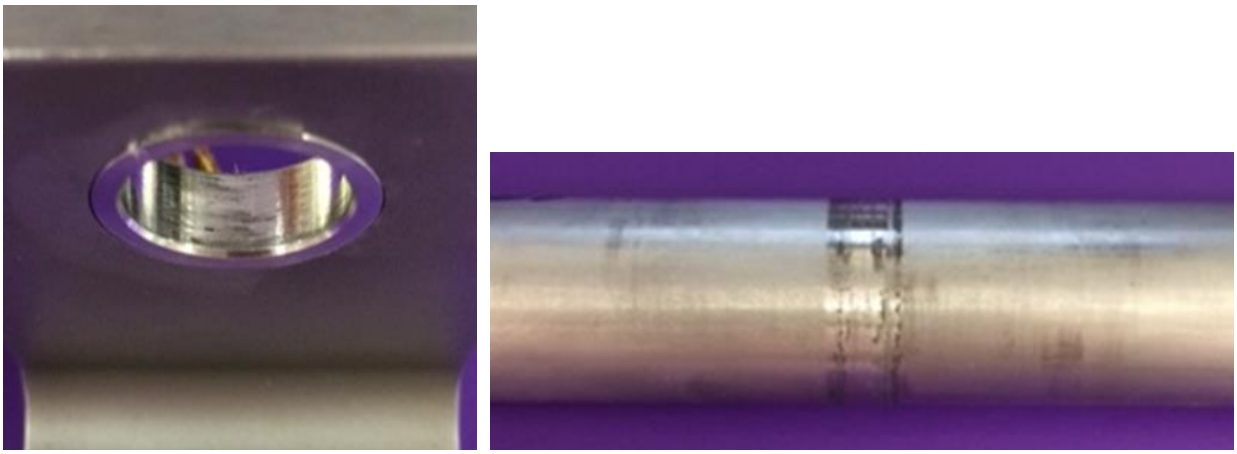

Figure 125. Results of NGCo-3A-7C Visual Inspection of 100 lb Load for both 0-100 Cycles and 100-200 Cycles Tests

Both the threshold and endurance bushing test methods were modified slightly in order to capture the initiation of galling. Although the two tests had different dynamic operations the two alloys produced similar performance results. After modifying the tests we were able to capture the initiation of galling with the available quantity of bushings that had been fabricated.

The endurance testing results were gathered and a summary chart prepared. A summary of the results are provided in Table 22. Bushing test data results provided by Metcut Industry from which the summary for the threshold and endurance testing was prepared are provided in the appendix.

Table 22. Summary of Endurance Bushing Testing Conditions and Visual Results

Endurance Bushing Test Summary						
Test #	Alloy	Bushing Geometry 0.09" X 0.07"	Applied Loading (Lbs)	Cycles (1 Cycle = 360°)	Max Load (Lbs)	Notes
1	NGCo-3A-4C	Chamfer	500	0-100	500	Galling Identified
2	NGCo-3A-5C	Chamfer	250	0-100	250	Galling Identified
3	CuBe-5C	Chamfer	250	0-100	250	Galling Identified
4a	CuBe -6C	Chamfer	100	0-100	100	Mild Material Transfer
4b	CuBe -6C	Chamfer	100	100-200	100	Galling Identified
5	NGCo-3A-6C	Chamfer	100	0-100	100	Galling Identified
6a	NGCo-3A-7C	Chamfer	100	0-100	100	Mild Material Transfer
6b	NGCo-3A-7C	Chamfer	100	100-200	100	Galling Identified

Use or disclosure of data contained on this sheet is subject to the restriction on the title page of this proposal.
Northrop Grumman Private/Proprietary Level I

6.0 ALTERNATIVE ALLOY HEALTH RISK ASSESSMENT

The need for a nontoxic replacement for Beryllium is apparent not only at the environmental health and safety level, but also from the standpoint of the cost reduction/avoidance and cycle time optimization.

First, a general background study was conducted to analyze and define significant material criteria and properties of the currently used material, as well as the necessary and usual test procedures. These parameters will be used as basis for an extensive literature research for alternative, non-toxic materials with similar properties. The behavior of the pre-selected, suitable materials under working conditions will be analyzed in a Finite Element Method.

A Heath Risk Assessment was performed on the Alternative Copper Beryllium Material NGCo-3A. A three phased approach was taken in evaluating the components in the newly developed alloy. Initially a comparison of the NGCo-3A with that of the Copper Beryllium was investigated utilizing the American Conference of Governmental Industrial Hygienists ACGIH Threshold Limit Values (TLV) and the Biological Exposure Indices (BEI) to present the typical hazard recommendation levels for the industry. These recommended levels are supported by quantitative tests which have been performed and the values have been based upon. In the second phase a review of the 5 tiered approach to a Health Risk assessment from the Air Quality Management District (AQMD) perspective. Typically this type of assessment is performed for a site specific material evaluation but the chronic pollutant index calculated by the formula in the first tier provides alloy comparison relevance in reference to hazardous air pollutant. For the third phase of the evaluation a hazardous review at the individual component level was performed. A hazardous ranking from least to greatest utilizing the TLV's, BEI's, Air Pollutant Index and some noted concerns is provided in the assessment. All referenced information indicates that Beryllium is far more hazardous, on the order of 100 times that of any component within the alternative alloy. Cobalt was ranked the highest health risk component within the new alloy followed by chrome which is inert as a standalone metal component but has a potential of reacting due its atomic valance characteristics and become trivalent or possibly even Hexavalent chrome during manufacturing. For this reason till tested otherwise the chrome element was ranked at the intermediate health risk level in support of this pending concern. An internet search to identify if any hexavalent chrome transformations have been reported for cobalt alloys was performed. One potential was found of the Cr (VI). Release of gas during the production (melting) of chrome containing alloys. The Health Risk Assment report which supports this summary is provided in the appendix.

7.0 CONCLUSIONS

The ultimate program goal is to design and develop alternative alloy materials that would be capable of replacing Cu-Be alloys currently used on military platforms. Alternative materials to be developed shall meet the following requirements:

- Tensile strength greater than 165,000 psi
- Yield strength at 0.2% offset greater than 140,000 psi
- Hardness of 36 to 45 Rockwell C (HRC)

Use or disclosure of data contained on this sheet is subject to the restriction on the title page of this proposal.
Northrop Grumman Private/Proprietary Level I

Alternative materials must also meet or exceed the performance of baseline Cu-Be alloy in terms of friction coefficient in dry sliding conditions against low-alloy steels, wear resistance, resistance to galling and spalling, axial fatigue, and rolling contact fatigue.

The results of preliminary alloy evaluations were utilized in the follow-on design and process modeling tasks for the detailed alternative alloys. Two alloy systems were targeted, one copper based alloy and one cobalt based alloy. Form these two systems six specific compositions were designed and produced, three copper based alloys and three cobalt based alloys. Each composition was investigated thoroughly in the design phases in order to obtain the desired performance characteristics and performance required from each material. Legacy materials composition and characteristics performance data was leveraged in producing the next generations of alternative materials. This information, new design alterations and the characteristics comparisons testing all supported the target of a down selected alternative alloy.

To evaluate the performance of these potential alternatives the Detail Alloy Evaluation/Characterization tasks were initiated. In doing so, the CuBe AMS 4533 material was procured and tested along with the newly designed alloys to provide comparison data and characteristic validation for the sub tasked coupon level evaluation.

Plans moved forward with the two alternative alloy systems that were down selected from the original six systems that had been identified. The two material systems were chosen because they both possessed the best potentials in producing an alloy that meets or surpasses the program requirements.

The design optimization of the copper and cobalt material systems was performed by QuesTek innovations with the use of several of their own development tools. Tools utilized by QuesTek included; Materials by Design, PrecipiCalc software and Thermal Phase Diagrams, all in support of producing the best alternative alloy and meeting the required program performance targets. These newly developed alloys were put through an initial series of tests. Testing was performed on both the newly designed alternative alloys along with the standard copper beryllium to support a side-by-side comparison and validation of performance. There were four initial tests performed as part of the alternative alloy materials down-selection. Initial alloy testing included Tensile, Compression, Pin-on-Disk and Reciprocating-Ball-on-Flat. In the initial round of testing the NGCo-1A cobalt based alternative alloy produced the best results and exceeded the program desired tensile strength but tensile yield strength fell slightly short of the desired program goal. Both copper-based materials were lower-strength than expected and were removed from the alternative selection.

The second group of alternative alloys was tested to the same set of tests that were performed on the initial group. Performance of the NGCo-3A material proved to be the best once again in comparison to the baseline copper beryllium only showing lower in the one category of the tensile yield strength where it fell behind the copper based Cuprium alternative alloy. The NGCo-1A material tested superior over both the NGCu-1A copper based and the standard copper beryllium alloy in producing a lower coefficient of friction. Upon completion of the 2nd round of testing a material down selection was made favoring the NGCo-3A cobalt based material. Two additional ASTM characterization tests, ASTM G98 Galling, and ASTM E606 Strain Controlled Fatigue, were performed on the down selected NGCo-3A and the standard copper beryllium alloys to evaluate these final performance characteristics. Galling results were similar in that they both yielded at the same load value before galling could be identified. The

Use or disclosure of data contained on this sheet is subject to the restriction on the title page of this proposal.
Northrop Grumman Private/Proprietary Level I

strain-life fatigue test results identified the NGCo-3A alloy as being the superior alloy in comparison to the baseline in both R-values and number of cycles occurring before failure.

The cobalt based alternative material supports a safe material replacement so the elimination of manufacturing controls for monitoring and hazardous material migration can be eliminated and provide a safer place to work for employees.

A predictive cost analysis was provided from QuesTek for the NGCo-3A alternative that was based on a quotation received from MetalWerks to produce the alloy at a larger scale. MetalWerks is capable of producing material via VIM + VAR processing at 2000 lb scale. The cost quotation provided is $41-43 dollars per pound of material. This is a costing based on toll-manufacturing overhead rates, and is likely not representative of a true cost of the material once sufficient market potential has been generated to justify production with a commercial entity capable of producing at larger scale (>10,000 lb), such as Carpenter Technology or Haynes International. Carpenter alternative alloy aCUBE 100 presently in production approximate costs range from the $22 to $36 dollars per pound of material. Material compositions are close and processing of the NGCo-3A material may not require as much work which supports a cost that could be competitive to what the market bears.

Use or disclosure of data contained on this sheet is subject to the restriction on the title page of this proposal.
Northrop Grumman Private/Proprietary Level I

REFERENCES:

1. Fodran, E.J., "Copper Beryllium Replacement Testing Phase 2 - Wear Tests" Internal F-35 Program Document 2ZZA00123, Distribution D, (2004).

2. Hsu, K. L., Ahn T.M. and Rigney D.A., "Friction, wear and microstructure of unlubricated austenitic stainless steels," Wear, 60 (1980), pp. 13-37.

3. B.R. Pearson, and R.B. Waterhouse, "Fretting corrosion of a nitrogen-bearing austenitic stainless steel in artificial seawater and 0.1 M H2SO4," Materials Characterization, 28 (1992), pp. 271-277.

4. G. Bolling and R. Richman, "The plastic deformation of paramagnetic FCC Fe-Ni-C alloys ", Acta Metallurgica, vol. 18, 1970.

5. Lim, C. M. and Ashby, M. F., "Wear-Mechanism Maps," Acta Metallurgica, 35 (1987), pp. 1-24.

6. NAVAIR Phase II SBIR Program, Contract # N68335-07-C-0108 *QuesTek* Proprietary Information – All information subject to Proprietary Information Agreement # MA11-09-13354 executed on December14th, 2009. 3

7. Teisanu, C, Dumitru, N., and Gheorghe S., (2011), "Analysis of the PM Bearing-Spindle Contact Using Finite Element Method", The Annals of "Dunarea De Jos" University of Galati, Fascicle VIII, Tribology, (XVII), Issue 1, ISSN 1221-4590, pp. 41-46

8. Molinari, J. F., Ortiz, M., Radovitzky R., and Repetto, E. A., (2001), "Finite-element Modeling of Dry Sliding Wear in Metals", Engineering Computations, Vol. 18, No. 3/4, pp. 592-609.

9. Kim, N. H., Won, D., Burris, D., Holtkamp, B., Gessel, G. R., Swanson, P., and Sawyer, W. G., (2005), "Finite Element Analysis and Experiments of Metal/Metal Wear in Oscillatory Contacts", Wear, Vol. 258, pp. 1787-1793.

10. ABAQUS, 2010, ABAQUS Users' Manual, Hibbit, Karlson and Sorenson Inc., Pawtucket, RI.

Use or disclosure of data contained on this sheet is subject to the restriction on the title page of this proposal.
Northrop Grumman Private/Proprietary Level I

APPENDIX A

1. ASTM E8 Tensile Testing/Evaluation Materials Test Results

ASTM E8 Tension (BL_Cu_Co).pdf
EUP3 Tensile Cuprium @ RTA.pdf
EUJY Tensile NGCO-3A Alt Cu-Be A
NOR149120256747002 Tensile 4in.PDF

2. ASTM E9 Compression Testing/Evaluation Materials Test Results

ASTM E9 Compression (BL_Cu_
NOR149120256747001 Comp 2in.PDF
NOR149120256747002 Comp 4in.PDF

3. ASTM G99 Pin on Disk Wear Testing/Evaluation Materials Test Results

TRB 120702 Northrop Grumman C
TRB 140116 Northrop Grumman C

4. ASTM G133 Reciprocating Ball on Flat Wear Testing/Evaluation Materials Test Results

TRB-L 120702 Northrop Grumman C
TRB-L 140116 Northrop Grumman C

5. ASTM G98 Galling Test Results

GallingReport13-165.pdf

6. Enhanced Busing Design and Development Report and Full Scale Bushing Test Results

Enhanced Bushing Design_Development
Metcut all up Threshold Testing File
Metcut all up Enduracne Testing Fil

7. Environmental Health Assessment Report

Copper Beryllium Alternative Alloy Heal

Use or disclosure of data contained on this sheet is subject to the restriction on the title page of this proposal.
Northrop Grumman Private/Proprietary Level I